In Silico Investigations into Lysosomal Arrhythmia Causation



Zhaozheng Meng

Linacre College

University of Oxford

Submission for the degree of Doctor of Philosophy

Hilary 2024

This thesis was jointly supervised by

Professor Rebecca Ann Beatrice Burton

Department of Pharmacology

And

Professor Alfonso Bueno-Orovio

Department of Computer Science

Abstract

During intracellular calcium overload, ryanodine receptors (RyRs) spontaneously release calcium, which can result in delayed afterdepolarizations that are strongly linked to potentially fatal arrhythmias. The sarcoplasmic reticulum acts as the primary calcium store in cardiomyocytes. Other organelles, such as mitochondria and lysosomes, may also act as calcium stores. Type 2 two-pore channels (TPC2) are principally responsible for releasing lysosomal calcium upon activation by NAADP. It has been demonstrated that knockout of two-pore channel 2 (TPC2) inhibits lysosomal calcium release, which decreases the occurrence of ventricular arrhythmias during β-adrenergic stimulation. There are currently no mechanistic studies examining how lysosomal function affects RyR spontaneous release. In this thesis, I study how lysosome function affects calcium loading, which in turn influences RyR spontaneous release. This allows us to understand how lysosomes might mediate arrhythmias. Understanding the role of lysosomal calcium as a potential contributor to the generation of arrhythmias can be approached by alternative approaches to controlled wet-lab experimentation, which restrain variability experimentally and statistically. Mechanistic investigations were conducted using a population of biophysically detailed mouse ventricular and human atrial cardiomyocyte models including lysosome calcium handling and incorporating variability, and calibrated by experimental findings. Here I demonstrate that lysosomal calcium uptake and release can synergistically form a pathway for fast calcium transport, by which lysosomal calcium release primarily modulates sarcoplasmic reticulum calcium ATPase reuptake and RyR release. Enhancing this pathway contributes to pro-arrhythmias. Notably, blocking this pathway revealed an antiarrhythmic impact on the cell. In ventricular cardiomyocytes, lysosomal calcium handling promotes RyR spontaneous release by elevating RyR open probability. In atrial cardiomyocytes, lysosomal release promotes early afterdepolarisations by increasing sodium calcium exchange inward current and late L-type calcium current. When considered collectively, the studies show that proarrhythmic mediators are directly influenced by lysosomal calcium handling, indicating potential antiarrhythmic approaches and revealing important modulators of lysosomal proarrhythmic action.

Acknowledgements

First of all, I would like to thank my supervisors sincerely, Professor Rebecca Burton and Professor Alfonso Bueno-Orovio, for being excellent supervisors and best friends, and for their continuous support, kindness and encouragement. I will be forever grateful to them for all the knowledge and wisdom they imparted to me and for their trust and patience throughout the course of my DPhil studies. I would like to express my sincere gratitude to my supervisor Professor Rebecca Burton for welcoming me to her lab, for her remarkable wisdom in shaping the direction of this work, and for her enormous effort in the development of my academic skills. I would like to express my sincere gratitude to my supervisor Professor Alfonso Bueno-Orovio for devoting so much effort for me and for helping me to rigorously cope with numerous difficulties in my work. In addition, I would like to thank my colleagues in our groups for their help and precious suggestions to improve my work. I would like to thank Dr. Rebecca Capel, Dr. Samuel J. Bose, Dr. Thamali Ayagama, Emily Akerman, Qianqian Song, and Matthew Read. I am grateful to Emily Akerman for proof reading my thesis and for her comments and edits.

The work of my thesis was built on the integration of experimental data and computational modelling. Here I would like to acknowledge my experimental collaborators and colleagues. I would like to thank Professor Derek Terrar for his continuous support and generosity during this course. I would like to thank Dr. Rebecca Capel and Dr. Samuel J. Bose for letting me have the invaluable experimental data for my work, as well as broadening my electrophysiological knowledge. I would like to thank Professor Niels Voigt group for letting me have the invaluable human experimental data for my work. Here I would like to acknowledge my computational collaborators and colleagues. I would like to thank Professor Blanca Rodriguez for her help. I would like to thank Professor Robert Planque and his students Erik Bosch and Sophia de Jong for the initial work.

I would like to thank Professor Alan Garfinkel for letting me attend the lecture course Dynamical Systems Modelling. I would like to thank Professor Vicente Grau for letting

me attend the lecture course Medical Imaging, Image Analysis and Microscopy. I would like to thank Professor Jotun Hein for letting me attend the lecture course Computational Biology.

Last but not least, I would like to thank my family and friends. I would like to thank my remarkable parents for their love and support. I would like to thank my mother for her always understanding me and encouraging me to pursue my dreams. I would like to thank my father for his faith on me and supporting me. Finally, I would like to thank all my family and friends for their help and support.

Abbreviation

ABC	Atrial fibrillation Better Care
ADP	adenosine diphosphate
AF	atrial fibrillation
APs	action potentials
APA	action potential amplitude
APD	action potential duration
ATP	adenosine triphosphate
AVN	atrioventricular node
AP_{AMP}	amplitude of the AP
AP_{APD90}	action potential duration at 90% repolarisation
AP_{peak}	peak membrane potential of the AP
AP_{RMP}	resting membrane potential of the AP
CA	catheter ablation
cAF	chronic atrial fibrillation
Ca^{2+}	calcium ion
Ca_{AMP}	calcium transient amplitude
Ca_{Dia}	diastolic calcium concentration
Ca_{RT50}	calcium transient at 50% relaxation
Ca_{RT80}	calcium transient at 80% relaxation
CICR	Ca^{2+}-induced Ca^{2+}-release
CLC	calcium loading channel
Cl^-	chloride ion
CTRL	control
DADs	delayed afterdepolarisations
dV/dt_{max}	maximum upstroke velocity
EADs	early afterdepolarisations
ER	endoplasmic reticulum
GPN	glycyl-L-phenylalanine 2-naphthylamide
H^+	hydrogen ion
IP3	inositol trisphosphate

IP3R	IP3 receptor
ISO	isoprenaline
I_{bCa}	Ca^{2+} background current
I_{bCl}	background Cl^- current
I_{bNa}	Na^+ background current
I_{CaL}	L-type Ca^{2+} current
I_{Cl}	Cl^- currents
$I_{Cl(Ca)}$	Ca^{2+}-activated Cl^- current
I_{KAch}	acetylcholine activated K^+ channel
I_{KATP}	ATP-sensitive K^+ channel
I_{Kr}	rapid component of the delayed rectifier repolarising K^+ currents
I_{Ks}	slow component of the delayed rectifier repolarising K^+ currents
I_{Kur}	ultrarapid delayed rectifier K^+ current
I_{K1}	inward rectifier K^+ current
I_{Na}	voltage-gated Na^+ current
I_{NaK}	Na^+/K^+ pump currents
I_{NCX}	Na^+/Ca^{2+} exchanger current
I_{to}	transient outward K^+ current
K^+	potassium ion
LSDs	lysosomal storage diseases
L-type	low threshold
MLIV	mucolipidosis type IV
NAADP	nicotinic acid adenine dinucleotide phosphate
NAADP-AM	membrane permeant analogue of NAADP
Na^+	sodium ion
NCX	Na^+/Ca^{2+} exchanger
NPC	Niemann Pick type C
nSR	normal sinus rhythm
PMCA	plasma membrane Ca^{2+} ATPase
RMP	resting membrane potential
RyRs	ryanodine receptors

SAN	sinoatrial node
SERCA	sarcoplasmic reticulum Ca^{2+}-ATPase
SR	sarcoplasmic reticulum
TASK-1	tandem of P domains in a weak inward-rectifying K^+ channel–related acid-sensitive K^+ channel-1
TPCs	two-pore channels
TPC2-KO	TPC2 knock-out
TWIK	two pore domain K^+ channel
T-tubule	transverse-tubular system
T-type	transient
V-ATPase	vacuolar-type H^+-ATPase
V_{20}	potential measured at 20% of the APD_{90} time

List of Figures

Figure 1.1	Human (Nerbonne *et al.*, 2001) and mouse ventricular AP morphology (traces of action potential and currents in the Morotti *et al.* ventricular model including lysosomal calcium handling at baseline at 1Hz).
Figure 1.2	Human ventricular (Grunnet, 2010) and atrial AP morphology (traces of action potential and currents in the Grandi *et al.* human atrial model including lysosomal calcium handling at baseline at 1Hz).
Figure 1.3	Electron micrograph of a lysosome in a ventricular cardiomyocyte.
Figure 1.4	Schematic diagram of NAADP signalling and modulation in cardiac myocytes.
Figure 1.5	Transmission electron microscopy of lysosomes.
Figure 2.1	Schematic diagram of including lysosome compartment in Morotti *et al.* and Grandi *et al.* models
Figure 2.2	Flowchart illustrating the process behind constructing an experimentally-calibrated population of models
Figure 3.1	Schematic cartoon showing the hypotheses for actions of lysosomal calcium handling
Figure 3.2	Validation of lysosomal calcium handling model against pharmacological protocols.
Figure 3.3	Lysosomal calcium release primarily modulates intracellular calcium handling by increasing SERCA reuptake and RyR release.
Figure 3.4	Ionic properties and calcium fluxes underlying spontaneous calcium events under hypercalcemia and sustained β-adrenergic stimulation.
Figure 3.5	Lysosomal calcium release promotes spontaneous calcium release in TPC-specific proarrhythmic models under hypercalcemia and β-adrenergic stimulation by increasing RyR open probability.
Figure 3.6	Loss of lysosomal calcium release flux reduced spontaneous calcium release from SR in TPC-specific proarrhythmic models

under hypercalcemia and β-adrenergic stimulation.
Figure 3.7 Lysosomal calcium release produces delayed afterdepolarisations by promoting spontaneous calcium release in TPC-specific proarrhythmic models under hypercalcemia and β-adrenergic stimulation.
Figure 3.8 TPC-specific proarrhythmic models with minor oscillatory behaviour under hypercalcemia and β-adrenergic stimulation.
Figure 3.9 Ionic properties and calcium fluxes underlying spontaneous calcium events under fast pacing at 10 Hz and sustained β-adrenergic stimulation.
Figure 3.10 Lysosomal calcium release promotes spontaneous calcium release in TPC-specific proarrhythmic models under fast pacing and β-adrenergic stimulation, by increasing RyR open probability.
Figure 3.11 Lysosomal calcium release promotes spontaneous calcium release in TPC-specific proarrhythmic profiles under fast pacing and β-adrenergic stimulation, by increasing RyR open probability.
Figure 3.12 Loss of lysosomal calcium release flux reduced spontaneous calcium release from SR in TPC-specific proarrhythmic models under fast pacing and β-adrenergic stimulation.
Figure 3.13 Loss of lysosomal calcium release flux reduced spontaneous calcium release from SR in TPC-specific proarrhythmic models under fast pacing and β-adrenergic stimulation.
Figure 3.14 Schematic cartoon showing the conclusions for actions of lysosomal calcium handling
Figure 4.1 Schematic cartoon showing the hypothesis for actions of lysosomal calcium release
Figure 4.2 Calibration of human atrial cardiomyocyte model incorporating lysosomal calcium handling.
Figure 4.3 Measurements of β-adrenergic response in human atrial cardiomyocytes.
Figure 4.4 Validation of β-adrenergic stimulation in the modified human atrial cardiomyocyte model.

Figure 4.5 Calibration of populations of models in nSR and cAF in baseline conditions.
Figure 4.6 Distributions of currents, fluxes, concentrations and action potentials.
Figure 4.7 Representative traces of the calcium concentrations and action potentials.
Figure 4.8 Representative traces of the currents and calcium fluxes.
Figure 4.9 Partial correlation coefficients between varied fluxes and currents and the biomarkers of calcium transient and action potential.
Figure 4.10 Distributions of currents, fluxes, concentrations and action potentials.
Figure 4.11 Representative traces of the calcium concentrations and action potentials.
Figure 4.13 Representative traces of the currents and calcium fluxes.
Figure 4.13 Partial correlation coefficients between varied fluxes and currents and the biomarkers of calcium transient and action potential.
Figure 4.14 Schematic cartoon showing the conclusion for actions of lysosomal calcium release
Figure 5.1 Schematic cartoon showing the hypothesis for actions of lysosomal calcium release
Figure 5.2 Traces of TPC-specific, and non-proarrhythmic models with early afterdepolarisation under mild hypercalcemia and β-adrenergic stimulation in nSR.
Figure 5.3 Comparisons of the TPC-specific, and non-proarrhythmic categories with early afterdepolarisation under mild hypercalcemia and β-adrenergic stimulation in nSR.
Figure 5.4 Lysosomal calcium release promoted early afterdepolarisation in proarrhythmic TPC-specific models under mild hypercalcemia and β-adrenergic stimulation in nSR.
Figure 5.5 Lysosomal calcium release promoted early afterdepolarisation in proarrhythmic TPC-specific models under mild hypercalcemia and β-adrenergic stimulation in nSR.

Figure 5.6 Traces of proarrhythmic TPC-specific, and non-proarrhythmic models with early afterdepolarisation under mild hypercalcemia and β-adrenergic stimulation in cAF.
Figure 5.7 Comparisons of TPC-specific, and non-proarrhythmic categories with early afterdepolarisation under mild hypercalcemia and β-adrenergic stimulation in cAF.
Figure 5.8 Lysosomal calcium release promoted early afterdepolarisation in proarrhythmic TPC-specific models under mild hypercalcemia and β-adrenergic stimulation in cAF.
Figure 5.9 Lysosomal calcium release promoted early afterdepolarisation in proarrhythmic TPC-specific models under mild hypercalcemia and β-adrenergic stimulation in cAF.
Figure 5.10 Schematic cartoon showing the conclusion for actions of lysosomal calcium release
Figure 6.1 Schematic cartoon showing the hypothesis for actions of lysosomal calcium release
Figure 6.2 Traces of TPC-specific and non-proarrhythmic models under I_{Kur} block and β-adrenergic stimulation in nSR.
Figure 6.3 Comparisons of TPC-specific and non-proarrhythmic categories under I_{Kur} block and β-adrenergic stimulation in nSR.
Figure 6.4 Lysosomal calcium release promoted EADs in proarrhythmic TPC-specific models under I_{Kur} block and β-adrenergic stimulation in nSR.
Figure 6.5 Lysosomal calcium release promoted EADs in proarrhythmic TPC-specific models under I_{Kur} block and β-adrenergic stimulation in nSR.
Figure 6.6 Traces of proarrhythmic TPC-specific, and non-proarrhythmic models with EADs under I_{Kur} block and β-adrenergic stimulation in cAF.
Figure 6.7 Comparisons of TPC-specific, and non-proarrhythmic categories under I_{Kur} block and β-adrenergic stimulation in cAF.
Figure 6.8 Lysosomal calcium release promoted EADs in proarrhythmic TPC-

specific models under I_{Kur} block and β-adrenergic stimulation in cAF

Figure 6.9 Lysosomal calcium release promoted EADs in proarrhythmic TPC-specific models under I_{Kur} block and β-adrenergic stimulation in cAF.

Figure 6.10 Schematic cartoon showing the conclusion for actions of lysosomal calcium release

Table of Contents

ABSTRACT.....**3**

ACKNOWLEDGEMENTS.....**4**

ABBREVIATION.....**6**

LIST OF FIGURES.....**9**

CHAPTER 1.....**18**

Introduction.....**18**

1.1 Physiology of the Heart.....**18**
1.1.1 Ion Channels.....18
1.1.2 Cardiac Electrophysiology.....21
1.1.3 Ionic Mechanisms of Arrhythmia.....24
1.1.4 Mechanisms of Atrial Fibrillation.....26
1.1.5 Atrial Fibrillation Therapy.....28

1.2 Lysosomes in the Heart.....**30**
1.2.1 Lysosome Identification.....30
1.2.2 Lysosomal Storage Disease.....31
1.2.3 Lysosomal Properties.....33
1.2.4 Lysosomes as Calcium Stores.....34
1.2.5 Lysosomes in the Cardiomyocyte.....37

1.3 Modelling Cardiomyocytes.....**39**
1.3.1 Development of Electrophysiological Models.....39
1.3.2 Ventricular Cardiomyocyte Models.....40
1.3.3 Atrial Cardiomyocyte Models.....42
1.3.4 Variability in Cardiac Electrophysiology.....44
1.3.5 Sampling Methods.....45

1.4 Aim.....**46**

CHAPTER 2.....**49**

Methods.....**49**

2.1 Modelling Lysosomal Calcium Loading in Mouse Ventricular Cardiomyocytes
.....**49**
2.1.1 Experimental Data.....49

2.1.2 Mathematical Modelling and Simulation Studies.....50
2.1.3 Including Lysosome Compartment in a Mouse Ventricular Cardiomyocyte Model.....50

2.2 Modelling Lysosomal Calcium Loading in Human Atrial Cardiomyocytes.....55
2.2.1 Experimental Data.....55
2.2.2 Mathematical Modelling and Simulation Studies.....56
2.2.3 Including Lysosome Compartment in a Human Atrial Cardiomyocyte Model. 56

2.3 Cellular Variability in Electrophysiology and Calcium Handling.....58

2.4 Quantitative Analysis of Ionic Features in Action Potential and Calcium Transient.....60
2.4.1 Definition of Proarrhythmic Events.....61
2.4.2 Models Extracted in Proarrhythmic Scenarios.....61
2.4.3 Statistics.....62

CHAPTER 3.....63

Lysosomal Calcium Loading Promotes Spontaneous Calcium Release by Potentiating Ryanodine Receptors.....63

3.1 Introduction.....64

3.2 Results.....66
3.2.1 Model Validation of Lysosomal Calcium Handling.....66
3.2.2 Lysosomal Calcium Release Primarily Modulates Intracellular Calcium Handling by Increasing SERCA Reuptake and RyR Release.....69
3.2.3 Lysosomal Calcium Release Promotes Spontaneous Calcium Release under Hypercalcemia and β-adrenergic Stimulation by Increasing RyR Open Probability..73
3.2.4 Lysosomal Calcium Release Promotes Spontaneous Calcium Release under Fast Pacing and β-adrenergic Stimulation by Increasing RyR Open Probability.....82

3.3 Discussion.....88
3.3.1 Limitations.....91

CHAPTER 4.....93

Lysosomal Calcium release Primarily Modulates Intracellular Calcium Handling by Increasing SERCA Reuptake and RyR Release in Human Atrial Cardiomyocytes.....93

4.1 Introduction.....94

4.2 Results.....96
4.2.1 Calibration of Human Atrial Cardiomyocyte Model Incorporating Lysosome Function.....96
4.2.2 Calibration of Populations of Validated Human Atrial Models in Normal Sinus Rhythm and Chronic Atrial Fibrillation.....103

4.2.3 Comparison of the Presence and Block of Lysosomal Release in Calcium Loading in Normal Sinus Rhythm.....106
4.2.4 Comparison of the Presence and Block of Lysosomal Release in Calcium Loading in Chronic Atrial Fibrillation.....113

4.3 Discussion.....119
4.3.1 Contribution of Lysosomal Calcium Release to Intracellular Calcium Handling in Normal Sinus Rhythm.....119
4.3.2 Contribution of Lysosomal Calcium Release to Intracellular Calcium Handling in Chronic Atrial Fibrillation.....121

CHAPTER 5.....123

Lysosomal Calcium Release Promotes EADs under Mild Hypercalcemia and β-adrenergic Stimulation in Human Atrial Cardiomyocytes.....123

5.1 Introduction.....123

5.2 Results.....125
5.2.1 Role of Lysosomal Calcium Release in EADs in Normal Sinus Rhythm.....126
5.2.2 Role of Lysosomal Calcium Release in TPC-specific Models in Normal Sinus Rhythm with EADs.....131
5.2.3 Role of Lysosomal Calcium Release in the Modulation of EADs in Chronic Atrial Fibrillation.....134
5.2.4 Role of Lysosomal Calcium Release in TPC-specific Models in Chronic Atrial Fibrillation with EADs.....138

5.3 Discussion.....140

CHAPTER 6.....144

Lysosomal Calcium Release Promotes EADs under I_{Kur} Block and β-adrenergic Stimulation in Human Atrial Cardiomyocytes.....144

6.1 Introduction.....144

6.2 Results.....146
6.2.1 Role of Lysosomal Calcium Release on generating EADs in Normal Sinus Rhythm under I_{Kur} Block and β-adrenergic Stimulation.....148
6.2.2 Role of Lysosomal Calcium Release on generating EADs in TPC-specific Models in Normal Sinus Rhythm under I_{Kur} Block and β-adrenergic Stimulation....151
6.2.3 Role of Lysosomal Calcium Release on generating EADs in Chronic Atrial Fibrillation under I_{Kur} Block and β-adrenergic Stimulation.....154
6.2.4 Role of Lysosomal Calcium Release on generating EADs in TPC-specific Models in Chronic Atrial Fibrillation under I_{Kur} Block and β-adrenergic Stimulation 158

6.3 Discussion.....161

CHAPTER 7.....164

Conclusions.....164

7.1 Summary.....164

7.2 Key Findings.....169

7.3 Future Directions.....171
7.3.1 Dimensions in Cardiac Modelling.....171
7.3.2 The Impact of Lysosomal Calcium Handling and Cardiac Fibrosis on Causing Atrial Arrhythmias at the Tissue Level.....172
7.3.3 Developing and Validating Computational Models of hiPSc-derived Cardiomyocytes.....173
7.3.4 Modelling Lysosomal Calcium Handling in hiPSC-aCMs in Atrial Fibrillation 174
7.3.5 Incorporating Anatomical Localisation of Lysosomes Information in Control vs Atrial Fibrillation Cellular Models.....176

7.4 Concluding Remarks.....177

REFERENCES.....179

Chapter 1
Introduction

1.1 Physiology of the Heart

1.1.1 Ion Channels

The electrical system of the heart is in charge of producing and transmitting the signals that cause the heart to beat. The cardiomyocyte is a type of excitable cell that initiates and propagates action potentials (APs). The cellular rhythm is maintained by the balance of cyclic ion flow, principally involving sodium (Na^+), potassium (K^+) and calcium (Ca^{2+}) ions, and cardiac performance is determined by relative balance of the ion movements (Qiu, 2004; Acharya *et al.*, 2006; Rawlins, Bhan and Sharma, 2009). The APs through the heart and the regional differences are the combining effects, resulting from selective permeability of ion channels which spread on the cell membrane (Zaza, 2000; Grant, 2009). The ion channels decrease the activation energy required for ion movement through the cell membrane (Grant, 2009). During the AP, the permeability of ion channels changes and each ion moves under its electrochemical gradient, given by the difference of membrane potential and the reversal potential of the moving ion, and the combining processes change the cellular membrane potential (Grant, 2009). Homeostasis of the intracellular ion concentrations is sustained by active and coupled transport processes, related to adenosine triphosphate (ATP) hydrolysis (Grant, 2009).

Ion channels possess two basic properties, ion permeation and gating (Eaton, 1984). The movement of ions across their open channel is ascribed to permeation. The selective permeability of channels to particular ions defines the class of ion channels, such as Na^+, K^+ and Ca^{2+} channels. Size, valency and hydration energy determine the ions selectivity (Grant, 2009). Ion channels offer multiple binding sites to ions to facilitate their movement, by which ions become charged by anions as the interaction of ions and binding sites is preferred by the interaction of ion and water (Grant, 2009). Thus, the function of ion channels is not just fluid-filled pores. The electrochemical potential is the driving force to move ions across the membrane, and the strength of ions movement forms the current. Most ion channels own a nonlinear relationship of voltage and current. Under the same absolute electrochemical potential, the current magnitude relies on the direction of ion movement inward or outward the cell. K^+ channels, which pass little outward current at depolarised and positive potentials, are known as rectification.

Gating is defined as the mechanism of opening and closing of ion channels, and can be divided into voltage-dependent, ligand-dependent and mechano-sensitive classes, with voltage-dependent gating as the commonest mechanism (Grant, 2009). The opening of most ion channels responds to depolarisation, and the pacemaker funny current channel opens in response to hyperpolarisation. The closing of ion channels has two mechanisms. Some Na^+ and Ca^{2+} channels reach a closed inactivated state during maintained depolarisation, and to re-obtain opening capability, the channel needs to go through a recovery process. The refractory period in cardiac muscle is vital to prevent premature reexcitation (Grant, 2009). The ligand-dependent class is the second largest gating mechanism. The acetylcholine activated K^+ channel (I_{KAch}) and ATP-sensitive K^+ channel (or adenosine diphosphate (ADP)-activated K^+ channel, I_{KATP}) are two representatives. Acetylcholine is the ligand to I_{KAch} receptor and activates the channel by G protein signalling. I_{KAch} shortens the AP and reduces the slope of diastolic depolarisation in pacemaker cells. I_{KAch} channels are most abundant in the atria, the sinoatrial node and the atrioventricular node. The I_{KATP} channel shows an abundant distribution across regions of the heart. I_{KATP} opening is gated by the proportion of ADP to ATP ratio. Since I_{KATP} couples the cellular metabolic energy, energy reduction during ischemia increases the ADP to ATP ratio, leading to the activated I_{KATP} to shorten the

AP (Grant, 2009). Mechano-sensitive channels can transduce a physical stretch to an electric signal by changing channel conductance and play an important role in arrhythmias caused by acute cardiac dilatation (Grant, 2009).

Na^+ channels are voltage-gated and each Na^+ channel opens in less than 1ms during depolarisation (Grant, 2009). The late component is more effective to block by class 1 antiarrhythmic drugs compared to the peak component, thus Na^+ channel is the substrate for class 1 antiarrhythmic drugs (Schwartz *et al.*, 1995).

Ca^{2+} channels are principal to the entry of Ca^{2+} in cardiac cells and there are L-type (low threshold) and T-type (transient) channels. L-type channels exist in all cardiac cellular types and T-type channels largely in pacemaker, atrial and Purkinje cells (Grant, 2009). The activation range is low transmembrane potentials (≈>-30mV) in L-type channels and high transmembrane potentials (≈>-60mV) in T-type channels(Grant, 2009). Inactivation of L-type channels occurs at low (≈-40mV) membrane potentials and is slow due to both voltage and calcium dependence, while it is fast by only voltage dependence in T-type channels. L-type channels are sensitive to isoprenaline (ISO) while T-type channels are not (Grant, 2009).

K^+ channels can be grouped into three main categories. First, a voltage-gated class, which includes the transient outward K^+ current (I_{to}), the ultrarapid delayed rectifier K^+ current (I_{Kur}), and the rapid and slow components of the delayed rectifier repolarising K^+ currents (I_{Kr} and I_{Ks}). Second, an inward rectifier class, including the inward rectifier K^+ current (I_{K1}), I_{KATP} and I_{KAch}. Finally, a background class, including channels such as tandem of P domains in a weak inward-rectifying K^+ channel–related acid-sensitive K^+ channel-1 (TASK-1) and two pore domain K^+ channel (TWIK) (Grant, 2009).

1.1.2 Cardiac Electrophysiology

The APs of pacemaker cells in the sinoatrial node (SAN) and atrioventricular node (AVN) are largely different from those cells in the working myocardium. The resting membrane potential in the beginning of phase 4 is more depolarised (-50 to -65 mV), proceeds with a slow depolarisation in diastole and merges into phase 0 (Grant, 2009). The velocity of depolarisation in phase 0 in SAN cells is much slower than the working cardiomyocytes, which results in slow propagation of the pulse in nodal regions (Grant, 2009). Cells in the His-Purkinje system may display phase 4 depolarisation in some circumstances (Grant, 2009). The AP characteristics change across the myocardial wall from endocardium, midmyocardium, to epicardium. Epicardial cells have an eminent phase 1 and shortest AP duration (Grant, 2009).

The initiated AP of pacemaker cells at the SAN spreads through cardiac cells. In brief, the rise of the transmembrane voltage during the onset of the AP in cardiomyocytes leads to Ca^{2+} entry via the L-type channels. This first wave of extracellular Ca^{2+} influx induces Ca^{2+} release by RyRs from the sarcoplasmic reticulum (SR), leading to the so-called Ca^{2+}-induced Ca^{2+}-release (CICR) mechanism, through which a larger additional Ca^{2+} flows into the cytosol and leads to cellular contraction (Bers, 2002). The L-type current is fast inactivated by voltage increase and by local Ca^{2+} through calmodulin associated with the channel (Bers, 2008). Ca^{2+} is pumped back into the SR via the sarcoplasmic reticulum Ca^{2+}-ATPase (SERCA), and simultaneously extruded outside the cell via the Na^{+}/Ca^{2+} exchanger (NCX) (Lin *et al.*, 2017). The SR is known as the principal intracellular Ca^{2+} store within cardiomyocytes, with total SR Ca^{2+} levels in the millimolar range (Michalak and Opas, 2009) (approximately 50.9 ± 7.4 µM for diastolic SR Ca^{2+} content in human atrial cardiomyocytes (Koivumäki, Korhonen and Tavi, 2011)).

Mouse and human ventricular APs (Figure 1.1), show a fast depolarisation upstroke (phase 0), which is mediated by the large, rapidly activating Na^+ current (I_{Na}) (Nerbonne *et al.*, 2001). The following repolarisation phase is under the balance of depolarising currents (I_{CaL}, I_{NCX}) and repolarising K^+ currents. The AP plateau (phase 2) comes after the fast repolarisation (phase 1) in human APs, which, in mouse APs, becomes a gradual repolarisation other than a plateau, due to the smaller L-type current contribution. Besides, a 4-aminopyridine–sensitive, slowly decaying outward K^+ current ($I_{K,slow}$) contributes to the gradual repolarisation (Nerbonne *et al.*, 2001).

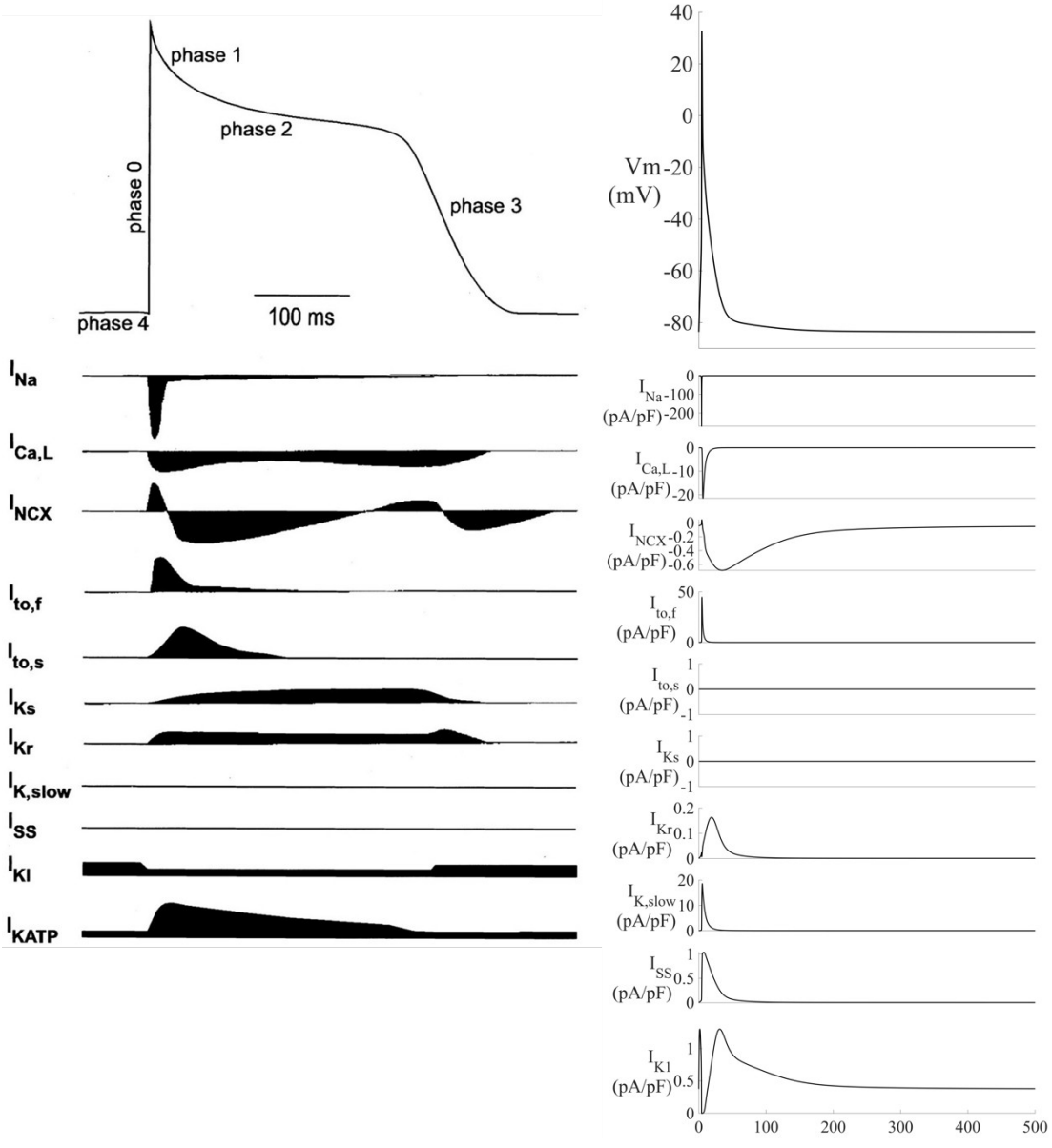


Figure 1.1: Human (Nerbonne *et al.*, 2001) **and mouse ventricular AP morphology (traces of action potential and currents in the Morotti *et al.* ventricular model including lysosomal calcium handling at baseline at 1Hz)**. Below the respective APs, the magnitudes and time windows of the main ionic currents underlying each AP waveform are shown. Figure 1.1 is reproduced with permission from Copyright Clearance Centre.

Human cardiac APs, both in atrial and ventricular cardiomyocytes, consist of five phases, numbered from 0 to 4 (Keating and Sanguinetti, 2001; Grant, 2009; Grunnet, 2010) (Figure 1.2). Phase 0, denoted as the depolarisation, is initiated instantaneously by the voltage-gated Na^+ current (I_{Na}) (Keating and Sanguinetti, 2001; Grant, 2009; Grunnet, 2010). Phase 1 occurs rapidly following the peak of depolarisation as a partial repolarisation of the membrane. The effects on phase 1 come from the closure of Na^+ channels and the opening of the I_{to} and the atrial-specific I_{Kur} (Keating and Sanguinetti, 2001; Grant, 2009; Grunnet, 2010). Phase 2 is the plateau phase, the long duration of which is unique to ventricular cardiomyocyte (Keating and Sanguinetti, 2001; Grant, 2009; Grunnet, 2010). Effects on phase 2 primarily result from the balance between inward L-type Ca^{2+} current (I_{CaL}), Na^+/Ca^{2+} exchanger current (I_{NCX}) and several outward K^+ currents such as I_{Kr}, I_{Ks} and I_{Kur} (Keating and Sanguinetti, 2001; Grant, 2009; Grunnet, 2010). I_{Kr} and I_{Ks} further contribute to the repolarisation of phase 3 as I_{CaL} decreases, together with I_{K1} (Keating and Sanguinetti, 2001; Grant, 2009; Grunnet, 2010). Besides, I_{KATP} and the atrial-specific I_{KAch} also contribute to the repolarisation of phase 3 (Grant, 2009). Relatively small changes of currents during phase 3 can have a large influence on the duration of the AP (Keating and Sanguinetti, 2001). I_{K1} contributes to the final repolarisation of the AP and maintains the level of membrane potential during phase 4 (Keating and Sanguinetti, 2001; Grant, 2009; Grunnet, 2010). I_{K1} current density is larger in ventricular than in atrial cardiomyocytes (Keating and Sanguinetti, 2001; Grant, 2009).

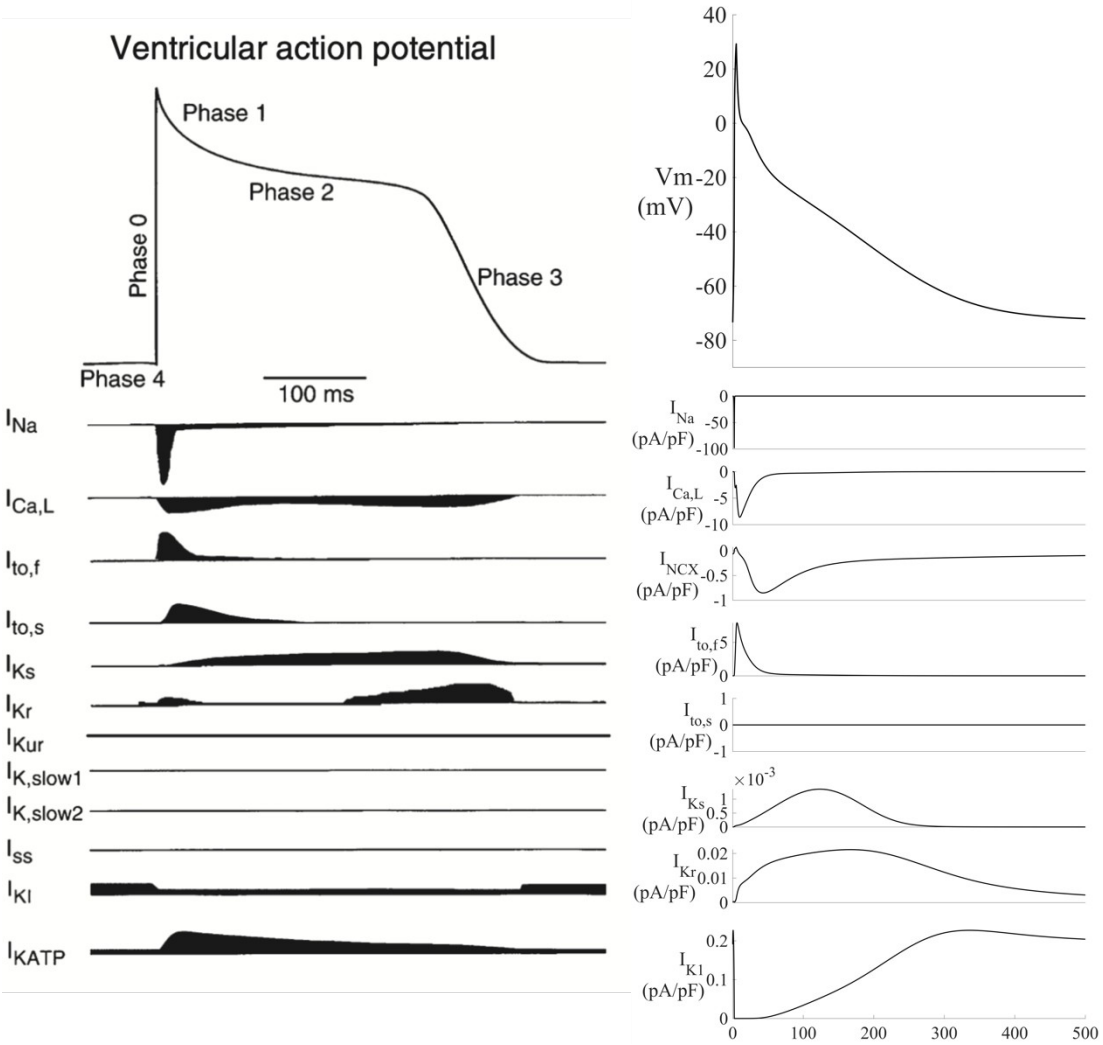


Figure 1.2: Human ventricular (Grunnet, 2010) **and atrial AP morphology (traces of action potential and currents in the Grandi *et al.* human atrial model including lysosomal calcium handling at baseline at 1Hz)**. Below the respective APs, the magnitudes and time windows of the main ionic currents underlying each AP waveform are shown. Figure 1.2 is reproduced with permission from Copyright Clearance Centre.

1.1.3 Ionic Mechanisms of Arrhythmia

Arrhythmias may lead to sudden cardiac death, and are one of most common causes of mortality throughout the world. The initiation of arrhythmia is complex, but regardless

of the underlying cause, the mechanisms leading to arrhythmogenesis can be broadly divided into those occurring at the cellular and tissue levels (Tse, 2016). Arrhythmogenesis at the cellular level can occur due to abnormal automaticity, afterdepolarisations, and alternans (Tse, 2016). Understanding of the underlying mechanisms requires detailed knowledge relating to the ionic contributions to the cellular AP (Tse, 2016).

Afterdepolarisations, such as early afterdepolarisations (EADs) and delayed afterdepolarisations (DADs), are abnormal depolarisations that arise in phase 2 and phase 3, or phase 4 of the AP respectively, and can lead to the generation of arrhythmias (Antzelevitch and Burashnikov, 2011).

EADs are generally associated with the prolongation of action potential duration (APD), and occur when there is a greater amplitude difference of total inward current over total outward current during the repolarisation phase of the AP (Tse, 2016). The main factor leading to EADs is APD prolongation, which allows I_{CaL} to recover from inactivation, resulting in depolarising inward current (Iwasaki *et al.*, 2011). Multiple factors can shift the balance to the inward direction, which include the increases of late Na^+ current, late L-type current, or the inward NCX current, as well as a decrease in repolarising K^+ currents (I_{Kr}, I_{Ks}, I_{K1}). The depolarisation during phase 2 or 3 of the AP derives from the net inward current (Antzelevitch and Burashnikov, 2011). Similarly, EADs can result from the effects of antiarrhythmic drugs, in which drugs that inhibit K^+ currents or increase inward currents predispose cardiomyocytes to develop EADs (Antzelevitch and Burashnikov, 2011). The increase of the inward currents which contributes to the depolarisation in an increasing loop to trigger an EAD (January and Riddle, 1989). Otherwise, when the membrane potential is below the threshold of L-type activation before full repolarisation, the increase of the inward NCX current by SR Ca^{2+} release or spontaneous Ca^{2+} release can lead to the depolarisation in the form of an EAD (SZABO *et al.*, 1994). The NCX forward mode (i.e., an inward current) is thus consistently enhanced, which promotes depolarisation in the form of an EAD (Tse, 2016). Though these factors are separately illustrated, it is obvious these factors can interact with each other. Thus, the involvement of inward currents can lead to EADs.

On the other hand, DADs occur after full repolarisation, and usually happen under conditions of elevated intracellular Ca^{2+} concentrations (Antzelevitch and Burashnikov, 2011). Rapid heart rates increase the probability of spontaneous Ca^{2+} release from the SR in cardiomyocytes by increasing SR Ca^{2+} loading. The spontaneously released Ca^{2+} depolarises the diastolic membrane potential by activating NCX and resulting in inward I_{NCX}; if the resulting depolarisation as a DAD suffices to reach the Na^{+} current excitation threshold, the DAD can trigger an AP (Weiss *et al.*, 2011). Commonly, when a DAD amplitude is sufficient to charge the potential to its threshold voltage, a spontaneous AP results in triggered events, which gives rise to extrasystoles and can precipitate into tachyarrhythmias (Antzelevitch and Burashnikov, 2011). Afterdepolarisations can propagate at tissue level initiating arrhythmia in the presence of decreased intercellular coupling, which is also linked to slower propagation, leading to re-entry, which can be either anatomical (anchoring around an anatomical obstacle) or functional (supported by regional refractoriness in the absence of anatomical defects) (Anumonwo and Pandit, 2015).

1.1.4 Mechanisms of Atrial Fibrillation

Atrial fibrillation (AF) is the most common sustained cardiac arrhythmia, leading to an increasing number of complications and deaths (Schotten *et al.*, 2011). AF features rapid and disorganised atrial activation causing impaired atrial function (Schotten *et al.*, 2011; Pellman and Sheikh, 2015). AF shortens atrial refractoriness and leads to loss of atrial contractility (Schotten *et al.*, 2011). AF may be defined as paroxysmal (converts to sinus rhythm within 7 days), persistent (converts to sinus rhythm after 7 days), and permanent (does not spontaneously convert to sinus rhythm) (Schotten *et al.*, 2011; Pellman and Sheikh, 2015; Brundel *et al.*, 2022).

The understanding of the basic mechanisms for AF occurrence and persistence has been increasing rapidly (Iwasaki *et al.*, 2011; Schotten *et al.*, 2011). AF can be maintained by rapid focal ectopic firing and/or re-entry (Iwasaki *et al.*, 2011; Schotten *et al.*, 2011). The irregular atrial discharge in AF may result from an irregular atrial response to a rapidly discharging regularly firing driver (the mechanism maintaining AF is often named as the driver) originating from either local ectopic firing or a single localised re-entry circuit (Iwasaki *et al.*, 2011; Schotten *et al.*, 2011). Otherwise, fibrillatory activity may be due to multiple functional re-entry circuits varying in time and space (Iwasaki *et al.*, 2011).

Basic mechanisms underlying ectopic firing involve enhanced automaticity, EADs, DADs (Iwasaki *et al.*, 2011; Schotten *et al.*, 2011). Enhanced automaticity occurs when cardiomyocytes possessing pacemaker activity enhance their rate of spontaneous discharge (Iwasaki *et al.*, 2011; Schotten *et al.*, 2011). EADs are mainly caused by APD prolongation and allowing L-type reactivation (Iwasaki *et al.*, 2011; Schotten *et al.*, 2011). DADs are caused by abnormal diastolic calcium release from the SR (Iwasaki *et al.*, 2011; Schotten *et al.*, 2011). Basic mechanisms underlying re-entry involve functional determinants and ion channel determinants (Iwasaki *et al.*, 2011). Re-entry may be conceptualised as either a leading circle or a spiral wave (Iwasaki *et al.*, 2011; Schotten *et al.*, 2011). The maintenance of continuous activity in both concepts relies on atrial substrate properties, with a proper balance between refractory and excitability functional determinants (Iwasaki *et al.*, 2011). In the leading circle concept, re-entry circuits spontaneously establish themselves in a circuit length (the wavelength, which is given by the product of refractory period and conduction velocity) (Allessie *et al.*, 2001; Comtois, Kneller and Nattel, 2005). When the wavelength is shorter, the atria can accommodate the larger number of simultaneous re-entry circuits (Iwasaki *et al.*, 2011; Schotten *et al.*, 2011). Thus, shortened refractory period and reduced conduction velocity leads to re-entrant AF (Iwasaki *et al.*, 2011). In the spiral wave concept, reduced refractory period also leads to spiral wave re-entry by accelerating and stabilising the rotors of spiral wave (Comtois, Kneller and Nattel, 2005; Iwasaki *et al.*, 2011). Either concept explains the AF occurrence by APD shortening (Iwasaki *et al.*,

2011; Schotten *et al.*, 2011). Further, abnormalities of refractory period and conduction velocity are the major determinants of AF re-entry substrates (Iwasaki *et al.*, 2011; Schotten *et al.*, 2011). Refractory period is determined by the balance between inward and outward currents, and conduction velocity by inward currents providing depolarisation energy and gap junction connexins providing cell-to-cell electric continuity (Iwasaki *et al.*, 2011; Schotten *et al.*, 2011).

Electrical and structural remodelling have become known as the key elements in the development of the AF substrates (Grandi *et al.*, 2011; Schotten *et al.*, 2011). Electrical remodelling comprises changes in Ca^{2+} and K^{+} currents resulting in shortening of the APD, while structural remodelling causes changes in atrial cardiomyocyte and tissue morphology (e.g. cell hypertrophy, fibrosis) (Grandi *et al.*, 2011; Schotten *et al.*, 2011). In human atrial cardiomyocytes in AF, the electrical remodelling of cardiac ion channels shows that peak I_{Na} density is significantly reduced (Sossalla *et al.*, 2010; Grandi *et al.*, 2011), I_{CaL} density is markedly reduced (Dobrev and Ravens, 2003; Christ *et al.*, 2004; Grandi *et al.*, 2011; Schotten *et al.*, 2011), I_{to} and I_{Kur} are markedly reduced (Dobrev and Ravens, 2003; Caballero *et al.*, 2010; Schotten *et al.*, 2011), I_{Ks} is increased (Caballero *et al.*, 2010) while I_{Kr} remains unchanged (Grandi *et al.*, 2011), I_{K1} is increased by nearly 2-fold (Dobrev *et al.*, 2001), NCX expression and function are upregulated (Schotten *et al.*, 2002; El-Armouche *et al.*, 2006; Neef *et al.*, 2010), the maximal pump rate of SERCA is reduced (Voigt *et al.*, 2009; Grandi *et al.*, 2011), and the sensitivity of RyR2 for luminal Ca^{2+} is increased (Neef *et al.*, 2010; Grandi *et al.*, 2011), respectively compared to in sinus rhythm.

1.1.5 Atrial Fibrillation Therapy

Currently, AF therapy is based on the Atrial fibrillation Better Care (ABC) pathway, in which A stands for avoiding stroke or anticoagulation, B the approach to optimise symptoms on rate or rhythm control, and C better management of cardiovascular risk

and comorbidity (Hindricks *et al.*, 2021). The objective by pharmacological therapy is towards rate or rhythm control, by pharmacological drugs targeted at ion channels (Brundel *et al.*, 2022). Drug therapy is not as effective as we would like it to be. For example, lack of effectiveness and propensity of proarrhythmic complications by antiarrhythmic drugs and bleeding by anticoagulants (Dobrev and Nattel, 2010). Catheter ablation (CA) therapy used to be used as a last resort for people who didn't respond to drug treatments and were experiencing symptoms. Now, CA is more commonly performed in certain patient cohorts. However, there are limitations to CA including significant fibrotic myopathy. The safety and effectiveness of CA only covers a constrained number of patients (Dobrev and Nattel, 2010). AF is managed by restoration and maintenance of sinus rhythm as rhythm control and by controlling ventricular response in patients with AF as rate control (Singh *et al.*, 2005; Dobrev and Nattel, 2010).

AF maintenance involves persistent rapid ectopic foci by DADs and EADs or re-entrant activity by a substrate with short refractoriness or slow conduction speed and an ectopic trigger. Complications of atrial electrical remodelling varies from paroxysmal AF to persistent AF. Treatment of persistent AF and the likelihood of AF recurrence in the first days following cardioversion has been shown in some studies (Dobrev and Nattel, 2010).

Conventional class III antiarrhythmic drugs (inhibiting K^+ currents) restrain re-entrant activity by prolonging refractory duration with side effects of torsade de pointes arrhythmias by EADs (Dobrev and Nattel, 2010). Class I drugs (inhibiting Na^+ currents) suppress ectopic activity by EADs and DADs, with potential risk of facilitating re-entry by slowing conduction (Dobrev and Nattel, 2010). Innovative drugs are multi-channel blockers, amiodarone, dronedarone and vernakalant. The current most effective drug (with its own limitations) in AF therapy is amiodarone but does have constrained proarrhythmic effects. Amiodarone and its analogues block Na^+, Ca^{2+} and K^+ channels by suppressing electrical remodelling (Nattel *et al.*, 2002), and shows the antiarrhythmic potential of all classes and the inhibition of alpha(α)-adrenergic and beta(β)-adrenergic stimulation (Singh, 2008). Amiodarone does have its own side effects with potential

extracardiac risk because of its long half-life (Singh, 2008). Dronedarone design is based on the amiodarone structure while minimising pharmacokinetic complexity and toxicity (Dobrev and Nattel, 2010). As a multichannel and antiadrenergic blocker, dronedarone increases APD, decreases heart rate and reduces the risk of torsade de pointes arrhythmias (Kathofer, Thomas and Karle, 2005). Vernakalant exerts effects on Na^+ and K^+ channels, including atrial selective currents I_{Kur} and I_{KAch}. Vernakalant is mainly used as intravenous treatment for suppression of recent onset AF (Dorian *et al.*, 2007; Dobrev and Nattel, 2010).

1.2 Lysosomes in the Heart

1.2.1 Lysosome Identification

Christian de Duve identified the lysosome as the major digestive compartment of the cell in 1955 (C. de Duve *et al.*, 1955; De Duve and Wattiaux, 1966; de Duve, 2005). It is described as a sedimentable particle encircled by an incessant membrane with enrichment in hydrolases, importantly, which was discrete from peroxisomes and mitochondria (De Duve and Wattiaux, 1966; Morgan *et al.*, 2011). He proposed the term lysosome as the specialised organelle, which was revealed by electron microscopy studies, and his reviews led the experimental path to the discovery of the lysosome, for which he was awarded the Nobel Prize for Physiology or Medicine in 1974 (De Duve and Wattiaux, 1966; Morgan *et al.*, 2011).

The notion of the lysosome dated from the work by Metchnikoff, who was the founding figure of innate immunity and awarded by the 1908 Nobel Prize in Physiology or Medicine for his seminal studies of phagocytosis (Tauber, 2003; Morgan *et al.*, 2011). His findings showed that particles absorbed in plain unicellular organisms and

mammalian phagocytes were broken down in an acidic organelle rich in digestive enzymes. In 1907, he used simple pH sensitive dyes to report phagosomes occurred with acidic reactions when peritoneal macrophages of guinea pig were fed by bacteria (Metchnikoff, 1907). Many years onwards, the general relevance of this finding to non-phagosomes cells was appreciated and the lysosome as the ubiquitous catabolic organelle was described (Morgan *et al.*, 2011).

The next crucial finding with lysosomes was genetic deficiencies in lysosomal enzymes accounted for a class of inherent metabolic disorders named lysosomal storage diseases (LSDs). Though the majority of LSDs was due to lysosomal enzyme deficiencies, meanwhile others could be caused by defects in proteins on lysosomal membrane (Morgan *et al.*, 2011). The seminal work by Hers uncovered that Pompe disease resulted from a defect in lysosomal α-glucosidase related to lysosomal glycogen catabolism. In the autophagy process, cytoplasmic glycogen moved into the lysosomal system where autophagosomes merge with lysosomes and α-glucosidase mediated glycogen catabolism (Hers, 1963).

Nowadays, it has been established that lysosome functions as the terminal organelle on the endocytic pathway and is involved with a complicated part in the multitude of homoeostasis in cells (Morgan *et al.*, 2011). Lysosomes have long been appreciated to be waste managing/recycling organelles, responsible for the degradation of macromolecules, but are also regulators of a number of signalling pathways, including apoptosis (Morgan *et al.*, 2011; Appelqvist *et al.*, 2013). Lysosomes are ubiquitous acidic intracellular organelles and mediate a complicated set of functions in eukaryotic cells (Appelqvist *et al.*, 2013).

1.2.2 Lysosomal Storage Disease

LSDs result from inherited defects in any area of lysosomal homeostasis and are caused by genetic mutations in lysosomal enzymes, transporters and ion channels (Morgan *et al.*, 2011). More than 70 LSDs have been described to date, characterised by accumulation of macromolecules, either undigested or partially digested, in the late endolysosomal system, leading to cellular dysfunction and clinical abnormalities (De Duve and Wattiaux, 1966; Morgan *et al.*, 2011). Although rare, cumulatively LSDs account for ~1 in 5000 births (Schröder *et al.*, 2010; Platt *et al.*, 2018).

The impaired function results in the amassing of undigested macromolecules in the lysosome. Currently, two LSDs have been found to be related to Ca^{2+} dysfunction of acidic store, Niemann Pick type C (NPC) and mucolipidosis type IV (MLIV), and they showed opposite defects. NPC features reduced nicotinic acid adenine dinucleotide phosphate (NAADP)-mediated Ca^{2+} release which results in hindered lysosomal function whereas the increased Ca^{2+} release in MLIV gives rise to enhanced endocytic pathway fusion (Morgan *et al.*, 2011).

Several types of LSDs are associated with cardiac disorders, including increased risk of arrhythmia (Laney, Gupta and Wechsler, 2018). As one such example, Anderson Fabry disease is the second most prevalent LSD (Klingelhöfer *et al.*, 2020). The classic type Fabry disease, with the alpha-galactosidase A deficiency, is estimated to have an incidence of approximately 1 in 50,000 males (Masson *et al.*, 2004; Brennan and Parkes, 2014), while the atypical type is more frequent than the classic type by approximately 3 to 10 fold (Spada *et al.*, 2006; Giugliani *et al.*, 2016). Over 50% of Fabry patients have a cardiac involvement, which is one of the most significant causes for disease-related death and reduces life expectancy amongst the patients (Shah *et al.*, 2005; Seydelmann *et al.*, 2015). Approximately over 50% of Fabry patients show cardiac manifestation, typically atrial or ventricular arrhythmias, with atrial arrhythmias more common (Mehta *et al.*, 2004; Morrissey, Philip and Schwarz, 2011). Longitudinal studies suggested the arrhythmias with Fabry disease occurred in 27–42% in male and 27% in female patients (Namdar, 2016). The frequently encountered atrial arrhythmias in patients of Fabry cardiomyopathy include supraventricular tachycardia, AF and atrial flutter (Neufeld, 2006). Typical traits of Fabry cardiomyopathy include myocyte

hypertrophy and fibrosis, and myocardial replacement fibrosis is a typical trait of the late stage cardiomyopathy (Morrissey, Philip and Schwarz, 2011; Seydelmann *et al.*, 2015). Fibrosis plays a role in sustained ventricular tachycardia, however, the causal relationship between the development of arrhythmia and left ventricular hypertrophy either with fibrosis or not is not clear (Namdar, 2016). Before left ventricular hypertrophy develops, early-stage Fabry cardiomyopathy occurs with left atrial enlargement (Boyd *et al.*, 2013). Left atrial enlargement predisposes to atrial arrhythmias, for example AF, possibly due to interstitial fibrosis in left atrial myocardium as in one patient's case (Akhtar and Elliott, 2018).

1.2.3 Lysosomal Properties

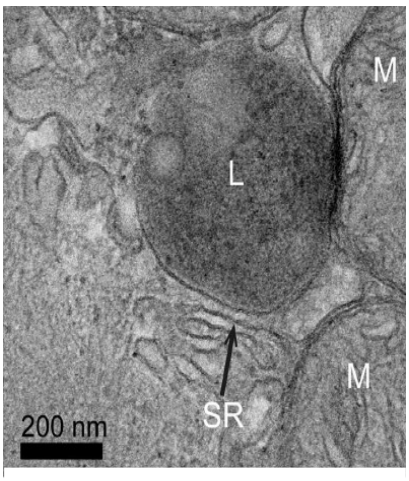


Figure 1.3: Electron micrograph of a lysosome in a ventricular cardiomyocyte. The lysosome (L) is in close proximity to the sarcoplasmic reticulum (SR) and mitochondria (M). From Aston et al. 2017 (Aston et al., 2017). Figure 1.3 is reproduced with permission from Copyright Clearance Centre.

Lysosomes have a 7-10 nm limiting phospholipid bilayer and ultra-structurally appear as cytosolic dense bodies (de Duve, 2005). Figure 1.3 shows an electron micrograph of a lysosome in a ventricular cardiomyocyte published by Aston *et al.* (Aston *et al.*, 2017). From recent electron micrograph studies, they are described as 383 nm long (306–580 nm) and 290 nm wide (220–455 nm) in medians in rabbit ventricular cardiomyocytes (Aston *et al.*, 2017). They can expand in number and size significantly with pathology due to accumulation of undigested material (Lloyd-Evans and Platt, 2011). The number of lysosomes was about 60 in rabbit ventricular cardiomyocytes. The size of the lysosomes was a median long axis of 414 nm (325–598 nm) and a short axis of 320 nm (248–483 nm) (Aston *et al.*, 2017). A lower limit on the volume fraction of the lysosomes

showed an estimate 0.3% of cell volume in neonatal rat atrial myocytes, compared to estimates of 0.08±0.4% of cell volume in rat hearts (Frenzel *et al.*, 1988; Capel *et al.*, 2024). Based on 4pi Single Molecule Switching imaging (4pi-SMS), lysosome volume in neonatal rat atrial myocytes has been estimated as 0.3µm^3 /1000µm^3 (0.3%) (Capel *et al.*, 2024). The volume of lysosome organelles is smaller than the volume of the SR (Morgan *et al.*, 2011). The endolysosomal system is composed of early endosomes, recycling endosomes, late endosomes and lysosomes. It was noted that differentiation between endosomes and small lysosomes may be difficult, thus a threshold of 200nm might be used to define a lysosome (Fameli *et al.*, 2014; Aston *et al.*, 2017). The lysosomes are basically distinguishable from endosomes by their larger size (Fameli *et al.*, 2014). The shortest apparent distances between lysosomes and the nearest T-tubule and Z-line were further away than the distance between lysosome and the nearest SR membrane (Aston *et al.*, 2017). The median distance between the majority of lysosomes and the SR was about 20nm (13-24nm). The shortest apparent distance between the lysosomes and the nearest T-tubule was 163 nm (123–870 nm), and the shortest apparent distance between the lysosomes and the nearest Z-line was 318 nm (176–529 nm) (Aston *et al.*, 2017).

Lysosomes carry more than 50 distinct acid hydrolases and respective activator proteins that are restricted primarily in the matrix (de Duve, 2005; Lübke, Lobel and Sleat, 2009). Luminal pH (4.5-6.5) and membrane potential of the lysosomes are important for its Ca^{2+} homeostasis (Morgan *et al.*, 2011). The uptake of hydrogen ion (H^+) in the lysosomal lumen requires energy from ATP, e.g. families of hydrogen pumps or by gradients of other ions, e.g. hydrogen exchangers (Morgan *et al.*, 2011). The V-ATPase (vacuolar-type H^+-ATPase) is the omnipresent chief pump that pushes H^+ into the lysosome against the gradient by spending ATP, thus the electrogenic process by the pump produces a lumen-positive potential, decreasing the pH (Morgan *et al.*, 2011). The hydrogen exchangers attune pH by connecting H^+ translocation to cation (Na^+, K^+, Ca^{2+}) or anion (Cl^-) movement, which reduces the luminal pH (Morgan *et al.*, 2011).

1.2.4 Lysosomes as Calcium Stores

Lysosomes Ca^{2+} stores contain up to 600 μM Ca^{2+} (Lloyd-Evans *et al.*, 2008). A common pathological feature in LSDs includes defective lysosomal Ca^{2+} signalling (Appelqvist *et al.*, 2013). Ca^{2+} has many roles in the endolysosomal system. It is crucial for the maintenance of trafficking, recycling, as well as vesicular fusion events (Lloyd-Evans and Platt, 2011). As Ca^{2+} enters into any Ca^{2+} store, only a small ratio of the entire Ca^{2+} is free while with the rest is bound, which facilitates the reduction in Ca^{2+} gradient for storing Ca^{2+}. In the SR, Ca^{2+} binds to calsequestrin which has highly acidic domains to bind Ca^{2+}. Lysosomal stores are acidic and emulate the concept by chelation through anionic groups including phosphate, sulfate and carboxylate (Morgan *et al.*, 2011).

Direct Ca^{2+} release by acidic stores in many cell types, stimulated by NAADP, gave rise to the notion of NAADP as a Ca^{2+}-mobilising messenger (Churchill *et al.*, 2002), and dissecting the involved mechanism led to the finding of a new class of endolysosomal channels, the TPCs (Calcraft *et al.*, 2009). The Ca^{2+} signals evoked by NAADP in many cells are considerable (Lee, 2005), however most lysosomal organelles are comprised of a smaller cellular volume than the endoplasmic reticulum (ER), which might result in small and localised Ca^{2+} signals in the cytosol (Duman *et al.*, 2006; Morgan *et al.*, 2011). The accurate difference between volumes of lysosomes and the SR has not been measured, since the lysosomes and SR volumes vary and might not be easily measured together (Capel *et al.*, 2024). In atrial and ventricular cardiomyocytes, the SR volume is about 3.5% of the cell volume (Page, McCallister and Power, 1971; Shannon *et al.*, 2004; Grandi *et al.*, 2011; Morotti *et al.*, 2014). A lower limit on the volume fraction of the lysosomes showed an estimate 0.3% of cell volume in neonatal rat atrial myocytes (Capel *et al.*, 2024), compared to estimates of 0.08±0.4% of cell volume in rat hearts (Frenzel *et al.*, 1988). The lysosome volume is about 0.2538% of cell volume in atrial cardiomyocytes from patients in sinus rhythm and about 0.4851% of cell volume in atrial cardiomyocytes from chronic AF patients (Capel *et al.*, 2024). The paradox could

be explained by the trigger hypothesis in which the NAADP-induced Ca^{2+} release could initiate CICR by inositol trisphosphate (IP3) and ryanodine receptors (IP3R and RyR), leading to more global Ca^{2+} signals (Cancela, Churchill and Galione, 1999).

Early finding of NAADP-mediated Ca^{2+} release from homogenates of sea urchin egg or brain showed its mechanism was not regulated by cytosolic Ca^{2+}, while the NAADP-mediated Ca^{2+} release could trigger an amplified Ca^{2+} release by recruitment of IP3R and RyR in the CICR process. This Ca^{2+} cascade could be via two routes, by the NAADP-mediated Ca^{2+} release as the trigger Ca^{2+} in CICR, but also by the trigger Ca^{2+} being uptaken into the ER (Patel, Churchill and Galione, 2001). As both routes potentiate the Ca^{2+} cycling in the ER in a positive feedback, it might not rule out that both occur in the NAADP-mediated cytosolic Ca^{2+} signals.

Major NAADP-gated Ca^{2+} release channels belong to the set of TPCs (Calcraft *et al.*, 2009), based on first their localisation in the endolysosomal system. Human TPC2 sequence showed a putative dileucine lysosome target motif and the homology with voltage-gated cation channels, as other cation channel blockers inhibit NAADP-mediated Ca^{2+} release (Genazzani *et al.*, 1997). Three isoforms of TPCs exist in animals, with an exception of primate and rodent genomes lacking TPC3, while two isoforms (TPC1 and TPC2) are in human. Although the three forms exist in endolysosomal system, TPC2 localises mainly in lysosomes and late endosomes, while TPC1 in endosomes and TPC3 largely in recycling endosomes (Morgan *et al.*, 2011). TPC2 is activated by NAADP and TPC2 openness is dependent on NAADP concentration (Pitt *et al.*, 2010, 2014). Though NAADP-mediated lysosomal Ca^{2+} release is mediated via TPC2, part of which, however, is by TPC1 (Ruas *et al.*, 2015), with TPC2 capable of greater Ca^{2+} release than TPC1 (Ruas *et al.*, 2015; Pitt, Reilly-O'Donnell and Sitsapesan, 2016).

1.2.5 Lysosomes in the Cardiomyocyte

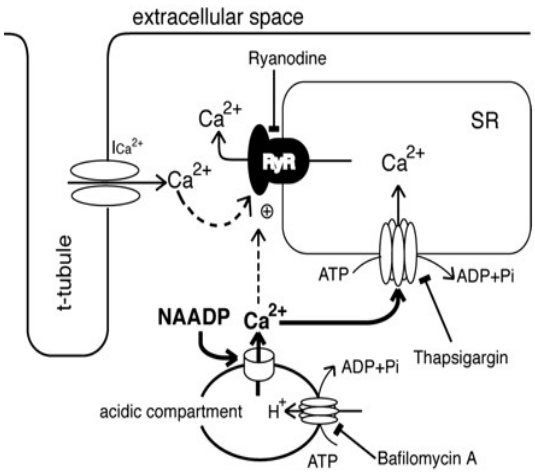


Figure 1.4: Schematic diagram of NAADP signalling and modulation in cardiac myocytes. Ca^{2+} is mobilized from an acidic store by NAADP. The SR takes up Ca^{2+}, and its load is increased. Subsequently, Ca^{2+} release is enhanced, increasing the Ca^{2+} transient. From Macgregor et al. (Macgregor et al., 2007) Figure 1.4 is reproduced with permission from Copyright Clearance Centre.

NAADP, a potent intracellular second messenger acting on TPCs, has been found to be responsible for stimulating Ca^{2+} release from lysosomes into the cytosol (Appelqvist *et al.*, 2013). Figure 1.4 shows the proposed mechanism in which NAADP enhances Ca^{2+} transients in cardiomyocytes. The role of NAADP in β-adrenergic stimulation is suggested to be mediated by the upregulated ADP-ribosyl cyclase, CD38, as the well-found form, for NAADP synthesis (Macgregor *et al.*, 2007). β-adrenergic stimulation by ISO increased the level of NAADP (Lewis *et al.*, 2012).

Previous studies have also shown that a membrane permeant analogue to NAADP (NAADP-AM), could not enhance the Ca^{2+} transient

in genetically-modified TPC2 knock-out (TPC2-KO) cardiomyocytes (Capel *et al.*, 2015). β-adrenergic stimulation by isoproterenol increased Ca^{2+} transients in both TPC2-KO and wild type (WT) cardiomyocytes, while the increased effect was reduced in TPC2-KO compared to WT (Capel *et al.*, 2015). Monophasic APs from the genetically-modified TPC2-KO whole hearts compared to WT under ventricular burst pacing protocols have showed a reduced tendency for arrhythmia and reduced threshold for arrhythmogenesis following acute or chronic β-adrenergic stimulation under isoproterenol, respectively (Capel *et al.*, 2015), further evidencing that Ca^{2+} release from the lysosome under β-adrenergic stimulation presents a tendency to be proarrhythmic (Capel *et al.*, 2015). Recently published data by our group have shown lysosomes neighbour the SR (Figure 1.5), by which lysosomal Ca^{2+} could amplify the CICR from RyRs or enhance SERCA reuptake to potentiate SR Ca^{2+} (Aston *et al.*, 2017). Taken together, these experimental findings might implicate lysosomal calcium handling as a fast calcium buffer between the junction and the cytosol.

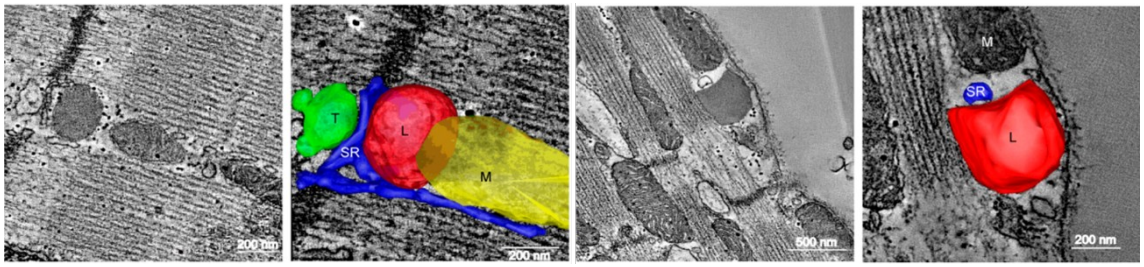


Figure 1.5: Transmission electron microscopy of lysosomes. 3D electron tomography reconstruction highlighting the proximity of lysosomes (L) to sarcoplasmic reticulum (SR), mitochondria (M) and T-tubule (T) (Aston *et al.*, 2017). Figure 1.5 is reproduced with permission from the original authors.

In atrial myocytes, the extensive transverse-tubular system (T-tubule) is not as well preserved as seen in ventricular myocytes which brings L-type channels close to RyRs for the homogeneous rise of global Ca^{2+} transients. The prominent SR elements are placed perpendicular to the long axis as Z-tubules with excitation initiated at the cellular surface where L-type channels and RyRs are located close together (Collins *et al.*, 2011). The Ca^{2+} transients propagate as a wave through the T-tubules into the cellular centre, which is determined by SR Ca^{2+} content. Though NAADP was able to release Ca^{2+} from cellular stores in a variety of cell types, NAADP increases Ca^{2+} transient amplitude by increasing SR Ca^{2+} while not by increasing L-type current amplitude in

atrial myocytes, and has no notable effects on AP traits including APD, maximum velocity during upstroke, peak amplitude and resting membrane potential (Collins *et al.*, 2011). Bafilomycin, (an inhibitor of V-type H^+ ATPase, affects the acidification of lysosomes) reduces Ca^{2+} transient amplitude (Collins *et al.*, 2011). It has been proposed that Ca^{2+} loading in lysosomes is through a process of a proton gradient by the Ca^{2+}-H^+ exchanger. Bafilomycin is an inhibitor of V-type H^+ ATPases, which are responsible for the acidification of lysosomes; NAADP-AM alkalinised lysosomes and ISO action showed a similar effect (Collins *et al.*, 2011). The Ca^{2+} transient amplitude by ISO and glycyl-L-phenylalanine 2-naphthylamide (GPN), which disrupts lysosomal function, is reduced compared to that by ISO (Collins *et al.*, 2011).

Lysosomal Ca^{2+} concentration is difficult to ascertain due to its pH and proteolytic surrounding (Yuan *et al.*, 2021). GPN disrupts proton gradient and osmotic pressure within lysosomes, thus affecting lysosomal uptake and release (Yuan *et al.*, 2021). The rapid leak of lysosomal Ca^{2+} by GPN into the cytosol may provide an estimate of Ca^{2+} content (Yuan *et al.*, 2021).

1.3 Modelling Cardiomyocytes

1.3.1 Development of Electrophysiological Models

The first mathematical model of cellular cardiac electrophysiology was published by Professor Denis Noble at Oxford in 1962, based on a Hodgkin and Huxley's

formulation (Hodgkin and Huxley, 1952; Noble, 1962). Ever since then, a number of electrophysiological models have been produced and these models expand the complexity with the availability of increasing experimental data (Amuzescu *et al.*, 2021). According to Professor Ronald Wilders, the phylogeny of models dating from Professor Denis Noble divides in the early stage from early 60s to 1988 and the advanced stage since 1989. The models in the early stage comprise Noble in 1962 (Noble, 1962), McAllister-Noble-Tsien (McAllister, Noble and Tsien, 1975), Beeler-Reuter in 1977 (Beeler and Reuter, 1977), DiFrancesco-Noble (DiFrancesco and Noble, 1985), and Hilgemann-Noble (Hilgemann and Noble, 1987), since their mathematical formulations of the properties of ion currents are similar to the Hodgkin and Huxley's model. The variables of property formulations involve conductance in current density, driving force, open probabilities of activation and inactivation gates, and modifications in kinetic equations by voltage dependent rates. These models, though simple, fit well with APs and currents by experimental recordings in Purkinje fibres and cardiomyocytes (Amuzescu *et al.*, 2021). Models in the advanced stage are more complicated since they comprise additional sets of differential equations of the kinetics of ion pumps and exchangers, and Ca^{2+} transport in subcellular compartments (Wilders, 2007).

1.3.2 Ventricular Cardiomyocyte Models

A ventricular-specific model was first developed by Beeler and Reuter in 1977, in which a fast Na^{+} current, a slower inward Ca^{2+} current, and two outward K^{+} currents were included in the system (Beeler and Reuter, 1977). In 1985, the DiFrancesco-Noble model added ion exchangers and pumps and intracellular Ca^{2+} release from the SR (DiFrancesco and Noble, 1985). In the 1990s, Luo and Rudy added a more detailed L-type Ca^{2+} current with both voltage and Ca^{2+} inactivation, to replace its previous

formulations as a simple slow inward current (Luo and Rudy, 1994a, 1994b). Till present, many types of cardiomyocyte models have been developed, including several models for the same cell type and species (Noble, 2002). Most ionic currents in cardiac electrophysiology models are similar regardless of cell type and species, comprising K^+ currents (I_{to}, I_{Kr}, I_{Ks}, I_{K1}), Na^+ currents (I_{Na}, with both fast and late components), Ca^{2+} currents (I_{CaL}), chloride (Cl^-) currents (I_{Cl}), Na^+/K^+ pump currents (I_{NaK}), Na^+/Ca^{2+} exchanger currents (I_{NCX}), and intracellular ionic homeostasis and Ca^{2+} handling (Grandi, Pasqualini and Bers, 2010; Carro *et al.*, 2011).

The first part of my DPhil is related to the modelling and simulation of lysosomal Ca^{2+} handling in mouse ventricular cardiomyocytes. In this regard, the state-of-the-art in mouse ventricular electrophysiological modelling is given by the recently developed model by Morotti *et al.* as an extension of the Soltis-Saucerman and the Shannon-Bers models for rabbit (Shannon *et al.*, 2004; Soltis and Saucerman, 2010; Morotti *et al.*, 2014).

The Morotti *et al.* model was specifically constructed in order to analyse the arrhythmogenic positive feedback between intracellular Na^+ elevation and intracellular Ca^{2+} loading. The model introduced features of cell size and geometry, ion currents, and Na^+ and Ca^{2+} handling parameters adapted to mouse reference data. In the cell size and geometry aspects, the larger surface area and fraction of t-tubules in junctions were considered (Soltis and Saucerman, 2010; Morotti *et al.*, 2014). As the main driver of repolarisation in mouse ventricular cardiomyocytes, especial attention was placed into I_{to}, consisting of a fast component only, and with current density and kinetics modified to fit experimental current-voltage relationships (Morotti *et al.*, 2014). The extracellular Ca^{2+} concentration was decreased and the magnitude of I_{CaL} was increased by 65% in order to reproduce the peak current and Ca^{2+} influx at 1 Hz pacing (Soltis and Saucerman, 2010; Li *et al.*, 2011, 2012; Morotti *et al.*, 2014). The SERCA maximal activity was increased and NCX maximal flux was reduced (Soltis and Saucerman, 2010; Morotti *et al.*, 2014). The description of Ca^{2+}/calmodulin-dependent protein kinase II (CaMKII) was unchanged from parent models (Shannon *et al.*, 2004; Soltis and Saucerman, 2010; Morotti *et al.*, 2014). The β-adrenergic stimulation from the

Yang-Saucerman model was implemented, substituting the original protein kinase A (PKA) activation (Soltis and Saucerman, 2010; Yang and Saucerman, 2012; Morotti *et al.*, 2014). The simulated administration of 100 nM of ISO was shown to enhance I_{CaL} availability by 56%, and to increase RyR open probability by 2 fold (Morotti *et al.*, 2014).

1.3.3 Atrial Cardiomyocyte Models

The second part of my DPhil was associated with modelling and simulation of lysosomal Ca^{2+} handling in existing cardiomyocyte models of human atrial electrophysiology. To date, eight major biophysically-detailed mathematical models of human atrial cardiomyocytes have been developed, which are Courtemanche *et al.*, 1998 (Courtemanche, Ramirez and Nattel, 1998), Nygren *et al.*, 1998 (Nygren *et al.*, 1998), Maleckar *et al.*, 2009 (Maleckar *et al.*, 2008), Koivumäki *et al.*, 2011 (Koivumäki, Korhonen and Tavi, 2011), Grandi *et al.*, 2011 (Grandi *et al.*, 2011), Colman *et al.*, 2013 (Colman *et al.*, 2018), Voigt *et al.*, 2013 (Voigt *et al.*, 2013), and Schmidt *et al.*, 2015 (Schmidt *et al.*, 2015).

For simplicity, those models are henceforth mentioned by their first author names. The Courtemanche, Nygren, Maleckar, Koivumäki and Grandi models include major transmembrane currents for AP generation, which are I_{Na}, I_{Kur}, I_{to}, I_{Kr}, I_{Ks}, I_{CaL}, I_{K1}, I_{NaK}, I_{NCX}, and the Ca^{2+} pump, plasma membrane Ca^{2+} ATPase (PMCA), the Ca^{2+} and Na^{+} background currents (I_{bCa} and I_{bNa}), and intracellular Ca^{2+} handling. As to inter-model differences by ion channels, the Maleckar model is the only one to include the I_{KACh} for modelling effects of vagal stimulation, while the Koivumäki model comprises a description of the hyperpolarising cation current, also known as funny current, active in phase 4 of the AP. The Grandi model contains a plateau K^{+} current (I_{Kur}), as well as a

Ca^{2+}-activated Cl^- current ($I_{Cl(Ca)}$) and a background Cl^- current (I_{bCl}). The five models differ on their specific mathematical formulations of transmembrane currents, intracellular Ca^{2+} handling, and number of intracellular compartments. The Courtemanche model, built on a previous guinea pig ventricular model (Luo and Rudy, 1994a, 1994b) , reformulated the currents I_{Na}, I_{CaL}, I_{Kur}, I_{to}, I_{Kr}, I_{Ks}, and I_{K1} based on experimental data in human atrial myocytes, and consists of an extracellular and an intracellular space, with currents flowing across them (Courtemanche, Ramirez and Nattel, 1998). The Nygren model was based on a previous rabbit atrial AP model (Lindblad *et al.*, 1996), and while using the same experimental data as the Courtemanche model (Courtemanche, Ramirez and Nattel, 1998), it accounts for an additional cleft space outside the subsarcolemma, permitting local accumulation and depletion of ions (Nygren *et al.*, 1998). The Maleckar model extended the Nygren model (Nygren *et al.*, 1998) reformulating its I_{Kur} and I_{to} currents with more recent experimental data, but otherwise has similar compartments as the Nygren model (Maleckar *et al.*, 2008).

The Grandi model adapted the human ventricular model from the same group in agreement with human atrial electrophysiology, for example, reducing the conductance of I_{K1} by a factor of 6 to match a smaller level of I_{K1} in atrial compared to ventricular cardiomyocytes, or including the currents I_{to} and atrial-specific I_{Kur} from the Maleckar model (Maleckar *et al.*, 2008; Grandi *et al.*, 2011). The Grandi model uses the Ca^{2+} handling from the rabbit ventricular model by Shannon-Bers, and features intracellular, subsarcolemmal and extracellular spaces, with the subsarcolemmal subspace (as an effective intracellular space with regard to the ionic concentrations seen by currents) connecting the intracellular and extracellular compartments (Shannon *et al.*, 2004; Grandi *et al.*, 2011). The Koivumäki model incorporated a spatial dimension to account for the lack of transverse tubules in human atrial cardiomyocytes, but is similar otherwise to the Grandi model in terms of compartment spaces (Koivumäki, Korhonen and Tavi, 2011). Further, the Colman model started from the Courtemanche model, included the I_{Kur} and I_{to} formulations from the Maleckar model and the two-compartment intracellular Ca^{2+} handling from the Koivumäki model (Colman *et al.*, 2018). The Voigt model extended the Grandi model by a subcellular structure to

describe the specific Ca^{2+} wave propagation in atrial cardiomyocytes, stochastic gating of RyR2 channels, and a further representation of the activation and inactivation properties in L-type Ca^{2+} currents (Voigt *et al.*, 2014), while the Schmidt model extended the Grandi model by incorporating I_{K1}, I_{KACh}, and two-pore-domain K^+ current, a K^+ current known as TASK-1 (Schmidt *et al.*, 2015). In summary, the Courtemanche, Maleckar, and Grandi models are well-established models for single-cell investigations, and the Koivumäki model has the most up-to-date description of the intracellular Ca^{2+} handling in human atrial cardiomyocytes.

1.3.4 Variability in Cardiac Electrophysiology

Variability and uncertainty exist in cardiac electrophysiology, and this variability can manifest in a variety of phenotypic responses in the physiological activity of cardiomyocytes to otherwise similar physiological interventions, such as drug action, stimulation protocols, or disease conditions. There are both intra-subject and inter-subject cardiac variability, the latter comprising the divergent responses of patients to the same type of clinical intervention.

Though studying each of the components of cellular electrophysiology in isolation is possible, it becomes increasingly difficult to study the interaction of their involved processes as they are in a simultaneous function (Sarkar, Christini and Sobie, 2012). Modelling and simulation studies represent a very powerful tool in the study of cardiac variability, as they allow for the deconstruction of its underlying cellular mechanisms through the complex interactions of ionic currents and intracellular fluxes, by introducing variability to the multiple model parameters. The formulas for describing the processes in mathematical modelling can be assembled in a comprehensive whole for studying their interactions to overcome the aforementioned difficulties (Shannon *et*

al., 2004; Morotti *et al.*, 2014). Biological variability exhibits in a variety of differences in a physiological function (Britton *et al.*, 2013; Muszkiewicz *et al.*, 2016). Further to understand the variable range of the responses in individual cells, the differences in expression and function of various ion channels within the same cells population would be simultaneously available (Sarkar, Christini and Sobie, 2012; Muszkiewicz *et al.*, 2016).

Using the ten Tusscher *et al.* model of the human ventricular AP, Romero *et al.* explored the effect of ±15% and ±30% modifications to one key parameter at a time, and sensitivity analysis quantified the contribution of each parameter to key cellular biomarkers such as APD, AP triangulation, AP rate dependence, and intracellular ion concentrations (Romero *et al.*, 2009). Sobie *et al.* used a multivariable sensitivity analysis on multiple parameters and partial least squares regression to explain the relationship between changes in single parameters to changes of APD, resting membrane potential, and peak AP values (Sobie, 2009). The overall variations in biomarkers were usually the combination of the multiple parameter variances (Sobie, 2009). Britton *et al.* generated a population of rabbit Purkinje cells in which 213 of 10,000 models were chosen through calibration against experimental data, predicting and explaining APD prolongation response to K^+ channel blockers, where parameter values considered a wider range of variability (up to ±100% changes) than previously investigated (Britton *et al.*, 2013). This methodology has been exploited in further studies. For example, two populations of models using the O'Hara-Rudy *et al.* model studied cells from healthy and failing hearts, sharing the same equations of similar ionic kinetics but different combinations of conductance parameters in individual currents, and APD properties and alternans generation were explained by linear regression analysis (Walmsley *et al.*, 2013). Other applications of these methods to encapsulate cardiac variability ranging from studies on AF to hypertrophic cardiomyopathy, can be found in the literature (Muszkiewicz *et al.*, 2016).

1.3.5 Sampling Methods

In brief, sampling takes input variables related to properties in currents and fluxes in the cardiomyocyte and returns output of the changes by the variables. If output variables resemble the real outputs by experiments, the sampling can be assumed accurate to represent the variability in the physiological process (McKay *et al.*, 1979). Representing the variability of physiological phenomena by mathematical formulations is usually dealing with the input choice of parameters, which is complicated in the physiological process in essence because each parameter in the system is affecting while feeding back on each other (McKay *et al.*, 1979). When the system parameters vary around nominal values, the uncertainty in variability can be ascertained by sampling with random variables as input (McKay *et al.*, 1979). There are random sampling, stratified sampling and Latin hypercube sampling. Random sampling takes random input in a known distribution. Stratified sampling enables the input as representative of each area of the sample space, the disjoint strata. Latin hypercube sampling extends stratified sampling to have an input with representatives of each stratum and of each portion of distribution in strata. The process is by partitioning the input range in N strata with equal marginal probability of 1/N and taking one random entity by each stratum. For example, let the number of parameters be K, and N as the number of desired samples, and N should be at least larger than K+1. This method proceeds by dividing the allowed space for each parameter into N regions, choosing without repetition the generated N samples for each of the K parameters, then producing as a population an N×K matrix of parameter sets.

Latin hypercube sampling is a uniform sampling method, which was introduced by McKay *et al.* in 1979 (McKay *et al.*, 1979). It enables an efficient and non-biased generation of variables over a multitude of parameters, and is based on the assumption that the sampling processes of each parameter are independent. The main advantages of this method are that it covers the whole parameter range at a minimum computing cost, independently of the number of parameters, and in an unbiased manner. It can be used to prevent under-sampling by a log scale, when the variation interval between several

parameters is big (Marino *et al.*, 2008). A drawback of the method, shared by other sampling techniques, is that the parameter space is not sampled in full at a given resolution, which quickly becomes computationally unfeasible as the number of parameters increases.

1.4 Aim

The main aim of my thesis is to incorporate lysosomal calcium handling in the established models of mouse ventricular and human atrial cell electrophysiology informed by experimental findings and to use the models to investigate proarrhythmic mechanisms. My work aims to understand the mechanisms of lysosomal calcium handling on pro-arrhythmias of RyR spontaneous calcium release in mouse ventricular cardiomyocyte model and of EADs in human atrial cardiomyocyte model. I aim to investigate the proarrhythmic mechanisms of lysosomal calcium handling by populations of biophysically detailed cardiomyocyte models. The general hypothesis of my thesis is that lysosomal calcium uptake and release forms a pathway for fast calcium transport via lysosome and enhancing this pathway contributes to pro-arrhythmias in proarrhythmic conditions.

The specific aims of the thesis are as follows:

1. To incorporate lysosomal calcium handling in mouse ventricular and human atrial cardiomyocyte model

2. To calibrate the responses of mouse ventricular and human atrial cardiomyocyte models by lysosomal calcium handling with experimental results

3. To investigate the proarrhythmic mechanisms of RyR spontaneous calcium release in the populations of mouse ventricular cardiomyocyte models and of EADs in the populations of human atrial cardiomyocyte models

Chapter 2 provides the methods and achieves the first aim in my thesis. I introduce the methods of incorporating lysosomal calcium handling in the mouse ventricular and human atrial cardiomyocyte models, based on experimental data. Then I describe the modelling of lysosomal calcium uptake and release fluxes. Finally, I introduce the cellular variability of ionic currents and intracellular fluxes that are used in the populations of mouse ventricular and human atrial cardiomyocyte models.

Chapter 3 achieves the second and third aims of the mouse ventricular cardiomyocyte model in my thesis. I introduce a paper of the role of lysosomal calcium handling on RyR spontaneous calcium release. I present the construction and calibration processes for the new mouse ventricular model including lysosome and for the populations of ventricular cardiomyocytes based on experimental findings. I introduce the proarrhythmic contributions of lysosomal function in RyR spontaneous calcium release. I reveal an antiarrhythmic impact by blocking lysosomal uptake or release.

Chapter 4 achieves the second aim of the human atrial cardiomyocyte model in my thesis. I present the construction and calibration processes for the new atrial model and for the population of atrial cardiomyocytes, based on experimental data. I introduce the investigation of the modulation of lysosomal calcium release in human atrial cellular electrophysiology. Specifically, I reveal the role of lysosomal calcium release on intracellular calcium handling.

Chapter 5 achieves the third aim of the human atrial cardiomyocyte model in my thesis. I present the mechanism underlying EADs using the population of human atrial cell models developed in Chapter 4 under the proarrhythmic condition of mild hypercalcemia and β-adrenergic stimulation. After comparing models showing the direct modulation, and no involvement of lysosomal calcium release on EADs, two types of ionic currents are found to be related to the generation of EADs. The ionic currents for the generation of EADs are investigated in the two types of models, and the role of lysosomal calcium release involved in the process is identified.

Chapter 6 achieves the third aim of the human atrial cardiomyocyte model in my thesis. I present the mechanism underlying EADs using the population of human atrial cell models developed in Chapter 4 under the proarrhythmic condition of I_{Kur} block and β-adrenergic stimulation. I introduce the categories of the models as directly modulated and non-involved by lysosomal calcium release. I investigate the ionic currents related to EADs onset in the two types of models. I explore the antiarrhythmic effect of blocking lysosomal calcium while maintaining the beneficial effect of increasing effective refractory period under I_{Kur} block.

Chapter 2
Methods

2.1 Modelling Lysosomal Calcium Loading in Mouse Ventricular Cardiomyocytes

2.1.1 Experimental Data

The experimental datasets in mouse ventricular cardiomyocytes, include Ca^{2+} transients and APs recordings at 1Hz under CTRL, NAADP-AM, ISO protocols, reproduced with permission from the original authors (Capel *et al.*, 2015).

2.1.2 Mathematical Modelling and Simulation Studies

The Morotti *et al.* (Morotti *et al.*, 2014) (mouse) model is used as the baseline for our investigations on mouse ventricular electrophysiology, because of matching species and inclusion of β-adrenergic stimulation module. The lysosome compartment is formulated into the model with details as following. Spontaneous calcium release events were identified by the occurrence after an initial pacing of 150 beats. The *[NAADP]* values used to respond TPC2 open probabilities are 1 nM, 15 nM and 15 nM for simulated CTRL, NAADP-AM and ISO protocols in the mouse ventricular cardiomyocyte model. The ISO ligand value used to respond β-adrenergic stimulation was 100 nM in the mouse model.

2.1.3 Including Lysosome Compartment in a Mouse Ventricular Cardiomyocyte Model

Figure 2.1 illustrates the integration of the lysosome compartment into the Morotti *et al.* (Morotti *et al.*, 2014) model, to account for the contribution of lysosomes to intracellular calcium handling. Based on organelle localisation and lysosome action in experimental findings in mouse electrophysiology (Pitt *et al.*, 2010, 2014; Lewis *et al.*, 2012; Nebel *et al.*, 2013; Capel *et al.*, 2015; Ruas *et al.*, 2015; Garrity *et al.*, 2016; Pitt, Reilly-O'Donnell and Sitsapesan, 2016; Aston *et al.*, 2017), the lysosomal subspace mediates a fast calcium transport, diverting calcium from the junctional to the cytosolic subspaces. In the populations of models under normal loading, lysosomal calcium release primarily modulated intracellular calcium handling by increasing SERCA reuptake and RyR release, not significantly influencing NCX activity. In the populations of models in proarrhythmic conditions, lysosomal calcium release enhanced the forward mode of NCX to extrude calcium. Basically, the TPC released calcium, together with the calcium released via RyR, was simultaneously re-uptaken by SERCA and extruded by NCX in the models. Calcium is up-taken from the junctional subspace into the lysosomal compartment by means of a calcium loading channel (CLC), and released to the cytosol by TPC2. The model also accounts for simultaneous slow calcium diffusion between the involved sub-compartments.

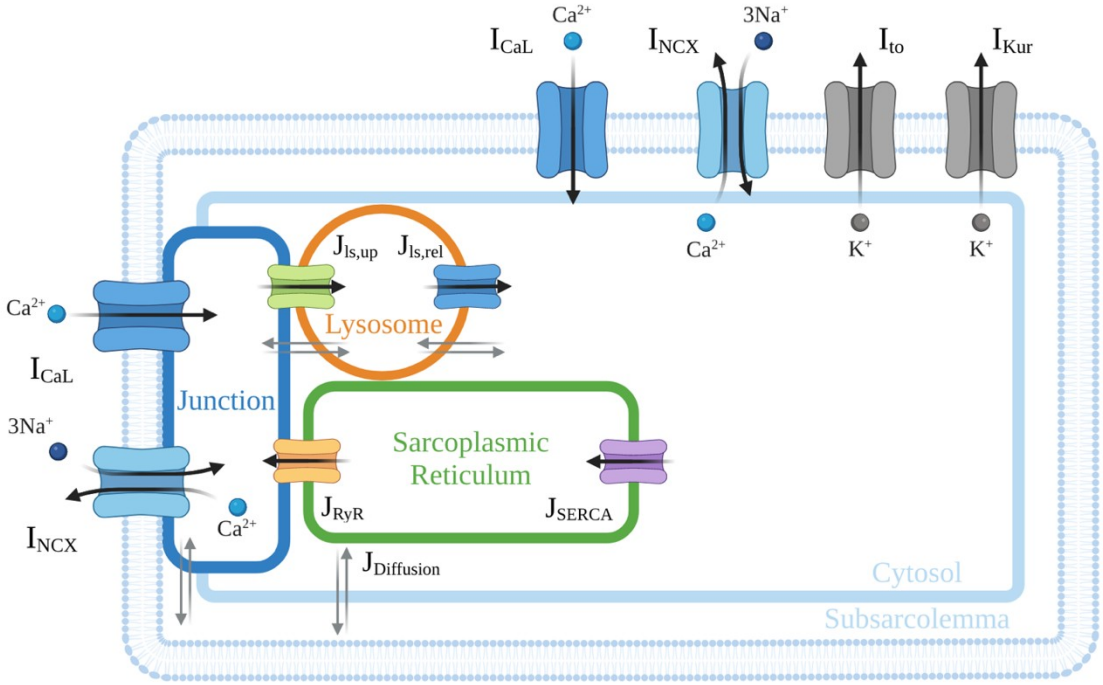


Figure 2.1. Schematic diagram of including lysosome compartment in Morotti *et al.* (Morotti *et al.*, 2014) and Grandi *et al.* (Grandi *et al.*, 2011) models.

The lysosomal calcium inward flux is modelled as a calcium loading channel (CLC) between junction and lysosome subspaces. The lysosomal calcium efflux is modelling NAADP-mediated calcium release via TPC2 from lysosomal subspace to cytosolic subspace. These are respectively given by:

$$J_{ls,up} = j_{clc} \cdot P_O \cdot (C_{ls} - C_j) + j_{clc,leak} \cdot (C_{ls} - C_j),$$
$$J_{ls,rel} = j_{tpc} \cdot P_O \cdot (C_{ls} - C_i) + j_{tpc,leak} \cdot (C_{ls} - C_i),$$

where j_{clc} and j_{tpc} denote the maximal CLC uptake and TPC release flux densities into the lysosomal and cytosolic subspaces; C_{ls}, C_j, and C_i are the calcium concentrations in the lysosomal, junctional, and cytosolic subspaces, respectively; $j_{clc,leak}$ and $j_{tpc,leak}$ denote the leak rates of calcium through the CLC and TPC channels to the junctional and cytosolic subspaces, respectively; and P_O represents the open probability of the lysosomal uptake and release channels. Based on previous experimental data (Nebel *et al.*, 2013; Aston *et al.*, 2017), we adopt the formulation of Penny *et al.* (Penny *et al.*, 2014) to describe the open probably of TPC channels. This is given by:

$$P_O = P_{Omax} \cdot \exp\left(\frac{\left(-\log\left([NAADP]\right) - \log\left(P_{Omean}\right)\right)^2}{2 \cdot P_{Osd}^2}\right),$$

where P_O follows a Gaussian distribution on the NAADP concentration, P_{Omax} denotes its maximum open probability, and P_{Omean} and P_{Osd} represent the mean and standard deviation of the distribution. For CLC channels, given the scarcity of experimental datasets, we adopted an analogous formulation for TPC channels. Such an assumption correctly recapitulated our calcium transient data under CTRL, NAADP-AM, ISO, and combined pharmacological protocols (see Figure 2.1, page 48). This modelling assumption can nevertheless be easily revisited, shall additional datasets on lysosomal calcium loading become available.

Conservation of mass for calcium ions then yields the following modified system of differential equations for intracellular calcium handling with respect to both models:

$$\dot{C}_{ls} = J_{ls,j}\frac{C_j - C_{ls}}{V_{ls}} - J_{ls,up} + J_{ls,i}\frac{C_i - C_{ls}}{V_{ls}} - J_{ls,rel},$$

$$\dot{C}_j = J_{j,sl}\frac{C_{sl} - C_j}{V_j} - I_{Ca,j} - J_{CaB,j} + J_{RyR}\frac{V_{SR}}{V_j} + J_{RyR,lk}\frac{V_c}{V_j} + J_{ls,up}\frac{V_{ls}}{V_j} + J_{ls,j}\frac{C_{ls} - C_j}{V_j},$$

$$\dot{C}_i = J_{sl,i}\frac{C_{sl} - C_i}{V_i} - J_{SERCA}\frac{V_{SR}}{V_i} - J_{CaB,i} + J_{ls,rel}\frac{V_{ls}}{V_i} + J_{ls,i}\frac{C_{ls} - C_i}{V_i},$$

where $\dot{C}_{ls}$, $\dot{C}_j$, and $\dot{C}_i$ denote the time derivatives of calcium concentrations in the lysosomal, junctional, and cytosolic subspaces, respectively, while V_{ls}, V_j, V_{SR}, and V_i represent the volumes of the lysosomal, junctional, SR, and cytosolic subspaces. In the equations above, $I_{Ca,j}$ denotes the junctional calcium fluxes via calcium currents, $J_{CaB,j}$ are the junctional calcium buffers, J_{RyR} and $J_{RyR,lk}$ the release and leak fluxes through ryanodine receptors, respectively, J_{SERCA} denotes the calcium reuptake fluxes by SERCA, and $J_{CaB,i}$ the cytosolic calcium buffers. In these equations, $J_{ls,j}$ and $J_{ls,i}$ are the rates of diffusion fluxes between the lysosome calcium pool and junctional or cytosolic subspaces, respectively.

Rest of equations in both models remain unaltered, including those describing calcium concentrations in the SR and subsarcolemmal compartments. Full parametrisation of the lysosomal compartment is provided in Table 2.1.

Parameters in Morotti *et al.* (Morotti *et al.*, 2014) **model**		**Units**	**Value**	**Ref.**
Volume	Total cell (V_{tot})	pL	33	(Morotti *et al.*, 2014) [1]
	Lysosome (V_{ls})	pL	2% V_{tot}	(Morotti *et al.*,

				2014; Penny *et al.*, 2014)[2, 3]
TPC	Maximum open probability (P_{Omax})		0.014	(Pitt *et al.*, 2010; Penny *et al.*, 2014)[2, 4]
	Variance (P_{Osd}^2)		2.25	this study
	Mean (P_{Omean})		23	(Penny *et al.*, 2014)[2]
	Leak rate ($j_{clc,leak}$, $j_{tpc,leak}$)	s^{-1}	1.13E-05	this study
Lysosome	TPC flux density into junction (j_{clc})	s^{-1}	9.708	this study
	TPC flux density into cytosol (j_{tpc})	s^{-1}	12.135	this study
	[*NAADP*] for CTRL protocol	nM	1	this study
	[*NAADP*] for NAADP-AM protocol	nM	15	this study
	[*NAADP*] for ISO protocol	nM	15	this study
	Diffusion flux rate to junction ($J_{ls,j}$)	L/ms	1.4219E-15	this study
	Diffusion flux rate to cytosol ($J_{ls,i}$)	L/ms	1.3858E-15	this study

Table 2.1. Baseline parameters for the lysosome compartment in the Morotti *et al.* (Morotti *et al.*, 2014) model. E+n displays numbers in exponential notation, in which E (exponent) multiplies the preceding number by 10 to the nth power.

2.2 Modelling Lysosomal Calcium Loading in Human Atrial Cardiomyocytes

2.2.1 Experimental Data

The datasets in human atrial cardiomyocytes, include Ca^{2+} transients and AP traces at 0.25Hz under protocols of ‘Before ISO’ and ‘After ISO’, and biomarkers of APs at pacing frequencies of 0.25, 0.5, 1, 2, 4, 6 and 8Hz under the protocol of after ISO (Prof Niels Voigt Group, Germany). The Ca^{2+} transient biomarkers include diastolic and systolic Ca^{2+} concentrations and Ca^{2+} transient amplitude, and the AP biomarkers include resting membrane potential (RMP), action potential amplitude (APA) and action potential durations at 50% of repolarisation (APD_{50}) and at 90% of repolarisation (APD_{90}). Experimental values in minimum and maximum in the protocol of ‘After ISO’, that are used to calibrate the initial populations in nSR and cAF, include APD_{20}, APD_{50}, APD_{90}, RMP, plateau potential, which was defined as the potential measured at 20% of the APD_{90} time (V_{20}), maximum upstroke velocity (dV/dt_{max}) in normal sinus rhythm (nSR) and chronic atrial fibrillation (cAF) (Sánchez *et al.*, 2014). The experimental values in the above biomarkers for validation are by mean ± standard deviation(Sánchez *et al.*, 2014).

2.2.2 Mathematical Modelling and Simulation Studies

The Grandi *et al.* (Grandi *et al.*, 2011) (human) model is used as the baseline to investigate on human atrial electrophysiology, because species were matched and β-adrenergic stimulation module was included. The lysosome compartment is formulated into the model with the following details. EADs were identified by the occurrence in any of the consecutive 5 beats after an initial pacing of 150 beats. The *[NAADP]* values used to respond TPC2 open probabilities are 1 nM and 15 nM for simulated Baseline and ISO protocols in the human atrial cardiomyocyte model. The ISO ligand value to respond β-adrenergic stimulation was 1μM in the human model. The different ISO concentrations used in the mouse ventricular and human atrial cardiomyocyte models showed enhanced effects on calcium transients. Due to the differences in calcium transient and AP morphologies between the models, the ISO concentrations used were different.

2.2.3 Including Lysosome Compartment in a Human Atrial Cardiomyocyte Model

The inclusion of lysosomal calcium handling was similarly incorporated in the Grandi *et al.* (Grandi *et al.*, 2011) model, due to its similarity to Morotti *et al.* (Morotti *et al.*, 2014) model in terms of mathematical formulation, as in the section 2.1.3. Rest of equations in the Grandi *et al.* (Grandi *et al.*, 2011) model remain unchanged. Full parametrisation of the lysosomal compartment is provided in Table 2.2.

Parameters in Grandi *et al.* (Grandi *et al.*, 2011) **model**		**Units**	**Value**	**Ref.**
Volume	Total cell (V_{tot})	pL	33	(Grandi *et al.*, 2011)
	Lysosome (V_{ls})	pL	2% V_{tot}	(Grandi *et al.*, 2011; Penny *et al.*, 2014)[2, 3]
TPC	Maximum open probability (P_{Omax})		0.014	(Pitt *et al.*, 2010; Penny *et al.*, 2014)[2, 4]
	Variance (P_{Osd}^2)		2.25	this study
	Mean (P_{Omean})		23	(Penny *et al.*, 2014)[2]
	Leak rate ($j_{clc,leak}$, $j_{tpc,leak}$)	s^{-1}	1.13E-05	this study
Lysosome	TPC flux density into junction (j_{clc})	s^{-1}	9.708	this study
	TPC flux density into cytosol (j_{tpc})	s^{-1}	12.135	this study
	[*NAADP*] for CTRL protocol	nM	1	this study
	[*NAADP*] for ISO protocol	nM	15	this study
	Diffusion flux rate to junction ($J_{ls,j}$)	L/ms	1.4219E-15	this study
	Diffusion flux rate to cytosol ($J_{ls,i}$)	L/ms	1.3858E-15	this study

Table 2.2. Baseline parameters for the lysosome compartment in the Grandi *et al.* (Grandi *et al.*, 2011) models. E+n displays numbers in exponential notation, in which E (exponent) multiplies the preceding number by 10 to the nth power.

2.3 Cellular Variability in Electrophysiology and Calcium Handling

A population of models approach (Figure 2.2 adapted from Muszkiewicz *et al.*, 2016, which thoroughly explains the creation and use of populations of models) (Britton *et al.*, 2013; Muszkiewicz *et al.*, 2016) to account for cellular variability in electrophysiology and calcium handling was adopted. Such an approach has been especially effective in investigating proarrhythmic mechanisms, including those associated with intracellular calcium handling (Britton *et al.*, 2013; Muszkiewicz *et al.*, 2016; Passini *et al.*, 2016; Zhou *et al.*, 2016). The variability of the main transmembrane ionic currents and intracellular fluxes regulating the AP and calcium transient is applied to an initial population of 1000 models, representing 1000 cells with different ionic properties, which is generated by means of uniform Latin hypercube sampling as scaling factors (scaling from half to two fold) for the following model components: I_{CaL}, as main driver of calcium influx into the cardiomyocyte; SR calcium release flux from RyR (J_{RyR}), SR calcium reuptake through SERCA (J_{SERCA}); lysosomal calcium uptake and release fluxes (j_{clc} and j_{tpc}), including calcium leak fluxes ($j_{clc,leak}$ and $j_{tpc,leak}$), NCX as principal mediator of calcium extrusion (I_{NCX}); and I_{to} and I_{Kr}, as the main variation of currents in mouse ventricular cardiomyocyte, and in human atrial cardiomyocyte model I_{Kr} is replaced with I_{Kur}. Only models characteristic of healthy physiological function were retained in the populations, if they do not exhibit spontaneous calcium arrhythmic triggers in mouse ventricular cardiomyocyte models in the protocols of CTRL, NAADP-AM and ISO, or EADs in human atrial cardiomyocyte models in nSR and cAF in the protocols of Baseline and ISO. The sampling method of Latin hypercube sampling produces a uniform distribution, in which each model has equal weight. This method generates parameter sets over a large parameter space efficiently and without bias (Britton *et al.*, 2013). The populations of mouse ventricular cardiomyocyte models recapitulated the

distributions of calcium transient amplitudes in the experimental data. The populations of human atrial cardiomyocyte models recapitulated the distributions of APDs in the experimental data. The remaining populations cover a wide range of ionic property. The above acceptance criteria allow us to investigate the role of lysosomal calcium handling under normal physiological function, as well as to dissect its contribution under specific proarrhythmic conditions.

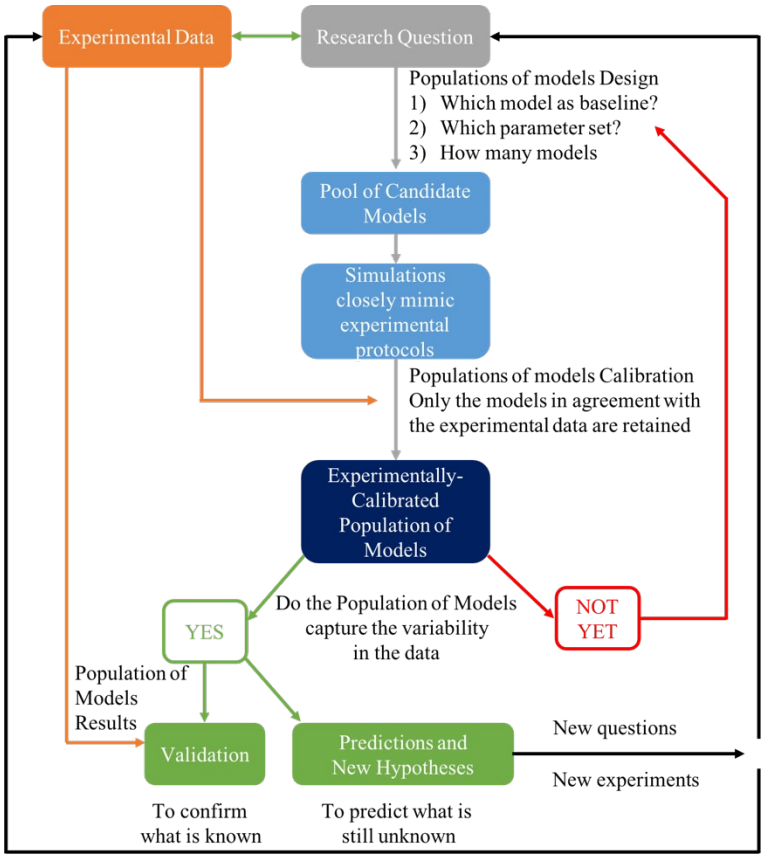


Figure 2.2. Flowchart illustrating the process behind constructing an experimentally-calibrated population of models adapted from Muszkiewicz *et al*. (Muszkiewicz *et al.*, 2016).

2.4 Quantitative Analysis of Ionic Features in Action Potential and Calcium Transient

Biomarkers summarised the morphology of the AP and calcium transient at steady-state. AP_{APD90} are calculated by the time required for the membrane to repolarise to the 90% of its membrane potential from the timepoint at maximum upstroke velocity. AP_{RMP} is the resting membrane potential of the AP. AP_{peak} is the peak membrane potential of the AP. AP_{AMP} is the difference of peak and resting membrane potentials of the AP.

The calcium transient biomarkers include calcium transient at 50% relaxation (Ca_{RT50}), calcium transient at 80% relaxation (Ca_{RT80}), diastolic calcium concentrations (Ca_{Dia}), calcium transient amplitude (Ca_{AMP}). Ca_{RT50} and Ca_{RT80} are calculated by the time required for the calcium transient to relax to 50% and 80% of its resting concentration from the timepoint at peak calcium. Ca_{Dia} is calculated by the resting calcium concentration. Ca_{AMP} biomarkers were calculated as the difference from the peak calcium to the diastolic calcium.

Distributions are presented in the form of boxplots, where the central line is the median, the box limits correspond to the 25^{th} and 75^{th} percentiles, whiskers extend to the most extreme data points not considered outliers, and outliers are depicted individually as independent data points. Fold changes of the calcium related amplitudes were calculated from the medians of the comparing populations. Partial correlation coefficients were used to find correlations between each varied flux and current and each biomarker. Pearson correlation coefficient was used to calculate the correlations in the study. It is a number between –1 and 1 that measures the strength and direction of the correlations.

2.4.1 Definition of Proarrhythmic Events

2.4.1.1 Definition of spontaneous calcium release event

The occurrence of spontaneous calcium release events is defined as oscillations during the relaxation phase of calcium transients. Only models exhibiting clear spontaneous calcium events (i.e., excluding those with minor oscillatory behaviour during relaxation) were retained for analysis.

2.4.1.2 Definition of early afterdepolarisation

The occurrence of EAD events is defined as oscillations at the plateau level of membrane potential or during phase 3 in the AP. EAD events are identified by occurrence in any of the consecutive 5 beats after an initial pacing of 150 beats.

2.4.2 Models Extracted in Proarrhythmic Scenarios

The proarrhythmic populations of mouse ventricular cardiomyocyte models are respectively sorted in the hypercalcemia and β-adrenergic stimulation, and fast to slow pacing transitions and β-adrenergic stimulation by the calibrated population. The proarrhythmic populations of human atrial cardiomyocyte models are respectively sorted in the proarrhythmic scenarios of mild hypercalcemia and β-adrenergic stimulation, I_{Kur} block and β-adrenergic stimulation, by the calibrated populations in nSR and cAF. The populations include non-TPC-specific proarrhythmic, TPC-specific proarrhythmic, and non-proarrhythmic populations. The non-TPC-specific populations are respectively extracted by proarrhythmic occurrence in the presence and block of lysosomal release, the TPC-specific populations are respectively extracted by proarrhythmic occurrence only in the presence of lysosomal release while not in the block scenario, and the non-proarrhythmic populations are respectively sorted by exhibiting absence of proarrhythmic occurrence in both scenarios.

2.4.3 Statistics

I acknowledge that no statistical comparisons were used in the thesis due to the aggregated form of the data. The research questions of the studies are mainly focused on investigating the proarrhythmic mechanisms of RyR spontaneous calcium release in the populations of mouse ventricular cardiomyocyte models and of EADs in the populations of human atrial cardiomyocyte models. Using boxplots and actual traces might be easier to present my results.

Chapter 3

Lysosomal Calcium Loading Promotes Spontaneous Calcium Release by Potentiating Ryanodine Receptors

Summary of contribution: This chapter presents a paper to investigate the role of lysosomal calcium loading in promoting spontaneous calcium release in mouse ventricular cardiomyocyte in Meng *et al.* 2023. I carried out the modelling of including lysosomal calcium handling in mouse ventricular cardiomyocyte model, conducted the calibration and validation of new model with experimental data, the simulation of populations of models, and the investigation of lysosomal calcium release and uptake in promoting spontaneous calcium release in proarrhythmic scenarios of hypercalcemia and fast to slow pacing transitions with β-adrenergic stimulation. Additionally, I did conceptualisation, methodology, software and writing of the project. Figures reproduced from the paper were my own work.

3.1 Introduction

Disruption in calcium signalling underlies many cardiac disorders, including contractile dysfunction and rhythm disorders (Scoote and Williams, 2004; Nattel, Burstein and Dobrev, 2008; Smith and Eisner, 2019; Burton and Terrar, 2021). In cardiomyocytes, the process of excitation-contraction coupling links depolarisation of the plasma membrane to muscle fibre contraction (Bers, 2002). Membrane depolarisation in response to the arrival of an AP leads to the activation of voltage gated L-type calcium channels located within the sarcolemma and transverse (t-)tubules. The resulting inward calcium current (I_{CaL}) causes an increase in the calcium concentration within the subsarcolemmal junctional space, located between the surface membrane and the SR. This elevation in junctional calcium activates RyRs, which then release calcium from the SR into the cytosol. If sufficient RyRs are activated, this process of CICR leads to a cellular calcium transient characterised by an initial rise in cytosolic calcium followed by a fall resulting from the combination of RyR closure, reuptake of calcium into SR via the SERCA, and extrusion from the cell via the NCX. Calcium transients are linked to cell contraction due to the binding and activation of cytosolic calcium to troponin on the muscle filaments (Bers, 2002). Tight regulation of cellular calcium is therefore essential in cardiac cells in order to maintain healthy rhythm and contractility.

Lysosomal dysfunction can be linked to cardiac disorders including arrhythmia and heart failure (Collins *et al.*, 2011; Capel *et al.*, 2015; Wu *et al.*, 2017; Simon *et al.*, 2021). Lysosomal calcium release occurs primarily through the opening of TPC2 following activation by NAADP (Churchill and Galione, 2001; Churchill *et al.*, 2002; Galione *et al.*, 2010; Capel *et al.*, 2015; Ruas *et al.*, 2015). Transmission electron microscopy has shown that, in cardiomyocytes, lysosomes are located within close proximity to the SR, mitochondria and t-tubules (Aston *et al.*, 2017) . Release of lysosomal calcium via TPC2 in response to NAADP enhances RyR calcium release from the SR (Macgregor *et al.*, 2007), and inhibition of NAADP pathway has been shown to be protective against β-adrenergic induced arrhythmias (Nebel *et al.*, 2013). Furthermore, lysosomes have been shown to generate oscillating calcium currents that can trigger potentially lethal cardiac arrhythmias, and these oscillations can also be supressed by the inhibition of NAADP (Davidson *et al.*, 2015). Despite these observations, the role of lysosomal calcium signalling in cardiomyocytes has been

relatively understudied and lysosomes are not included in current mathematical models of cardiac calcium handling (Shannon *et al.*, 2004; Morotti *et al.*, 2014).

Mathematical models based purely on experimental data can suffer from the loss of individuality resulting from the averaging of biological data (Sarkar, Christini and Sobie, 2012). However, the use of more recent advances in approaches for studying variability such as experimentally calibrated populations-of-models frameworks, enables such biological variability to be incorporated into models of cardiac electrophysiological signalling (Britton *et al.*, 2013; Muszkiewicz *et al.*, 2016). Here I modify an existing model of mouse ventricular calcium handling by Morotti *et al.* (Morotti *et al.*, 2014) to include a lysosomal compartment based on experimental data on spatial organisation and lysosomal action. I adopt a population of models-based approach to account for variability in electrophysiology and calcium handling (Britton *et al.*, 2013; Muszkiewicz *et al.*, 2016). This model was used to investigate mechanisms of lysosomal calcium handling in arrhythmogenesis and RyR spontaneous release under conditions of calcium overload (hypercalcemia and fast pacing) in conjunction with β-adrenergic stimulation. The modelling data supports the hypothesis that lysosomes can act as an additional intracellular calcium store, providing an additional transport for intracellular calcium, and can influence the driving force for spontaneous calcium release from the SR to the junctional space.

I hypothesise that lysosomal calcium handling might modulate intracellular calcium handling by increasing SERCA reuptake and RyR release in normal loading condition, and that enhanced lysosomal calcium handling might promote RyR spontaneous calcium release by increasing RyR open probability and RyR release in calcium overload conditions of hypercalcemia or fast to slow pacing transitions additionally with β-adrenergic stimulation (Figure 3.1).

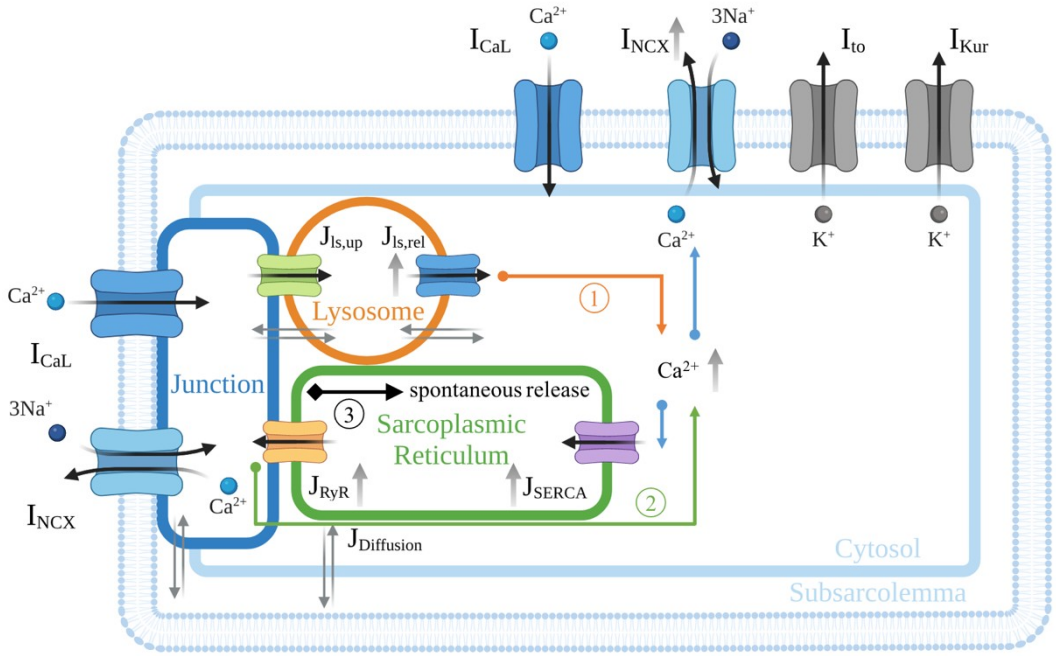


Figure 3.1. Schematic cartoon showing the hypotheses for actions of lysosomal calcium handling.

3.2 Results

3.2.1 Model Validation of Lysosomal Calcium Handling

To investigate the role of lysosomal calcium handling on ventricular function, the mouse ventricular model of Morotti *et al.* (Morotti *et al.*, 2014) was extended to include a lysosomal compartment (see Methods on Chapter 2). In brief, based on experimental evidence on organelle localisation and function (Capel *et al.*, 2015; Ruas *et al.*, 2015;

Garrity *et al.*, 2016; Aston *et al.*, 2017), lysosome action was modelled as an additional calcium pool, with function primarily driven by calcium loading from the junctional subspace, and NAADP-modulated release to the cytosol via TPC2 channels. The lysosome pool can thereby act as an additional calcium source depending on lysosomal calcium concentration, contributing to the CICR process.

Lysosome model calibration was conducted as follows. Without activating ligands, NAADP-modulated TPC2 openings are typically very brief, with open probability P_O<0.0009(Pitt *et al.*, 2010). The single channel recording took place at 22 ± 2 °C (Pitt *et al.*, 2010). The effect of temperature on the TPC P_O is currently unknown. These were described by adopting a previously validated Gaussian distribution on NAADP concentration and an endogenous *[NAADP]* value of 1 nM (Penny *et al.*, 2014), yielding an upper bound for P_O of 0.016, close to the experimental findings. *[NAADP]* was increased to 15 nM when simulating opened TPC2 channels, resulting in a $P_O = 0.0134$, close to the maximum open probability observed in experiments (Pitt *et al.*, 2010).

The magnitudes of lysosomal calcium fluxes were then calibrated based on experimental data from both WT and genetically-modified TPC2-KO mouse cardiomyocytes (Capel *et al.*, 2015). In these experiments (see Figure 3.2), application of exogenous NAADP (NAADP-AM) increased calcium transient amplitude in WT, but not in TPC2-KO cardiomyocytes. Simulated NAADP-AM action by increased *[NAADP]* resulted in a stronger calcium release from the lysosome compartment via TPC2, recapitulating the increase of cytosolic calcium amplitude (Figure 3.2A). When lysosomal calcium release ($J_{ls,rel}$) was set to zero (denoted as TPC2-KO) to mimic the genetically-modified TPC2-KO cardiomyocytes, cytosolic calcium transient features were unaltered by an increase in *[NAADP]*, in agreement with the experimental data (Figure 3.2B).

Further validation of the lysosomal calcium handling model was conducted under additional pharmacological protocols exerting an action on the CICR process. Experimentally, β-adrenergic stimulation by ISO increased calcium transient amplitude

in both WT and TPC2-KO, with the response of TPC2-KO significantly reduced compared to WT (Figure 3.2C, 3.2D). Both cardiomyocyte types also showed faster calcium transient relaxation in response to ISO. Likewise, the activation of the β-adrenergic response in the model by application of 100 nM ISO replicated these effects, with a larger response in WT.

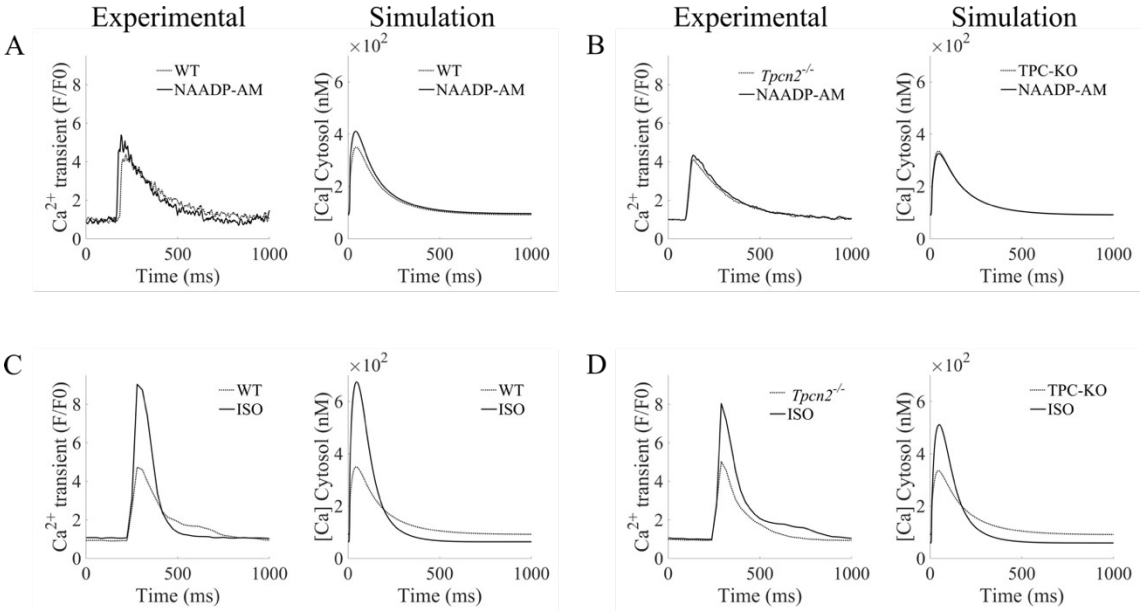


Figure 3.2. Validation of lysosomal calcium handling model against pharmacological protocols. **3.2A, 3.2B:** Calibration of Ca^{2+} transients under increased lysosomal release by NAADP-AM (WT vs TPC2-KO, respectively). **3.2C, 3.2D:** Validation of Ca^{2+} transients under β-adrenergic stimulation by ISO (WT vs TPC2-KO, respectively). The experimental data were presented as $F/F0$ such that fluorescence data were presented relative to diastolic fluorescence (Capel *et al.*, 2015). The simulated data were presented as cytosolic [Ca^{2+}] which showed the calcium concentration in cytosol (Morotti *et al.*, 2014).

3.2.2 Lysosomal Calcium Release Primarily Modulates Intracellular Calcium Handling by Increasing SERCA Reuptake and RyR Release

In brief, in the modified model containing the lysosome as a compartment capable of taking up and releasing calcium, the calcium released from the lysosome enables an additional direct transport of calcium between the junctional and cytosolic spaces. In the absence of this transport mechanism, junctional calcium can only flow into the cytosol by pure intracellular diffusion, which is characterised by slower transport kinetics.

To investigate how these effects modulate intracellular calcium handling at the whole cellular level, a population of models approach was exploited to account for cellular variability in ionic currents and intracellular calcium fluxes, and their modulation of the full CICR process (Britton *et al.*, 2013; Muszkiewicz *et al.*, 2016). To further enable investigations of the role of lysosomal calcium handling on arrhythmogenesis, only models characteristic of healthy physiological function (i.e., not exhibiting spontaneous calcium arrhythmic triggers in any of the described simulated pharmacological protocols) were retained in the population, giving a total of 423 accepted models (see Methods on Chapter 2). Subsequent data are reported using this final population.

The boxplots in Figure 3.3 show the amplitude distributions of calcium concentrations in the lysosome (Figure 3.3Ai) and cytosolic compartments (Figure 3.3Bi), and the intracellular calcium fluxes of SERCA reuptake (Figure 3.3Ci) and RyR release (Figure 3.3Di) involved in intracellular calcium handling. Example selected traces are shown for basal conditions (CTRL) and the investigated protocols of increased lysosomal function (NAADP-AM and ISO), as well as for WT vs TPC2-KO cardiomyocytes

(Figures 3.3Aii, 3.3Dii, 3.3Aiii, 3.3Diii). For CTRL, lysosomal calcium concentration was higher in TPC2-KO than WT, as a result of the modelled genetic deletion of TPC in TPC2-KO cardiomyocytes (Figures 3.3Ai, 3.3Aiii), which precludes calcium from being released from the lysosomal compartment. No main median differences in cytosolic calcium amplitude were observed between WT and TPC2-KO (Figures 3.3Bi, 3.3Biii) in CTRL, consistent with non-significant experimental differences in calcium transient amplitude between both cardiomyocyte types in basal conditions (Capel *et al.*, 2015). Evaluation of SERCA and RyR amplitudes showed no main median differences in CTRL (Figures 3.3Ci, 3.3Ciii, 3.3Di, 3.3Diii).

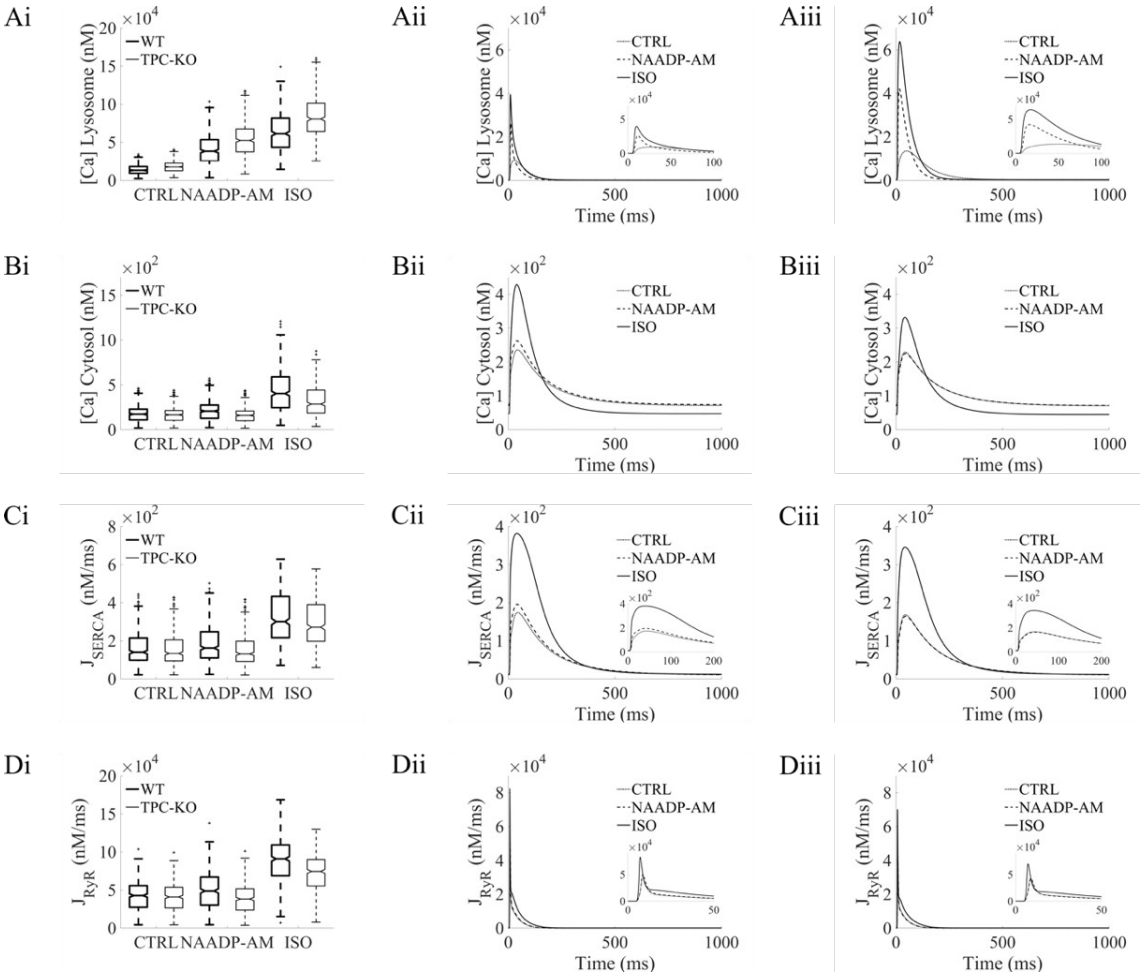


Figure 3.3. Lysosomal calcium release primarily modulates intracellular calcium handling by increasing SERCA reuptake and RyR release. Example selected traces for steady-state are shown for: lysosomal calcium concentration (**3.3Ai-iii**), cytosolic calcium concentration (**3.3Bi-iii**), SERCA reuptake (**3.3Ci-iii**) and RyR release (**3.3Di-iii**). For each quantity, the distribution of amplitudes under each experimental condition is shown in (i). Wild-type (WT) data is presented in black and TPC2 knock-out, TPC2-KO, in red. The central line represents the median, boxes the inter-quartile range and dotted lines the range. Each quantity is reported under control conditions (CTRL), in the presence of NAADP (NAADP-AM, 15 nM) and in the presence of β-adrenergic stimulation with ISO (ISO, 100 nM). Representative traces of model outputs for WT and TPC2-KO are presented in (ii) and (iii) respectively (CTRL in dotted lines, NAADP-AM, in dashed lines, ISO in solid lines).

Under application of exogeneous NAADP (NAADP-AM protocol), the increased lysosomal calcium loading and the increased lysosomal calcium release led to a 1.19-fold amplitude increase of cytosolic calcium in WT, compared to CTRL (Figure 3.3Bi). Under NAADP-AM protocol, the lysosomal calcium uptake flux was increased by uptake of junctional calcium, and contributed to the increase of lysosomal calcium concentration. The increased lysosomal calcium loading led to the enhanced lysosomal calcium release which positively feedback to lysosomal calcium loading by contributing to SERCA potentiation, SR content, RyR release, and increasing junctional calcium loading and lysosomal calcium uptake flux. This difference was also apparent in the example selected traces of cytosolic calcium concentration (Figure 3.3Bii). In particular, these effects led to a systolic increase in cytosolic calcium and similar diastolic levels in WT cardiomyocytes under NAADP-AM compared to CTRL (Figure 3.3Bii), while the cytosolic calcium transient was unaltered upon NAADP-AM application in TPC2-KO cardiomyocytes (Figure 3.3Biii). Quantitatively, the calibrated population predicted a normalised increase in cytosolic calcium amplitude under NAADP-AM relative to CTRL of 0.200±0.003 (mean ± standard error) in WT vs –0.035±0.001 in TPC2-KO. These values are in agreement with the ranges of 0.16±0.05 for WT and –0.06±0.04 for TPC2-KO in experimental findings (Capel *et al.*, 2015), further validating model predictions. Mechanistically, the increased cytosolic calcium loading under NAADP-AM in WT cells consequently promoted calcium reuptake by SERCA, causing a 1.15-fold increase in SERCA amplitude (Figure 3.3Ci), which was also linked to a 1.14-fold increase calcium release by RyR, respectively compared to the CTRL protocol (Figure 3.3Di). No main median differences with respect to basal conditions were observed in the amplitude of these fluxes for TPC2-KO cardiomyocytes in the comparison of NAADP-AM and CTRL protocols.

When β-adrenergic stimulation by ISO was simulated, the activation of PKA phosphorylation targets (I_{CaL}, RyR, phospholamban, and phospholemman in the model) resulted in a higher lysosomal calcium load and release compared to the NAADP-AM protocol (Figure 3.3Ai). Matching the experimental findings, there was also a greater response to ISO in WT cells than in TPC2-KO; ISO application increased the cytosolic calcium amplitude by 2.32-fold compared to CTRL for WT, and by 1.41-fold in WT

versus TPC2-KO models in ISO (Figure 3.3Bi). In terms of relative changes of cytosolic calcium amplitude, the population predicted increases of 1.439±0.027 in WT and 0.898±0.021 in TPC2-KO are in agreement with the ranges of 1.23±0.24 and 0.57±0.17 increase in experimental findings, respectively(Capel *et al.*, 2015). ISO application led to a stronger 1.11-fold increase in calcium reuptake by SERCA in WT versus TPC2-KO (Figure 3.3Ci), and a 1.22-fold increase of calcium release by RyR (Figure 3.3Di).

Altogether, the results presented in this section qualitatively and quantitatively recapitulate the findings associated with experimental observations of lysosomal function on the calcium transient in both WT and genetically-modified TPC2-KO mouse cardiomyocytes (Capel *et al.*, 2015). These results also illustrate an impact of lysosomal calcium in intracellular calcium handling by increasing the cytosolic calcium peak concentration, which in turn potentiates SERCA reuptake, increases the SR calcium load, and promotes CICR via RyR release.

3.2.3 Lysosomal Calcium Release Promotes Spontaneous Calcium Release under Hypercalcemia and β-adrenergic Stimulation by Increasing RyR Open Probability

Following our model validation and mechanistic findings of a lysosomal modulation of CICR under normal calcium loading, we further tested the model to investigate mechanisms of lysosomal involvement under proarrhythmic conditions.

Firstly, I simulated conditions of calcium overload by hypercalcemia (raising extracellular calcium from 1.0 to 1.8 mM), coupled with β-adrenergic stimulation. Only models exhibiting either normal calcium transients or clear spontaneous calcium events (i.e., excluding those with minor oscillatory behaviour during relaxation) under this protocol were retained for analysis, leaving a total of 357 models. Out of the 357 cellular profiles (none exhibiting spontaneous release events in basal conditions), 52% of the models displayed spontaneous calcium release events (in the presence of 1.8 mM extracellular calcium and β-adrenergic stimulation) in WT compared to 44% in TPC2-KO models, highlighting a lysosomal involvement in the triggering of intracellular calcium proarrhythmic events.

To better understand the mechanisms where lysosomal calcium handling is directly responsible for these potentially proarrhythmic events, TPC-specific proarrhythmic models (n=30) were extracted from the population, meaning that the selected models exhibited spontaneous calcium release in WT (i.e., with active lysosomal TPC2 release) but not in their paired TPC2-KO configurations. The rest of proarrhythmic models featured spontaneous occurrence in both WT and TPC2-KO, while non-proarrhythmic models did not show spontaneous events in either WT or TPC2-KO. In terms of ionic properties underlying variability in cell-to-cell response, TPC-specific proarrhythmic profiles favoured larger lysosomal calcium release than non-proarrhythmic models ($J_{ls,rel}$, Figure 3.4A). Importantly, the TPC-specific proarrhythmic profiles were characterised by smaller densities in L-type calcium current compared to non-proarrhythmic profiles (I_{CaL}, Figure 3.4A).

Taken together, our findings highlight that, in the example selected traces of TPC-specific proarrhythmic models with similar I_{CaL} influx to the non-proarrhythmic ones (Figure 3.4B), lysosomal calcium release provided sufficient additional calcium load to the cytosol to potentiate SERCA reuptake for SR loading (Figures 3.4C, 3.4D, 3.4E), which increased RyR open probability for RyR release (Figures 3.4F, 3.4G).

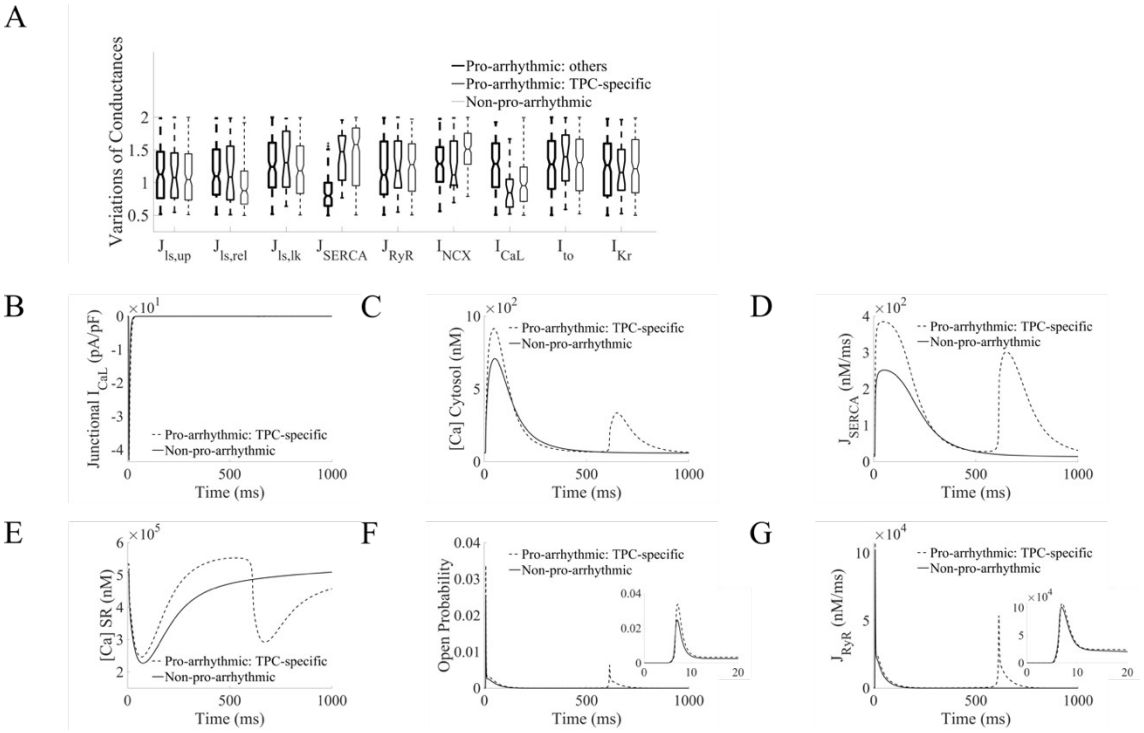


Figure 3.4. Ionic properties and calcium fluxes underlying spontaneous calcium events under hypercalcemia and sustained β-adrenergic stimulation. **3.4A:** Comparison of ionic properties of TPC-specific proarrhythmic models (intermediate lines), other proarrhythmic models (thick lines), and non-proarrhythmic models (thin lines) in WT. **3.4B-3.4G:** Traces of junctional L-type calcium current, cytosolic and SR calcium concentrations, SERCA flux, RyR open probability, and RyR flux, respectively, comparing example selected TPC-specific proarrhythmic and non-proarrhythmic models in WT under similar I_{CaL} influx.

A further analysis of lysosome modulation of spontaneous calcium release events is presented in Figures 3.5 and 3.6. Figure 3.5 illustrates the traces of the main calcium concentrations and fluxes involved in lysosomal calcium release under hypercalcemia and β-adrenergic stimulation for the TPC-specific proarrhythmic profiles, while Figure 3.6 shows representative traces of under WT and TPC2-KO for further detailed mechanistic analysis. In the population of models, hypercalcemia resulted in lysosomal overload (Figure 3.5Ai) compared to basal conditions (Figure 3.3Ai), which contributed to a stronger calcium release from lysosome to cytosol (Figure 3.5Ci). This was confirmed by an increase of total calcium reuptake by SERCA (Figures 3.5Ei), leading

to a higher SR calcium concentration and consequently increasing the likelihood of spontaneous events via RyRs (Figures 3.5Fi).

Continuing to focus on models with TPC-dependent arrhythmias, the influence of lysosomal calcium handling in mediating spontaneous calcium release events was further dissected by blocking each of the respective lysosomal fluxes in the WT. The block of lysosomal calcium uptake ($J_{ls,up}$) precluded calcium loading in the lysosome compartment (Figure 3.5Aii), reducing spontaneous calcium release events to 37% (11/30) compared to TPC-specific proarrhythmic models in WT (Figure 3.5Dii). In terms of impact on function, the block of the lysosomal uptake flux impeded the loading of the lysosomal compartment, resulting in the loss of lysosomal calcium release (Figure 3.5Aii-3.5Cii). The absence of the lysosomal calcium transport decreased calcium transient amplitude (Figure 3.5Dii) and thus calcium reuptake by SERCA (Figures 3.5Eii), and the magnitude of RyR release (Figures 3.5Fii).

On the other hand, loss of the lysosomal release in TPC2-KO cardiomyocytes (as mimicked by setting $J_{ls,rel}=0$) had a dual antiarrhythmic effect, resulting in the complete abolishment of spontaneous calcium release events in all TPC-specific proarrhythmic models. First, although the lysosome compartment now gets loaded (Figure 3.5Aiii), the block of lysosomal release precludes its calcium load from flowing directly into the cytosol, getting transiently stored for a longer period of time in this compartment. The absence of the fast lysosomal pathway thus resulted in a similar antiarrhythmic mechanism as above described in the case of lysosomal uptake block (decreased calcium transient amplitude, Figure 3.5Diii, 3.6A; reduced SERCA uptake, Figures 3.5Eiii, 3.6B; reduced SR concentration, Figure 3.6C; and therefore, smaller RyR open probability, Figure 3.6D; smaller magnitude of RyR release, Figures 3.5Fiii, 3.6E; and smaller junctional loading, Figure 3.6F). Second, a significant part of the lysosomal calcium concentration (approximately 86% in median) is reverted into the junctional space through the lysosomal loading channels, which is even noticeable in steady-state conditions (positive peak in Figure 3.5Biii). The additional calcium being released back into the junction contributes to reduce CICR, which reduced calcium load in the cytosol, SR, and junction (Figures 3.6A, 3.6C, 3.6F), drastically diminishing RyR

open probability (Figure 3.6D), and therefore for spontaneous calcium release, when RyRs open.

In summary, approximately 16% (30/186) of our investigated models exhibiting spontaneous calcium release events under hypercalcemia and β-adrenergic stimulation were directly linked to lysosomal action, due to an increased RyR open probability. Such lysosome-specific events can be effectively counteracted by inhibition of lysosomal calcium release, in agreement with experimental findings of decreased arrhythmic propensity in TPC2-KO mice (Capel *et al.*, 2015).

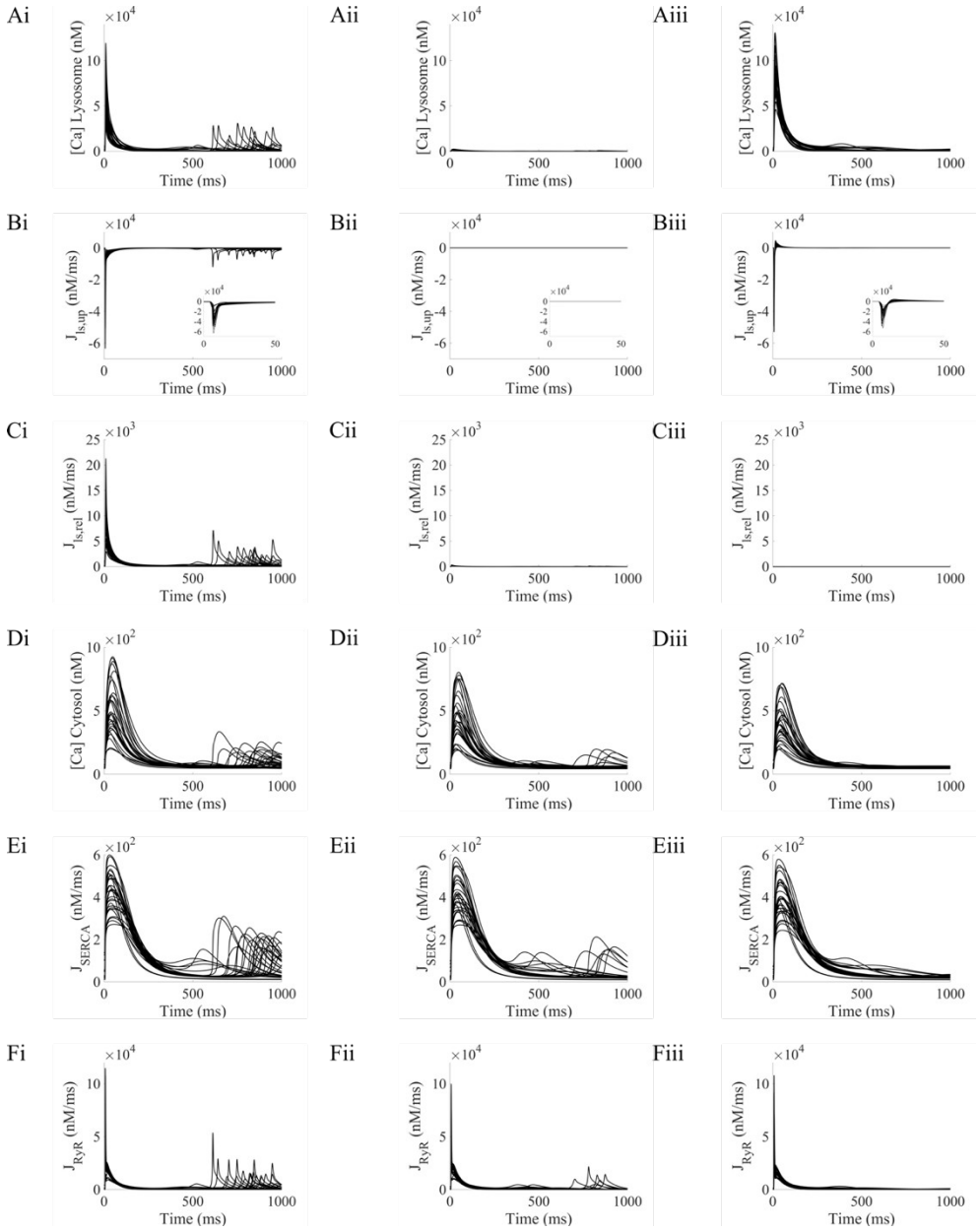


Figure 3.5. Lysosomal calcium release promotes spontaneous calcium release in TPC-specific proarrhythmic models under hypercalcemia and β-adrenergic stimulation by increasing RyR open probability. **3.5Ai-3.5Fi:** Lysosomal calcium concentration, lysosomal uptake and release, cytosolic calcium concentration, and SR reuptake and release fluxes, respectively, in basal conditions. **3.5Aii-3.5Fii:** Calcium concentrations and fluxes under lysosomal uptake block ($J_{ls,up}=0$). **3.5Aiii-3.5Fiii:** Calcium concentrations and fluxes under lysosomal release block ($J_{ls,rel}=0$).

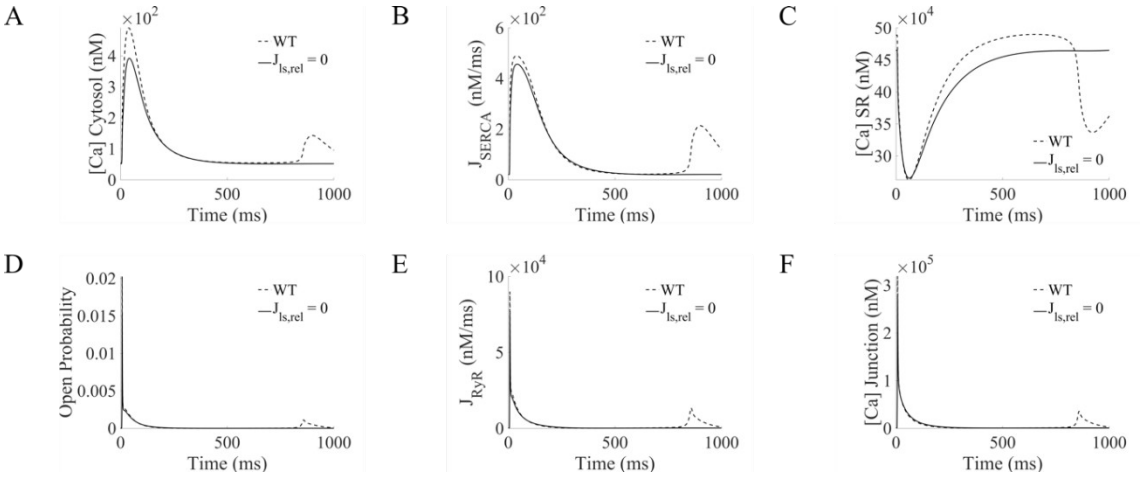


Figure 3.6. Loss of lysosomal calcium release flux reduced spontaneous calcium release from SR in TPC-specific proarrhythmic models under hypercalcemia and β-adrenergic stimulation. **3.6A-3.6F:** Example selected traces of cytosolic, SR and junctional calcium concentrations, SERCA flux, RyR open probability, and RyR flux, comparing scenarios in WT (dashed line), and blocking lysosomal calcium release ($J_{ls,rel}=0$, solid line).

The relationship of spontaneous calcium release events with DADs at the AP level is presented in Figure 3.7. The spontaneous calcium release events mediated by lysosomal calcium release in TPC-specific proarrhythmic models activates the forward mode of NCX (Figure 3.5Di). This results in calcium extrusion through the membrane with an accompanying inward current, which elevates transmembrane voltage in the AP as DADs (Figure 3.7Ai), by comparison to the absence of spontaneous release events and DADs in such models under block of lysosomal release (Figures 3.5Diii, 3.7Aiii).

Since NCX current directly mediates DAD formation, we generated an additional population of models with enhanced NCX current by 3-fold to investigate its relationship with DAD amplitude. In the new population, 671 models were calibrated in CTRL, NAADP-AM, and ISO protocols by not exhibiting spontaneous calcium release events. Under hypercalcemia, we newly excluded for analysis those models with minor oscillatory behaviour during relaxation that might not be clearly ascribed to spontaneous calcium release events. The extraction of those models was based on the spontaneous calcium release events during diastolic stage. Figures 3.8Ai-3.8Aiii, 3.8Ci-3.8Ciii show

minor oscillatory behaviour during relaxation that might not be clearly ascribed to spontaneous calcium release events. These calcium oscillations translated into minor oscillatory behaviour in AP (Figures 3.8Bi-3.8Biii, 3.8Di-3.8Diii), which might not clearly represent DADs. This exhaustive pruning led to a total of 7 TPC-specific models (compared to 30 TPC-specific models in basal variation), all exhibiting larger DADs than those in basal current variation (Figures 3.7Ai, 3.7Bi). We therefore find that an increase of NCX current contributes to DAD amplitude in TPC-specific models (Figure 3.7Bi), which can be successfully counteracted by block of TPC2 lysosomal release (Figure 3.7Biii).

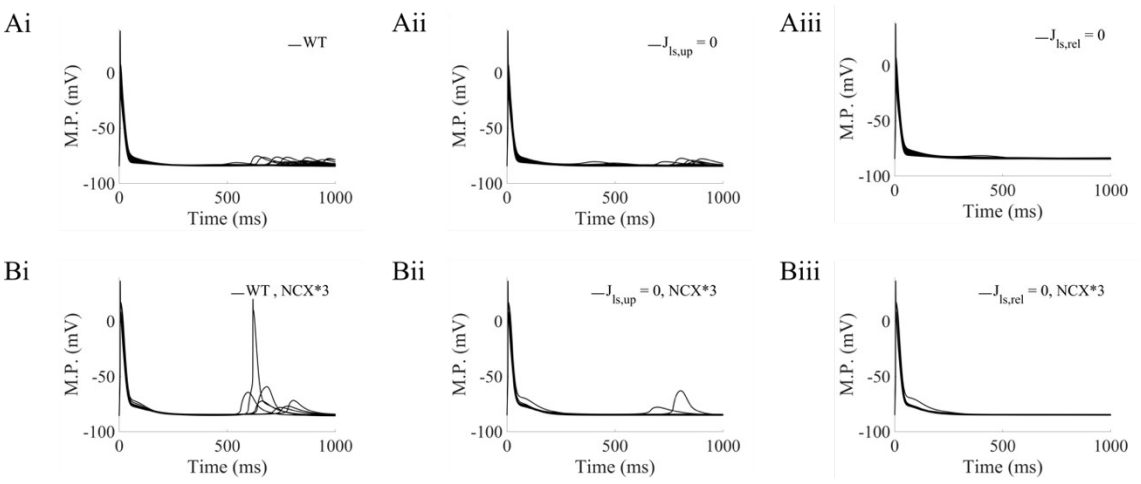


Figure 3.7. Lysosomal calcium release produces delayed afterdepolarisations by promoting spontaneous calcium release in TPC-specific proarrhythmic models under hypercalcemia and β-adrenergic stimulation. **3.7Ai-3.7Aiii:** Action potentials in the TPC-specific category with NCX current under basal variation (range of 0.5 to 2-fold changes), comparing scenarios in WT, blocking lysosomal calcium loading ($J_{ls,up}=0$), and blocking lysosomal calcium release ($J_{ls,rel}=0$), respectively. **3.7Bi-3.7Biii:** Action potentials in the TPC-specific category when NCX current variation is increased by 3-fold (range of 0.5×3 to 2×3-fold changes), comparing scenarios in WT, blocking lysosomal calcium loading ($J_{ls,up}=0$), and blocking lysosomal calcium release ($J_{ls,rel}=0$), respectively. M.P.: membrane potential.

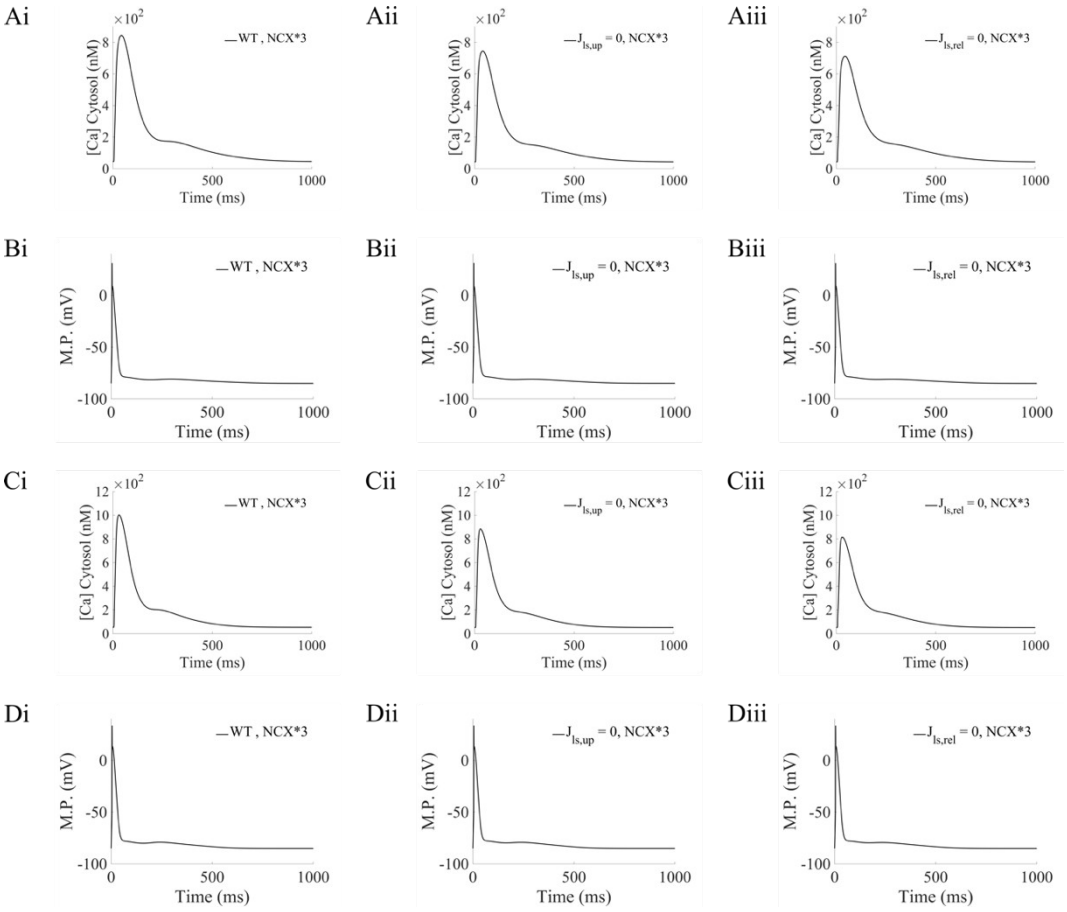


Figure 3.8. TPC-specific proarrhythmic models with minor oscillatory behaviour under hypercalcemia and β-adrenergic stimulation. **3.8Ai-3.8Aiii, 3.8Bi-3.8Biii:** One model of calcium transients and action potentials in the TPC-specific category when NCX current variation is increased by 3-fold (range of 0.5×3 to 2×3-fold changes), comparing scenarios in WT, blocking lysosomal calcium loading ($J_{ls,up}=0$), and blocking lysosomal calcium release ($J_{ls,rel}=0$), respectively. M.P.: membrane potential. **3.8Ci-3.8Ciii, 3.8Di-3.8Diii:** Another model of calcium transients and action potentials in the TPC-specific category when NCX current variation is increased by 3-fold (range of 0.5×3 to 2×3-fold changes), comparing scenarios in WT, blocking lysosomal calcium loading ($J_{ls,up}=0$), and blocking lysosomal calcium release ($J_{ls,rel}=0$), respectively. M.P.: membrane potential.

3.2.4 Lysosomal Calcium Release Promotes Spontaneous Calcium Release under Fast Pacing and β-adrenergic Stimulation by Increasing RyR Open Probability

Following experimental evidence of an involvement of lysosomal calcium handling in mediating arrhythmic events under chronic β-adrenergic stimulation and burst pacing (Capel *et al.*, 2015), we hypothesised similar proarrhythmic mechanisms due to intracellular calcium accumulation by fast pacing as in concomitant hypercalcemia and sustained β-adrenergic stimulation. For these investigations, our populations of cardiomyocyte models were paced at 10 Hz for 150 beats to raise intracellular calcium, followed by a transition to slow pacing at 1 Hz for 5 consecutive beats, where spontaneous calcium release events were recorded.

From the original 423 models in the population, 8 were excluded for proarrhythmic analysis in fast pacing under the same criteria as aforementioned (oscillation in calcium transient no clearly ascribed to spontaneous calcium release). Out of the 415 calibrated cellular profiles, 59% of WT models displayed spontaneous calcium release events during their transitions from fast to slow pacing, compared to 44% in TPC2-KO models, newly evidencing a lysosomal contribution to intracellular calcium proarrhythmic events. TPC-specific proarrhythmic profiles (n=60) were extracted from the new population, based on those exhibiting spontaneous calcium release events when transitioning from fast to slow pacing in WT, while not in their paired TPC2-KO configuration. In terms of ionic properties underlying cellular variability, TPC-specific proarrhythmic profiles were characterised by smaller I_{CaL} and I_{NCX} densities, together with smaller levels of SERCA reuptake (J_{SERCA}) and RyR release (J_{RyR}), respectively compared to non-arrhythmic profiles (Figure 3.9A).

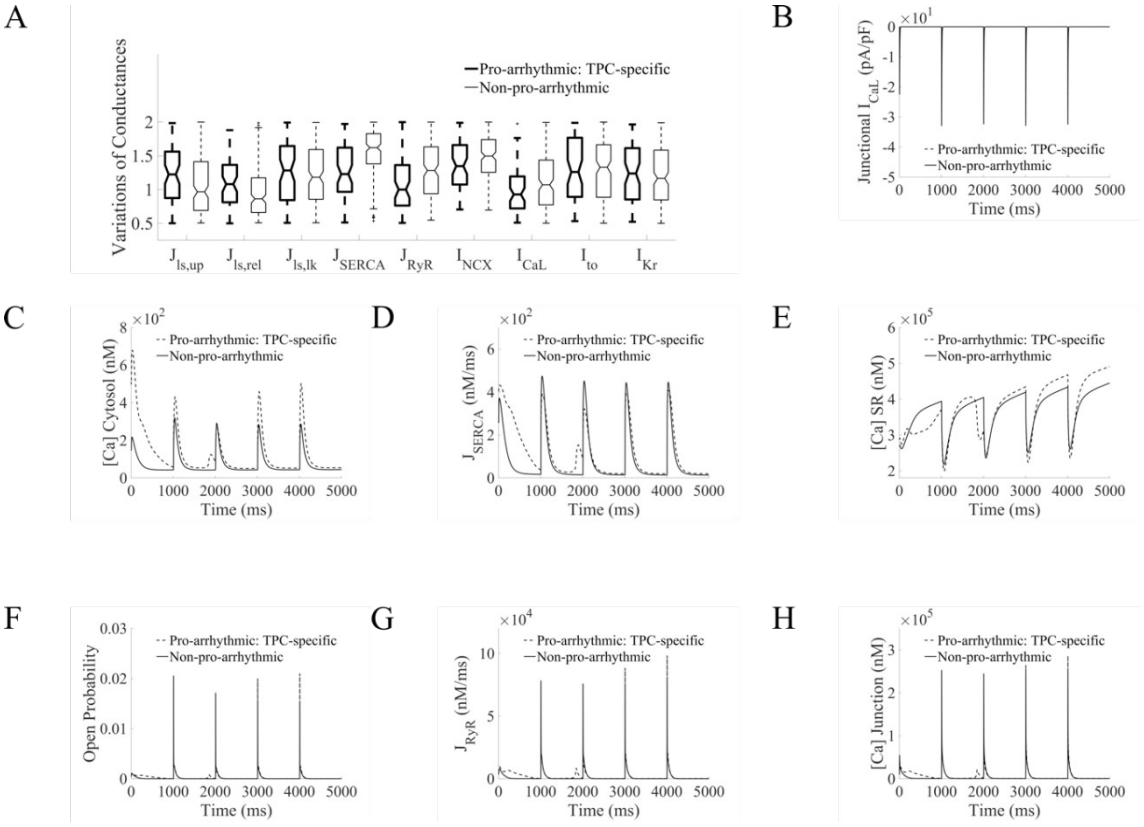


Figure 3.9. Ionic properties and calcium fluxes underlying spontaneous calcium events under fast pacing at 10 Hz and sustained β-adrenergic stimulation. **3.9A:** Comparison of ionic properties of TPC-specific proarrhythmic models (thick lines), and non-proarrhythmic models (thin lines) in WT. **3.9B-3.9H:** Traces of junctional L-type calcium current, cytosolic, SR and junctional calcium concentrations, SERCA flux, RyR open probability, and RyR flux, comparing TPC-specific proarrhythmic models, and non-proarrhythmic models in WT.

The key intracellular concentrations and calcium fluxes involved in CICR are presented in Figure 3.10 for the TPC-specific proarrhythmic models during their transition from fast to slow pacing. In WT, intracellular calcium accumulation due to the fast pacing portion of the protocol is apparent at the start of the transition (Figure 3.10Di), compared to basal conditions (Figure 3.3Bii). This calcium overload is taken back up

into the SR by SERCA (Figure 3.10Ei), leading to subsequent SR overload and a persistent release by RyR in the form of spontaneous calcium events during the entire transition in slow pacing (Figure 3.10Fi). Fast pacing model runs were repeated at a faster pacing rate of 25 Hz and analogous findings were observed (Figure 3.11).

The influence of lysosomal calcium handling in mediating these spontaneous calcium release events was investigated by blocking each of the respective lysosomal fluxes (Figure 3.10, middle and right columns). While for the hypercalcemia case simulations were in a stable state, the transition from fast to slow pacing produced beat-by-beat changes in different models. Example selected traces of a proarrhythmic TPC-specific model under WT and TPC-KO are presented in Figure 3.12. Similar to the hypercalcemia case, block of the lysosomal release ($J_{ls,rel}=0$) was accompanied by an additional reversal of part of the lysosomal calcium concentration into the junctional space via the lysosomal loading channel (positive peaks in Figure 3.10Biii), and precluded calcium load in the lysosome (Figures 3.10Aiii-3.10Ciii), leading to the abolition of the fast calcium pathway from the junctional space into the cytosol. This resulted into the previously discussed cascade of decreased cytosolic calcium transient amplitude (Figures 3.10Diii, 3.12A), reduced SERCA uptake (Figures 3.10Eiii, 3.12B), decreased SR loading (Figure 3.12C), and smaller RyR open probability as driving force for RyR release (Figures 3.10Fiii, 3.12D, 3.12E), and reduced junctional loading (Figure 3.12F). Block of the lysosomal uptake ($J_{ls,up}=0$) decreased the incidence of spontaneous calcium release events to only 25% (15/60) of the TPC-specific proarrhythmic models. The same findings were obtained under faster pacing rates (Figure 3.13).

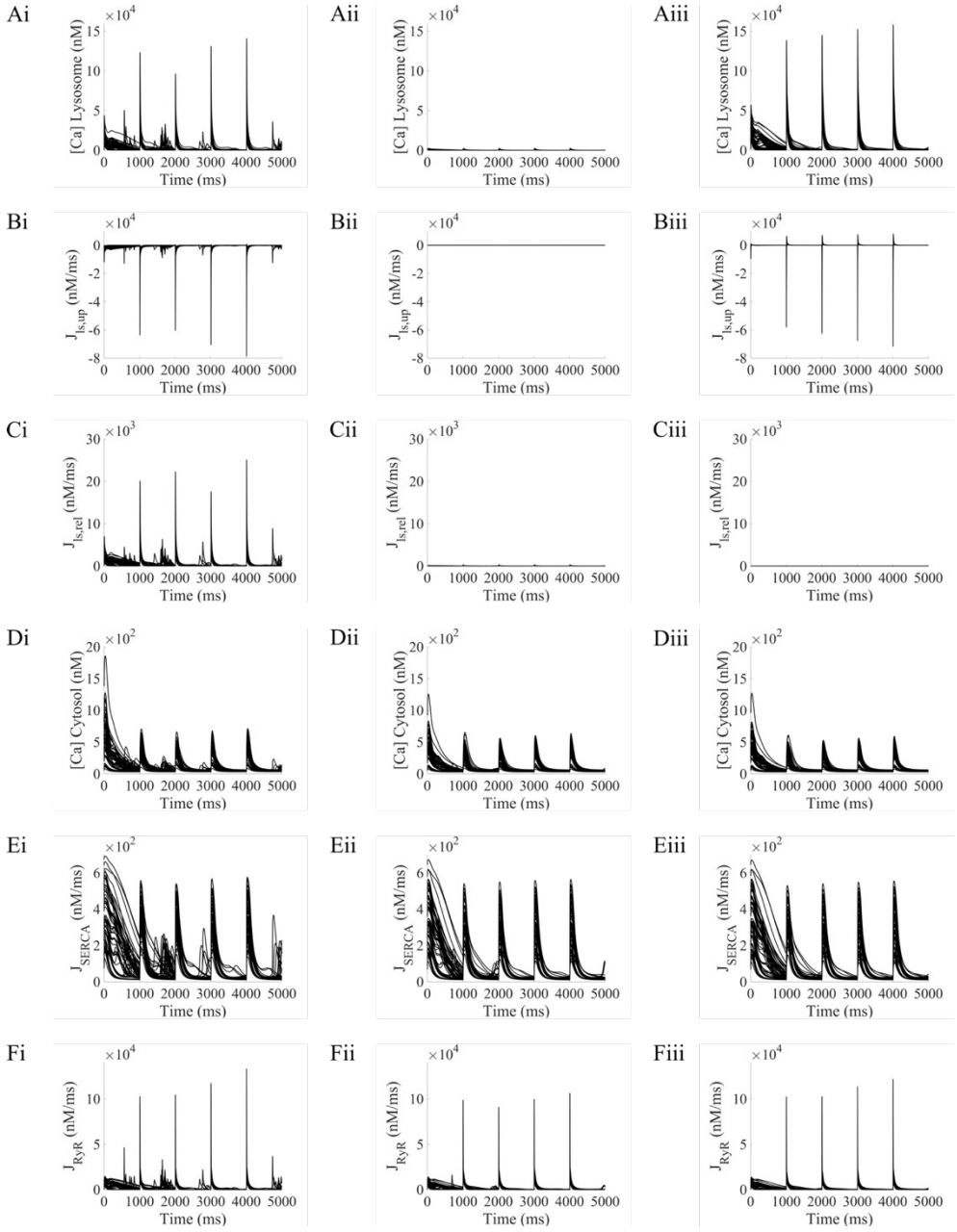


Figure 3.10. Lysosomal calcium release promotes spontaneous calcium release in TPC-specific proarrhythmic models under fast pacing and β-adrenergic stimulation, by increasing RyR open probability. All results presented under initial fast pacing at 10 Hz. The transition from fast to slow pacing occurred at time 0. **3.10Ai-3.10Fi:** Lysosomal calcium concentration, lysosomal uptake and release, cytosolic calcium concentration, and SR reuptake and release fluxes, respectively, in basal conditions. **3.10Aii-3.10Fii:** Calcium concentrations and fluxes under lysosomal uptake block ($J_{ls,up}=0$). **3.10Aiii-3.10Fiii:** Calcium concentrations and fluxes under lysosomal release block ($J_{ls,rel}=0$).

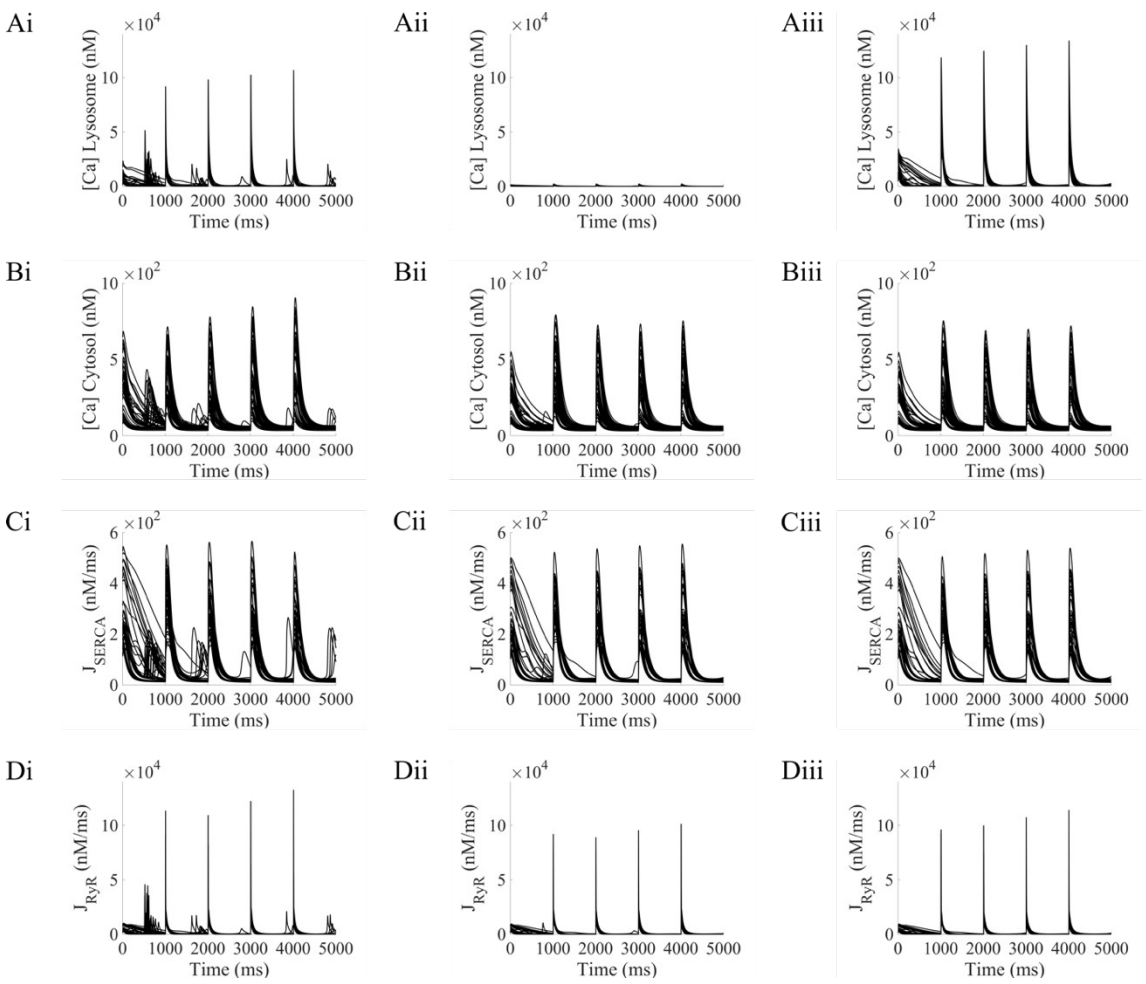


Figure 3.11. Lysosomal calcium release promotes spontaneous calcium release in TPC-specific proarrhythmic profiles under fast pacing and β-adrenergic stimulation, by increasing RyR open probability. **3.11Ai-3.11Di:** Lysosomal calcium concentration, cytosolic calcium concentration, and SR reuptake and release fluxes, respectively, in basal conditions. **3.11Aii-3.11Dii:** Calcium concentrations and fluxes under lysosomal uptake block ($J_{ls,up}=0$). **3.11Aiii-3.11Diii:** Calcium concentrations and fluxes under lysosomal release block ($J_{ls,rel}=0$). All results presented under preliminary fast pacing at 25 Hz.

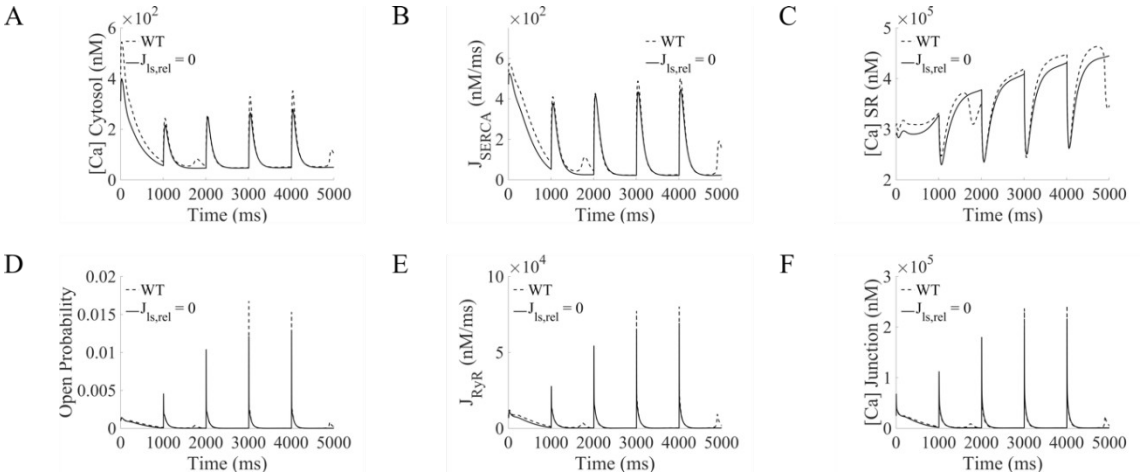


Figure 3.12. Loss of lysosomal calcium release flux reduced spontaneous calcium release from SR in TPC-specific proarrhythmic models under fast pacing and β-adrenergic stimulation. All results presented under initial fast pacing at 10 Hz. The transition from fast to slow pacing occurred at time 0. **3.12A-3.12F:** Example selected traces of cytosolic, SR and junctional calcium concentrations, SERCA flux, RyR open probability, and RyR flux, comparing scenarios in WT (dashed lines), and blocking lysosomal calcium release ($J_{ls,rel}=0$, solid lines).

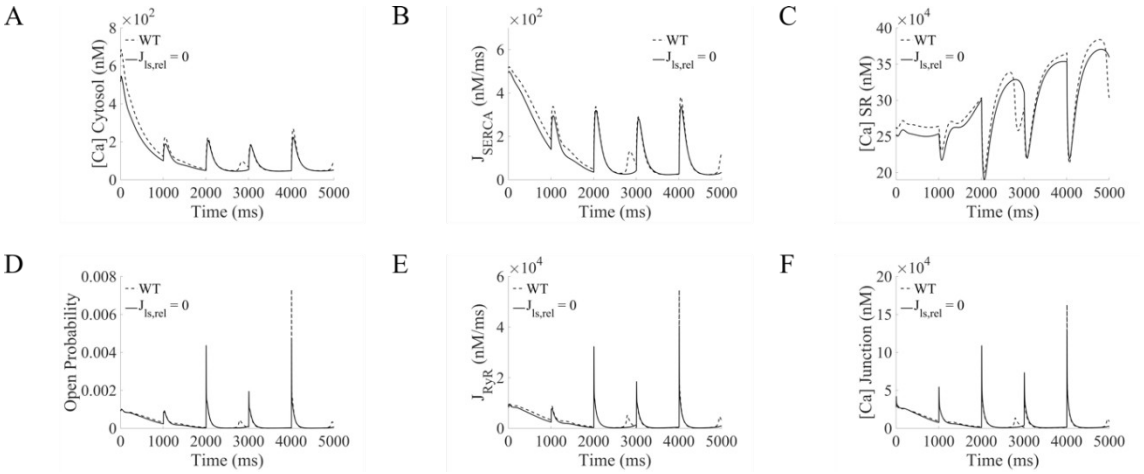


Figure 3.13. Loss of lysosomal calcium release flux reduced spontaneous calcium release from SR in TPC-specific proarrhythmic models under fast pacing and β-adrenergic stimulation. **3.13A-3.13F:** Traces of cytosolic, SR and junctional calcium concentrations, SERCA flux, RyR open probability, and RyR flux, comparing scenarios in WT (dashed lines), and blocking lysosomal calcium release ($J_{ls,rel}$=0, solid lines). The beats presented in the results are at 1Hz following 25Hz fast pacing protocol.

3.3 Discussion

In this chapter I present modifications to the well-established Morotti *et al.* cardiomyocyte model (Morotti *et al.*, 2014) to include a lysosomal calcium pool. To our knowledge, this work represents the first cardiac computational model to include a lysosomal compartment as part of beat-to-beat calcium signalling. Lysosomes are a store of calcium (Lloyd-Evans *et al.*, 2008) and release calcium in response to the endogenous second-messenger NAADP (Churchill *et al.*, 2002). Work published from our group and others has confirmed that lysosomal calcium signalling is constitutively active in both ventricular (Macgregor *et al.*, 2007; Nebel *et al.*, 2013) and atrial (Collins

et al., 2011) cardiomyocytes and contributes to β-adrenergic responses (Macgregor *et al.*, 2007; Collins *et al.*, 2011; Lewis *et al.*, 2012; Nebel *et al.*, 2013; Capel *et al.*, 2015). Further, abolishing lysosomal calcium signalling, either pharmacologically or by genetic ablation of the NAADP effector channel TPC2, is protective against cardiac hypertrophy and arrhythmias (Nebel *et al.*, 2013; Capel *et al.*, 2015). This modified model was used to probe the impacts of lysosomal calcium signalling under both physiological and proarrhythmic conditions.

After initial model construction, testing and validation (Figure 3.2), I used a population of models approach to generate a pool of models with a range of expression levels in other signalling proteins (e.g., I_{CaL}, RyR, SERCA). The model population was able to recapitulate experimental data: 'wild-type' cells responded to NAADP with an increase in calcium transient amplitude, TPC2-KO cells did not (Figure 3.3); TPC2-KO cells exhibited a reduced response to β-adrenergic stimulation by ISO (Figure 3.3) and a reduced propensity to arrhythmogenesis under proarrhythmic conditions (Figures 3.5 and 3.10). The major results of our simulation studies are consistent with a role for lysosomes in increasing calcium uptake to the SR by SERCA, release from the SR by RyRs and RyR open probability (Figures 3.4 and 3.9). The overall effect is to increase calcium release from the SR during CICR. In a small fraction of the models in our population, lysosomal calcium was found to be the direct cause of arrhythmogenesis under proarrhythmic conditions. Our further trials (Figures 3.6, 3.12 and 3.13) suggested that, when the balance of other signalling effectors is appropriate, lysosomes acting as a fast transport can effectively shunt the location of calcium to promote DAD formation.

In our simulations using this population of models, lysosomal calcium release primarily modulated intracellular calcium handling by increasing SERCA reuptake and subsequently RyR release. This is consistent with published data which suggest that stimulation of lysosomal calcium release with NAADP leads to an increase in SR calcium load, as measured by caffeine transient (Macgregor *et al.*, 2007; Collins *et al.*, 2011).

Our published work in ventricular cardiomyocytes and ex vivo cardiac tissue suggest that TPC2-KO is protective against the development of cardiac arrhythmias under conditions of acute or chronic high-dose β-adrenergic stimulation (Capel *et al.*, 2015). This is also true of acute ISO exposure in single cells where TPC2 channels have been inhibited pharmacologically (Nebel *et al.*, 2013). As an analogous set of experiments, we exposed the population of 423 accepted models to proarrhythmic conditions in both WT and TPC2-KO configurations. Similar to published data, we found that TPC2-KO is protective against the genesis of arrhythmia: 52% of WT models exhibited spontaneous events under β-adrenergic stimulation and high calcium, but this fell to 44% in TPC2-KO. Moreover, 59% of WT models exhibited spontaneous events under β-adrenergic stimulation and fast pacing, but this fell to 44% in TPC2-KO.

In a sub-population of the accepted models exposed to proarrhythmic conditions, the WT model was found to be arrhythmic and the corresponding TPC2-KO was not. These models comprised n=30 for raised extracellular calcium with β-adrenergic stimulation and n=60 for rapid pacing and β-adrenergic stimulation, or 16% (30/186) and 25% (60/243) of all models which exhibited arrhythmia for each proarrhythmic condition respectively. Analysis of the intracellular calcium traces during the genesis of spontaneous activity showed a profile of DADs arising from spontaneous SR calcium release (Figures 3.5 and 3.7).

One way to consider the specific effects of lysosomal fluxes on models exhibiting TPC2-dependent arrhythmias is to investigate the consequence of removing lysosomal calcium contributions, flux-by-flux, from the WT versions of the models in question. Removing these fluxes from the models with TPC2-dependent arrhythmias (Figures 3.5 and 3.10), regardless of the specific proarrhythmic condition, led to decreases in: SERCA calcium flux, RyR calcium flux, SR calcium content and RyR open probability. Taken together, this would suggest a conclusion consistent with that seen in our physiological signalling study: the presence of lysosomal calcium release boosts SR calcium content and release by acting as a fast transport.

I conclude that lysosomal calcium handling primarily modulates intracellular calcium handling by increasing SERCA reuptake and RyR release in normal loading condition, and that enhanced lysosomal calcium handling in calcium overload conditions promotes RyR spontaneous calcium release by increasing RyR open probability and RyR release (Figure 3.14).

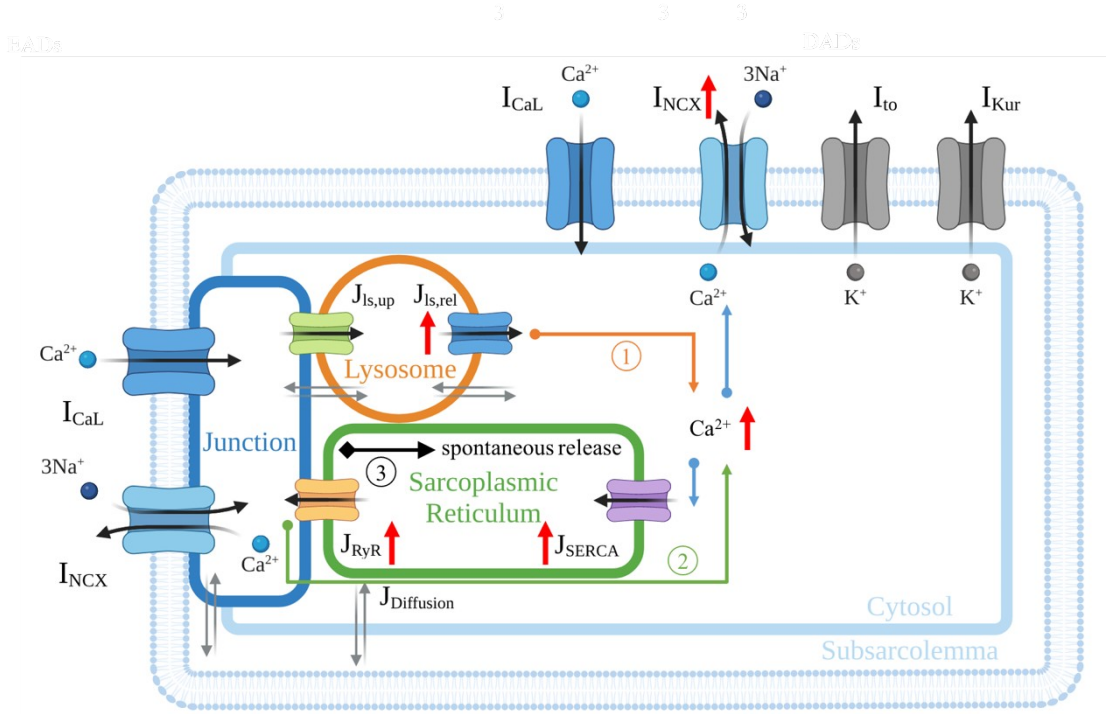


Figure 3.14. Schematic cartoon showing the conclusions for actions of lysosomal calcium handling.

3.3.1 Limitations

The approach for lysosomal calcium handling modelling effectively considers the lysosomes as a separate compartment, feeding from the junctional space (shared by I_{CaL} channels and RyRs) and releasing their calcium load into the cytosol. This, together

with appropriate considerations of lysosomal volume size, allows the lysosomal compartment to achieve high local calcium concentrations compared to the cytosol. Given that the cytosolic space is shared by CaMKII and phospholamban/SERCA, the lysosomal compartment can therefore be conceptually interpreted as in close proximity to these proteins, with lysosomal calcium release via TPC2 being able to directly modulate their function. Shall sufficient evidence become available; the proposed modelling could be expanded to consider different (nano-)domain configurations.

Previous studies (Capel *et al.*, 2015) have shown that TPC2-KO reduced arrhythmic propensity under adrenergic stress conditions, and that calcium transient amplitude was reduced when blocking lysosomal release. Although these findings were replicated by our model, the reduced calcium transient could also have knock on effects on other downstream targets, not directly described in the model formulation. In addition, pharmacological observations (Capel *et al.*, 2015) have also shown that CaMKII is required for responses to NAADP in ventricular myocytes from guinea pig and mice. Although CaMKII is accounted for in the Morotti *et al.* model (Morotti *et al.*, 2014), we did not investigate in detail its interactions with lysosomal function. We hope to address these aspects in future research.

Chapter 4

Lysosomal Calcium release Primarily Modulates Intracellular Calcium Handling by Increasing SERCA Reuptake and RyR Release in Human Atrial Cardiomyocytes

Summary of contribution: This chapter presents my work to incorporate lysosomal calcium handling in human atrial cardiomyocyte, calibrate the atrial model including lysosome with experimental data, and to investigate the role of lysosomal calcium release in normal loading. I carried out the modelling of including lysosomal calcium handling in human atrial cardiomyocyte model, conducted the calibration and validation of the atrial model with experimental data, the simulation of populations of models, and the investigation of the role of lysosomal calcium release in normal loading under baseline and ISO protocols. Additionally, I did methodology and writing of the project.

4.1 Introduction

Several types of LSDs are related to cardiac disorders with increased risk of arrhythmia (Laney, Gupta and Wechsler, 2018). Anderson Fabry disease is the second most prevalent LSD (Klingelhöfer *et al.*, 2020) and about over 50% of Fabry patients show cardiac symptoms, typically atrial or ventricular arrhythmias, with atrial arrhythmia more common (Mehta *et al.*, 2004; Morrissey, Philip and Schwarz, 2011). Currently, there are two types of LSDs related to calcium dysfunction of acidic store, NPC (Niemann Pick type C) and MLIV (mucolipidosis type IV). NPC shows reduction in calcium release mediated by NAADP, resulting in hindered lysosomal function while the increased calcium release in MLIV leads to enhanced endocytic pathway fusion (Morgan *et al.*, 2011).

A previous study showed that inhibition of lysosomal release by TPC2-KO reduced the tendency of ventricular arrhythmias under β-adrenergic stimulation (Capel *et al.*, 2015). In atrial cardiomyocytes, though the SR was regarded as the essential role in regulating calcium transient, NAADP acted on acidic stores (lysosomes) to release calcium (Collins *et al.*, 2011). NAADP increased the calcium transient amplitude with no effect on AP or L-type calcium current (Collins *et al.*, 2011). Disruption of lysosomes by GPN reduced the increased calcium transient by ISO, showing that lysosome calcium release actively contributed to calcium transient increase under β-adrenergic stimulation (Collins *et al.*, 2011). However, the proarrhythmic role of lysosomal release in human atrial cardiomyocytes is currently unknown.

Currently, there is no direct experimental evidence for the lysosome in pro-arrhythmia in human atrial cardiomyocytes. Based on my modelling work of lysosomal calcium handling in mouse ventricular cardiomyocytes presented in Chapter 3 of this thesis (by expanding the computational model by Morotti *et al.* (Morotti *et al.*, 2014)), the role of lysosome in human atrial electrophysiology will be addressed by including lysosomal calcium handling in the human atrial cardiomyocyte model by Grandi *et al.* (Grandi *et*

al., 2011). The Morotti *et al.* mouse ventricular model and Grandi *et al.* human atrial model were different in calcium transient and AP morphologies, currents densities, and fluxes densities in intracellular calcium handling, although their mathematical formulations were similar. The models were used in different investigations of spontaneous calcium release and EADs and were able to incorporate lysosomal calcium handling to investigate its proarrhythmic role. Given their similarities in terms of mathematical formulation of the two models, lysosomal calcium handling has been successfully incorporated into the human Grandi model in this Chapter. This chapter aims to investigate the role of lysosomal calcium release in human atrial cardiomyocyte in normal loading.

The human atrial baseline Grandi *et al.* (Grandi *et al.*, 2011) model including lysosomal calcium handling is calibrated with experimental traces of calcium transient and AP, and with experimental values of calcium transient and AP biomarkers at increasing pacing frequencies under ISO administration. The baseline model is used to construct a population of human atrial cardiomyocyte models, which are calibrated by experimental values (obtained from our collaborators lab Prof Niels Voigt, Germany) of AP biomarkers in nSR and cAF (Sánchez *et al.*, 2014).

I hypothesise that lysosomal calcium release might modulate intracellular calcium handling by increasing SERCA reuptake and RyR release (Figure 4.1).

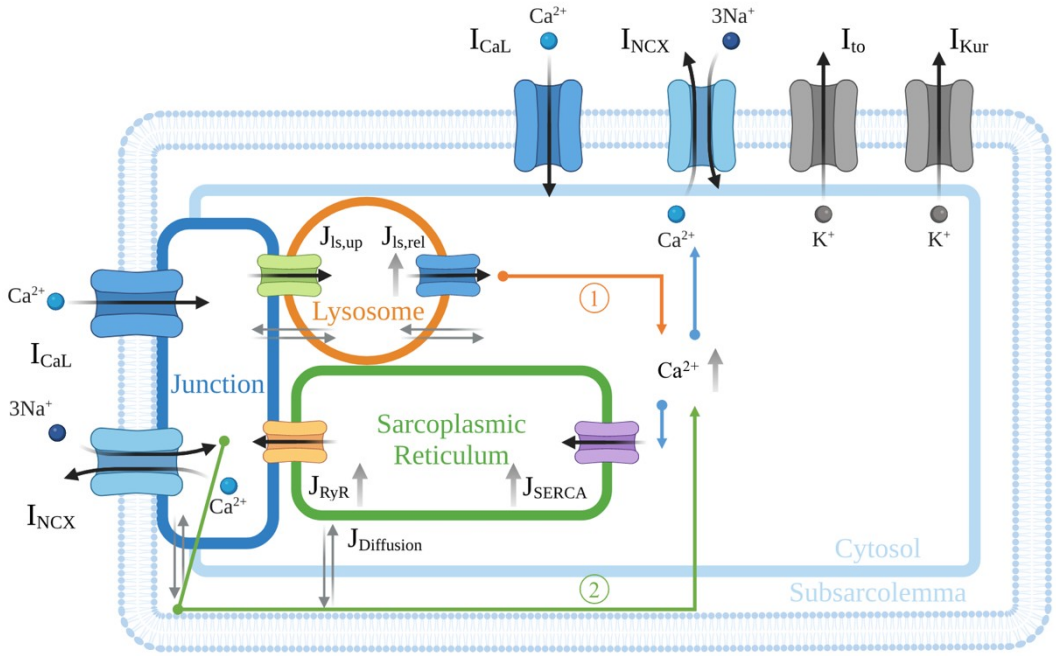


Figure 4.1. Schematic cartoon showing the hypothesis for actions of lysosomal calcium release.

4.2 Results

4.2.1 Calibration of Human Atrial Cardiomyocyte Model Incorporating Lysosome Function

To investigate the role of lysosomal calcium handling in atrial function, we extended the human atrial model by Grandi *et al.* (Grandi *et al.*, 2011) with a lysosome compartment. In brief, based on experimental evidence on lysosomal function and human two-pore

channels (Pitt *et al.*, 2010, 2014; Lewis *et al.*, 2012; Nebel *et al.*, 2013; Capel *et al.*, 2015; Ruas *et al.*, 2015; Garrity *et al.*, 2016; Pitt, Reilly-O'Donnell and Sitsapesan, 2016; Aston *et al.*, 2017), lysosomal calcium handling was modelled as a fast buffer for mediating calcium loading in junctional subspace to cytosolic subspace via TPC channels. NAADP activated TPC1 and TPC2 while TPC2 is more selective for calcium and capable of greater calcium release than TPC1 (Pitt *et al.*, 2010, 2014; Ruas *et al.*, 2015; Pitt, Reilly-O'Donnell and Sitsapesan, 2016). We adopted the TPC2 open probability distribution on NAADP concentration to describe the TPC opening (Pitt *et al.*, 2010; Penny *et al.*, 2014). Thus, the lysosome subspace directly modulates calcium handling in junction during the CICR process.

Model calibration was conducted as follows. TPC openings are very brief with open probability P_O<0.0009, without activating ligands NAADP (Pitt *et al.*, 2010). The response of TPC opening to NAADP concentration was based on a previously validated Gaussian distribution. TPC showed an upper bound for P_O of 0.0016 by an endogenous *[NAADP]* value at 1 nM for $P_O = 0.0134$, and by the *[NAADP]* value at 15 nM for opened channel, as observed in experimental findings (Pitt *et al.*, 2010). Next, lysosomal calcium release mediated by the *[NAADP]* concentrations were calibrated in experimental data, respectively in nSR and cAF.

My previous study in the modelling of lysosomal release in mouse ventricular cardiomyocytes showed the involvement of lysosomal calcium release in the onset of cardiac arrhythmias by acute or chronic high dose β-adrenergic stimulation (Meng *et al.*, 2023). To focus on these findings, I went through a thorough calibration and validation of β-adrenergic stimulation in the modified human atrial model against simultaneously acquired calcium transient and AP recordings from human atrial nSR and cAF cardiomyocytes in the absence and presence of ISO administration.

Experimentally, β-adrenergic stimulation by 1 μM ISO increased calcium transient amplitude with similar diastolic calcium at 0.25Hz, respectively by nearly 2-fold in nSR vs nearly 1.6-fold in cAF, compared to the application 'Before ISO' (Figures 4.2A, 4.2B). Recapitulation of the experimental traces by the original Grandi *et al.* (Grandi *et*

al., 2011) led to an overestimation in the rise of calcium transient amplitude and to obviously reduced diastolic calcium levels by ISO action (Figures 4.2Ai, 4.2Bi). This might be due to the L-type calcium influx, RyR release and SERCA reuptake were too large, thus a larger CICR led to the rise of calcium transient amplitude and reduced diastolic calcium levels. In the calibration of calcium transient, I increased the amplitudes of RyR and SERCA fluxes, and L-type current in β-adrenergic stimulation, respectively by 2.6-fold, 1.8-fold, and 1.6-fold in nSR and by 1.7-fold, 1.6-fold and 1.7-fold in cAF. This led to recapitulate the experimental traces by the modified human atrial model. Simulated ISO application at 1μM, recapitulated the increases in calcium transient amplitudes by around 2-fold in nSR and around 1.4-fold in cAF and preserved the diastolic calcium levels, respectively in nSR and cAF (Figures 4.2Aii, 4.2Bii).

Experimental traces of AP in nSR and cAF exhibited prolonged APD at 20% and 50% (APD_{20} and APD_{50}), and similar values of APD_{90} in 'Before ISO' and 'After ISO' (Figures 4.2C, 4.2D). By simulation of 1μM ISO, the original Grandi *et al.* (Grandi *et al.*, 2011) model led to considerable prolongation of AP in nSR and cAF (Figures 4.2Ci, 4.2Di). In calibration of the AP, I kept the modifications for the calcium transients. The modifications of the calcium transient might also contribute to the calibration of AP. I focused on recapitulating the similar duration at APD_{90} in the comparison of 'After ISO' and 'Before ISO'. In nSR, I applied a 1.7-fold amplitude increase of the I_{Ks} in After ISO compared to Before ISO, while in cAF I additionally applied a 5-fold amplitude increase of the I_{K1} compared to in nSR in After ISO (Figures 4.2Cii, 4.2Dii right panels). The modifications of I_{Ks} and I_{K1} contributed to repolarisation of phase 3 in the AP, and led to the recapitulation of APD in nSR and cAF. I acknowledge the limitations that the simulated APs still look different to the experimental traces. Given the scarcity of experimental data, I focused on recapitulation of calcium transients and APD at 90%. As the investigation was focused on the proarrhythmic role of lysosomal calcium handling, this recapitulation fits the research aim.

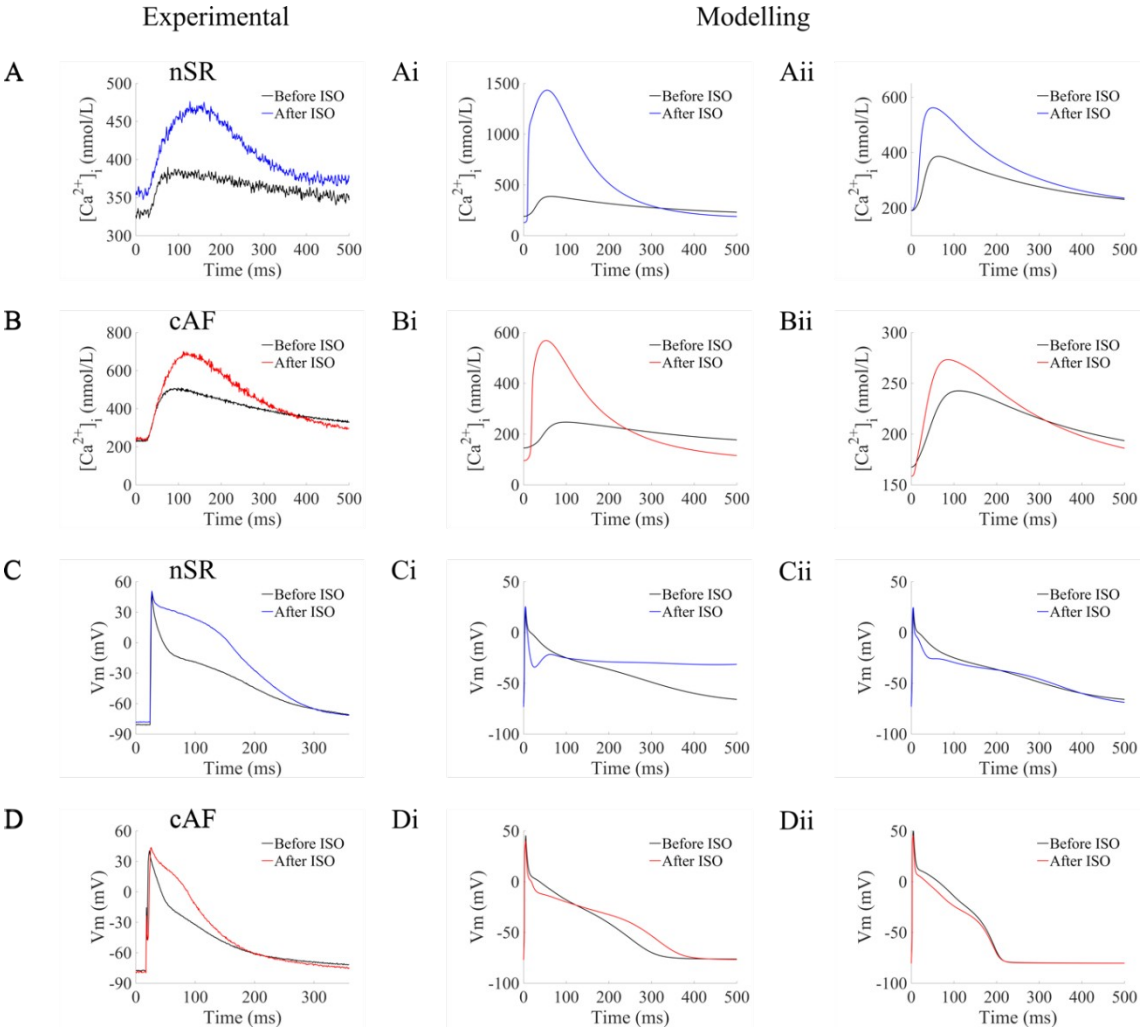


Figure 4.2. Calibration of human atrial cardiomyocyte model incorporating lysosomal calcium handling. **4.2A, 4.2B:** Experimental traces of calcium transient at 0.25Hz before and after ISO at 1 μmol/L on atrial myocytes from patients in nSR and cAF. **4.2Ai, 4.2Bi:** Simulated traces of calcium transient at 0.25Hz before and after ISO by the original Grandi *et al.* (Grandi *et al.*, 2011) model in nSR and cAF, respectively. **4.2Aii, 4.2Bii:** Simulated traces of calcium transient at 0.25Hz before and after ISO by the modified model in nSR and cAF, respectively. **4.2C, 4.2D:** Experimental traces of action potential before and after ISO at 1 μmol/L on atrial myocytes in nSR and cAF. **4.2Ci, 4.2Di:** Simulated traces of action potential before and after ISO by the original Grandi *et al.* (Grandi *et al.*, 2011) model in nSR and cAF, respectively. **4.2Cii, 4.2Dii:** Simulated traces of action potential before and after ISO by the modified model in nSR and cAF.

The values of the experimental data were summarised in the metrics of diastolic calcium, calcium transient amplitude, resting membrane potential, AP amplitude, APD_{50} and APD_{90}, comparing the experimental findings before and after ISO application. In diastolic calcium, no overall significant trend was shown in nSR while diastolic calcium tended to elevate in ISO in cAF (Figure 4.3A). Calcium transient amplitude showed an increasing trend in nSR and no overall significant trend in cAF (Figure 4.3B). Resting membrane potential showed increasing trends in nSR and cAF (Figure 4.3C). AP amplitude showed no overall significant trends in either nSR or cAF (Figure 4.3D). In terms of APD_{50}, great variability in cardiomyocytes response was observed, but without overall significant trends (Figure 4.3E). APD_{90} showed no overall significant trend in nSR while a decreasing trend in cAF (Figure 4.3F).

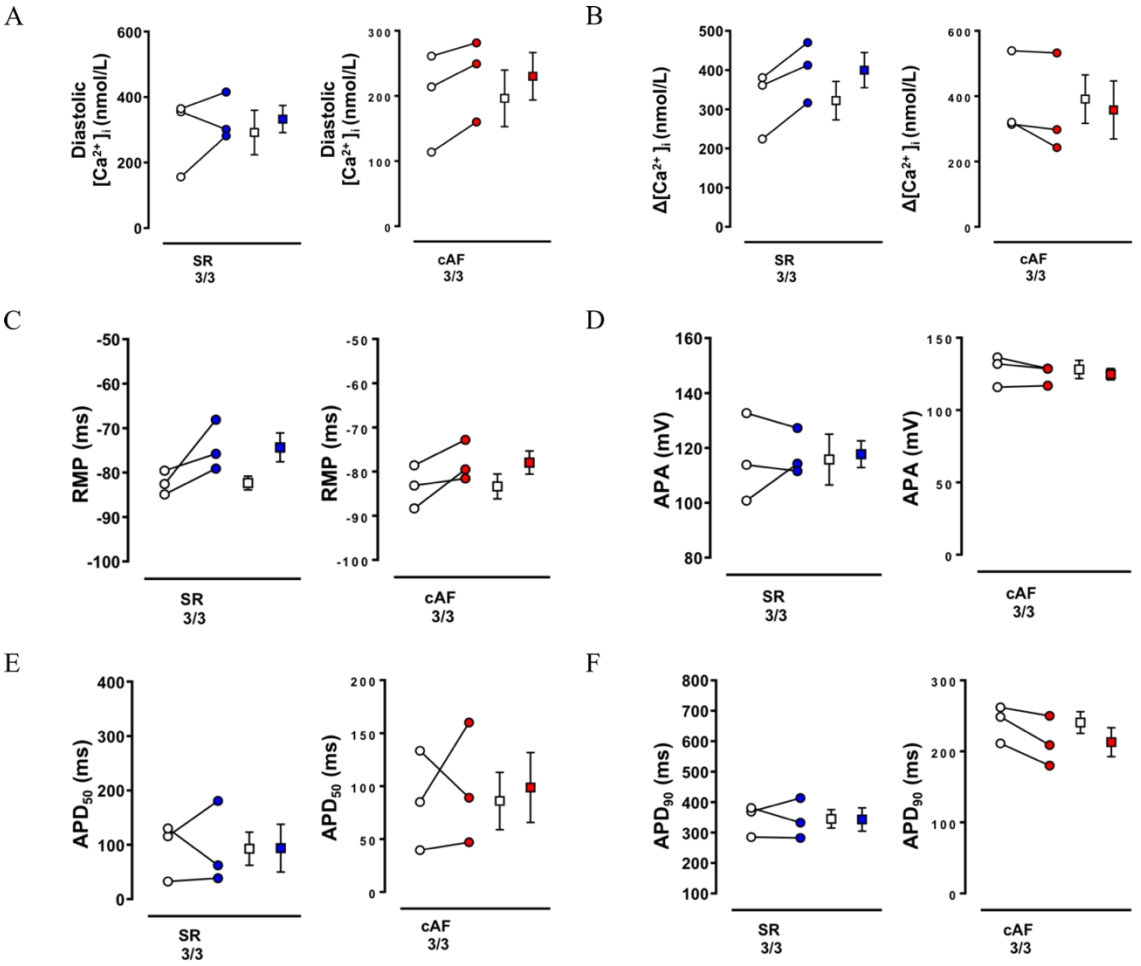


Figure 4.3. Measurements of β-adrenergic response in human atrial cardiomyocytes. Experimental data of calcium transient and action potential after 1 μM ISO in human atrial cardiomyocytes are presented as mean±SD in nSR and cAF, respectively (Data provided by Professor Neils Voigt group). **4.3A:** Diastolic intracellular calcium concentration. **4.3B:** Calcium transient amplitude (Δ¿¿). **4.3C:** Resting membrane potential (RMP). **4.3D:** Action potential amplitude (APA). **4.3E:** Action potential duration at 50% of repolarisation (APD_{50}). **4.3F:** Action potential duration at 90% of repolarization (APD_{90}).

Further validation was conducted by comparing biomarkers (diastolic calcium concentrations, calcium transient amplitudes, RMP, APA, APD_{50} and APD_{80}) after ISO application, by gradually increasing pacing frequencies from 0.25, 0.5, 1, 2, 4, 6 to 8 Hz in both nSR and cAF. The modified model (solid lines) better recapitulated diastolic calcium levels at faster pacing rates than the original Grandi *et al.* model (Grandi *et al.*,

2011) (dashed lines) in nSR and cAF (Figure 4.4A). The modified model also better recapitulated the calcium transient amplitude in nSR than the original model, especially at low pacing frequencies, and the non-monotonic trend in the observation of calcium transient amplitude rise in cAF (Figure 4.4B). In RMP and APA, both model variants showed similar trends, which relatively agreed with the experimental data (Figures 4.4C, 4.4D). In APD_{50}, the responses of both models were similar, and both models showed greater triangulation than the experimental trend in nSR, while a relatively closer agreement with the experimental trend in cAF (Figure 4.4E). In APD_{90}, the modified model also better retrieved the responses at lower pacing in nSR and in the whole frequency range in cAF (Figure 4.4F). In summary, these findings revealed that the modified model outperformed the capabilities of the original Grandi *et al.* model (Grandi *et al.*, 2011) in terms of rate response in both calcium transient and AP biomarkers under β-adrenergic stimulation.

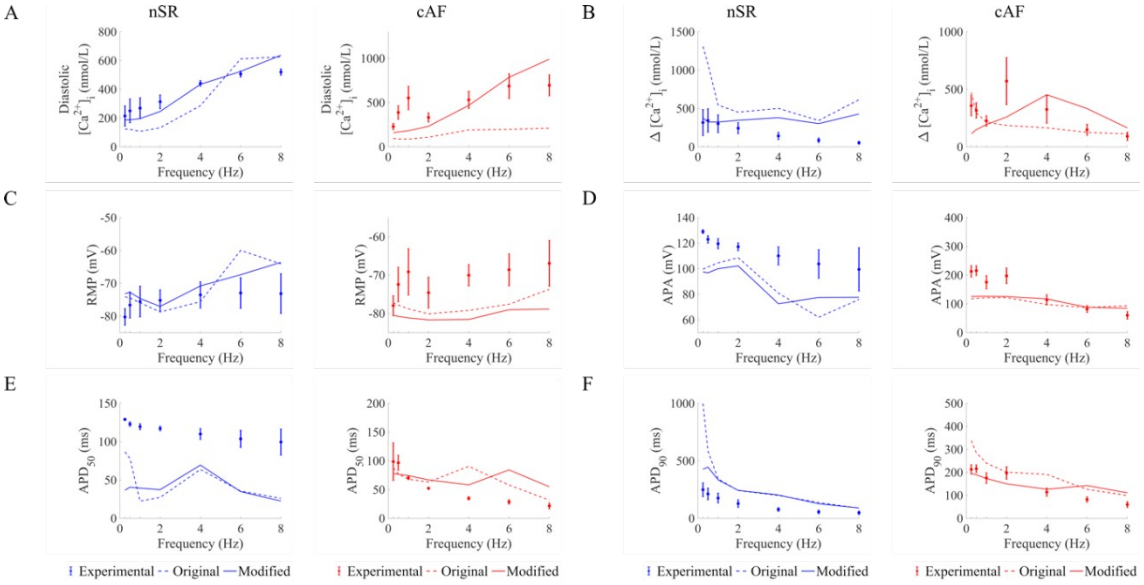


Figure 4.4. Validation of β-adrenergic stimulation in the modified human atrial cardiomyocyte model. Experimental calcium transient and action potential data after 1 μM ISO in human atrial cardiomyocytes are presented as mean±SD in nSR and cAF, respectively. Dashed/solid lines: the original Grandi *et al.* model/the modified model. **4.4A:** Diastolic calcium concentration. **4.4B:** Calcium transient amplitude (Δ¿¿). **4.4C:** Resting membrane potential (RMP). **4.4D:** Action potential amplitude (APA). **4.4E:** Action potential duration at 50% of repolarisation (APD_{50}). **4.4F:** Action potential duration at 90% of repolarisation (APD_{90}).

4.2.2 Calibration of Populations of Validated Human Atrial Models in Normal Sinus Rhythm and Chronic Atrial Fibrillation

To investigate the role of lysosomal calcium handling in human atrial electrophysiology, a population of models approach was exploited to account for cellular variability in ionic currents and intracellular calcium fluxes (Britton *et al.*, 2013; Muszkiewicz *et al.*, 2016). Initial populations of 1000 models were generated by means of uniform Latin hypercube sampling in nSR and cAF. For calibration against human experimental data, models were first filtered by exhibiting normal APs under scenarios of active lysosomal release in either baseline or ISO conditions, in both nSR and cAF.

In terms of experimental data considered for calibration in nSR and cAF, the minimum and maximum values used for the different AP biomarkers are listed in Table 4.1 (Sánchez *et al.*, 2014). 627 and 825 models were accepted as representative of human atrial physiological function within the experimental data ranges of nSR and in cAF, respectively. The populations formed by the 627 models in nSR and 825 models in cAF predict and resemble the distributions of AP biomarkers observed in the experimental data, as further validated in Figure 4.5 (Sánchez *et al.*, 2014). Subsequent data are reported using the populations.

In the distributions of APDs, the population of models agreed strongly with the experimental distributions of APD_{90} and APD_{20} values in nSR (Figures 4.5A, 4.5Ai, 4.5B, 4.5Bi). In cAF, good agreement was found between the distributions of

experimental and simulated APD_{90} and APD_{50} values (Figures 4.5C, 4.5Ci, 4.5D, 4.5Di).

experimental data	**nSR**		**cAF**	
	minimum value	**maximum value**	**minimum value**	**maximum value**
APD_{90} (ms)	190	440	140	330
APD_{50} (ms)	6	200	30	180
APD_{20} (ms)	1	60	1	75
APA (mV)	75	120	80	130
RMP (mV)	−85	−65	-85	-65
V_{20} (mV)	−35	10	-30	20
dV/dt_{max} (V/s)	40	420	40	420

Table 4.1. Calibration of the population of human atrial cardiomyocyte models in baseline by the action potential biomarkers in the experimental findings (Sánchez *et al.*, 2014). Biomarkers include action potential duration at 90 percent (APD_{90}), action potential duration at 50 percent (APD_{50}), action potential duration at 20 percent (APD_{20}), action potential amplitude (APA), resting membrane potential (RMP), plateau potential defined as the potential measured at 20% of the APD_{90} time (V_{20}), maximum upstroke velocity (dV/dt_{max}).

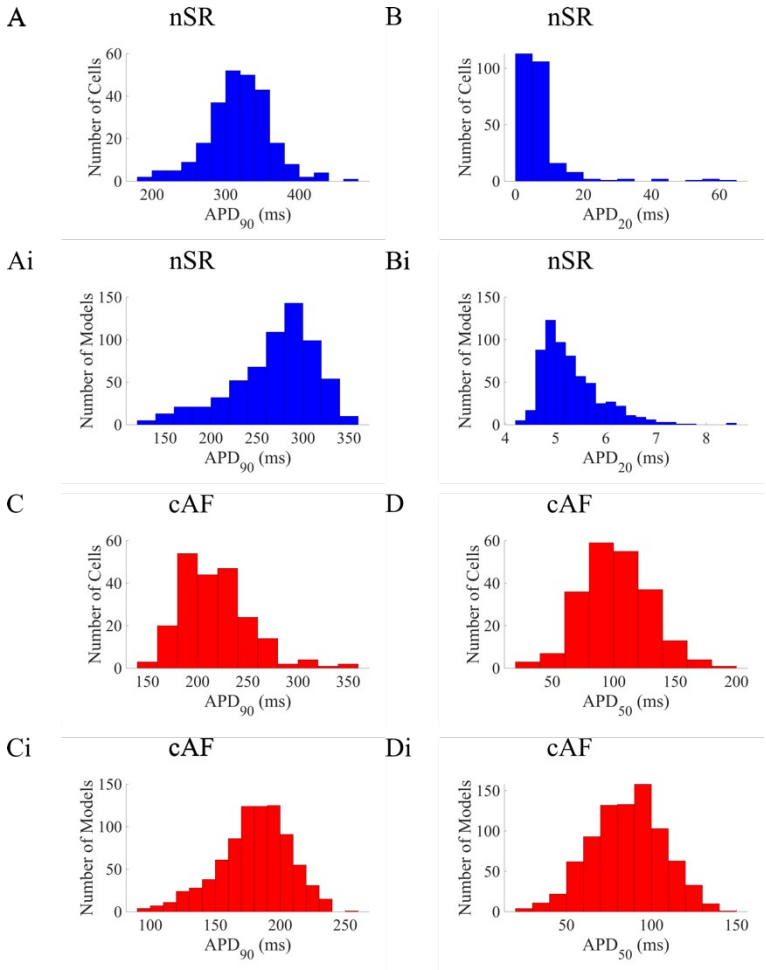


Figure 4.5. Calibration of populations of models in nSR and cAF in baseline conditions. **4.5A-4.5B, 4.5Ai-4.5Bi:** Histograms of APD_{90} and APD_{20} distributions, respectively, in experimental (A-B) and simulated (Ai-Bi) values in nSR. **4.5C-4.5D, 4.5Ci-4.5Di:** Histograms of APD_{90} and APD_{50} distributions, respectively, in experimental (C-D) and simulated (Ci-Di) values in cAF.

4.2.3 Comparison of the Presence and Block of Lysosomal Release in Calcium Loading in Normal Sinus Rhythm

The boxplots in Figure 4.6 show amplitude distributions of currents, calcium fluxes and concentrations that are involved in the intracellular calcium handling in nSR. Representative traces of calcium concentrations in each subspace, and the associated currents and calcium fluxes are shown in Figure 4.7 and 4.8, respectively. Results are presented for the two investigated pharmacological protocols (Baseline, ISO), as well as for the presence and the block of lysosomal release. In terms of the Baseline protocol, no main differences are observed in terms of effective sizes (medians difference) in comparison of the presence and the block of lysosomal release, though with larger lysosomal calcium release (Figures 4.6E, 4.8E, 4.8F) in the presence scenario and larger lysosomal calcium concentration (Figures 4.6B, 4.7A, 4.7B) in the block scenario. With a smaller lysosomal concentration and without its direct calcium release into cytosol (Figure 4.6E), the lysosomal calcium did not contribute to a significant amplitude increase in cytosol (Figures 4.6B, 4.6H).

For the ISO protocol, the β-adrenergic stimulation increased the intracellular calcium influx via the I_{CaL} with a similar extent in the presence and block scenarios (Figures 4.6A, 4.8A, 4.8B). For abbreviation, the fold changes of comparing ISO to Baseline were presented in the form of the presence versus block of lysosomal release. The higher 1.43-fold versus 2.11-fold lysosomal calcium loading (Figures 4.6B, 4.7A, 4.7B) resulted from the increased 7.52-fold versus 4.30-fold in lysosomal uptake flux (Figures 4.6C, 4.8C, 4.8D) and resulted in a 13.01-fold versus 2.23-fold in calcium release flux (Figures 4.6E, 4.8E, 4.8F). Blocking lysosomal release diminished adding calcium to cytosol without significant contribution to cytosolic amplitude increase (Figures 4.6H, 4.7G, 4.7H), although lysosomal calcium was loaded and part of it reverted to the

junction (Figures 4.6D, 4.8D). The increase in cytosolic calcium is mediated by both SR calcium release via RyR and lysosomal calcium release by TPC2. In the Figure 4.7H of TPC2-KO in ISO, the diastolic cytosolic calcium is reduced and the peak cytosolic calcium is increased, thus the calcium transient amplitude may be increased by normalising the diastolic calcium level in ISO and in baseline. An increased transport by lysosomal uptake and release took junctional calcium to cytosol, which gave rise to the increase of SERCA reuptake (Figures 4.8C, 4.8D, 4.8E, 4.8F, 4.8I, 4.8J). Thus, a higher SR calcium concentration led to (Figures 4.7I, 4.7J) a larger SR release (Figures 4.8K, 4.8L) into junction (Figures 4.7C, 4.7D).

The main consequence of this increased lysosomal calcium release was a 1.19-fold (comparing ISO to Baseline in WT) versus 1.01-fold (comparing ISO to Baseline in TPC2-KO), amplitude elevation of calcium load in the cytosolic space (Figures 4.6H, 4.7G), as the additional calcium load in the junctional subspace quickly mobilised through diffusion into the subsarcolemma (Figures 4.6D, 4.6F, 4.7C, 4.7E). In particular, the above-described changes led to a systolic increase in the calcium transient with a similar diastolic level, and the diastolic level in ISO was reduced in both scenarios (Figures 4.7G, 4.7H). In both cases, increased calcium load in subsarcolemma (Figures 4.6F, 4.7E, 4.7F) activated the forward mode of NCX current with calcium extrusion, respectively compared to Baseline (Figures 4.6G, 4.8G, 4.8H), while this was negligible by comparing the presence and block of lysosomal release (Figures 4.6G, 4.8G, 4.8H). However, the increased calcium loading in cytosol enhanced the 1.28-fold (comparing ISO to Baseline in WT) versus 1.09-fold (comparing ISO to Baseline in TPC2-KO) SERCA reuptake (Figures 4.6I, 4.8I, 4.8J). This consequently led to a higher 1.05-fold versus 0.95-fold SR calcium load (Figures 4.6J, 4.7I, 4.7J) and a stronger 1.27-fold versus 1.14-fold calcium release through RyR (Figures 4.6K, 4.8K, 4.8L), the latter therefore contributing to the larger systolic peak of the cytosolic calcium (Figures 4.6H, 4.7G, 4.7H). There exists a small difference in cytosolic calcium in baseline versus ISO for the TPC2-KO, which can be viewed in the traces in Figure 4.7H. In TPC2-KO in ISO, cytosolic calcium showed a reduced diastolic level and the peak is increased, thus the calcium transient amplitude is increased. Nevertheless, the increase might be small due to the loss of positive feedback between lysosomal calcium release

and SERCA reuptake. This increased loading in cytosolic calcium by lysosome did not lead to significant change of APD (Figures 4.6L, 4.7K, 4.7L). The populations in comparison of Before ISO and After ISO, predicted 0.22±0.01 or 0.04±0.01 in the range of the normalised amplitude increase of cytosolic calcium, respectively in the presence and block of lysosomal release. In summary:

- Lysosomal release increased cytosolic calcium loading to potentiate SERCA reuptake in ISO. The increased SR calcium content promoted RyR release.
- Blocking lysosomal release decreased calcium loading in cytosol and SERCA reuptake in ISO. The reduced SR calcium content decreased RyR release.

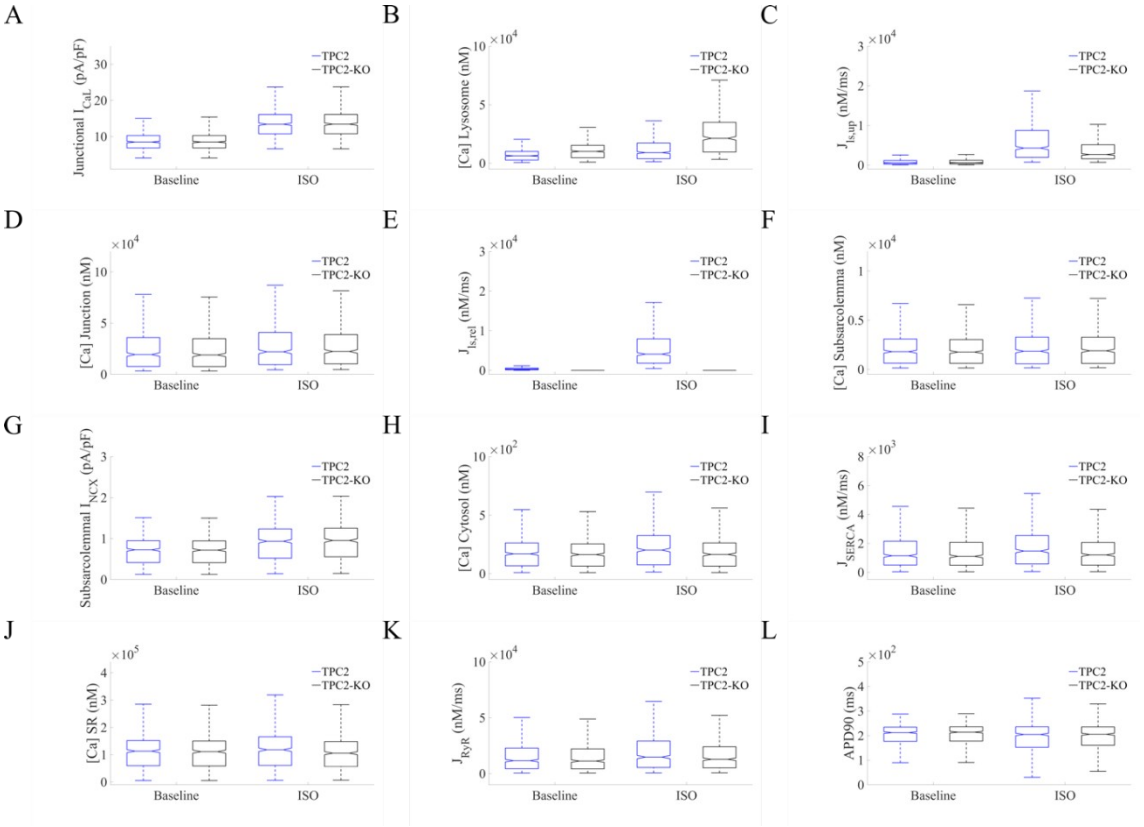


Figure 4.6. Distributions of currents, fluxes, concentrations and action potentials. **4.6A-4.6L** are the boxplots of amplitudes of currents and calcium fluxes, calcium concentrations in each subspace, and APD_{90}, across protocols of baseline and ISO, respectively.

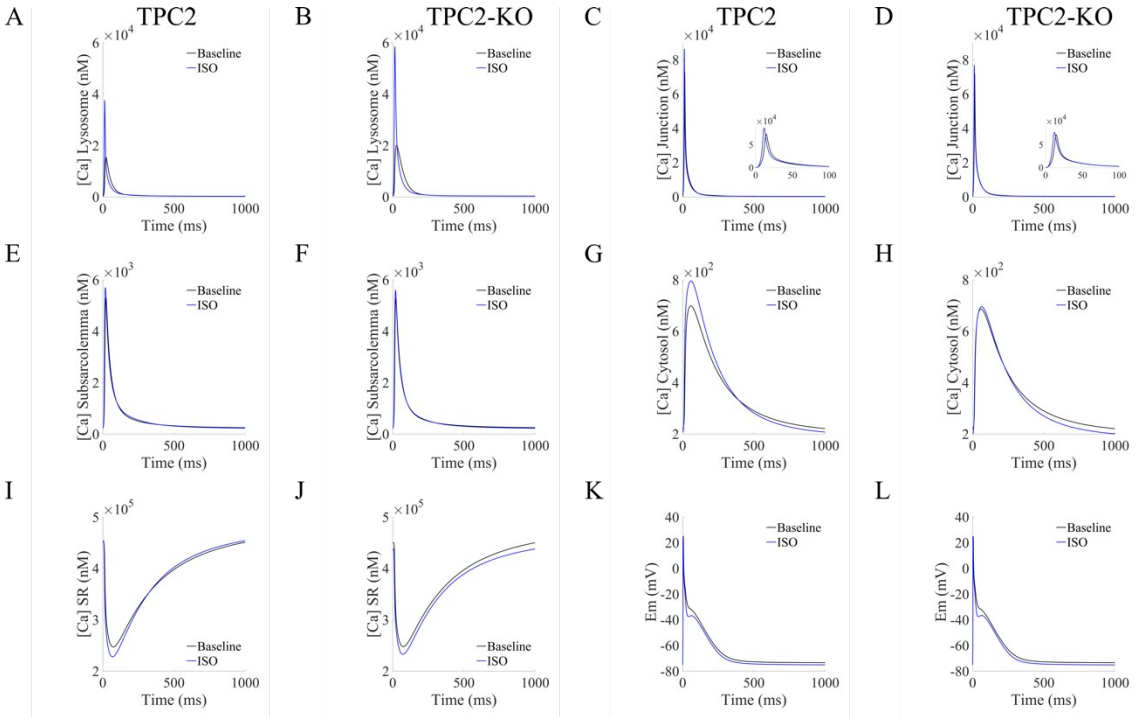


Figure 4.7. Representative traces of the calcium concentrations and action potentials. **4.7A, 4.7C, 4.7E, 4.7G, 4.7I, 4.7K** shows for a representative model the traces of calcium concentrations and action potential in subspaces across baseline and ISO protocols in the presence of lysosomal release (TPC2). **4.7B, 4.7D, 4.7F, 4.7H, 4.7J, 4.7L** the same model is shown under the block of lysosomal release (TPC2-KO).

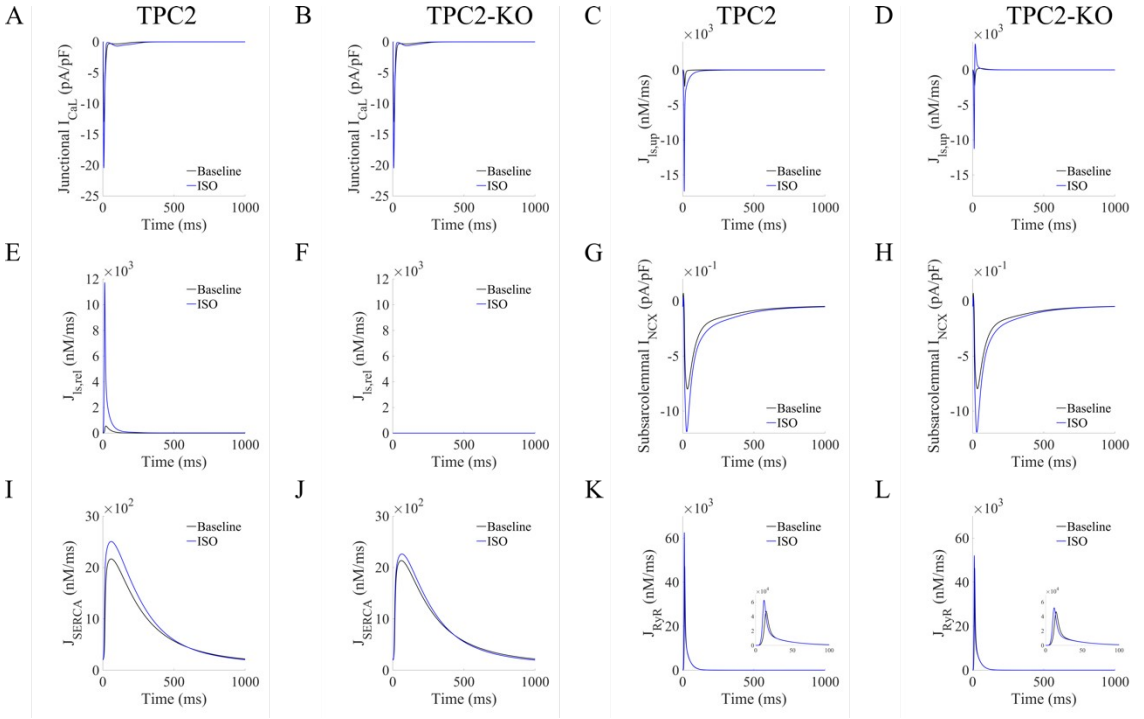


Figure 4.8. Representative traces of the currents and calcium fluxes. **4.8A, 4.8C, 4.8E, 4.8G, 4.8I, 4.8K** shows for a representative model the traces of calcium currents and fluxes across baseline and ISO protocols in the presence of lysosomal release (TPC2). **4.8B, 4.8D, 4.8F, 4.8H, 4.8J, 4.8L** the same model is shown under the block of lysosomal release (TPC2-KO).

To further analyse the influence of lysosomal calcium on calcium transient and AP biomarkers, partial correlation coefficients were used to quantify the correlations between each flux or current that was varied in the accepted population and each biomarker across the investigated protocols, in the presence and block of lysosomal release (Figure 4.9). Across the protocols in nSR, the influence of lysosomal uptake and release fluxes ($J_{ls,up}$ and $J_{ls,rel}$), on the calcium transient amplitude (Ca_{AMP}) became more important in ISO (Figure 4.9C), even though their contributions were minimum in baseline (Figure 4.9A). In ISO, $J_{ls,rel}$ became more important in modulating calcium transient biomarkers, such as the Ca_{AMP}, even surpassing SERCA flux (J_{SERCA}) (Figure 4.9C). The partial correlation coefficient value of J_{SERCA} in the TPC2-KO may be small. This might show loss of lysosomal calcium release to cytosol, might reduce the SERCA potentiation, and lysosomal calcium release and SERCA reuptake may be in a positive feedback. In baseline and ISO, the influence of $J_{ls,rel}$ on the biomarkers of calcium

transient was all reduced under block of lysosomal release, compared to in the presence scenario (Figures 4.9A, 4.9B, 4.9C, 4.9D).

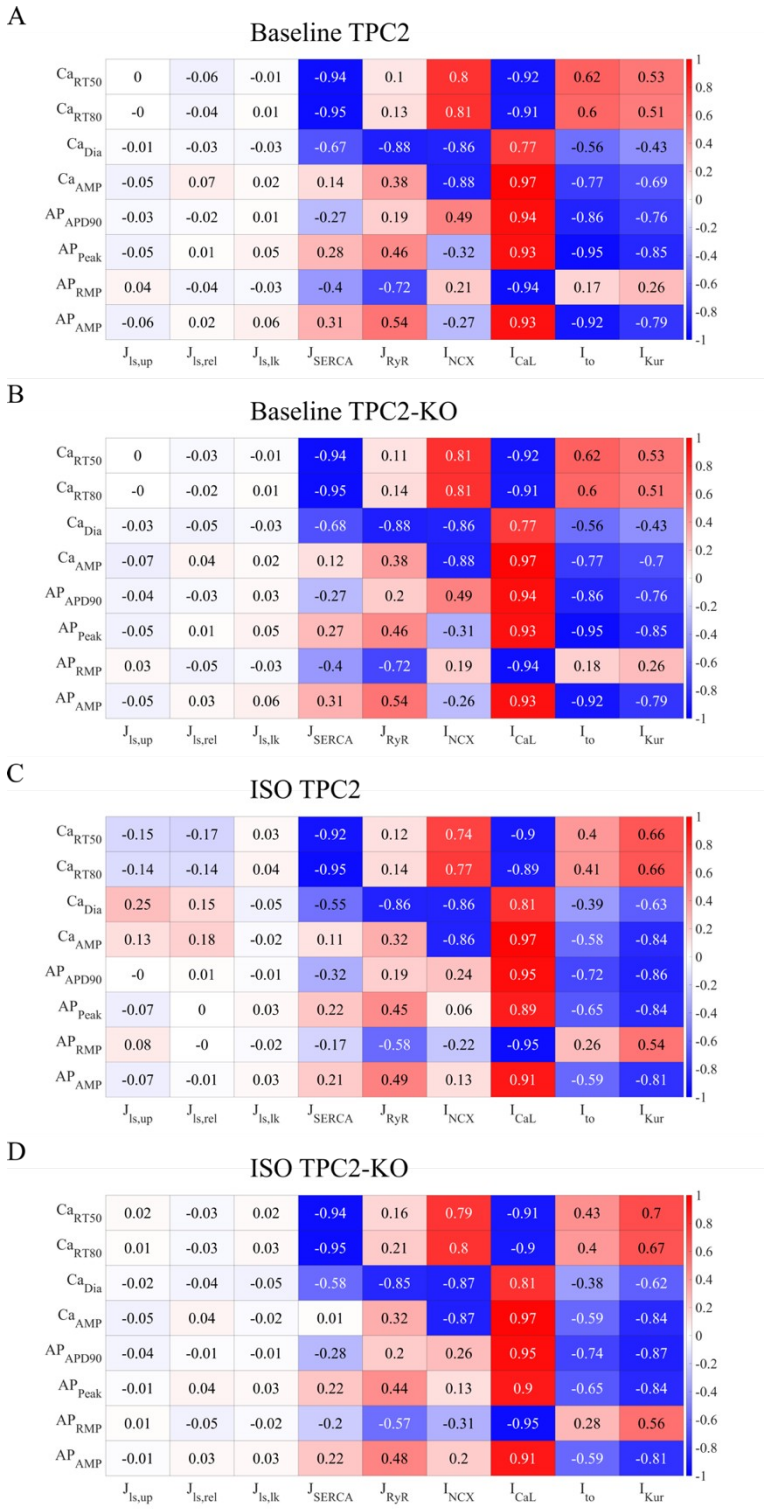


Figure 4.9. Partial correlation coefficients between varied fluxes and currents and the biomarkers of calcium transient and action potential. **4.9A-4.9D** showed the Spearman partial correlation coefficients in heatmaps across Baseline and ISO in the presence and block of lysosomal release (TPC2, TPC2-KO), respectively.

4.2.4 Comparison of the Presence and Block of Lysosomal Release in Calcium Loading in Chronic Atrial Fibrillation

The boxplots in Figure 4.10 show the amplitude distributions of currents, calcium fluxes and concentrations involved in intracellular calcium handling in cAF. Representative traces of calcium concentration in each compartment and the associated currents and calcium fluxes are shown in Figures 4.11 and 4.12, respectively. Results are also shown in Baseline and ISO, as well as the presence and block of lysosomal release. In Baseline, no main differences were observed in medians in the presence and block of lysosomal release, except lysosomal calcium uptake and release (Figures 4.10C, 4.10E, 4.12C, 4.12D, 4.12E, 4.12F) and concentration (Figures 4.10B, 4.11A, 4.11B). Blocking lysosomal calcium release did not contribute to an amplitude increase in cytosolic calcium (Figures 4.10B, 4.10H, 4.11A, 4.11B, 4.11G, 4.11H).

For the ISO protocol in cAF, the increased L-type calcium current brought a similar extent of calcium influx in the presence and block scenarios (Figures 4.10A, 4.12A, 4.12B). For abbreviation, the fold changes of comparing ISO to Baseline are presented in the form of the presence versus block of lysosomal release. An increase of 8.43-fold versus 3.70-fold in lysosomal uptake flux (Figures 4.10C, 4.12C, 4.12D) resulted in the higher 1.43-fold versus 1.97-fold calcium load in lysosome, in comparison of Baseline and ISO (Figures 4.10B, 4.11A, 4.11B). Thus, lysosomal release flux was increased by a 12.12-fold versus a 2.05-fold (Figures 4.10E, 4.12E, 4.12F).

The main consequence of this larger lysosomal release is a 1.31-fold versus 1.14-fold amplitude elevation of calcium loading in the cytosol, by comparison of Baseline and ISO protocols (Figures 4.10H, 4.11G, 4.11H). Under block of lysosomal release, the loaded lysosomal calcium did not contribute to the amplitude increase in the cytosol (Figures 4.10B, 4.10H, 4.11A, 4.11B, 4.11G, 4.11H), although it flowed backward to the junction (Figures 4.11D, 4.12D), which showed a smaller junctional loading compared to in the presence scenario (Figures 4.10D, 4.11C, 4.11D). Meanwhile, calcium in the junctional subspace fast mobilised through diffusion into the subsarcolemma (Figure 4.10D, 4.10F, 4.11C, 4.11E), also contributing to the increased cytosolic calcium load (Figure 4.10H, 4.11G). In particular, the increased loading in the cytosol in ISO was observed with a systolic increase in the active lysosome release scenario compared to the block scenario and a similar diastolic level in both scenarios, while both diastolic levels were reduced in ISO compared to Baseline (Figures 4.11G, 4.11H). The increased calcium load in the subsarcolemma (Figures 4.10F, 4.11E, 4.11F) led to stronger calcium extrusion by NCX forward mode (Figures 4.10G, 4.12G, 4.12H) in ISO compared to in Baseline, while minimal in the comparison of the presence and block scenarios in ISO (Figures 4.12G, 4.12H).

The increased calcium loading in the cytosol strengthened 1.28-fold versus 1.12-fold the calcium reuptake by SERCA (Figures 4.10I, 4.12I, 4.12J). This led to a higher 1.11-fold versus 1.01-fold SR calcium load (Figures 4.10J, 4.11I, 4.11J) and an increased 1.36-fold versus 1.25-fold calcium release by RyR (Figures 4.10K, 4.12K, 4.12L), the latter consequently contributing to the higher loading in junction and therefore the larger systolic peak of the calcium transient (Figures 4.11C, 4.11G). The increased loading in intracellular subspaces by active lysosome release did not lead to changes of APD (Figures 4.10L, 4.11K, 4.11L). At the population level, the comparison between Before ISO and After ISO protocols predicted an increase of normalised cytosolic calcium amplitude of 0.28 ± 0.01 or 0.11 ± 0.00, in the presence and block of lysosomal release, respectively. In summary:

- Lysosomal release potentiated SERCA reuptake by increasing cytosolic calcium loading in ISO. The increased SR calcium content promoted RyR release.

- Blocking lysosomal release decreased SERCA reuptake by reducing calcium loading in cytosol in ISO. The reduced SR calcium content decreased RyR release.

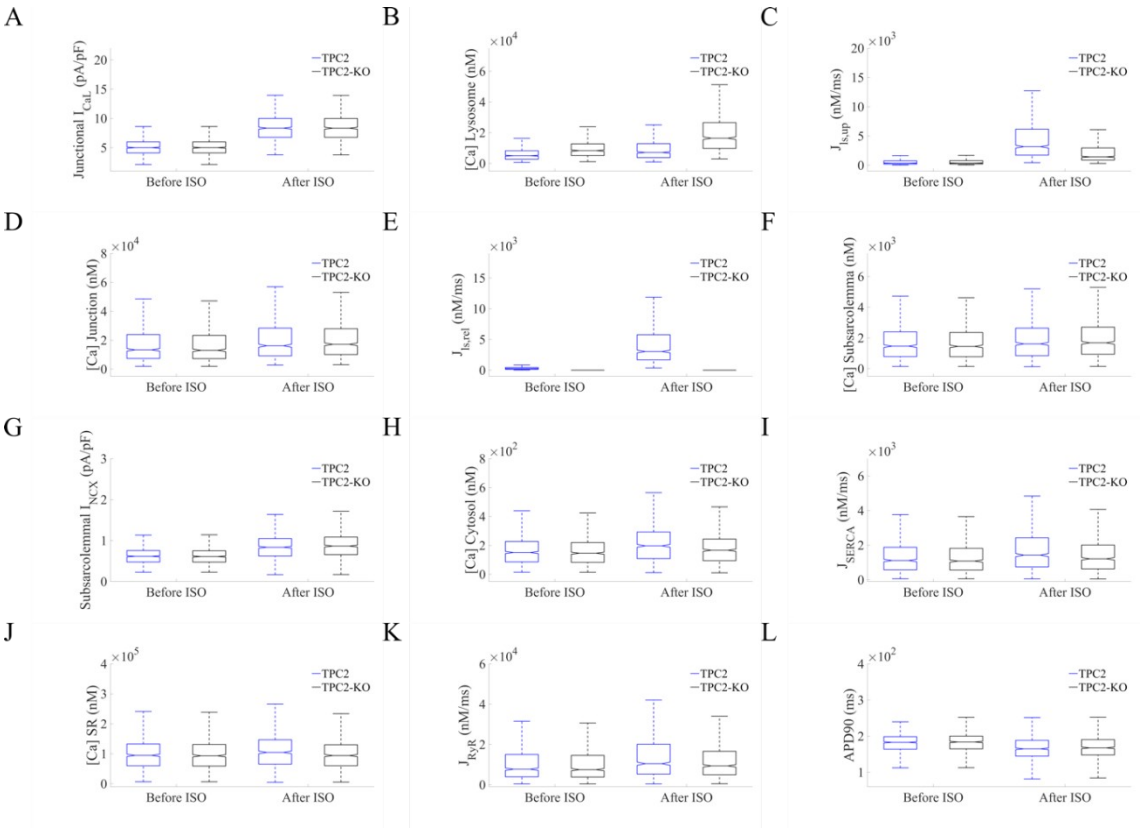


Figure 4.10. Distributions of currents, fluxes, concentrations and action potentials**. 4.10A-4.10L** are the boxplots of amplitudes of currents and calcium fluxes, calcium concentration in each subspace, and and APD_{90}, across protocols of baseline and ISO, respectively.

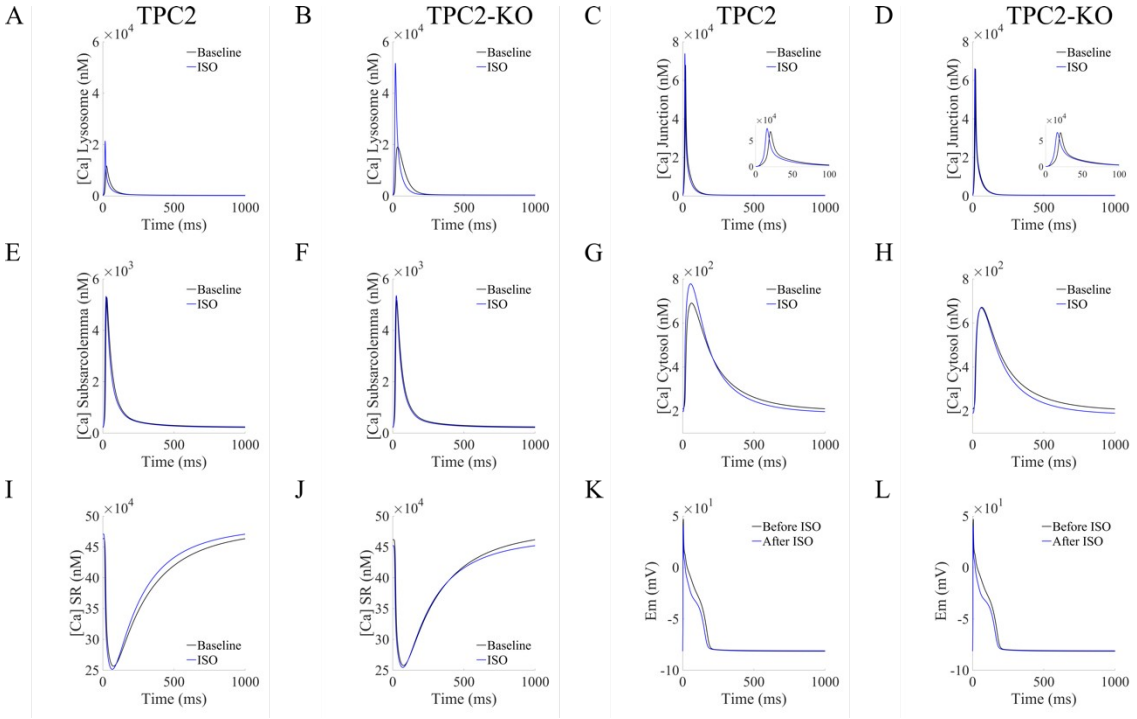


Figure 4.11. Representative traces of the calcium concentrations and action potentials. **4.11A, 4.11C, 4.11E, 4.11G, 4.11I, 4.11K** shows for a representative model the traces of calcium concentrations and action potentials in subspaces across baseline and ISO protocols in the presence of lysosomal release (TPC2). **4.11B, 4.11D, 4.11F, 4.11H, 4.11J, 4.11L** the same model is shown under the block of lysosomal release (TPC2-KO).

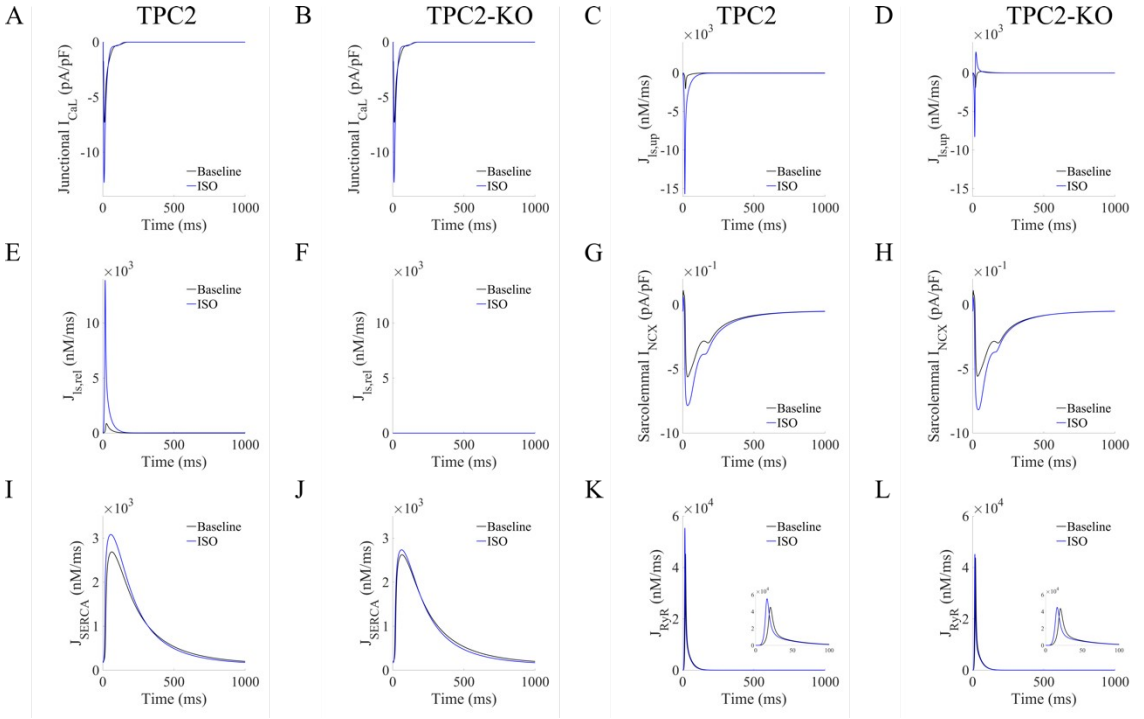


Figure 4.12. Representative traces of the currents and calcium fluxes. **4.12A, 4.12C, 4.12E, 4.12G, 4.12I, 4.12K** shows for a representative model the traces of calcium currents and fluxes across baseline and ISO protocols in the presence of lysosomal release (TPC2). **4.12B, 4.12D, 4.12F, 4.12H, 4.12J, 4.12L** the same model is shown under the block of lysosomal release (TPC2-KO).

To further characterise the influence of lysosomal calcium on calcium transient and AP biomarkers in cAF, correlations between each flux or current and each biomarker were compared in both scenarios using partial correlation coefficients (Figure 4.13). Comparing Baseline and ISO, the influence of lysosomal uptake and release fluxes ($J_{ls,up}$ and $J_{ls,rel}$) on the calcium transient biomarkers, such as Ca_{AMP}, became notably more significant (Figure 4.13C), although their contributions were negligible in Baseline (Figure 4.13A). $J_{ls,up}$ and $J_{ls,rel}$ became more important in modulating calcium transient amplitude, Ca_{AMP}, even surpassing SERCA flux (J_{SERCA}) in comparison of Baseline and ISO (Figures 4.13A, 4.13C). In ISO, the influence of $J_{ls,rel}$ on the calcium transient biomarkers all plummeted in the block scenario, compared to the presence of lysosomal release (Figures 4.13C, 4.13D).

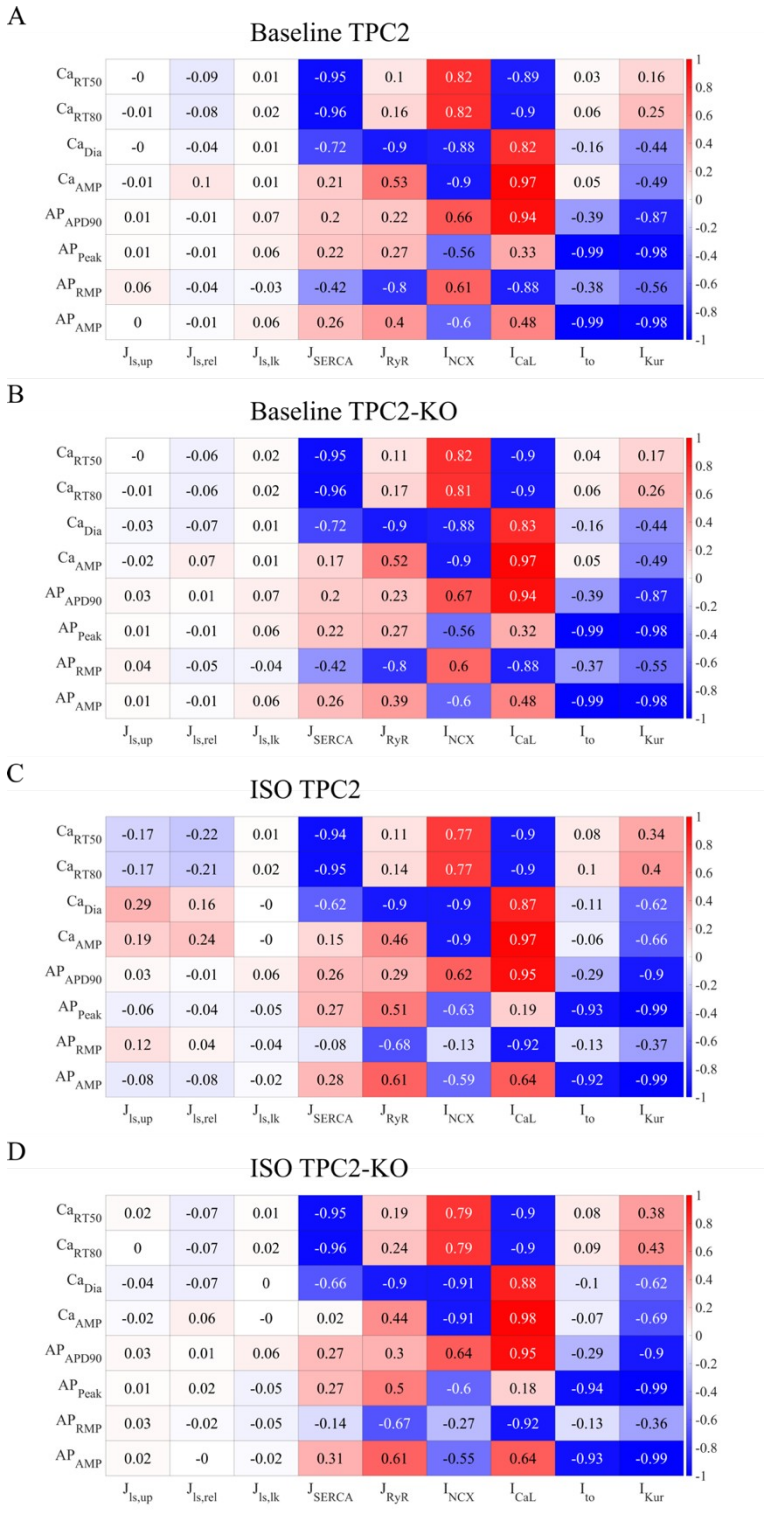


Figure 4.13. Partial correlation coefficients between varied fluxes and currents and the biomarkers of calcium transient and action potential. **4.13A-4.13D** showed the Spearman partial correlation coefficients in heatmaps across Baseline and ISO in the presence and block of lysosomal release (TPC2, TPC2-KO), respectively.

4.3 Discussion

In this chapter, I have presented my work to incorporate, for the first time, lysosomal calcium handling in computational models of the human atrial cardiomyocyte, and calibrated the baseline model by experimental data in calcium transient and AP traces and biomarkers. To add model credibility, we refined the model response under ISO exposure, and exploited a unique dataset of simultaneously recorded APs and calcium transients in human atrial cardiomyocytes at multiple stimulation frequencies. The model response of increased cytosolic calcium transient amplitude under β-adrenergic stimulation agreed with experimental findings in both atrial (Collins *et al.*, 2011) and ventricular (Capel *et al.*, 2015) cardiomyocytes.

4.3.1 Contribution of Lysosomal Calcium Release to Intracellular Calcium Handling in Normal Sinus Rhythm

I calibrated the population of models by experimental ranges in AP biomarkers. The results presented in this chapter predict the role of lysosomal calcium in nSR. The variations of calcium transient amplitude were attributed to the delicate balance of intracellular fluxes and currents. To understand the specific role of lysosomal calcium release, a population of ionic profiles, varying lysosomal fluxes and the other

intracellular fluxes and currents, was used. The population was calibrated by the individual values of AP features in human atrial cardiomyocytes, and therefore characterised the voltage morphology for each individual calibrated profile. Thus, each profile in a calibrated voltage morphology showed a scenario of intracellular flux variations, which also defined the commensurate lysosomal fluxes. For the specific role of lysosomes on calcium transient, we focused on its release flux and explored a scenario of blocking the direct effect of calcium transport from the lysosome to the cytosol in the calibrated population. Block of lysosomal release reduced calcium transient amplitude by lessening the systolic peak, which became apparent when larger calcium was loaded into the lysosome under β-adrenergic stimulation.

Compared to Baseline, the increase of calcium transient amplitude observed under β-adrenergic stimulation was by raising the systolic peak and slightly reducing the diastolic level. Precluded from being released in the block scenario, the calcium in the lysosome grew bigger than in the active release scenario; however, this calcium, when returned to the junction, did not add up to a similar level. Because the SERCA potentiation to SR calcium was reduced by block of lysosomal release, this small reverting calcium to the junction under the block scenario did not trigger a larger CICR. Under active lysosomal release, the influx of calcium by the I_{CaL} was not significantly changed by lysosomal loading, thus lysosomal loading mainly effected on intracellular calcium handling. The NCX forward mode in the junction and subsarcolemma was also not significantly changed between the presence and block of lysosomal release, thus lysosomal loading mainly mediated SR refilling. Taken together, this modelling study predicted that lysosomal release increased cytosolic calcium transient to potentiate SERCA reuptake and the SR content, contributing to the increase of RyR release. This effect was mainly on modulating intracellular calcium handling. In summary, lysosomal calcium release primarily modulated intracellular calcium handling by increasing SERCA reuptake and RyR release in nSR.

4.3.2 Contribution of Lysosomal Calcium Release to Intracellular Calcium Handling in Chronic Atrial Fibrillation

Following the inclusion of lysosomal calcium handling in nSR, I applied the cellular ionic remodelling associated with cAF without modifying the lysosomal fluxes in such incorporation. The magnitudes of lysosomal fluxes were driven by the gradients of their neighbouring subspaces concentrations and the open probabilities of their respective lysosomal fluxes. Their open probabilities were the same in Baseline and ISO, thus their magnitudes were defined by the concentrations in the intracellular subspaces. Next, I calibrated the initial population by experimental values of AP features in cAF (Sánchez *et al.*, 2014), which resulted in a new population in cAF. Thus, using individual population in nSR and in cAF could reveal more of the role of lysosomal release in the variation of intracellular calcium handling.

The role of lysosomal loading was changed under the ionic remodelling associated with cAF, where the intracellular calcium handling was altered by a decrease of the I_{CaL}, and increases of SERCA reuptake and NCX current, as implemented in the Grandi *et al.* model (Grandi *et al.*, 2011). To identify the role of lysosomal calcium handling on the calcium transient, I simulated protocols of lysosomal release block to halt the direct calcium transport from the lysosome to the cytosol. Block of lysosomal release decreased calcium transient amplitude by reducing the systolic peak in ISO. The slight increase in calcium transient amplitude was by reducing the diastolic level in the block scenario, while the increase in the active release scenario was by raising the systolic peak and slightly reducing the diastolic level.

Under TPC2 block conditions, the calcium accumulates in the lysosome and does not contribute to junctional loading like in the active release scenario, therefore block of

lysosomal release has an effect on SR calcium reuptake. In the release scenario, calcium from the lysosome increases calcium loading in the cytosol to potentiate SERCA reuptake. The higher SR content led to an increase of RyR release. The calcium extrusion by NCX forward mode in the junction and subsarcolemma remained similar to the block scenario. Besides, lysosomal loading did not significantly change L-type calcium influx. Thus, lysosomal release mainly contributed to SR calcium refilling by increasing SERCA reuptake. In summary, this modelling study predicted that lysosomal release increased intracellular calcium transient to potentiate SERCA reuptake. The increased SR content contributed to increase RyR release. Lysosomal calcium release primarily modulated intracellular calcium handling by increasing SERCA reuptake and RyR release also in cAF.

I conclude that lysosomal calcium release primarily modulates intracellular calcium handling by increasing SERCA reuptake and RyR release (Figure 4.14).

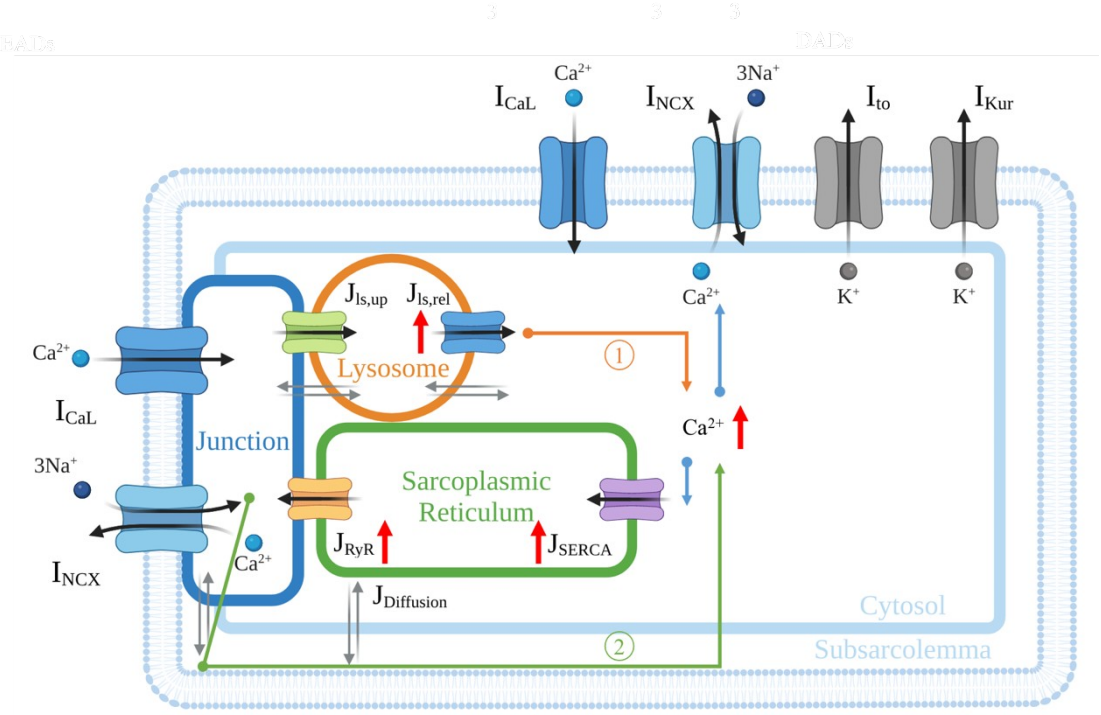


Figure 4.14. Schematic cartoon showing the conclusion for actions of lysosomal calcium release.

Chapter 5

Lysosomal Calcium Release Promotes EADs under Mild Hypercalcemia and β-adrenergic Stimulation in Human Atrial Cardiomyocytes

Summary of contribution: This chapter presents my work to investigate the role of lysosomal calcium release on EADs under mild hypercalcemia and β-adrenergic stimulation. I carried out the simulation of calibrated populations of models in Chapter 4 under mild hypercalcemia and β-adrenergic stimulation and the investigation of the role of lysosomal calcium release on EADs in the proarrhythmic scenario. Additionally, I did methodology and writing of the project.

5.1 Introduction

EADs are defined as oscillations at the plateau level of the membrane potential or during phase 3 of the AP (Wit and Rosen, 1992; Volders *et al.*, 2000). I_{CaL} reactivation is the key underlying mechanism for generating EADs, meanwhile EADs are known to

be facilitated by abnormalities in intracellular calcium handling and calcium overload (Zeng and Rudy, 1995; Weiss *et al.*, 2010; Passini *et al.*, 2016).

The importance of I_{CaL} for EADs is because its voltage-dependent activation reaching the range of membrane potentials (-35 to 0 mV) in which EADs arise (Volders *et al.*, 2000). To induce EADs, this requires 1) a conditioning phase that is controlled by the sum of membrane currents present near the AP plateau and is characterised by the prolonging of the plateau within a voltage range where, 2) the recovery from inactivation and reactivation of I_{CaL} to bring in a sufficient depolarising current can happen (Volders *et al.*, 2000). The inward I_{NCX} plays an important role at the initial delay in repolarisation (January and Riddle, 1989; Zeng and Rudy, 1995), named the conditioning phase. Besides, the conditioning phase is typically manifested as an AP prolongation during repolarisation which could, while does not have to, be followed by an EAD upstroke.

EADs have been reported in human atrial cardiomyocytes (Kettlewell *et al.*, 2019); however, whether lysosomal calcium loading may play a role in this phenomenon remains unknown. To mechanistically investigate such a possible contribution of lysosomal calcium release in human atrial cardiomyocytes, I explore conditions of calcium overload under mild hypercalcemia and β-adrenergic stimulation by means of computer modelling and simulation in order to investigate the proarrhythmic and antiarrhythmic roles of lysosomal calcium release. I hypothesise that raising extracellular calcium concentration in β-adrenergic stimulation would enhance the lysosomal calcium release, contributing to EADs. This is explored by exploiting the calibrated populations of human atrial cardiomyocyte models developed in Chapter 4 under scenarios of nSR and cAF.

I hypothesise that lysosomal calcium release might promote EADs by increasing NCX inward current and late L-type calcium current under hypercalcemia and β-adrenergic stimulation (Figure 5.1).

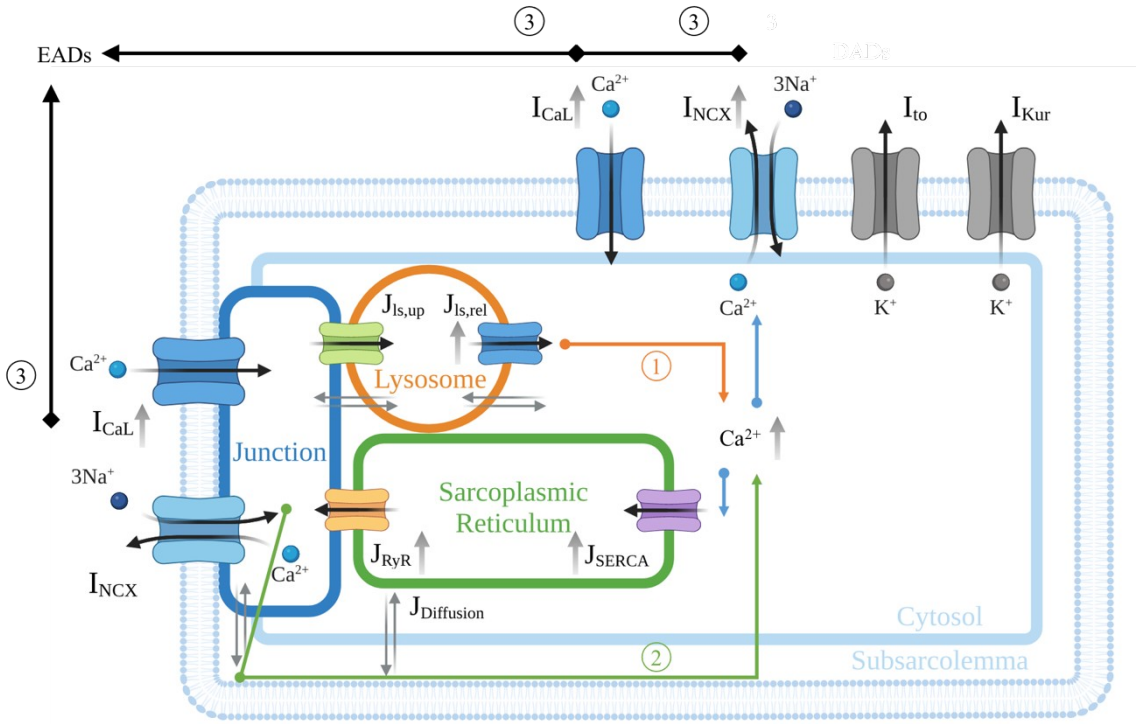


Figure 5.1. Schematic cartoon showing the hypothesis for actions of lysosomal calcium release.

5.2 Results

I investigated the role of lysosomal calcium release in EADs under mild hypercalcemia by simulating an elevation of extracellular calcium concentration to 2.8 mM in nSR and cAF. Based on the comparison of EADs formation under the presence vs the block of lysosomal calcium release, the models in the population were classified as: (i) non-TPC-specific proarrhythmic models, when EADs occurred both in the presence and block of lysosomal release; (ii) TPC-specific proarrhythmic models, when EADs occurred only in the presence of lysosomal release while not in the block scenario; and (iii) non-proarrhythmic models, exhibiting absence of EADs in both scenarios (Table 5.1). In brief, the presence of lysosomal release led to a higher incidence of EADs in the proarrhythmic categories (non-TPC-specific and TPC-specific) by 151 (119 + 32) and

161 (142 + 19) models in nSR and cAF, respectively. The non-proarrhythmic categories accounted for 336 and 472 atrial cell models in nSR and in cAF, respectively. EADs were identified by occurrence in any of the consecutive 5 beats after an initial pacing of 150 beats.

EAD occurrences in mild hypercalcemia and β-adrenergic stimulation	**non-TPC-specific proarrhythmic**		**TPC-specific proarrhythmic**		**Non-proarrhythmic**	
	nSR	**cAF**	**nSR**	**cAF**	**nSR**	**cAF**
	119 / 627	142 / 825	32/ 627	19/ 825	336/ 627	472/ 825

Table 5.1. Distributions of proarrhythmic occurrences with EADs, in non-TPC-specific proarrhythmic, TPC-specific proarrhythmic, and non-proarrhythmic categories under mild hypercalcemia and β-adrenergic stimulation in nSR and cAF.

5.2.1 Role of Lysosomal Calcium Release in EADs in Normal Sinus Rhythm

To understand the mechanism of lysosomal calcium release involvement in EADs generation in nSR under mild hypercalcemia, I focused on the proarrhythmic behaviour exhibited by models in the *TPC-specific* (EADs directly promoted by lysosomal calcium release, i.e., EADs present only under active TPC2 channels, but not when blocked) and *non-proarrhythmic* (no EADs) categories. Representative traces in each category are presented in Figure 5.2.

The presence of active lysosomal calcium release promoted EADs in the TPC-specific category, while had no effect in non-proarrhythmic models (Figure 5.2A). Lysosomal

release promoted RyR release (Figures 5.2B, 5.2C). The increase of RyR release further increased calcium loading in both the junctional and in subsarcolemmal subspaces (Figures 5.2D, 5.2E). In brief, larger lysosomal calcium loading in the TPC-specific category of proarrhythmic models contributed to a larger junctional and subsarcolemmal calcium loading, compared to the non-proarrhythmic models. The increase of junctional and subsarcolemmal calcium loading contributed to enhanced NCX forward modes, with a larger extent in its subsarcolemmal contribution, and this led to an increase of inward NCX current (Figures 5.2F, 5.2G).

The TPC-specific proarrhythmic models showed larger peaks in calcium concentration in the junction and subsarcolemmal subspaces (Figures 5.2D, 5.2E). As a result, the L-type calcium-dependent inactivation exhibited lower minima, leading to a protracted recovery, especially in the subsarcolemmal component of I_{CaL} (Figures 5.2H, 5.2J). Because of the calcium-dependent inactivation taking longer to fully inactivate (Figures 5.2H, 5.2J), the time-window of I_{CaL} can get prolonged during the portion of the AP where the transmembrane potential is in the range enabling its reactivation (Figures 5.2I, 5.2K). The resultant increases of junctional and subsarcolemmal inward late L-type currents, together with the increase of subsarcolemmal NCX inward current, led to elevation of the plateau voltage of the AP and set the conditions for the reopening of the L-type voltage-dependent activation gate (Figure 5.2L), thus contributing to the generation of the EADs.

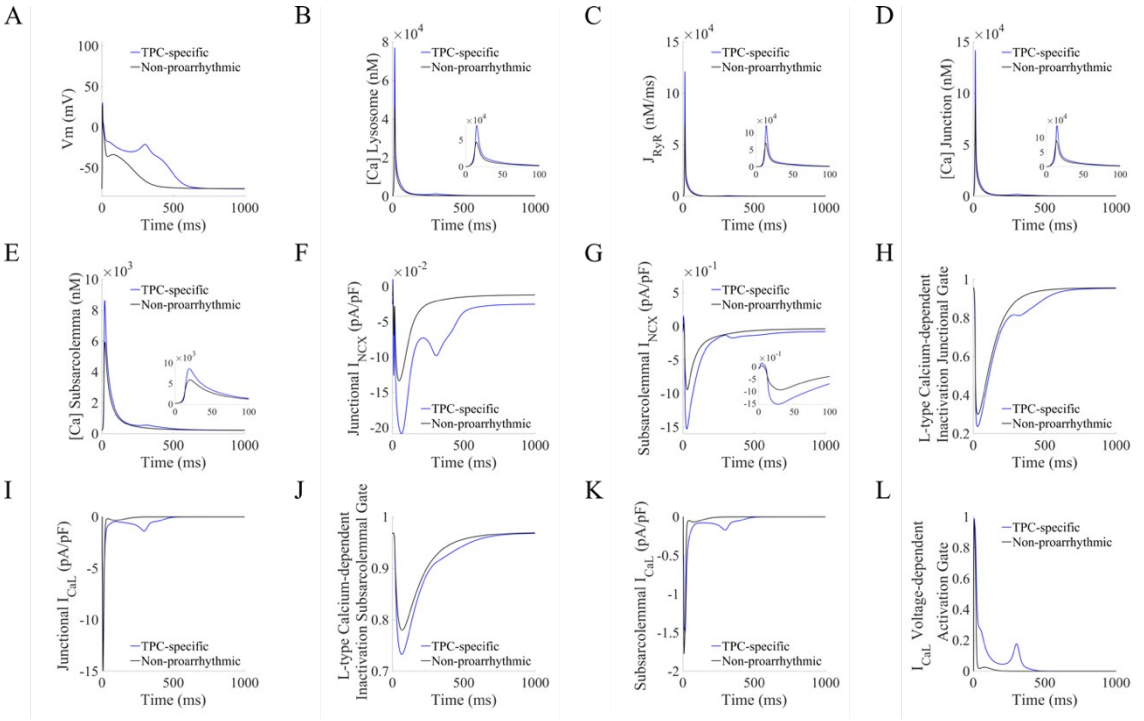


Figure 5.2. Traces of TPC-specific, and non-proarrhythmic models with early afterdepolarisation under mild hypercalcemia and β-adrenergic stimulation in nSR. **5.2A-5.2L:** Representative traces of action potential, lysosomal calcium concentration, RyR release, junctional and subsarcolemmal calcium concentrations, junctional and subsarcolemmal I_{NCX}, L-type calcium-dependent inactivation junctional and subsarcolemmal gates, junctional and subsarcolemmal I_{CaL}, and I_{CaL} voltage-dependent activation gate, respectively in the presence of lysosomal calcium release.

In terms of ionic properties, the magnitude of the I_{CaL} conductance showed a sharp trend in the comparison of the non-proarrhythmic and TPC-specific proarrhythmic category (Figure 5.3A). The non-proarrhythmic models showed smaller I_{CaL} densities, while TPC-specific models presented larger values (Figure 5.3A). This shows that lysosomal calcium release may promote the adequate disruption in intracellular calcium handling to transition models from the non-proarrhythmic category into a proarrhythmic state. I_{NCX} conductance magnitude showed a less evident trend, but still being smaller in the non-proarrhythmic models (Figure 5.3A). For intracellular fluxes, lysosomal release, SERCA, and RyR permeabilities showed evidently smaller differences in the comparison of the TPC-specific proarrhythmic category and non-proarrhythmic category (Figure 5.3A).

Next, I explored at the population level to check if the above-described mechanisms were preserved. Lysosomal release promoted RyR release and increased calcium loading in junction and subsarcolemma (Figures 5.3B, 5.3C, 5.3D, 5.3E). During the initial upstroke of the AP, junctional and subsarcolemmal NCX currents showed upward peaks by reaching above zero while working in reverse mode (Figures 5.2F, 5.2G), as revealed in the TPC-specific category (Figures 5.3F, 5.3G). The inward calcium by NCX reverse mode was larger in the subsarcolemma than in the junction in the TPC-specific proarrhythmic category (Figures 5.3F, 5.3G). This inward calcium in the subsarcolemma contributed to its calcium loading (Figures 5.3E, 5.3G), promoting the subsarsolemmal NCX forward mode (Figure 5.3I). With its reverse mode persisting for a while, NCX functions in forward mode for the rest of the AP by extruding calcium from the junction and subsarcolemma. Because calcium loading in the junction was fast depleted by active lysosomal calcium transport, differences in calcium extrusion were not evident in the junctional NCX forward mode, while they became evident in the subsarcolemmal NCX forward mode in the TPC-specific proarrhythmic category compared to non-proarrhythmic models (Figures 5.3H, 5.3I).

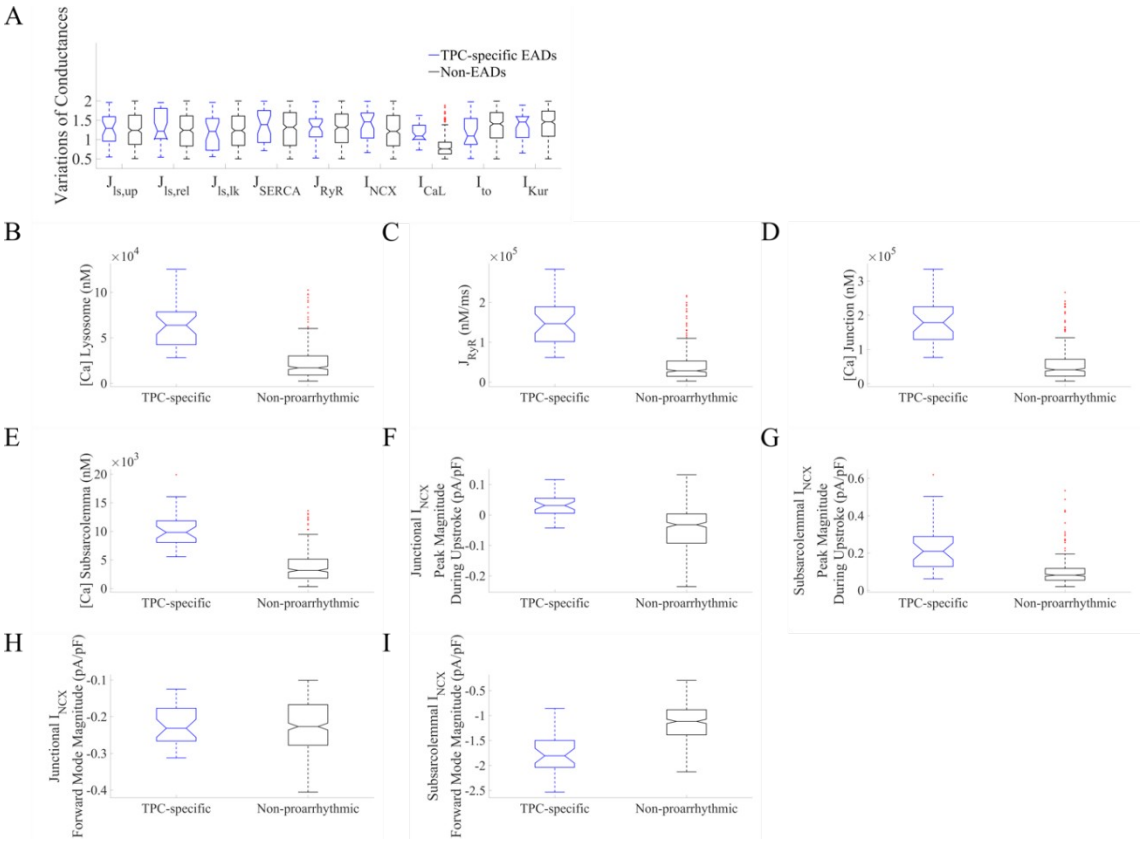


Figure 5.3. Comparisons of the TPC-specific, and non-proarrhythmic categories with early afterdepolarisation under mild hypercalcemia and β-adrenergic stimulation in nSR. **5.3A:** Ionic properties in TPC-specific profiles (blue) and non-proarrhythmic profiles (black). **5.3B-5.3I:** Distributions of amplitudes of lysosomal, junctional and subsarcolemmal calcium concentrations and RyR release, peak magnitudes during upstroke of junctional and subsarcolemmal I_{NCX}, and forward mode magnitudes of junctional and subsarcolemmal I_{NCX}, respectively comparing models in the TPC-specific, and non-proarrhythmic categories.

5.2.2 Role of Lysosomal Calcium Release in TPC-specific Models in Normal Sinus Rhythm with EADs

To understand the specific role of lysosomal release, here I focused on the TPC-specific models in nSR. Lysosomal release promoted EADs while block of lysosomal release prevented EADs in the TPC-specific category of cell models (Figures 5.4A, 5.4B). Lysosomal release increased RyR release with a larger junctional calcium loading (Figures 5.4C, 5.4D). The larger junctional loading was fast depleted by loading into the lysosomal subcompartment, which reduced the involvement of calcium extrusion by NCX resulting in a similar magnitude of NCX forward mode compared to the block scenario (Figures 5.4F). By contrast, the subsarcolemmal NCX forward mode was larger in magnitude and longer in duration, because more calcium diffused from the junction into the subsarcolemma when lysosome loading was present (Figures 5.4D, 5.4E, 5.4G). Meanwhile, the larger junctional and subsarcolemmal calcium loading resulted in lower minima and protracted recovery of the L-type calcium-dependent inactivation (Figures 5.4H, 5.4J), and therefore prolonged the time-window of I_{CaL} during the plateau potential yielding to L-type voltage-dependent reactivation gate (Figures 5.4I, 5.4K, 5.4L). The resultant increases of junctional and subsarcolemmal L-type inward current and subsarcolemmal NCX inward current (Figures 5.4G, 5.4I) contributed to the elevation of the plateau voltage (Figure 5.4A). The plateau voltage elevation further increased the opening of the L-type voltage-dependent activation gate (Figure 5.4L), leading to an increase in inward late L-type currents in junction and subsarcolemma (Figures 5.4I, 5.4K). This process of increased inward currents, plateau potential and voltage-dependent activation potentiated the upstroke of depolarisation during EAD formation.

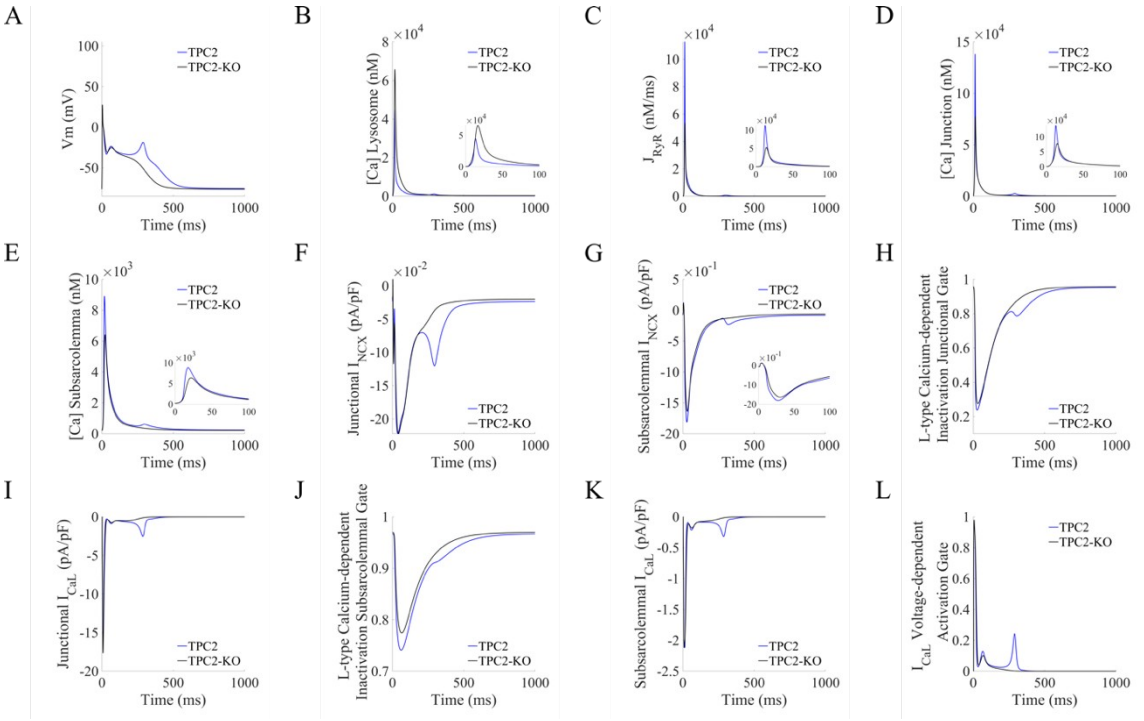


Figure 5.4. Lysosomal calcium release promoted early afterdepolarisation in proarrhythmic TPC-specific models under mild hypercalcemia and β-adrenergic stimulation in nSR. **5.4A-5.4L:** Representative traces of action potential, lysosomal calcium concentration, RyR release, junctional and subsarcolemmal calcium concentrations, junctional and subsarcolemmal I_{NCX}, L-type calcium-dependent inactivation junctional and subsarcolemmal gates, junctional and subsarcolemmal I_{CaL}, and I_{CaL} voltage-dependent activation gate, respectively comparing the presence and block of lysosomal release.

Next, I checked whether the previously described mechanisms were preserved at the population level. Lysosomal release promoted RyR release, which increased calcium loading in junction and subsarcolemma (Figures 5.5A, 5.5B, 5.5C, 5.5D). The calcium influxes by junctional and subsarcolemmal NCX reverse mode were respectively similar in the presence and block of lysosomal release (Figures 5.5E, 5.5F). Thus, the larger subsarcolemmal loading resulted from the larger calcium diffusion from junctional loading, and contributed to an enhanced NCX forward mode (Figures 5.5D, 5.5H). By comparison, the junctional loading, though larger, was mainly depleted by lysosomal calcium loading, thus the junctional NCX forward mode featured a similar magnitude in the presence and block scenarios (Figures 5.5C, 5.5G). In summary, the increases of

subsarcolemmal NCX inward current and of the junctional and subsarcolemmal late components of the L-type current promoted EAD in TPC-specific models.

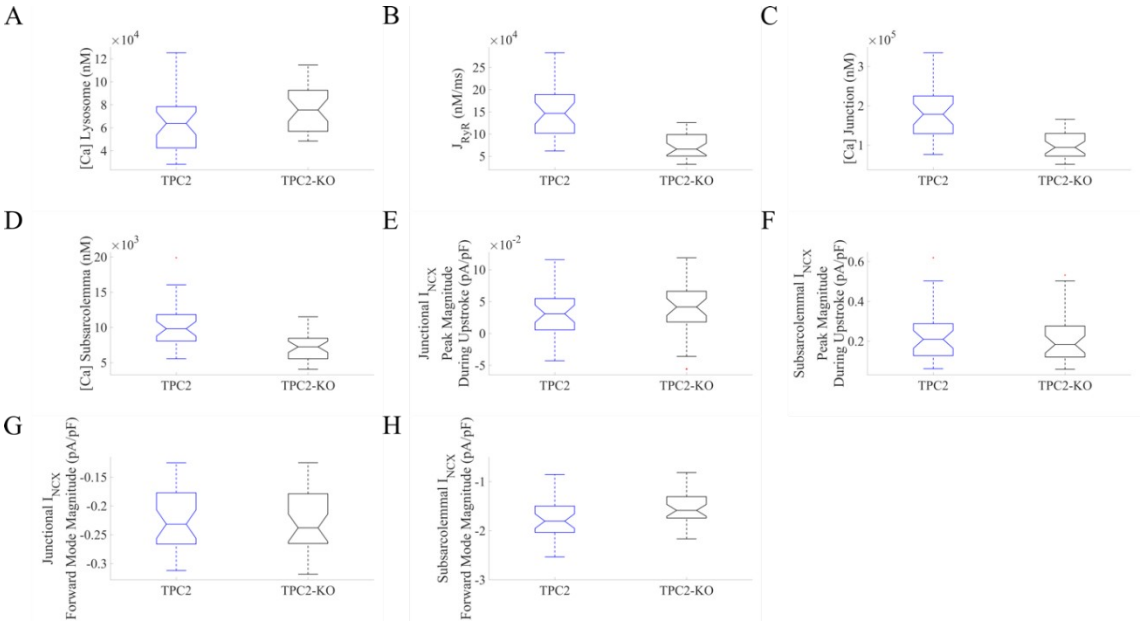


Figure 5.5. Lysosomal calcium release promoted early afterdepolarisation in proarrhythmic TPC-specific models under mild hypercalcemia and β-adrenergic stimulation in nSR. **5.5A-5.5H:** Distributions of amplitudes of lysosomal, junctional and subsarcolemmal calcium concentrations and RyR release, peak magnitudes during upstroke of junctional and subsarcolemmal I_{NCX}, and forward mode magnitudes of junctional and subsarcolemmal I_{NCX}, respectively comparing the presence and block of lysosomal release in the TPC-specific models.

5.2.3 Role of Lysosomal Calcium Release in the Modulation of EADs in Chronic Atrial Fibrillation

To understand the role of lysosomal release in EADs formation in cAF, I analysed its involvement in proarrhythmia in atrial cellular models from the TPC-specific and non-proarrhythmic categories. One set of representative traces in each category is presented in Figure 5.6.

The EADs resulted from the increases of subsarcolemmal NCX inward current and late junctional and subsarcolemmal L-type currents in nSR. Similarly, in cAF, lysosomal release led to a series of events to increase the currents, which contribute to the elevation of plateau voltage and reopening of L-type voltage-dependent activation (Figures 5.6A, 5.6L). First, lysosomal release promoted RyR release and increased calcium loading in junction and subsarcolemma (Figures 5.6B, 5.6C, 5.6D, 5.6E). Second, the increased junctional calcium and subsarcolemmal calcium loading led to enhanced NCX forward mode (Figures 5.6F, 5.6G). The larger junctional and subsarcolemmal loading led to the protracted recovery of L-type calcium-dependent inactivation, prolonging the time-window of I_{CaL} during the plateau potential (Figures 5.6H, 5.6J), and this resulted in larger late currents by reopening of the L-type voltage activation gate (Figures 5.6I, 5.6K, 5.6L).

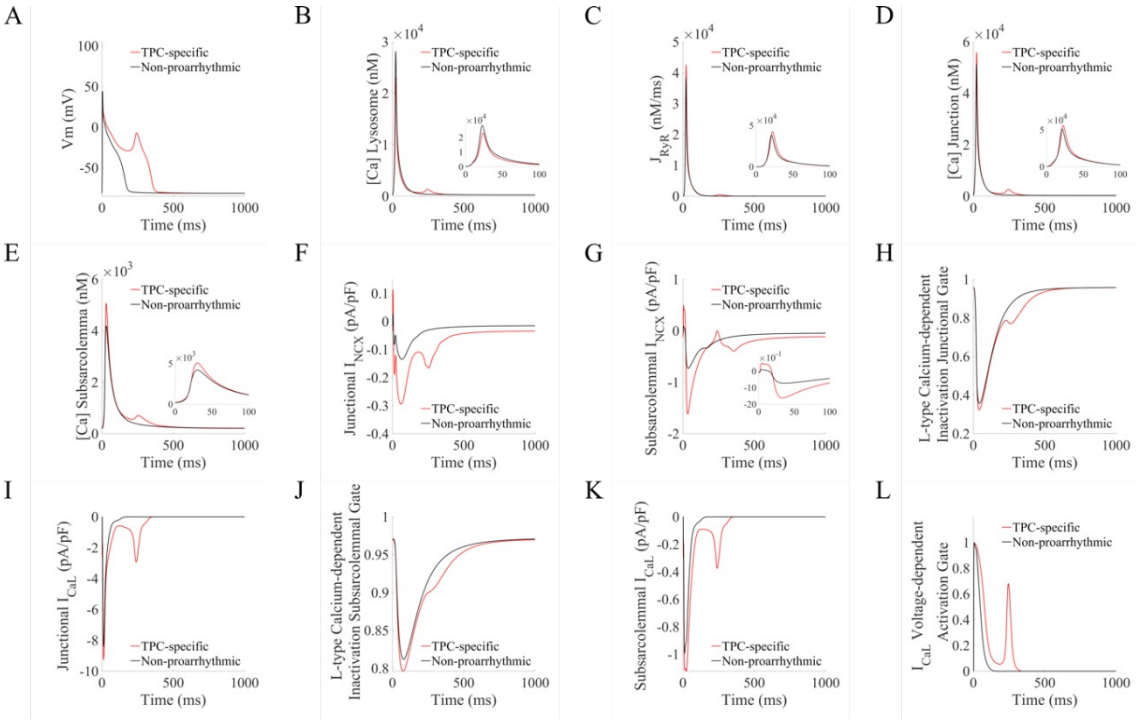


Figure 5.6. Traces of proarrhythmic TPC-specific, and non-proarrhythmic models with early afterdepolarisation under mild hypercalcemia and β-adrenergic stimulation in cAF. **5.6A-5.6L:** Representative traces of action potential, lysosomal calcium concentration, RyR release, junctional and subsarcolemmal calcium concentrations, junctional and subsarcolemmal I_{NCX}, L-type calcium-dependent inactivation junctional and subsarcolemmal gates, junctional and subsarcolemmal I_{CaL}, and I_{CaL} voltage-dependent activation gate, respectively in the presence of lysosomal calcium release.

In terms of ionic properties, the magnitude of I_{CaL} conductance showed a distinct trend in the comparison of the TPC-specific proarrhythmic and the non-proarrhythmic categories (Figure 5.7A). L-type conductance magnitudes were in a descending order in TPC-specific profiles and non-proarrhythmic profiles, respectively (Figure 5.7A). This shows that lysosomal calcium release could promote models in a non-proarrhythmic category into a proarrhythmic state. I_{NCX} conductance magnitudes showed a less obvious trend (Figure 5.7A). In terms of intracellular fluxes, lysosomal release, SERCA, and RyR permeabilities showed noticeably smaller differences in the comparison of the TPC-specific proarrhythmic and non-proarrhythmic categories (Figure 5.7A).

Next, I explored in the populations of the TPC-specific proarrhythmic category and non-proarrhythmic category to check whether the above mechanism held. Lysosomal release increased RyR release and this resulted in larger calcium loading in junction and subsarcolemma in the models of the TPC-specific proarrhythmic category, compared to non-proarrhythmic category (Figures 5.7B, 5.7C, 5.7D, 5.7E). Besides, calcium influx by NCX reverse mode in junction and subsarcolemma was also larger in models of the TPC-specific proarrhythmic category, compared to non-proarrhythmic category (Figures 5.7F, 5.7G). The larger junctional calcium loading in TPC-specific models, under active lysosomal calcium release, reduced the involvement of calcium extrusion by junctional NCX forward mode (Figures 5.7C, 5.7H, 5.7J). Besides, the larger subsarcolemmal loading in the TPC-specific proarrhythmic category promoted an enhanced NCX forward mode (Figures 5.7E, 5.7I). Taken together, lysosomal release promoted EADs in cAF by increasing subsarcolemmal NCX inward current in TPC-specific models.

In summary, lysosomal release promoted EADs by increasing inward currents in nSR and cAF. In nSR, the EADs were mediated by subsarcolemmal NCX inward current and junctional and subsarcolemmal L-type inward current. In cAF, the above mechanism applied to the TPC-specific category.

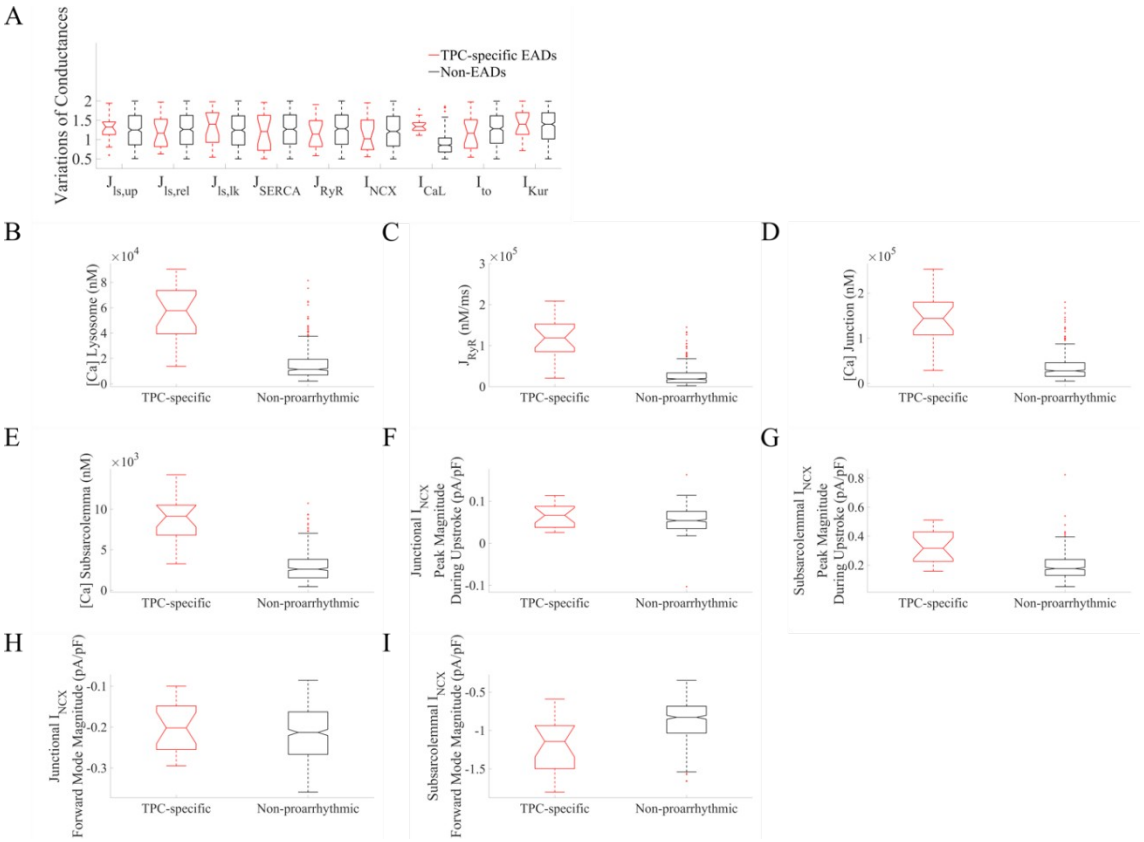


Figure 5.7. Comparisons of TPC-specific, and non-proarrhythmic categories with early afterdepolarisation under mild hypercalcemia and β-adrenergic stimulation in cAF. **5.7A:** Ionic properties in TPC-specific profiles (red) and non-proarrhythmic profiles (black). **5.7B-5.7I:** Distributions of amplitudes of calcium concentrations and flux, and peak magnitudes during upstroke and forward mode magnitudes of junctional and subsarcolemmal I_{NCX}, respectively comparing models in the TPC-specific and non-proarrhythmic categories.

5.2.4 Role of Lysosomal Calcium Release in TPC-specific Models in Chronic Atrial Fibrillation with EADs

To understand the specific role of lysosomal release in EADs, I focused on the TPC-specific models in cAF. Lysosomal release promoted EADs in the TPC-specific model (Figure 5.8A). Lysosomal release increased RyR release with larger junctional and subsarcolemmal calcium loading, respectively compared to the corresponding TPC2-block scenario (Figures 5.8B, 5.8C, 5.8D, 5.8E). The larger junctional loading was fast depleted by lysosomal calcium loading, which decreased the calcium extrusion by junctional NCX forward mode (Figures 5.8D, 5.8F). The larger junctional loading also contributed to a protracted recovery of L-type calcium-dependent inactivation and prolonged time-window of I_{CaL} during plateau stage (Figure 5.8H). Otherwise, without the direct lysosomal transport, the larger subsarcolemmal loading increased the calcium extrusion by subsarcolemmal NCX forward mode and prolonged the recovery of subsarcolemmal L-type calcium-dependent inactivation gate and the time-window of I_{CaL} for reactivation (Figures 5.8E, 5.8G, 5.8J). Thus, the larger subsarcolemmal NCX inward current and junctional and subsarcolemmal late L-type current contributed to the reopening of L-type voltage-dependent activation gate to promote EAD formation (Figure 5.8L).

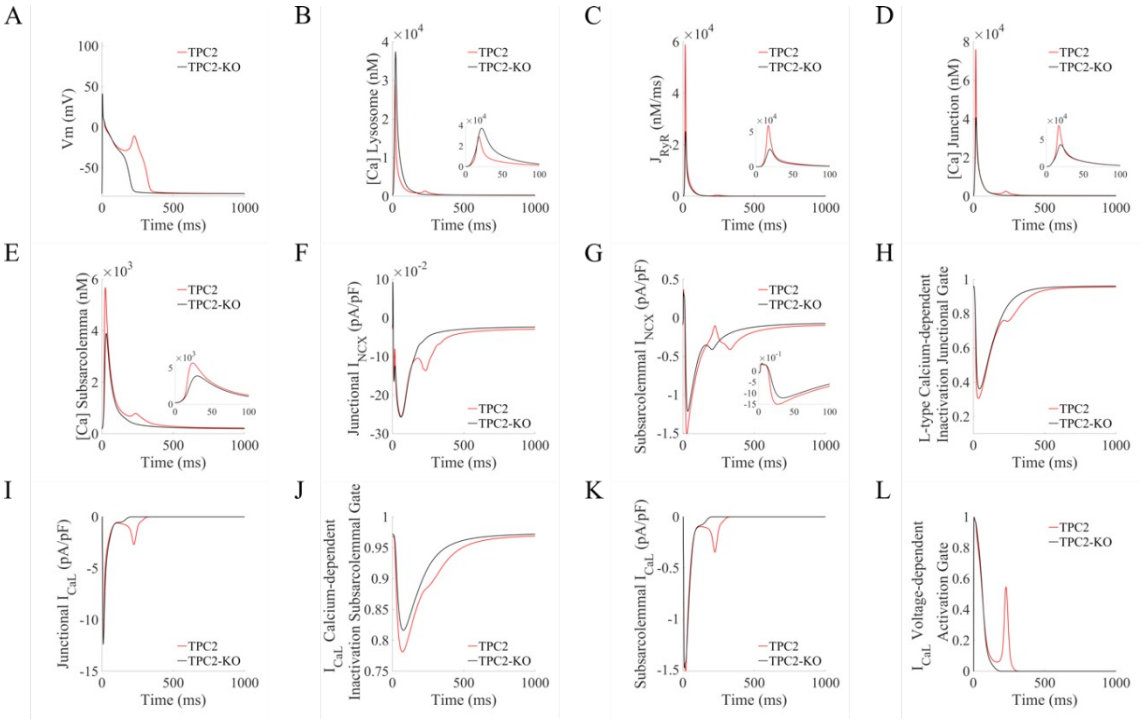


Figure 5.8. Lysosomal calcium release promoted early afterdepolarisation in proarrhythmic TPC-specific models under mild hypercalcemia and β-adrenergic stimulation in cAF. **5.8A-5.8L:** Representative traces of action potential, lysosomal calcium concentration, RyR release, junctional and subsarcolemmal calcium concentrations, junctional and subsarcolemmal I_{NCX}, L-type calcium-dependent inactivation junctional and subsarcolemmal gates, junctional and subsarcolemmal I_{CaL}, and I_{CaL} voltage-dependent activation gate, respectively comparing the presence and block of lysosomal release.

Further, I tested if the mechanism above applied at the population level. Lysosomal release increased RyR release, which promoted junctional and subsarcolemmal calcium loading (Figures 5.9A, 5.9B, 5.9C, 5.9D). The inward calcium by NCX reverse mode were similar between the presence and block of lysosomal release in junction and subsarcolemma (Figures 5.9E, 5.9F). With lysosome loading deleting junctional calcium, junctional NCX forward mode was not enhanced (Figure 5.9G). This larger subsarcolemmal loading promoted an enhanced subsarcolemmal NCX forward mode (Figure 5.9H). In summary, TPC-specific models in nSR and in cAF showed, lysosomal release promoted EADs by increasing subsarcolemmal NCX inward current and junctional and subsarcolemmal late L-type current.

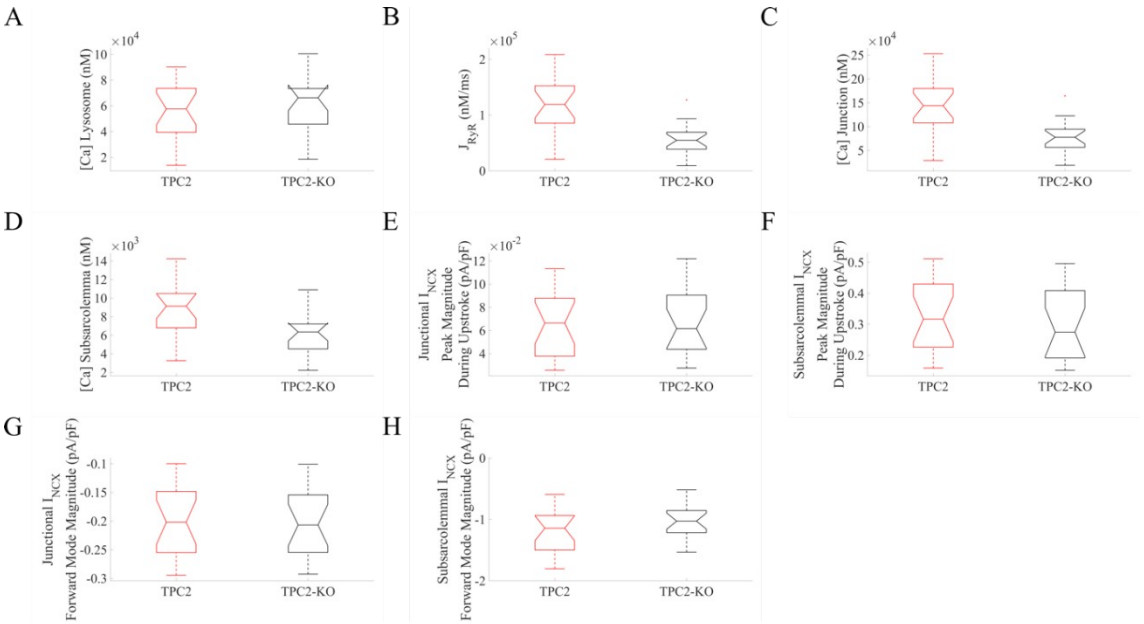


Figure 5.9. Lysosomal calcium release promoted early afterdepolarisation in proarrhythmic TPC-specific models under mild hypercalcemia and β-adrenergic stimulation in cAF. **5.9A-5.9H:** Distributions of amplitudes of lysosomal, junctional and subsarcolemmal calcium concentrations and RyR release, peak magnitudes during upstroke of junctional and subsarcolemmal I_{NCX}, and forward mode magnitudes of junctional and subsarcolemmal I_{NCX}, respectively comparing the presence and block of lysosomal release in the TPC-specific models.

5.3 Discussion

These modelling results show the role of lysosomal calcium release in EAD formation in human atrial cardiomyocytes under mild hypercalcemia and β-adrenergic stimulation. Lysosomal release mediated a fast buffering, which transported junctional calcium to cytosol to potentiate SR reuptake and increase RyR release. This process promoted

calcium loading in junction and subsarcolemma. Blocking lysosomal release decreased RyR release and junctional and subsarcolemmal calcium loading by taking calcium in junction, holding it in lysosome and reverting to junction. Lysosomal calcium handling was involved with L-type calcium currents by L-type calcium-dependent inactivation gates in junction and subsarcolemma, and involved with NCX currents by their junctional and subsarcolemmal calcium loading. The resultant increases of NCX and L-type inward currents contributed to elevation of plateau potential in the AP, therefore the increase of the opening of L-type voltage-dependent activation gate.

Proarrhythmic occurrences in the plateau stage of the AP exhibited single or multiple depolarisations as single or multiple EADs. The reactivation of the L-type voltage-dependent activation gate determined the onset of such depolarisations, which resulted from the inward currents by subsarcolemmal NCX inward current and junctional and subsarcolemmal late L-type inward currents. Thus, in the increasing loop of plateau voltage, L-type voltage-dependent activation gate and the inward currents mediated EADs in the plateau phase in AP.

The proarrhythmic involvement included non-TPC-specific proarrhythmic, TPC-specific proarrhythmic and non-proarrhythmic categories in nSR and cAF. The TPC-specific proarrhythmic category in nSR and cAF showed the increase of the opening of L-type voltage-dependent activation gate resulted from the elevation of plateau voltage, by subsarcolemmal NCX inward current and junctional and subsarcolemmal late L-type currents. Non-proarrhythmic models displayed with decreased inward currents which prevented EADs.

In TPC-specific models in nSR and cAF, blocking lysosomal release inhibited the fast transport of calcium from the junction to the cytosol. This reduced junctional and subsarcolemmal calcium loading, and consequently shortened the recovery of junctional and subsarcolemmal L-type calcium-dependent inactivation. Besides, blocking lysosomal release reduced the inward current in the subsarcolemma carried by the NCX forward mode. Thus, the reduced NCX inward current and decreased L-type inward current contributed to reduce the plateau potential, which prevented EADs. In brief,

blocking lysosomal release reduced the disturbance of intracellular calcium handling to contribute to antiarrhythmic activity.

Previous studies have shown that the NCX inward current promoted APD and the generation of EADs (Zhao *et al.*, 2012; Morotti *et al.*, 2016). This study shows that the increase of NCX inward current contributed to elevation of plateau voltage with the increases of the opening of L-type voltage-dependent activation gate and late inward current. The NCX inward current was the primary mediator for the elevation of plateau voltage and the late L-type current contributed to maintain the elevation. This sets the condition for the increasing process of plateau voltage, L-type voltage-dependent activation gate and late L-type current, which determined the onset of EADs.

Previous studies have shown that, in EAD occurrences mediated by hydrogen peroxide or by ISO and BayK8644, L-type reactivation during the plateau phase was the main cause for EAD upstroke since plateau L-type current was enhanced, and inhibition of NCX current by SEA0400 reduced the EAD occurrence (Zhao *et al.*, 2012). This showed that the L-type reactivation resulted from the inward NCX current which was involved in the critical phase in mediating the elevation of plateau voltage, though SEA0400 does not completely inhibited NCX current and also targeted L-type current (Zhao *et al.*, 2012). The EAD occurrences in this study showed that both subsarcolemmal NCX inward current and late L-type current in nSR and cAF, mediated the elevation of plateau voltage and the increase of the opening of L-type voltage-dependent activation gate. Thus, the NCX inward current primarily contributed to elevation of plateau voltage, which was additionally promoted by late L-type current when APD was longer in nSR. Further, these results showed subsarcolemmal NCX current and late L-type current promoted the increasing loop of plateau voltage, L-type voltage-dependent activation gate and late L-type current.

I conclude that lysosomal calcium release under hypercalcemia and β-adrenergic stimulation promotes EADs by increasing NCX inward current and late L-type calcium current (Figure 5.10).

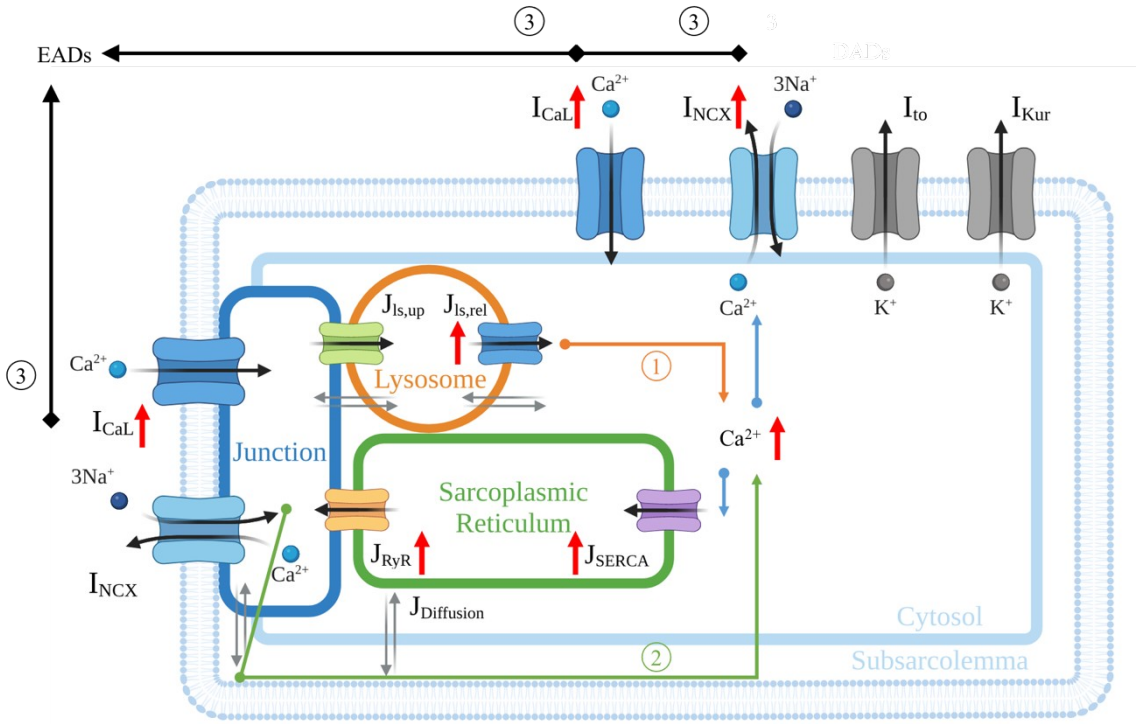


Figure 5.10. Schematic cartoon showing the conclusion for actions of lysosomal calcium release.

Chapter 6

Lysosomal Calcium Release Promotes EADs under I_{Kur} Block and β-adrenergic Stimulation in Human Atrial Cardiomyocytes

Summary of contribution: This chapter presents my work to investigate the role of lysosomal calcium release on EAD formation under I_{Kur} block and β-adrenergic stimulation. I carried out the simulation of calibrated populations of models in Chapter 4 under I_{Kur} block and β-adrenergic stimulation and the mechanistic investigation of the role of lysosomal calcium release on EAD formation in the proarrhythmic scenario. Besides, I did methodology and writing of the project.

6.1 Introduction

As discussed in the previous chapter, EADs can result from a decrease of outward currents, an increase of inward currents, or the combinations of the two so that repolarisation becomes unbalanced at the ionic level (Volders *et al.*, 2000; Qu *et al.*,

2013). The repolarisation of the human atrial AP is related to several outward potassium currents, namely I_{to}, I_{Kr}, I_{Ks}, I_{K1}, and the atrial-specific I_{Kur}. The redundancy of the currents is termed as repolarisation reserve, in which blocking one of the currents can be compensated to some extent by recruiting other currents (Osadchii, 2017). However, estimating how alterations of individual currents may impact atrial repolarisation features is challenging, due to the complex dynamics and the overlapping of subsarcolemmal ionic currents and fluxes[1].

The I_{Kur} is a major repolarising current in human atrial cardiomyocytes (Wettwer *et al.*, 2004). I_{Kur} is a sustained outward current, and contributes to early and late repolarisation in human atrial cardiomyocytes (Maleckar *et al.*, 2009). I_{Kur} block in human atrial cardiomyocytes has been also associated with secondary increases in L-type current, with smaller changes in AF than in sinus rhythm (Wettwer *et al.*, 2004).

I_{Kur} is viewed as a potential target to develop atrial-specific antiarrhythmic drugs: with either little or none I_{Kur} expressed in human ventricular cardiomyocytes, selective I_{Kur} blockers could prevent adverse effects of potassium channel blockers in prolonging APD in the ventricles (Tsujimae, Murakami and Kurachi, 2008). Blocking I_{Kur} and the subsequent atrial-specific APD prolongation are anticipated to be beneficial in chronic AF, since AF induces APD and effective refractory period shortening, by means of electrical remodelling in the expression and function of the involved ionic channels, with reported I_{Kur} reduction by around 50% (Dobrev and Ravens, 2003; Caballero *et al.*, 2010).

This chapter aims to understand the role of lysosomal release in EAD occurrence under I_{Kur} block. As mentioned above, block of I_{Kur} might reduce repolarisation reserve and contribute to EADs onset. In this context, in this chapter I aim to explore if concomitant pharmacological inhibition of lysosomal calcium release might constitute a potential antiarrhythmic strategy to decrease EADs incidence while maintaining the beneficial increase of effective refractory period associated to I_{Kur} block. These mechanisms are explored in the calibrated populations of human atrial cardiomyocyte models in Chapter 4 in nSR and cAF.

I hypothesise that lysosomal calcium release might promote EADs by increasing NCX inward current and late L-type calcium current under I_{Kur} block and β-adrenergic stimulation (Figure 6.1).

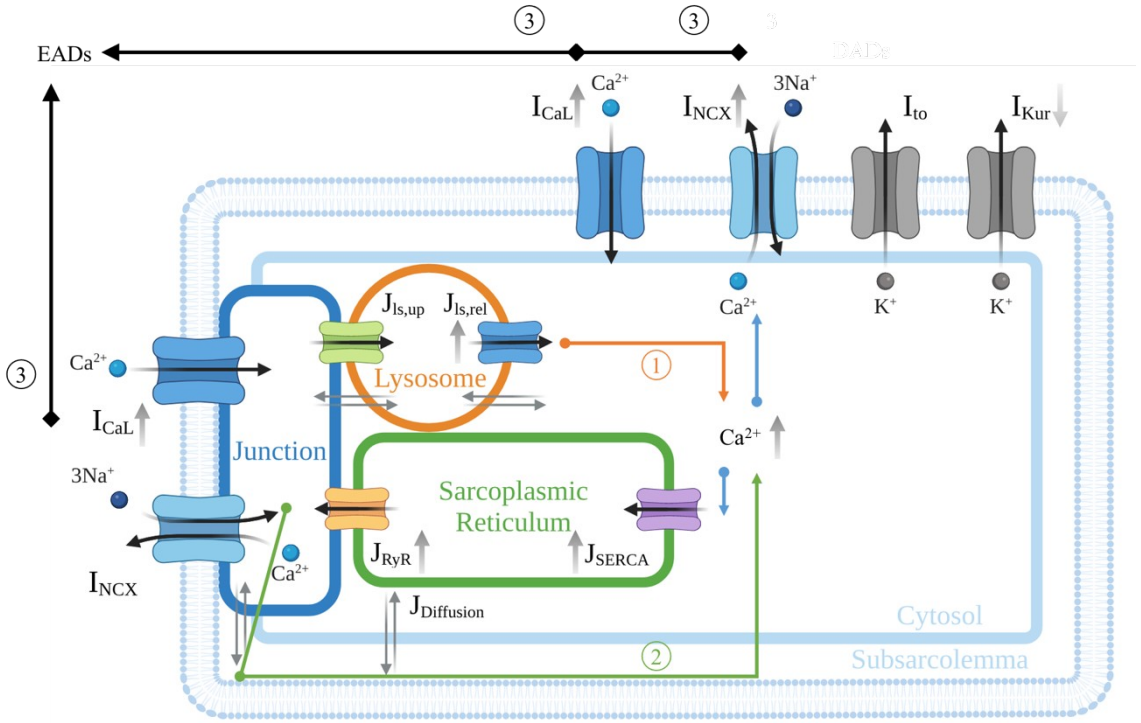


Figure 6.1. Schematic cartoon showing the hypothesis for actions of lysosomal calcium release.

6.2 Results

Here I investigated the role of lysosomal calcium release in EADs by blocking I_{Kur} by 50% in nSR and cAF. This is due to blocking I_{Kur} at 50% in ISO caused EADs in the experimental data and modelling results (Olson *et al.*, 2006; Grandi *et al.*, 2011). In human atrial cardiomyocytes in AF, the electrical remodelling of cardiac ion channels showed I_{Kur} was reduced by around 50% (Dobrev and Ravens, 2003; Caballero *et al.*,

2010). Thus, I_{Kur} is additionally reduced in the investigated condition. By the comparison of the presence and block of lysosomal release, I extracted *non-TPC-specific proarrhythmic* models (exhibiting EADs in both in the presence and block of lysosomal release), *TPC-specific proarrhythmic* models (EADs in the presence scenario, but not in the block scenario), and *non-proarrhythmic* models (normal APs in both scenarios), as detailed in Table 6.1. Lysosomal release led to a higher incidence of EADs in proarrhythmic (including non-TPC-specific and TPC-specific) categories by 71 (49+22) and 78 (64+14) models in nSR and cAF, respectively. The number of non-proarrhythmic models were 431 in nSR and 663 in cAF. EADs were sorted by their first occurrence in either of the 5 beats after the pacing of 150 beats.

EAD occurrences in I_{Kur} block and β-adrenergic stimulation	**non-TPC-specific proarrhythmic**		**TPC-specific proarrhythmic**		**Non-proarrhythmic**	
	nSR	**cAF**	**nSR**	**cAF**	**nSR**	**cAF**
	49/ 627	64/ 825	22/ 627	14/ 825	431/ 627	663/ 825

Table 6.1. Distributions of proarrhythmic occurrences with EADs, in non-TPC-specific proarrhythmic, TPC-specific proarrhythmic, and non-proarrhythmic categories under I_{Kur} block and β-adrenergic stimulation in nSR and cAF.

6.2.1 Role of Lysosomal Calcium Release on generating EADs in Normal Sinus Rhythm under I_{Kur} Block and β-adrenergic Stimulation

To understand the role of lysosomal calcium release in EADs in nSR under I_{Kur} block, I focused first on the proarrhythmic modulation of EADs by lysosomal calcium release in models from the TPC-specific and non-proarrhythmic categories. Representative traces for each category are presented in Figure 6.2.

Lysosomal calcium release promoted EADs in TPC-specific proarrhythmic models (Figure 6.2A). Active lysosomal release increased RyR release, and raised junctional and subsarcolemmal calcium loading (Figures 6.2B, 6.2C, 6.2D, 6.2E). The larger loading enhanced and prolonged their NCX forward modes, and to a larger extent in the subsarcolemma (Figures 6.2F, 6.2G). The larger junctional and subsarcolemmal loading contributed to a protracted recovery of calcium-dependent inactivation of the L-type calcium current, by lowering its minima and increasing the time-window of I_{CaL} during the plateau phase of the AP (Figures 6.2H, 6.2J). These resulting increased subsarcolemmal NCX current and junctional and subsarcolemmal L-type currents acted as additional contributing inward sources, elevating the plateau voltage of the AP (Figures 6.2A, 6.2G, 6.2I). Besides, blocking I_{Kur} prolonged the time-window of elevated plateau voltage. This fact, together with enhanced inward currents, promoted the reopening of the L-type voltage-dependent activation gate (Figures 6.2G, 6.2I, 6.2L), establishing the positive feedback loop between inward currents, plateau voltage, and voltage-dependent activation gate for EAD onset (Figures 6.2A, 6.2I, 6.2L).

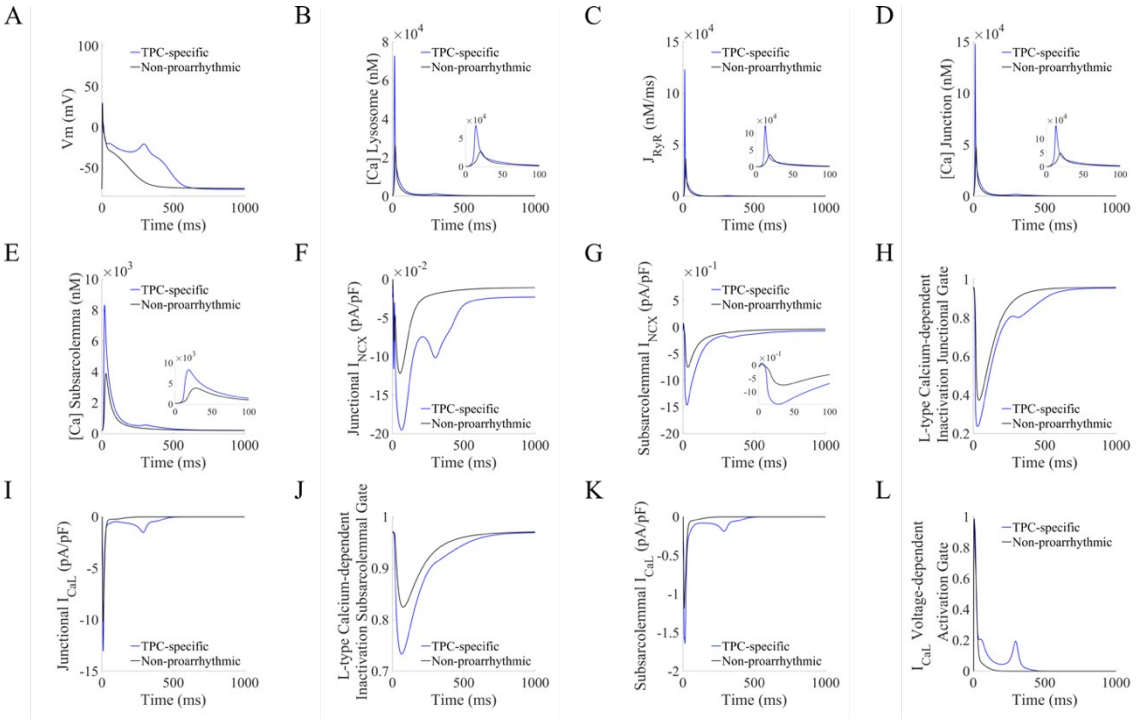


Figure 6.2. Traces of TPC-specific and non-proarrhythmic models under I_{Kur} block and β-adrenergic stimulation in nSR. **6.2A-6.2L:** Representative traces of action potential, lysosomal calcium concentration, RyR release, junctional and subsarcolemmal calcium concentrations, junctional and subsarcolemmal I_{NCX}, L-type calcium-dependent inactivation junctional and subsarcolemmal gates, junctional and subsarcolemmal I_{CaL}, and I_{CaL} voltage-dependent activation gate, respectively in the presence of lysosomal calcium release.

In terms of ionic properties, an evident trend in the conductance of the I_{CaL} showed that the TPC-specific category shared larger conductance magnitude, compared to the non-proarrhythmic category (Figure 6.3A). In addition, TPC-specific proarrhythmic models showed larger I_{Kur} conductance magnitudes to regulate their repolarisation (and oppose their larger I_{CaL}), which would render them more sensitive to I_{Kur} block (Figure 6.3A). The TPC-specific proarrhythmic category also presented larger I_{NCX} conductance sizes (Figure 6.3A).

I further explored to confirm that the above-described mechanisms were preserved at the population level. In the TPC-specific proarrhythmic category, lysosomal release promoted an increase in calcium loading in the junctional and subsarcolemmal spaces

by enhanced RyR release, compared to the non-proarrhythmic category (Figures 6.3B, 6.3C, 6.3D, 6.3E). The junctional loading increased the NCX forward mode, especially in the subsarcolemma (Figures 6.3B, 6.3F, 6.3G). The increase in subsarcolemmal loading, together with calcium influx by NCX reverse mode, led to enhanced calcium extrusion by NCX forward mode (Figures 6.3E, 6.3H, 6.3I). Thus, the inward source of NCX current promoted the EADs in the TPC-specific proarrhythmic category.

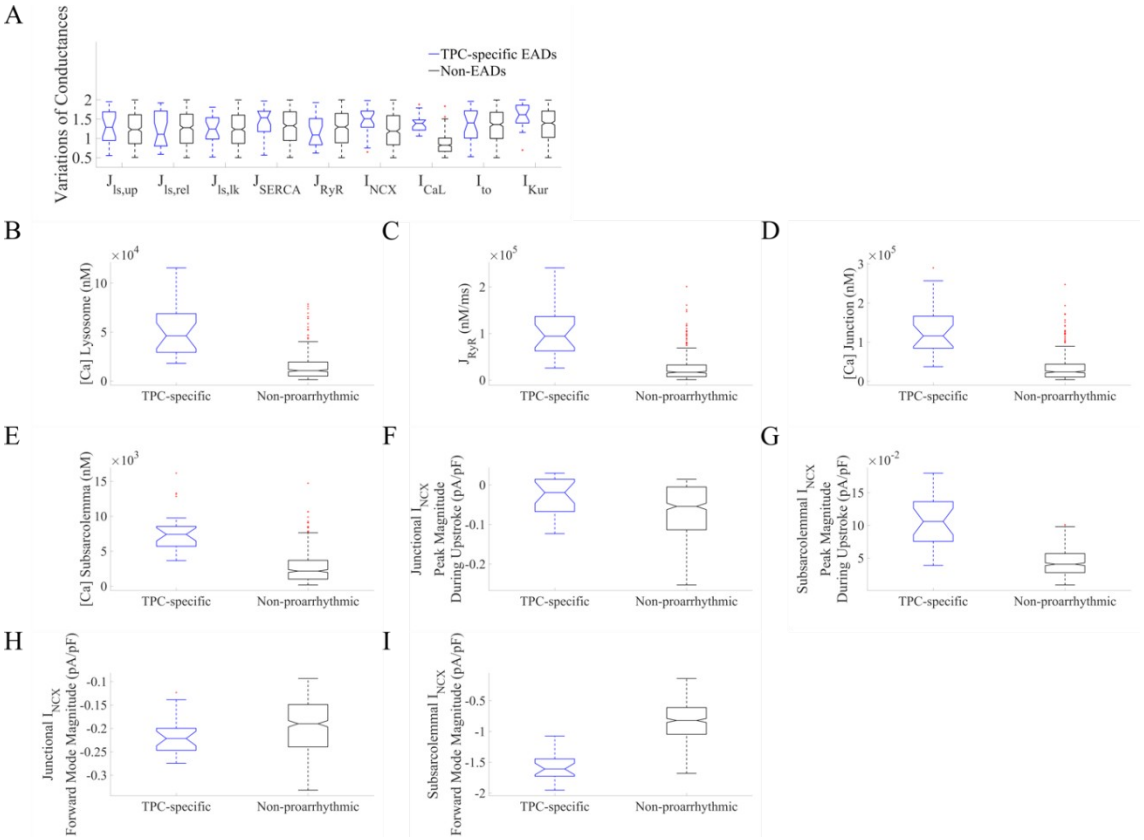


Figure 6.3. Comparisons of TPC-specific and non-proarrhythmic categories under I_{Kur} block and β-adrenergic stimulation in nSR. **6.3A:** Ionic properties in TPC-specific (blue), and non-proarrhythmic profiles (black). **6.3B-6.3I:** Distributions of amplitudes of lysosomal, junctional and subsarcolemmal calcium concentrations and RyR release, peak magnitudes during upstroke of junctional and subsarcolemmal I_{NCX}, and forward mode magnitudes of junctional and subsarcolemmal I_{NCX}, respectively comparing models in the TPC-specific and non-proarrhythmic categories.

6.2.2 Role of Lysosomal Calcium Release on generating EADs in TPC-specific Models in Normal Sinus Rhythm under I_{Kur} Block and β-adrenergic Stimulation

To better understand the mechanisms of modulation of EADs by lysosomal calcium release, I focused on the TPC-specific models in nSR. In this category of models, active lysosomal release promoted EADs while block of lysosomal release prevented their occurrence (Figure 6.4A), so here I detail changes directly associated to the block of TPC2 channels. Lysosomal release increases RyR release contributing to increased junctional and subsarcolemmal calcium loading (Figures 6.4B, 6.4C, 6.4D, 6.4E). These differences in calcium loading during active lysosomal release especially increased the forward mode of the subsarcolemmal component of the NCX current (Figure 6.4G). The increased junctional and subsarcolemmal calcium loading also promoted a protracted recovery of L-type calcium-dependent inactivation, especially in the subsarcolemma (Figures 6.4H, 6.4J), prolonging the time-window of I_{CaL} with slightly larger inward current during the plateau phase of the AP (Figures 6.4I, 6.4K). The resultant inward currents contributed to elevation of plateau voltage, and the increase in the opening of L-type voltage dependent activation gate, which further increased the late L-type currents for EAD formation (Figures 6.4A, 6.4I, 6.4K, 6.4L).

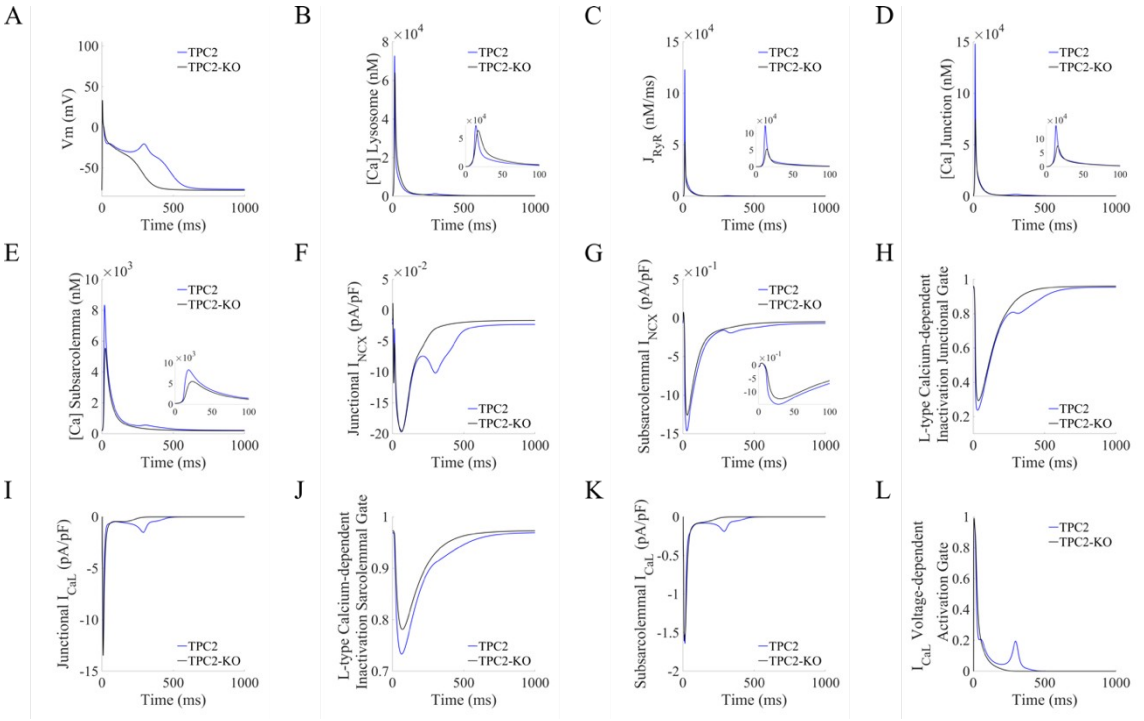


Figure 6.4. Lysosomal calcium release promoted EADs in proarrhythmic TPC-specific models under I_{Kur} block and β-adrenergic stimulation in nSR. **6.4A-6.4L:** Representative traces of action potential, lysosomal calcium concentration, RyR release, junctional and subsarcolemmal calcium concentrations, junctional and subsarcolemmal I_{NCX}, L-type calcium-dependent inactivation junctional and subsarcolemmal gates, junctional and subsarcolemmal I_{CaL}, and I_{CaL} voltage-dependent activation gate, respectively comparing the presence and block of lysosomal release.

Next, I tested at the population level to further corroborate whether the aforesaid mechanisms were preserved. Lysosomal release increased junctional and subsarcolemmal calcium loading by RyR release (Figures 6.5A, 6.5B, 6.5C, 6.5D). With minimum inward calcium by NCX reverse mode, lysosomal release mediated the depletion of junctional calcium, reducing the activity of the junctional NCX forward mode (Figures 6.5E, 6.5G). The larger subsarcolemmal loading by lysosomal release enhanced the forward mode of NCX in this compartment, leading to a larger inward current, under similar calcium influx by the reverse NCX mode (Figures 6.5F, 6.5H).

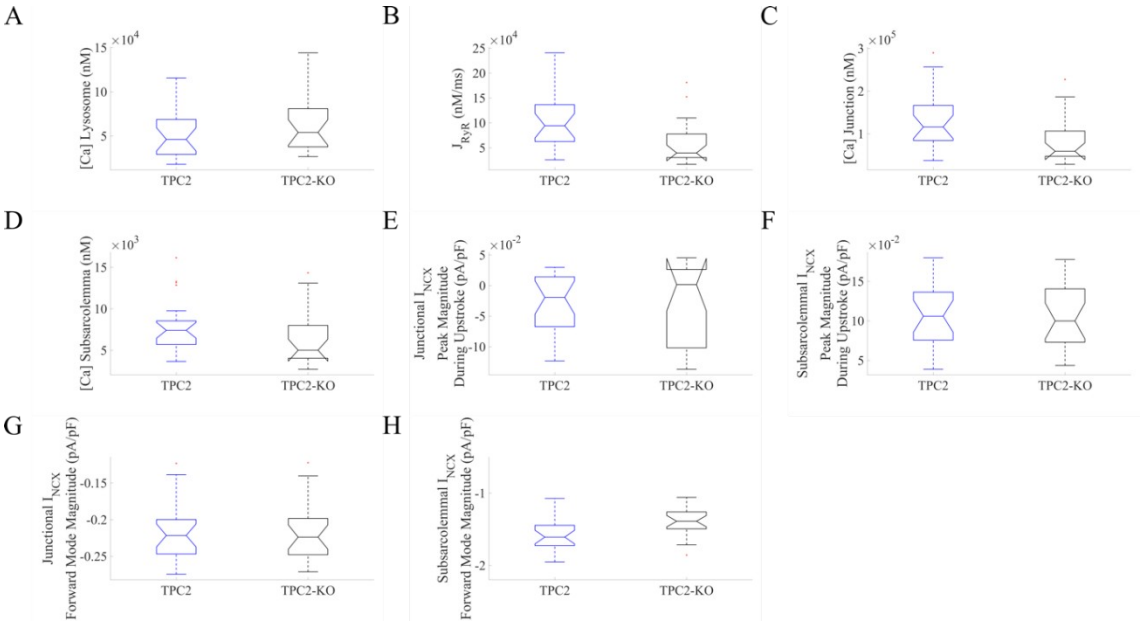


Figure 6.5. Lysosomal calcium release promoted EADs in proarrhythmic TPC-specific models under I_{Kur} block and β-adrenergic stimulation in nSR. **6.5A-6.5H:** Distributions of amplitudes of lysosomal, junctional and subsarcolemmal calcium concentrations and RyR release, peak magnitudes during upstroke of junctional and subsarcolemmal I_{NCX}, and forward mode magnitudes of junctional and subsarcolemmal I_{NCX}, respectively comparing the presence and block of lysosomal release in TPC-specific models.

6.2.3 Role of Lysosomal Calcium Release on generating EADs in Chronic Atrial Fibrillation under I_{Kur} Block and β-adrenergic Stimulation

To understand the contribution of lysosomal release to EADs in cAF, the role of lysosomal release was explored in the TPC-specific and non-proarrhythmic categories. Representative traces in each category are presented in Figure 6.6.

The mechanisms of EADs observed in nSR was preserved in cAF. Lysosomal release promoted EADs in TPC-specific models (Figure 6.6A). First, lysosomal release increased calcium loading in both the junction and subsarcolemma spaces via enhanced RyR release (Figures 6.6B, 6.6C, 6.6D, 6.6E). Second, the larger loading enhanced calcium extrusion by NCX, and to a larger extent in the subsarcolemma (Figures 6.6F, 6.6G). The increased junctional and subsarcolemmal calcium contributed to the protracted recovery of the L-type calcium-dependent inactivation, prolonging the time-window of I_{CaL} (Figures 6.6H, 6.6J). Finally, both inward sources of NCX and L-type currents contributed to the increase and reopening of the L-type voltage-dependent activation gate, which further promoted the late component of the L-type inward current (Figures 6.6I, 6.6K, 6.6L).

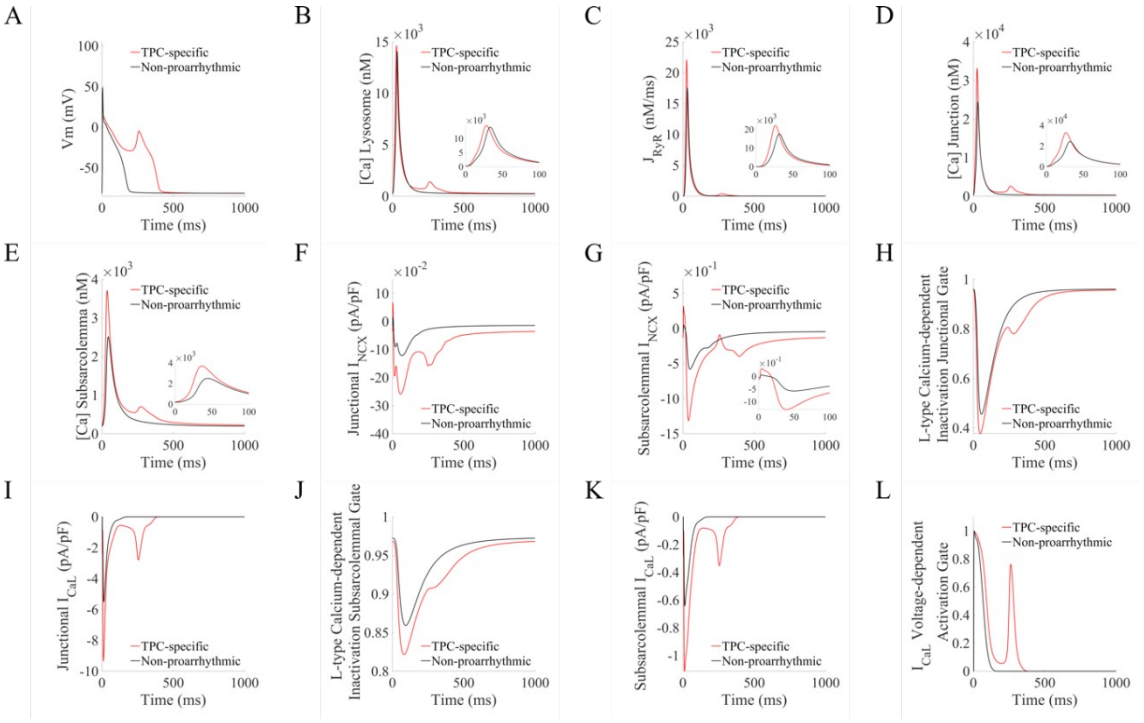


Figure 6.6. Traces of proarrhythmic TPC-specific, and non-proarrhythmic models with EADs under I_{Kur} block and β-adrenergic stimulation in cAF. **6.6A-6.6L:** Representative traces of action potential, lysosomal calcium concentration, RyR release, junctional and subsarcolemmal calcium concentrations, junctional and subsarcolemmal I_{NCX}, L-type calcium-dependent inactivation junctional and subsarcolemmal gates, junctional and subsarcolemmal I_{CaL}, and I_{CaL} voltage-dependent activation gate, respectively, in the presence of lysosomal calcium release.

Regarding ionic properties, a clear trend in the magnitude of I_{CaL} conductance was observed between the different categories as the main determinant of EAD propensity in cAF (Figure 6.7A). Non-proarrhythmic models showed the lowest I_{CaL} conductance, while TPC-specific models exhibited larger magnitudes. In addition, the magnitudes of I_{Kur} conductance were also larger in the TPC-specific proarrhythmic category, therefore making them more vulnerable to I_{Kur} block (Figure 6.7A).

I then tested whether the above mechanisms for lysosomal-induced EADs were also preserved at the population level. As expected, lysosomal release increased RyR release and resulted in increased calcium loading in both the junction and subsarcolemma

(Figure 6.7B, 6.7C, 6.7D, 6.7E). Under similar inward calcium by NCX, lysosomal release mediated junctional calcium depletion, reducing the activity of junctional NCX forward mode (Figures 6.7F, 6.7H). The increased subsarcolemmal calcium, with larger inward calcium by NCX, led to an enhanced subsarcolemmal component NCX forward mode (Figure 6.7G, 6.7I).

In summary, lysosomal release promoted EADs primarily by increasing the subsarcolemmal component of the NCX inward current in both nSR and cAF. This increase in total inward current contributed to the elevation of plateau voltage, which promoted the reactivation of the L-type calcium channel leading to EADs.

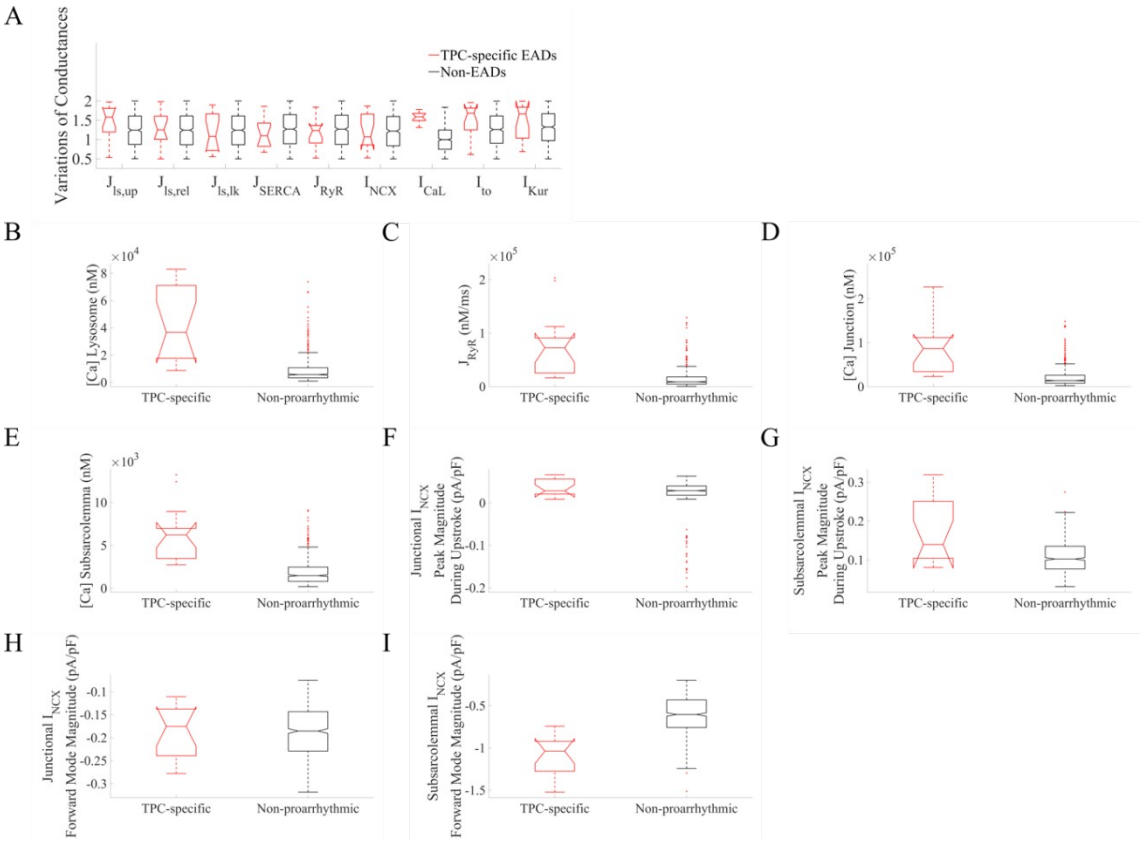


Figure 6.7. Comparisons of TPC-specific, and non-proarrhythmic categories under I_{Kur} block and β-adrenergic stimulation in cAF. **6.7A:** Ionic properties in TPC-specific (red) and non-proarrhythmic profiles (black). **6.7B-6.7I:** Distributions of amplitudes of lysosomal, junctional and subsarcolemmal calcium concentrations and RyR release, and peak magnitudes during upstroke of junctional and subsarcolemmal I_{NCX}, and forward mode magnitudes of junctional and subsarcolemmal I_{NCX}, respectively comparing models in TPC-specific, and non-proarrhythmic categories.

6.2.4 Role of Lysosomal Calcium Release on generating EADs in TPC-specific Models in Chronic Atrial Fibrillation under I_{Kur} Block and β-adrenergic Stimulation

Finally, to better characterise the mechanisms of modulation of EADs by lysosomal calcium release under I_{Kur} block in cAF, I again focused on TPC-specific models by analysing in detail the changes exhibited by this subset of models under simulated TPC2 channel block. In these models, active lysosomal release promoted EADs, while TPC2 channel block prevented their onset (Figure 6.8A).

Similar to the nSR case, lysosomal release also increased RyR release and calcium loading in cAF in both the junction and the subsarcolemma spaces (Figures 6.8B, 6.8C, 6.8D, 6.8E). The resulting differences in calcium loading during active lysosomal release newly led to a net increase in inward currents, especially of the NCX forward mode in the subsarcolemma (Figure 6.8G). The increased calcium loading also promoted a protracted recovery of L-type calcium-dependent inactivation, in particular in the subsarcolemma (Figures 6.8H, 6.8J), leading to a prolonged time-window of I_{CaL} with slightly larger inward current during the plateau phase of the AP (Figures 6.8I, 6.8K). Therefore, the larger inward NCX and L-type currents promoted the reopening of L-type voltage-dependent activation, leading to EAD formation (Figure 6.8L).

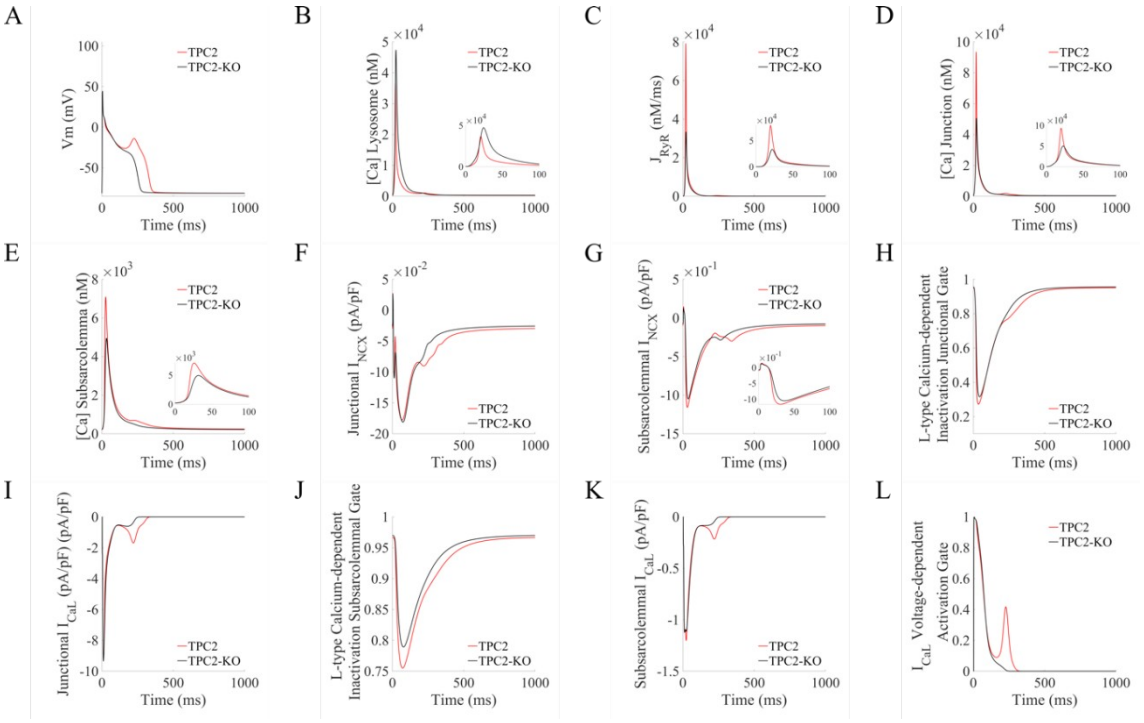


Figure 6.8. Lysosomal calcium release promoted EADs in proarrhythmic TPC-specific models under I_{Kur} block and β-adrenergic stimulation in cAF. **6.8A-6.8L:** Representative traces of action potential, lysosomal calcium concentration, RyR release, junctional and subsarcolemmal calcium concentrations, junctional and subsarcolemmal I_{NCX}, L-type calcium-dependent inactivation junctional and subsarcolemmal gates, junctional and subsarcolemmal I_{CaL}, and I_{CaL} voltage-dependent activation gate, respectively comparing the presence and block of lysosomal release.

To complement the previous results, I tested if the above-described mechanisms also held at the population level. In the population (Figure 6.9), lysosomal release increased RyR release, which further increased calcium loading in both the junction and subsarcolemma (Figures 6.9A, 6.9B, 6.9C, 6.9D). The larger junctional loading contributed to similar junctional NCX forward mode due to the involvement of lysosomal transport, leading to a similar inward calcium intake by the NCX reverse mode between the presence and block of lysosomal release (Figures 6.9E, 6.9G). On the other hand, the larger subsarcolemmal loading, together with an additional increase of inward calcium by reverse NCX, concomitantly contributed to an enhanced NCX

forward mode in the subsarcolemma, then leading to AP prolongation and increased plateau voltage levels (Figure 6.9F, 6.9H).

In summary, lysosomal release promoted EADs by increasing subsarcolemmal NCX inward current, and junctional and subsarcolemmal late L-type currents, in TPC-specific models in both nSR and cAF under I_{Kur} block and β-adrenergic stimulation.

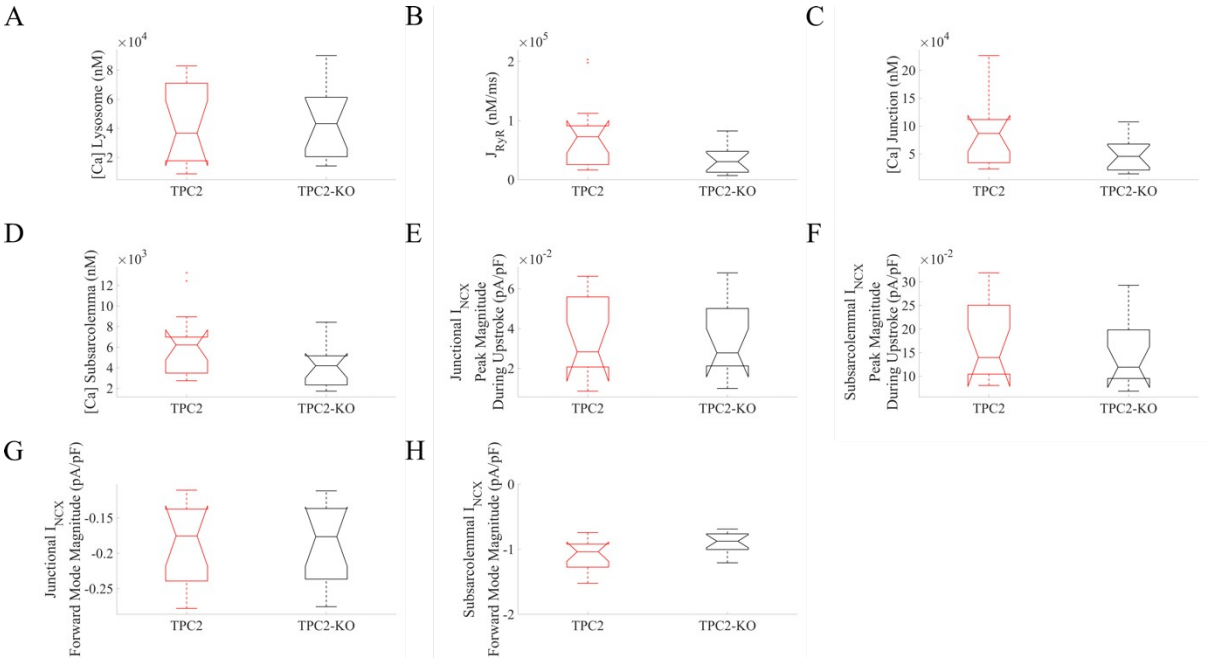


Figure 6.9. Lysosomal calcium release promoted EADs in proarrhythmic TPC-specific models under I_{Kur} block and β-adrenergic stimulation in cAF. **6.9A-6.9H:** Distributions of amplitudes of lysosomal, junctional and subsarcolemmal calcium concentrations and RyR release, peak magnitudes during upstroke of junctional and subsarcolemmal I_{NCX}, and forward mode magnitudes of junctional and subsarcolemmal I_{NCX}, respectively comparing the presence and block of lysosomal release in the TPC-specific models.

6.3 Discussion

The modelling and simulation results presented in this chapter illustrate the proarrhythmic mechanisms of lysosomal calcium release in inducing EADs under I_{Kur} block and β-adrenergic stimulation. Blocking I_{Kur} prolonged the duration of the plateau of the AP to yield the conditions for reactivation of the L-type calcium channel. The EADs resulted from an increase inward NCX current and late L-type current, which were mediated by active lysosomal calcium release. The inward currents contributed to the elevation of the plateau potential, which mediated the reopening of L-type voltage-dependent activation and the density of the late L-type current.

Lysosomal release, forming a component of calcium transport, functions to transport junctional calcium to the cytosol to potentiate SR reuptake. This calcium transport had the effects of depleting junctional calcium and potentiating subsarcolemmal calcium loading. The increase in junctional calcium loading contributed to promote a protracted recovery of the calcium-dependent inactivation of junctional I_{CaL} and thus to prolong its active time-window. The increase of subsarcolemmal calcium loading, by inward NCX calcium and junctional calcium diffusion, contributed to an increase of NCX forward mode, which promotes the protracted recovery of the calcium-dependent inactivation of subsarcolemmal I_{CaL} and its time-window. Thus, the increase in inward currents included both subsarcolemmal NCX, and junctional and subsarcolemmal L-type calcium currents. These currents mediated the formation of EAD in the models of TPC-specific proarrhythmic category in nSR and in cAF.

The investigations conducted on the proarrhythmic modulation of EADs by lysosomal calcium release included non-TPC-specific proarrhythmic, TPC-specific proarrhythmic and non-proarrhythmic categories in both nSR and cAF. The TPC-specific proarrhythmic category showed that the increases of subsarcolemmal NCX inward current and junctional and subsarcolemmal late L-type currents mediated the EADs.

Non-proarrhythmic models were characterised by smaller NCX and late L-type inward currents.

In TPC-specific models, lysosomal release contributed to an enhanced NCX forward mode in the subsarcolemma, and the protracted recovery of the junctional and subsarcolemmal L-type calcium-dependent inactivation gates with prolonged I_{CaL} time-window. Therefore, subsarcolemmal NCX inward current, and junctional and subsarcolemmal late L-type calcium current mediated the EADs. These TPC-specific models illustrate lysosomal calcium release as a sufficient mediator of EAD occurrence, contributing the sufficient instability to change intracellular calcium handling to promote the above-described downstream mechanisms. On the other hand, blocking lysosomal release inhibited EADs by reducing junctional loading (by transporting junctional calcium into lysosome, holding it, and reverting only a fraction to the junction). This reduced calcium loading in the junction also contributed to a reduced subsarcolemmal loading, which further decreased the NCX forward mode and shortened the recovery of junctional and subsarcolemmal calcium-dependent inactivation, hence reducing the I_{CaL} active time-window.

I conclude that lysosomal calcium release under I_{Kur} block and β-adrenergic stimulation promotes EADs by increasing NCX inward current and late L-type calcium current (Figure 6.10).

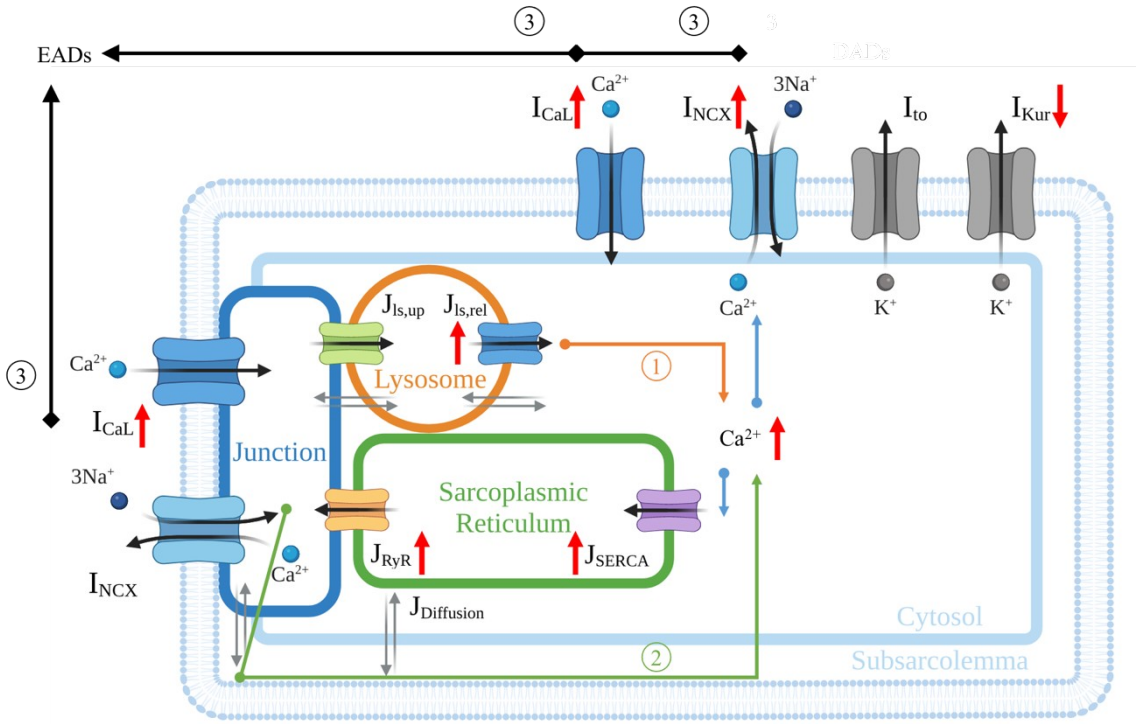


Figure 6.10. Schematic cartoon showing the conclusion for actions of lysosomal calcium release.

Chapter 7
Conclusions

I conclude my thesis by outlining its primary accomplishments. In this chapter, I highlight the reasons behind the doctoral dissertation and providing an overview of my work that was done. I outline the main conclusions, which include integrating lysosomal calcium handling into models of human atrial cardiomyocytes and mouse ventricular myocytes, as well as examining the proarrhythmic processes of lysosomal calcium handling in ventricular and atrial electrophysiology. I will then conclude my work with closing thoughts after outlining an overview of potential future research topics.

7.1 Summary

My thesis is related to the modelling and simulation of lysosomal Ca^{2+} handling in mouse ventricular and human atrial cardiomyocytes, in order to better understand lysosomal function and its potential contribution to arrhythmias.

The SR is known as the principal intracellular Ca^{2+} store within cardiomyocytes. Christian de Duve identified the lysosome as the major digestive compartment of the cell in 1955 (C. de Duve *et al.*, 1955; De Duve and Wattiaux, 1966; de Duve, 2005). Lysosomes have long been appreciated to be waste managing/recycling organelles, responsible for the degradation of macromolecules, but are also regulators of a number of signalling pathways, including apoptosis (Morgan *et al.*, 2011; Appelqvist *et al.*, 2013). Lysosomes are ubiquitous organelles in eukaryotic cells. They contain more than 50 different acid hydrolases and several activator proteins that are localised mainly in the matrix (de Duve, 2005; Lübke, Lobel and Sleat, 2009). Lysosomes have a 7-10 nm

limiting phospholipid bilayer and ultra-structurally appear as cytosolic dense bodies (de Duve, 2005). Lysosomes are also Ca^{2+} stores and contain up to 600 μM Ca^{2+} (Lloyd-Evans *et al.*, 2008). Ca^{2+} has many roles within the endolysosomal system; it is crucial for the maintenance of trafficking, recycling, as well as vesicular fusion events (Lloyd-Evans and Platt, 2011). NAADP, a potent intracellular second messenger acting on TPCs, has been found to be responsible for stimulating Ca^{2+} release from the lysosome into the cytosolic compartment (Capel *et al.*, 2015).

Previous studies have also shown that NAADP-AM could not enhance the Ca^{2+} transient in genetically-modified TPC2-KO cardiomyocytes (Capel *et al.*, 2015). β-adrenergic stimulation by ISO increased the level of NAADP (Lewis *et al.*, 2012). TPC2 openness was dependent on NAADP concentration (Pitt *et al.*, 2010; Penny *et al.*, 2014). β-adrenergic stimulation by ISO increased Ca^{2+} transients in both TPC2-KO and WT cardiomyocytes, while the increased effect was reduced in TPC2-KO compared to WT (Capel *et al.*, 2015). Monophasic APs from the genetically-modified TPC2-KO whole hearts compared to WT under ventricular burst pacing protocols have showed a reduced tendency for arrhythmia and reduced threshold for arrhythmogenesis following acute or chronic β-adrenergic stimulation under ISO respectively, further evidencing that Ca^{2+} release from the lysosome under β-adrenergic stimulation presents a tendency to be proarrhythmic (Capel *et al.*, 2015). Recently published data by my main supervisor's group have shown lysosomes to be in close proximity to the SR, by which lysosomal Ca^{2+} could directly promote CICR from RyRs or result in enhanced SR Ca^{2+} release indirectly (Aston *et al.*, 2017). However, the mechanisms by lysosomal calcium handling in pro-arrhythmia remain poorly understood.

Calcium handling operates in simultaneous function with a broad range of systems, complexes, and proteins and it becomes difficult to study the interaction of their involved processes (Shannon *et al.*, 2004; Morotti *et al.*, 2014). Such processes can be formally described by means of mathematical modelling and assembled in a comprehensive fashion for studying their interactions and overcome experimental difficulties (Shannon *et al.*, 2004; Morotti *et al.*, 2014). Biological variability in physiological function, often difficult to treat in experimental research, is generally

addressed by averaging data to reduce errors (Sarkar, Christini and Sobie, 2012; Britton *et al.*, 2013; Muszkiewicz *et al.*, 2016). Populations of models are a methodology accomplished by computational simulation and has proved to link mechanisms with their physiological variations by calibration against experimental data (Britton *et al.*, 2013; Muszkiewicz *et al.*, 2016; Passini *et al.*, 2016; Zhou *et al.*, 2016). I therefore proposed to utilise computational mechanistic studies using a population of models approach to investigate the mechanisms mediated by lysosomal calcium handling on cellular proarrhythmia.

Based on the localisation and function of the lysosome and using a rodent model that matches with the experiments (Capel *et al.*, 2015; Ruas *et al.*, 2015; Garrity *et al.*, 2016; Aston *et al.*, 2017), I extended the mouse ventricular cardiomyocyte model with β-adrenergic stimulation by Morotti *et al.* (Morotti *et al.*, 2014) to include lysosomal calcium handling. Next, to understand the role of lysosomal calcium release in human atrial electrophysiology, I aimed to address its possible proarrhythmic mechanisms in both nSR and cAF. At present, there is no experimental evidence of that calcium from the lysosomes can contribute to pro-arrhythmia in human atrial cardiomyocytes, so my research will be important in informing such experiments. To this end, I have extended the human atrial Grandi *et al.* (Grandi *et al.*, 2011) model with intracellular lysosomal calcium handling, based on its similar mathematical formulation to the mouse model by Morotti *et al.* (Morotti *et al.*, 2014) where I have already successfully incorporated lysosome function (Meng *et al.*, 2023).

Therefore, the goal of this thesis was to investigate proarrhythmic mechanisms of lysosomal calcium handling by populations of biophysically detailed cardiomyocytes models. In this thesis, I investigated four proarrhythmic conditions: hypercalcemia and fast to slow pacing transitions with β-adrenergic stimulation in mouse ventricular cardiomyocytes, mild hypercalcemia and I_{Kur} block with β-adrenergic stimulation in human atrial cardiomyocytes.

In Chapter 1, I began by introducing physiology in the heart. I focused on ion channels which mediated the different phases of an AP, cellular proarrhythmic mechanisms by

explaining spontaneous calcium release and DAD, and EAD, and chronic AF ionic remodelling and chronic AF therapy by pharmacological drugs. Then I introduced alternative calcium stores, namely lysosomes in the heart. I presented the discovery of lysosomes, lysosomal storage diseases, lysosomal calcium stores and calcium signalling in cardiomyocytes. Particular attention was paid to NAADP signalling and modulation in cardiomyocytes. Finally, I presented important computational techniques, such as development of computational models and method of population of models. This method is to address the variability in the cardiac electrophysiology.

In Chapter 2, I described the incorporation of lysosomal calcium handling in mouse ventricular and human atrial cardiomyocyte models. First, I presented the experimental data that were used in the modelling. Second, I presented the modelling of TPC2 opening response to NAADP concentration and lysosomal uptake and release fluxes. I then presented the incorporation of lysosomal calcium handling into the established models. Next, I presented the cellular variability of ionic currents and calcium fluxes that were used in this study. Finally, I described the analyses of biomarker features and proarrhythmic events.

In Chapter 3, I presented my study on the role of lysosomal calcium handling in mouse ventricular cardiomyocytes (Meng *et al.*, 2023). I investigated the proarrhythmic contributions of variability in lysosomal function in the spontaneous calcium release by RyRs in hypercalcemia or fast to slow pacing transitions in addition to β-adrenergic stimulation. The results identified an involvement of lysosomal release in spontaneous calcium release events by exerting a modulation of the RyR open probability. In cellular models where pro-arrhythmia was directly linked to lysosome function, lysosomal calcium handling enabled a fast calcium transport pathway which promoted spontaneous calcium release by elevating RyR open probability. Inhibition of either lysosomal uptake or release revealed an antiarrhythmic impact.

In Chapter 4, I showed the function of lysosomal calcium release in human atrial cardiomyocytes. I performed a comprehensive calibration and validation of β-adrenergic response in our modified human atrial model against simultaneously

acquired calcium transient and AP recordings from human atrial control and cAF cardiomyocytes in the absence and presence of ISO application. To investigate the modulation of lysosomal calcium handling in human atrial cellular electrophysiology, I exploited a population of models approach to account for cellular variability in ionic currents and calcium fluxes. I further calibrated the populations in nSR and cAF by AP biomarkers. Next, I revealed that lysosomal release primarily modulated intracellular calcium handling by increasing SERCA reuptake and RyR release in nSR and cAF. This led to the hypothesis that this intracellular mechanism could be of relevance under proarrhythmic conditions of calcium overload, by lysosomes acting as secondary calcium sources.

In Chapter 5, I investigated the proarrhythmic mechanisms of lysosomal calcium release in EADs under conditions of calcium overload by mild hypercalcemia and β-adrenergic stimulation. First, by analysing their proarrhythmic involvement, I revealed non-TPC-specific proarrhythmic models (proarrhythmic regardless of the presence or block of lysosomal calcium release), TPC-specific proarrhythmic models (proarrhythmic only during active lysosomal release), and non-proarrhythmic models. Second, I found that increased subsarcolemmal calcium loading promoted an enhanced subsarcolemmal NCX forward mode, and larger junctional and subsarcolemmal loading led to a protracted recovery of L-type calcium-dependent inactivation and prolonged I_{CaL} time-window during plateau stage of the AP. The resultant inward currents contributed to elevate the plateau potential, which caused the reopening of L-type voltage-dependent activation gate and facilitated the EADs in nSR. In cAF, despite shorter APD and smaller L-type conductance, the above mechanism was still preserved.

In Chapter 6, I investigated the role of lysosomal calcium release in EADs under I_{Kur} block and β-adrenergic stimulation. Based on the hypothesis, blocking I_{Kur} might reduce repolarisation reserve, and contribute to EADs onset. In this context, I aimed to explore whether the concomitant pharmacological inhibition of lysosomal calcium release might make a potential antiarrhythmic strategy to reduced EADs incidence meanwhile maintaining the beneficial increase of effective refractory period by I_{Kur} block. Lysosomal calcium release promoted EADs by increasing the subsarcolemmal NCX

inward current, junctional and subsarcolemmal L-type inward current in nSR and cAF. These inward sources contributed to elevation of plateau potential, and this promoted the reactivation of L-type calcium channel which facilitated EADs onset. The mechanisms in nSR and cAF were consistent with those underpinning EADs formation in the context of mild hypercalcemia.

7.2 Key Findings

The initial part of the thesis developed novel models which incorporated lysosomal calcium handling in mouse ventricular and human atrial cardiomyocytes, based on experimental findings. Inclusion of the lysosomal compartment in mouse ventricular cardiomyocytes led to validated model predictions of increased cytosolic calcium transient amplitude under NAADP-AM and ISO protocols compared to control (CTRL). This response was mediated by an enhanced SERCA reuptake and RyR release under active lysosomal calcium release. The incorporation of lysosomal subspace in human atrial cardiomyocytes led to model prediction of the increase of calcium transient amplitude under β-adrenergic stimulation, in agreement with experimental findings in atrial cardiomyocytes. This process showed lysosomal calcium release primarily modulated intracellular calcium handling by increasing SERCA reuptake and RyR release.

The following part of the thesis investigated the proarrhythmic mechanisms of lysosomal calcium handling in spontaneous calcium release in mouse ventricular cardiomyocyte models and EADs in human atrial cardiomyocyte models. In mouse ventricular cardiomyocytes, lysosomal calcium handling promoted spontaneous calcium release via RyR from the SR by elevating the RyR open probability in hypercalcemia and in fast to slow pacing transitions, additionally coupled with β-adrenergic stimulation. Blocking either lysosomal calcium uptake or release revealed an antiarrhythmic impact. In the conditions of calcium overload, these results showed that

these responses were largely modulated by intercellular variability in L-type calcium current, RyR release, and SERCA reuptake. This investigation identified that lysosomal calcium handling directly modulated RyR spontaneous release by regulating RyR open probability, suggesting antiarrhythmic strategies and identifying key modulators of lysosomal proarrhythmic action.

In human atrial cardiomyocytes, lysosomal calcium release promoted EADs by increasing subsarcolemmal NCX inward current, junctional and subsarcolemmal late L-type current in mild hypercalcemia and I_{Kur} block with β-adrenergic stimulation. In this process, lysosomal calcium release promoted NCX forward mode by increasing subsarcolemmal calcium loading, and promoted late L-type current by protracting the recovery of L-type calcium-dependent inactivation and by prolonging I_{CaL} time-window. Blocking lysosomal calcium release revealed an antiarrhythmic strategy. Under the condition of calcium overload by mild hypercalcemia and the condition of reducing repolarisation reserve by I_{Kur} block, these results indicated that these responses were largely modulated by intercellular variability in L-type calcium and NCX currents. This revealed lysosomal release as a sufficient mediator of EADs onset, capable of contributing the sufficient instability to alter intracellular calcium handling and drive the downstream mechanisms. This investigation identified that active lysosomal calcium release directly modulated EADs onset by regulating inward sources of currents, revealing antiarrhythmic strategies, and identifying key modulators of lysosomal proarrhythmic action.

7.3 Future Directions

7.3.1 Dimensions in Cardiac Modelling

This work concentrates on single cell models that include a certain level of detail in describing the mechanisms leading to the forms of arrhythmias observed in experiments. Nonetheless, multicellular phenomena underlie clinically significant heart rhythm abnormalities, and numerous efforts have been made to create complex models of cardiac electromechanical activity (Garny, Noble and Kohl, 2005). In this thesis, I used single cardiomyocyte models and simulations to investigate the proarrhythmic mechanisms of lysosomal calcium handling in mouse ventricular and human atrial electrophysiology. However, cardiac arrhythmias occur at the tissue level, and the impact of gap junction coupling and 3D tissue structure might affect the origin of arrhythmias. Afterdepolarisations can propagate at tissue level initiating arrhythmia in the presence of decreased intercellular coupling, which is also linked to slower propagation, leading to re-entry, which can be either anatomical (anchoring around an anatomical obstacle) or functional (supported by regional refractoriness in the absence of anatomical defects) (Anumonwo and Pandit, 2015). In this regard, multicellular models are necessary for the simulation of the spread of both normal and abnormal cardiac excitation.

Several proarrhythmic conditions, including re-entry, might only be studied in 2D or 3D simulations. 2D models can be used to explore complex associated re-entry patterns or fibrillation, and they get around many of the shortcomings of lower dimensionality model. However, 3D implementations further enable research on scroll waves (transmural re-entry); they are the most realistic (Garny, Noble and Kohl, 2005). Research indicates that 2D models are a useful first step towards anatomically accurate simulations because they provide a reasonable balance between computer power, the

intricacy of electrophysiological models, and their suitability for basic science applications. Thus, I believe it is a promising direction of future investigations to extend the results of this thesis to tissue modelling.

Due to time constraints, I was unable to explore 2D or 3D modelling approaches. Future studies involving 3D tissue simulation for a biophysically detailed model would require supercomputing resources, and performing simulation studies with a population of models. Thus, the next research step might begin with simple 2D simulations for the TPC-specific models (exhibiting pro-arrhythmias when lysosomal calcium release is present, while not when blocked). It would be intriguing to explore the generation of the afterdepolarisations by lysosomal calcium handling under the influence of electrical coupling.

7.3.2 The Impact of Lysosomal Calcium Handling and Cardiac Fibrosis on Causing Atrial Arrhythmias at the Tissue Level

Building on the work from atrial cellular modelling, I would extend my findings to simulation studies of atrial tissue to investigate the impact of lysosomal calcium handling on conduction (Liberos *et al.*, 2016; Sánchez *et al.*, 2017; Aronis *et al.*, 2019). Given the well-documented involvement of fibrosis in lysosomal disease, it would be interesting to investigate the interplay of lysosome calcium dysregulation and cardiac fibrosis in promoting suitable substrates for re-entry in AF. At the tissue level, this would be made possible by integrating the modelling and simulation technologies with those for the generation of physiologically accurate patterns of cardiac fibrosis (Jakes *et al.*, 2019). Cellular models extracted from the populations of human atrial cardiomyocyte models in this thesis would be integrated into the tissue models and simulated under protocols of fast pacing, to explore mechanisms of arrhythmia initiation

under different fibrosis types (interstitial, diffuse, patchy) as characteristic of lysosomal disease. In particular, my initial hypothesis would be that the stronger loading effects of patchy fibrosis will predispose the generation of re-entry associated to lysosomal calcium handling compared to other fibrosis types. The proposed simulation studies might be initially performed in 2D and extended to realistic 3D atrial anatomies as needed. Experimental validation of the observed conduction phenomena might be possible through optical mapping experiments in cardiac monolayers.

7.3.3 Developing and Validating Computational Models of hiPSc-derived Cardiomyocytes

Computational methods are still in their infancy when it comes to handling interactions at the global and subcellular levels. Human induced pluripotent stem cell (hiPSc) cultures are extremely accessible to computer modelling techniques due to their 2D shape and ability to remain viable for several days. By adding details on organelle signalling compartmentalisation, physiologically accurate hiPSc atrial models can be improved and utilised to assess the relative contributions of the main ionic pathways linked to lysosome activity to human atrial APs and Ca^{2+} transients. Electrophysiological and structural heterogeneities in refractoriness and propagation velocity as characterised experimentally can be represented in the model by introducing changes in single cell properties and cell-to-cell coupling for the purpose of testing hypotheses regarding mechanisms of re-entry in AF at the tissue level.

The methods developed in this thesis may be applied to other LSDs. LSDs result from inherited defects in any aspect of lysosomal homeostasis and are caused by genetic mutations in lysosomal enzymes, transporters, and ion channels (Morgan *et al.*, 2011). A common pathological feature in LSDs includes defective lysosomal calcium signalling (Appelqvist *et al.*, 2013). Several types of LSDs are associated with cardiac

disorders, including increased risk of arrhythmia (Laney, Gupta and Wechsler, 2018). As one such example, Anderson Fabry disease is the second most prevalent LSD (Klingelhöfer *et al.*, 2020). Approximately over 50% of Fabry patients have cardiac manifestation, usually atrial or ventricular arrhythmias, with atrial arrhythmia more common (Mehta *et al.*, 2004; Morrissey, Philip and Schwarz, 2011).

To investigate the proarrhythmic role of lysosomal calcium handling in cardiac manifestation in Fabry disease, we might use the Fabry-patient induced pluripotent stem cell-derived cardiomyocytes (iPSC-CMs). iPSC-CMs contain donor-specific genotype and phenotype relationships and display cell-to-cell cardiac variability. Computational modelling and simulation offers a high throughput approach to reconcile multiple datasets of lysosomal calcium signalling by iPSC-CMs (Kernik *et al.*, 2019). Such a framework would link the molecular activities to cellular outputs in arrhythmia by utilising model parameters linked to known iPSC-CMs phenotypes in Fabry disease. Further, the iPSC-CMs models could be extended to include genetic mutations and pharmacological interventions to study the proarrhythmic mechanisms of the role of lysosomal calcium handling in rare events in Fabry disease. This integration of experimental datasets and computational modelling might provide the capability of predicting patient-to-patient vulnerability in the onset of cardiac arrhythmias.

7.3.4 Modelling Lysosomal Calcium Handling in hiPSC-aCMs in Atrial Fibrillation

AF is the most frequently encountered clinical arrhythmia, associated with increased morbidity and mortality (Dobrev and Nattel, 2010). Ectopic activity and re-entry are considered major arrhythmogenic mechanisms contributing to the initiation and maintenance of AF (Dobrev and Nattel, 2010). “Improving our understanding on the onset and maintenance of atrial arrhythmias depends on details such as geometry,

electrical state, anisotropic cellular and sub-cellular structures such as the sarcoplasmic reticulum, and heterogeneities" (Trayanova, 2014; Aston *et al.*, 2017; Beneke and Molina, 2021). Work from the lab I belong to has demonstrated that NAADP-induced calcium release from lysosomes increases the calcium transient amplitude and sarcoplasmic calcium load in atrial myocytes, potentially leading to AF (Capel *et al.*, 2015) (unpublished results). The key question is how NAADP-induced calcium release leads to these results.

Using these cells, it will allow a better understanding of the basic biological mechanisms of sub-cellular calcium signalling in atria and the aetiology of AF by investigating the importance of NAADP signalling in human induced pluripotent stem cell-derived atrial cardiomyocytes (hiPSC-aCM). Augmenting *in-silico* hiPSC-aCM models (Paci *et al.*, 2013) with accurate descriptions of lysosomal calcium signalling would provide a better understanding of the pathway in AF, and qualify such models as an alternative to animal use in calcium dysregulation research. Recent studies (Ayagama *et al.*, 2023) have suggested that endolysosomes play an important role in atrial function and contribute to the development of AF over longer time frames. There is mounting evidence that calcium contribution from the lysosomes in cardiomyocytes is important in atrial function, and that perturbations in lysosomal calcium in disease processes may lead to initiation and maintenance of AF (Collins *et al.*, 2011; Ayagama *et al.*, 2023; Capel *et al.*, 2024). Computational modelling incorporating lysosomal calcium handling in hiPSC-aCM models (Paci *et al.*, 2013) and investigating proarrhythmic mechanisms offer a step-by-step method for increasing dimensionality and complexity in cardiac modelling.

7.3.5 Incorporating Anatomical Localisation of Lysosomes Information in Control vs Atrial Fibrillation Cellular Models

From the functional electrophysiological modelling of lysosomal calcium handling in cardiomyocytes, I additionally believe there is scope for incorporating anatomical localisation information on lysosomes in anatomical modelling of intracellular calcium stores.

Lysosomes are closely associated with the SR with a median separation of 20nm in 2D electron microscopy and 3.3nm in 3D electron tomography (Aston *et al.*, 2017). Membrane contact sites (MCS) were defined as regions in which the membranes of neighbouring organelles were 5 to 30nm apart (Barral *et al.*, 2022). MCS provided platforms for protein interactions, signalling events, lipid exchange and calcium flux (Martello, Platt and Eden, 2020). Lysosome biogenesis and function are affected by links with other organelles at MCS, such as the MCS that form between ER and late endocytic organelles (Barral *et al.*, 2022). Lysosomes not just form MCS with the ER, but also with the mitochondria (Barral *et al.*, 2022) by a median separation of 6.2nm in 3D studies. In terms of calcium signalling, ER-lysosomes MCS were implicated in the refilling of lysosome calcium stores (Garrity *et al.*, 2016; Atakpa *et al.*, 2018), and generating local calcium signals (Kilpatrick *et al.*, 2013; Morgan *et al.*, 2013), which may regulate the extent of contact (Kilpatrick *et al.*, 2017). This might imply a calcium regulated calcium signalling mechanism at MCS. ER-lysosome calcium cross-talk seems likely at these MCS (Burgoyne, Patel and Eden, 2014). Mathematical modelling supports the concept (Burgoyne, Patel and Eden, 2014; Fameli *et al.*, 2014; Penny *et al.*, 2014). Modelling of calcium fluxes at ER-lysosome MCS in fibroblasts (Penny *et al.*, 2014) and SR-lysosome MCS in pulmonary artery smooth muscle cells (Fameli *et al.*,

2014) supports and predicts that lysosomal calcium release is sufficient to trigger CICR by the ER/SR (Burgoyne, Patel and Eden, 2014).

To extend the current modelling framework of lysosomal calcium handling into structure-function modelling, the lysosome anatomical experimental measurements could be incorporated in the modelling of diffusion fluxes in the membrane contact site between lysosome and the neighbouring organelles.

A previous study of calcium microdomains at the MCS of lysosome and ER showed a computational model of the coupling of lysosomal calcium leak as trigger and ER calcium as amplifier by IP3 receptor (Penny *et al.*, 2014). This model was adapted for the studies in which NAADP-mediated lysosomal calcium release in the microdomain of lysosome and ER could lead to global calcium oscillations (Penny *et al.*, 2014). Previous studies also showed that a computational closed-cell model of calcium dynamics accounted for ER-mitochondria calcium microdomains as a compartment with calcium influx and efflux (Moshkforoush *et al.*, 2019). IP3 receptors have been reported to populate at the ER-lysosome MCS, and facilitated the localised calcium delivery from ER to lysosomes (Atakpa *et al.*, 2018). Further, TPC1 was revealed to localise at ER-endosome MCS and antagonising action of NAADP inhibited the TPC1, buffered local calcium fluxes and this enlarged lysosomes (Kilpatrick *et al.*, 2017). Further, mobilisation of lysosomal calcium stores was sufficient for ER-dependent calcium release, probably through lysosomes-ER MCS, which was similar to the action of calcium mobilisation by NAADP (Kilpatrick *et al.*, 2013).

7.4 Concluding Remarks

Since the discovery of lysosomes more than sixty years ago, experiments have provided invaluable insight on the role of lysosomal calcium in cardiovascular diseases. My thesis is now part of the long series of milestones that show how modelling lysosomal calcium handling might contribute to existing knowledge of cardiac electrophysiology,

especially in untangling proarrhythmic mechanisms. I presented the following main novel contributions. First, based on experimental findings, I included lysosomal calcium handling in mouse ventricular and human atrial cardiomyocyte models. Second, I calibrated the model responses by lysosomal calcium handling with experimental results. Third, I investigated the proarrhythmic mechanisms of spontaneous calcium release by lysosomal calcium handling in mouse ventricular cardiomyocytes and the proarrhythmic mechanisms of EADs by lysosomal calcium release in human atrial cardiomyocytes. My findings reveal an antiarrhythmic impact of blocking lysosomal calcium release.

References

Acharya, U. R. *et al.* (2006) ‘Heart rate variability: A review’, *Medical and Biological Engineering and Computing*. doi: 10.1007/s11517-006-0119-0.

Akhtar, M. M. and Elliott, P. M. (2018) ‘Anderson-Fabry disease in heart failure’, *Biophysical Reviews*. doi: 10.1007/s12551-018-0432-5.

Allessie, M. A. *et al.* (2001) ‘Pathophysiology and prevention of atrial fibrillation’, *Circulation*, 103, pp. 769–777. doi: 10.1161/01.CIR.103.5.769.

Amuzescu, B. *et al.* (2021) ‘Evolution of mathematical models of cardiomyocyte electrophysiology’, *Mathematical Biosciences*, 334. doi: 10.1016/j.mbs.2021.108567.

Antzelevitch, C. and Burashnikov, A. (2011) ‘Overview of Basic Mechanisms of Cardiac Arrhythmia’, *Cardiac Electrophysiology Clinics*. doi: 10.1016/j.ccep.2010.10.012.

Anumonwo, J. M. and Pandit, S. V. (2015) ‘Ionic mechanisms of arrhythmogenesis’, *Trends in Cardiovascular Medicine*, 25(6), pp. 487–96. doi: 10.1016/j.tcm.2015.01.005.

Appelqvist, H. *et al.* (2013) ‘The lysosome: From waste bag to potential therapeutic target’, *Journal of Molecular Cell Biology*, 5(4), pp. 214–26. doi: 10.1093/jmcb/mjt022.

Aronis, K. N. *et al.* (2019) ‘Understanding AF mechanisms through computational modelling and simulations’, *Arrhythmia and Electrophysiology Review*, 8(3), pp. 210–219. doi: 10.15420/aer.2019.28.2.

Aston, D. *et al.* (2017) ‘High resolution structural evidence suggests the Sarcoplasmic Reticulum forms microdomains with Acidic Stores (lysosomes) in the heart’, *Scientific Reports*. Nature Publishing Group, 7(March 2016), p. 40620. doi: 10.1038/srep40620.

Atakpa, P. *et al.* (2018) ‘IP3 Receptors Preferentially Associate with ER-Lysosome Contact Sites and Selectively Deliver Ca2+ to Lysosomes’, *Cell Reports*, 25(11), pp. 3180–3193. doi: 10.1016/j.celrep.2018.11.064.

Ayagama, T. *et al.* (2023) ‘Compartmentalisation proteomics revealed endolysosomal protein network changes in a goat model of atrial fibrillation’, *bioRxiv*. doi: https://doi.org/10.1101/2023.03.10.532119.

Barral, D. C. *et al.* (2022) ‘Current methods to analyze lysosome morphology, positioning,

motility and function', *Traffic*, 23(5), pp. 238–269. doi: 10.1111/tra.12839.

Beeler, G. W. and Reuter, H. (1977) 'Reconstruction of the action potential of ventricular myocardial fibres', *The Journal of Physiology*. doi: 10.1113/jphysiol.1977.sp011853.

Beneke, K. and Molina, C. E. (2021) 'Molecular Basis of Atrial Fibrillation Initiation and Maintenance', *Hearts*, 2(1), pp. 170–187. doi: 10.3390/hearts2010014.

Bers, D. M. (2002) 'Cardiac excitation-contraction coupling', *Nature*, 415, pp. 198–205. doi: 10.1038/415198a.

Bers, D. M. (2008) 'Calcium cycling and signaling in cardiac myocytes', *Annual Review of Physiology*. doi: 10.1146/annurev.physiol.70.113006.100455.

Boyd, A. C. *et al.* (2013) 'Left atrial enlargement and reduced atrial compliance occurs early in fabry cardiomyopathy', *Journal of the American Society of Echocardiography*. doi: 10.1016/j.echo.2013.08.024.

Brennan, P. and Parkes, O. (2014) 'Case-finding in Fabry disease: Experience from the North of England', *Journal of Inherited Metabolic Disease*. doi: 10.1007/s10545-013-9629-8.

Britton, O. J. *et al.* (2013) 'Experimentally calibrated population of models predicts and explains intersubject variability in cardiac cellular electrophysiology', *Proceedings of the National Academy of Sciences of the United States of America*, 110(23), pp. E2098-105. doi: 10.1073/pnas.1304382110.

Brundel, B. J. J. M. *et al.* (2022) 'Atrial fibrillation', *Nature Reviews Disease Primers*, 8(1), p. 21. doi: 10.1038/s41572-022-00347-9.

Burgoyne, T., Patel, S. and Eden, E. R. (2014) 'Calcium signaling at ER membrane contact sites', *Biochimica et Biophysica Acta - Molecular Cell Research*, 1853(9), pp. 2012–2017. doi: 10.1016/j.bbamcr.2015.01.022.

Burton, R.-A. B. and Terrar, D. A. (2021) 'Emerging Evidence for cAMP-calcium Cross Talk in Heart Atrial Nanodomains Where IP 3 -Evoked Calcium Release Stimulates Adenylyl Cyclases', *Contact*. doi: 10.1177/25152564211008341.

C. de Duve *et al.* (1955) 'Tissue Fractionation Studies', *The Biochemical Journal*, 60, pp. 604–617.

Caballero, R. *et al.* (2010) 'In Humans, Chronic Atrial Fibrillation Decreases the Transient Outward Current and Ultrarapid Component of the Delayed Rectifier Current Differentially on Each Atria and Increases the Slow Component of the Delayed

Rectifier Current in Both', *Journal of the American College of Cardiology*, 55(21), pp. 2346–2354. doi: 10.1016/j.jacc.2010.02.028.

Calcraft, P. J. *et al.* (2009) 'NAADP mobilizes calcium from acidic organelles through two-pore channels', *Nature*, 459(7246), pp. 596–600. doi: 10.1038/nature08030.

Cancela, J. M., Churchill, G. C. and Galione, A. (1999) 'Coordination of agonist-induced Ca2+-signalling patterns by NAADP in pancreatic acinar cells', *Nature*, 398(6722), pp. 74–76. doi: 10.1038/18032.

Capel, R. A. *et al.* (2015) 'Two-pore Channels (TPC2s) and Nicotinic Acid Adenine Dinucleotide Phosphate (NAADP) at Lysosomal-Sarcoplasmic Reticular Junctions Contribute to Acute and Chronic beta-Adrenoceptor Signaling in the Heart', *J Biol Chem*. 2015/10/07. From the Department of Pharmacology, BHF Centre of Research Excellence, University of Oxford, Mansfield Road, Oxford OX1 3QT. the Faculty of Life Science, University of Manchester, Manchester M13 9NT, and. the Department of Physiology, Anatomy and Genetic, 290(50), pp. 30087–98. doi: 10.1074/jbc.M115.684076.

Capel, R. A. *et al.* (2024) 'Lysosomal signalling pathways influence heart rhythm, and regulate atrial function', *bioRxiv*. doi: https://doi.org/10.1101/2024.06.10.597905.

Carro, J. *et al.* (2011) 'A human ventricular cell model for investigation of cardiac arrhythmias under hyperkalaemic conditions', *Philosophical Transactions of the Royal Society A: Mathematical, Physical and Engineering Sciences*. doi: 10.1098/rsta.2011.0127.

Christ, T. *et al.* (2004) 'L-type Ca2+ current downregulation in chronic human atrial fibrillation is associated with increased activity of protein phosphatases', *Circulation*, 110(17), pp. 2651–2657. doi: 10.1161/01.CIR.0000145659.80212.6A.

Churchill, G. C. *et al.* (2002) 'NAADP mobilizes Ca2+ from reserve granules, lysosome-related organelles, in sea urchin eggs', *Cell*, 111(5), pp. 703–708. doi: 10.1016/S0092-8674(02)01082-6.

Churchill, G. C. and Galione, A. (2001) 'NAADP induces Ca2+ oscillations via a two-pool mechanism by priming IP3- and cADPR-sensitive Ca2+ stores', *EMBO J*, 20(11), pp. 2666–2671. doi: 10.1093/emboj/20.11.2666.

Collins, T. P. *et al.* (2011) 'NAADP influences excitation-contraction coupling by releasing calcium from lysosomes in atrial myocytes', *Cell Calcium*. Elsevier Ltd, 50(5), pp. 449–458. doi: 10.1016/j.ceca.2011.07.007.

Colman, M. A. *et al.* (2018) 'Description of the human atrial action potential derived from a single, congruent data source: Novel computational models for integrated experimental-

numerical study of atrial arrhythmia mechanisms', *Frontiers in Physiology*. doi: 10.3389/fphys.2018.01211.

Comtois, P., Kneller, J. and Nattel, S. (2005) 'Of circles and spirals: Bridging the gap between the leading circle and spiral wave concepts of cardiac reentry', *Europace*, 7(2), pp. 10–20. doi: 10.1016/j.eupc.2005.05.011.

Courtemanche, M., Ramirez, R. J. and Nattel, S. (1998) 'Ionic mechanisms underlying human atrial action potential properties: Insights from a mathematical model', *American Journal of Physiology - Heart and Circulatory Physiology*. doi: 10.1152/ajpheart.1998.275.1.h301.

Davidson, S. M. *et al.* (2015) 'Inhibition of NAADP signalling on reperfusion protects the heart by preventing lethal calcium oscillations via two-pore channel 1 and opening of the mitochondrial permeability transition pore', *Cardiovascular Research*, 108(3), pp. 357–366. doi: 10.1093/cvr/cvv226.

DiFrancesco, D. and Noble, D. (1985) 'A model of cardiac electrical activity incorporating ionic pumps and concentration changes.', *Philosophical transactions of the Royal Society of London. Series B, Biological sciences*, 307, pp. 353–998. doi: 10.1098/rstb.1985.0001.

Dobrev, D. *et al.* (2001) 'Molecular basis of downregulation of G-protein -coupled inward rectifying k+ current (ik,ach) in chronic human atrial fibrillation decrease in GIRK4 mrna correlates with reduced IK,ACh and muscarinic receptor-mediated shortening of action potentials', *Circulation*, 104(21), pp. 2551–2557. doi: 10.1161/hc4601.099466.

Dobrev, D. and Nattel, S. (2010) 'New antiarrhythmic drugs for treatment of atrial fibrillation', *The Lancet*, 375(9721), pp. 1212–1223. doi: 10.1016/S0140-6736(10)60096-7.

Dobrev, D. and Ravens, U. (2003) 'Remodeling of cardiomyocyte ion channels in human atrial fibrillation', *Basic Research in Cardiology*, 98, pp. 137–148. doi: 10.1007/s00395-003-0409-8.

Dorian, P. *et al.* (2007) 'The effect of vernakalant (RSD1235), an investigational antiarrhythmic agent, on atrial electrophysiology in humans', *Journal of Cardiovascular Pharmacology*, 50, pp. 35–40. doi: 10.1097/FJC.0b013e3180547553.

Duman, J. G. *et al.* (2006) 'Contributions of intracellular compartments to calcium dynamics: Implicating an acidic store', *Traffic*, 7(7), pp. 859–872. doi: 10.1111/j.1600-0854.2006.00432.x.

de Duve, C. (2005) 'The lysosome turns fifty', *Nature Cell Biology*. doi: 10.1038/ncb0905-847.

De Duve, C. and Wattiaux, R. (1966) ‘Functions of lysosomes.’, *Annual review of physiology*. doi: 10.1146/annurev.ph.28.030166.002251.

Eaton, D. C. (1984) *Ionic channels of excitable membranes. Bertil Hille. Sunderland, Ma: Sinauer Associates, 1984, Journal of Neuroscience Research*. doi: 10.1002/jnr.490130415.

El-Armouche, A. *et al.* (2006) ‘Molecular determinants of altered Ca2+ handling in human chronic atrial fibrillation’, *Circulation*, 114, pp. 670–680. doi: 10.1161/CIRCULATIONAHA.106.636845.

Fameli, N. *et al.* (2014) ‘Cytoplasmic nanojunctions between lysosomes and sarcoplasmic reticulum are required for specific calcium signaling’, *F1000Research*, 3, p. 93. doi: 10.12688/f1000research.3720.1.

Frenzel, H. *et al.* (1988) ‘Regression of cardiac hypertrophy: Morphometric and biochemical studies in rat heart after swimming training’, *Journal of Molecular and Cellular Cardiology*, 20(8), pp. 737–751. doi: 10.1016/S0022-2828(88)80018-X.

Galione, A. *et al.* (2010) ‘NAADP as an intracellular messenger regulating lysosomal calcium-release channels’, *Biochem Soc Trans*, 38(6), pp. 1424–1431. doi: 10.1042/BST0381424.

Garny, A., Noble, D. and Kohl, P. (2005) ‘Dimensionality in cardiac modelling’, *Progress in Biophysics and Molecular Biology*, 87(1), pp. 47–66. doi: 10.1016/j.pbiomolbio.2004.06.006.

Garrity, A. G. *et al.* (2016) ‘The endoplasmic reticulum, not the pH gradient, drives calcium refilling of lysosomes’, *eLife*, 5, p. e15887. doi: 10.7554/eLife.15887.

Genazzani, A. A. *et al.* (1997) ‘Pharmacological properties of the Ca2+-release mechanism sensitive to NAADP in the sea urchin egg’, *British Journal of Pharmacology*, 121(7), pp. 1489–1495. doi: 10.1038/sj.bjp.0701295.

Giugliani, R. *et al.* (2016) ‘A 15-year perspective of the fabry outcome survey’, *Journal of Inborn Errors of Metabolism and Screening*. doi: 10.1177/2326409816666298.

Grandi, E. *et al.* (2011) ‘Human atrial action potential and Ca 2+ model: Sinus rhythm and chronic atrial fibrillation’, *Circulation Research*, 109, pp. 1055–1066. doi: 10.1161/CIRCRESAHA.111.253955.

Grandi, E., Pasqualini, F. S. and Bers, D. M. (2010) ‘A novel computational model of the human ventricular action potential and Ca transient’, *Journal of Molecular and Cellular*

Cardiology, 48(1), pp. 112–121. doi: 10.1016/j.yjmcc.2009.09.019.

Grant, A. O. (2009) 'Cardiac ion channels: Basic science for the clinical electrophysiologist.', *Circulation: Arrhythmia and Electrophysiology*, 2(2), pp. 185–194.

Grunnet, M. (2010) 'Repolarization of the cardiac action potential. Does an increase in repolarization capacity constitute a new anti-arrhythmic principle?', *Acta Physiologica*. doi: 10.1111/j.1748-1716.2009.02072.x.

Hers, H. G. (1963) 'α-Glucosidase deficiency in generalized glycogen storage disease (Pompe's disease)', *Biochem. J*, 86, pp. 11–16.

Hilgemann, D. W. and Noble, D. (1987) 'Excitation-contraction coupling and extracellular calcium transients in rabbit atrium: reconstruction of basic cellular mechanisms.', *Proceedings of the Royal Society of London. Series B, Containing papers of a Biological character. Royal Society (Great Britain)*, 230, pp. 163–205. doi: 10.1098/rspb.1987.0015.

Hindricks, G. *et al.* (2021) '2020 ESC Guidelines for the diagnosis and management of atrial fibrillation developed in collaboration with the European Association for Cardio-Thoracic Surgery (EACTS)', *Russian Journal of Cardiology*, 42(5), pp. 373–498. doi: 10.15829/1560-4071-2021-4701.

Hodgkin, A. L. and Huxley, A. F. (1952) 'A quantitative description of membrane current and its application to conduction and excitation in nerve', *The Journal of Physiology*. doi: 10.1113/jphysiol.1952.sp004764.

Iwasaki, Y. *et al.* (2011) 'Atrial Fibrillation Pathophysiology', *Circulation*, 124(20), pp. 2264–2274. doi: 10.1161/circulationaha.111.019893.

Jakes, D. *et al.* (2019) 'Perlin noise generation of physiologically realistic patterns of fibrosis', *bioRxiv*.

January, C. T. and Riddle, J. M. (1989) 'Early afterdepolarizations: Mechanism of induction and block. A role for L-type Ca2+ current', *Circulation Research*, 64, pp. 977–990. doi: 10.1161/01.RES.64.5.977.

Kathofer, S., Thomas, D. and Karle, C. A. (2005) 'The novel antiarrhythmic drug dronedarone: Comparison with amiodarone', *Cardiovascular Drug Reviews*, 23, pp. 217–230. doi: 10.1111/j.1527-3466.2005.tb00167.x.

Keating, M. T. and Sanguinetti, M. C. (2001) 'Molecular and cellular mechanisms of cardiac arrhythmias', *Cell*. doi: 10.1016/S0092-8674(01)00243-4.

Kernik, D. C. *et al.* (2019) ‘A computational model of induced pluripotent stem-cell derived cardiomyocytes incorporating experimental variability from multiple data sources’, *Journal of Physiology*, 597(17), pp. 4533–4564. doi: 10.1113/JP277724.

Kettlewell, S. *et al.* (2019) ‘Dynamic clamping human and rabbit atrial calcium current: narrowing ICaL window abolishes early afterdepolarizations’, *Journal of Physiology*, 597(14), pp. 3619–3638. doi: 10.1113/JP277827.

Kilpatrick, B. S. *et al.* (2013) ‘Direct mobilisation of lysosomal Ca2+ triggers complex Ca2+ signals’, *Journal of Cell Science*, 126(0 1), pp. 60–66. doi: 10.1242/jcs.118836.

Kilpatrick, B. S. *et al.* (2017) ‘An Endosomal NAADP-Sensitive Two-Pore Ca2+ Channel Regulates ER-Endosome Membrane Contact Sites to Control Growth Factor Signaling’, *Cell Reports*, 18(7), pp. 1636–1645. doi: 10.1016/j.celrep.2017.01.052.

Klingelhöfer, D. *et al.* (2020) ‘Global research on Fabry’s disease: Demands for a rare disease’, *Molecular Genetics and Genomic Medicine*, 8(9), p. e1163. doi: 10.1002/mgg3.1163.

Koivumäki, J. T., Korhonen, T. and Tavi, P. (2011) ‘Impact of sarcoplasmic reticulum calcium release on calcium dynamics and action potential morphology in human atrial myocytes: A computational study’, *PLoS Computational Biology*, 7(1), p. e1001067. doi: 10.1371/journal.pcbi.1001067.

Laney, D. A., Gupta, D. and Wechsler, S. B. (2018) ‘Getting to the Heart of the Matter: Lysosomal Storage Diseases That Manifest a Cardiac Phenotype’, *Current Genetic Medicine Reports*, 6, pp. 28–42. doi: 10.1007/s40142-018-0135-z.

Lee, H. C. (2005) ‘Nicotinic acid adenine dinucleotide phosphate (NAADP)-mediated calcium signaling’, *Journal of Biological Chemistry*, pp. 33693–33696. doi: 10.1074/jbc.R500012200.

Lewis, A. M. *et al.* (2012) ‘beta-Adrenergic receptor signaling increases NAADP and cADPR levels in the heart’, *Biochemical and Biophysical Research Communications*, 427(2), pp. 326–329. doi: 10.1016/j.bbrc.2012.09.054.

Li, L. *et al.* (2011) ‘Calcium dynamics in the ventricular myocytes of SERCA2 knockout mice: A modeling study’, *Biophysical Journal*. doi: 10.1016/j.bpj.2010.11.048.

Li, L. *et al.* (2012) ‘Sodium accumulation in SERCA knockout-induced heart failure’, *Biophysical Journal*. doi: 10.1016/j.bpj.2012.03.045.

Liberos, A. *et al.* (2016) ‘Balance between sodium and calcium currents underlying chronic atrial fibrillation termination: An in silico intersubject variability study’, *Heart Rhythm*,

13(12), pp. 2358–2365. doi: 10.1016/j.hrthm.2016.08.028.

Lin, W. K. *et al.* (2017) ‘Synthesis of the Ca 2+ -mobilizing messengers NAADP and cADPR by intracellular CD38 enzyme in the mouse heart: Role in -adrenoceptor signaling’, *Journal of Biological Chemistry*, 292(32), pp. 13243–13257. doi: 10.1074/jbc.M117.789347.

Lindblad, D. S. *et al.* (1996) ‘A model of the action potential and underlying membrane currents in a rabbit atrial cell’, *American Journal of Physiology - Heart and Circulatory Physiology*. doi: 10.1152/ajpheart.1996.271.4.h1666.

Lloyd-Evans, E. *et al.* (2008) ‘Niemann-Pick disease type C1 is a sphingosine storage disease that causes deregulation of lysosomal calcium’, *Nature Medicine*, 14(11), pp. 1247–1255. doi: 10.1038/nm.1876.

Lloyd-Evans, E. and Platt, F. M. (2011) ‘Lysosomal Ca2+ homeostasis: Role in pathogenesis of lysosomal storage diseases’, *Cell Calcium*. doi: 10.1016/j.ceca.2011.03.010.

Lübke, T., Lobel, P. and Sleat, D. E. (2009) ‘Proteomics of the lysosome’, *Biochimica et Biophysica Acta - Molecular Cell Research*. doi: 10.1016/j.bbamcr.2008.09.018.

Luo, C. H. and Rudy, Y. (1994a) ‘A dynamic model of the cardiac ventricular action potential: I. Simulations of ionic currents and concentration changes’, *Circulation Research*. doi: 10.1161/01.RES.74.6.1071.

Luo, C. H. and Rudy, Y. (1994b) ‘A dynamic model of the cardiac ventricular action potential: II. Afterdepolarizations, triggered activity, and potentiation’, *Circulation Research*. doi: 10.1161/01.RES.74.6.1097.

Macgregor, A. *et al.* (2007) ‘NAADP controls cross-talk between distinct Ca2+ stores in the heart’, *Journal of Biological Chemistry*, 282(20), pp. 15302–15311. doi: 10.1074/jbc.M611167200.

Maleckar, M. M. *et al.* (2008) ‘Mathematical simulations of ligand-gated and cell-type specific effects on the action potential of human atrium’, *Progress in Biophysics and Molecular Biology*. doi: 10.1016/j.pbiomolbio.2009.01.010.

Maleckar, M. M. *et al.* (2009) ‘K+ current changes account for the rate dependence of the action potential in the human atrial myocyte’, *American Journal of Physiology - Heart and Circulatory Physiology*, 297(4), pp. H1398–H1410. doi: 10.1152/ajpheart.00411.2009.

Marino, S. *et al.* (2008) ‘A methodology for performing global uncertainty and sensitivity

analysis in systems biology', *Journal of Theoretical Biology*, 254(1), pp. 178–196. doi: 10.1016/j.jtbi.2008.04.011.

Martello, A., Platt, F. M. and Eden, E. R. (2020) 'Staying in touch with the endocytic network: The importance of contacts for cholesterol transport', *Traffic*, 21(5), pp. 354–363. doi: 10.1111/tra.12726.

Masson, C. *et al.* (2004) 'Fabry disease: A review', *Joint Bone Spine*. doi: 10.1016/j.jbspin.2003.10.015.

McAllister, R. E., Noble, D. and Tsien, R. W. (1975) 'Reconstruction of the electrical activity of cardiac Purkinje fibres.', *The Journal of Physiology*, 251, pp. 1–59. doi: 10.1113/jphysiol.1975.sp011080.

McKay, M. D. *et al.* (1979) 'A Comparison of Three Methods for Selecting Values of Input Variables in the Analysis of Output from a Computer Code', *Technometrics*, 42(1), pp. 55–61. doi: 10.2307/1268522.

Mehta, A. *et al.* (2004) 'Fabry disease defined: Baseline clinical manifestations of 366 patients in the Fabry Outcome Survey', *European Journal of Clinical Investigation*, 34(3), pp. 236–42. doi: 10.1111/j.1365-2362.2004.01309.x.

Meng, Z. *et al.* (2023) 'Lysosomal calcium loading promotes spontaneous calcium release by potentiating ryanodine receptors', *Biophysical Journal*, 122(15), pp. 3044–3059. doi: 10.1016/j.bpj.2023.06.007.

Metchnikoff, E. (1907) *Immunity to Infective Disease*. Cambridge University Press, Cambridge.

Michalak, M. and Opas, M. (2009) 'Endoplasmic and sarcoplasmic reticulum in the heart', *Trends in Cell Biology*. doi: 10.1016/j.tcb.2009.03.006.

Morgan, A. J. *et al.* (2011) 'Molecular mechanisms of endolysosomal Ca 2+ signalling in health and disease', *Biochemical Journal*, 439(1), pp. 349–74. doi: 10.1042/BJ20110949.

Morgan, A. J. *et al.* (2013) 'Bidirectional Ca2+ signaling occurs between the endoplasmic reticulum and acidic organelles', *Journal of Cell Biology*, 200(6), pp. 789–805. doi: 10.1083/jcb.201204078.

Morotti, S. *et al.* (2014) 'A novel computational model of mouse myocyte electrophysiology to assess the synergy between Na+ loading and CaMKII', *Journal of Physiology*, 592(6), pp. 1181–1197. doi: 10.1113/jphysiol.2013.266676.

Morotti, S. *et al.* (2016) 'Atrial-selective targeting of arrhythmogenic phase-3 early afterdepolarizations in human myocytes', *Journal of Molecular and Cellular Cardiology*, 96, pp. 63–71. doi: 10.1016/j.yjmcc.2015.07.030.

Morrissey, R. P., Philip, K. J. and Schwarz, E. R. (2011) 'Cardiac abnormalities in Anderson-Fabry disease and Fabry's cardiomyopathy', *Cardiovascular Journal of Africa*, 22(1), pp. 38–44.

Moshkforoush, A. *et al.* (2019) 'Modeling the role of endoplasmic reticulum-mitochondria microdomains in calcium dynamics', *Scientific Reports*, 9(1), p. 17072. doi: 10.1038/s41598-019-53440-7.

Muszkiewicz, A. *et al.* (2016) 'Variability in cardiac electrophysiology: Using experimentally-calibrated populations of models to move beyond the single virtual physiological human paradigm', *Progress in Biophysics and Molecular Biology*, 120(1–3), pp. 115–27. doi: 10.1016/j.pbiomolbio.2015.12.002.

Namdar, M. (2016) 'Electrocardiographic Changes and Arrhythmia in Fabry Disease', *Frontiers in Cardiovascular Medicine*. doi: 10.3389/fcvm.2016.00007.

Nattel, S. *et al.* (2002) 'New approaches to atrial fibrillation management: A critical review of a rapidly evolving field', *Drugs*, 62, pp. 2377–2397. doi: 10.2165/00003495-200262160-00005.

Nattel, S., Burstein, B. and Dobrev, D. (2008) 'Atrial remodeling and atrial fibrillation: mechanisms and implications.', *Circulation. Arrhythmia and electrophysiology*, 1(1), pp. 62–73. doi: 10.1161/CIRCEP.107.754564.

Nebel, M. *et al.* (2013) 'Nicotinic acid adenine dinucleotide phosphate (NAADP)-mediated calcium signaling and arrhythmias in the heart evoked by β-adrenergic stimulation', *Journal of Biological Chemistry*, 288(22), pp. 16017–16030. doi: 10.1074/jbc.M112.441246.

Neef, S. *et al.* (2010) 'CaMKII-Dependent diastolic SR Ca2+ leak and elevated diastolic Ca2+ levels in right atrial myocardium of patients with atrial fibrillation', *Circulation Research*, 106(6), pp. 1134–1144. doi: 10.1161/CIRCRESAHA.109.203836.

Nerbonne, J. M. *et al.* (2001) 'Genetic Manipulation of Cardiac K + Channel Function in Mice', *Circulation Research*, 89(11), pp. 944–956. doi: 10.1161/hh2301.100349.

Neufeld, E. F. (2006) *Fabry Disease: Perspectives from 5 Years of FOS, Enzyme replacement therapy – a brief history*.

Noble, D. (1962) ‘A modification of the Hodgkin—Huxley equations applicable to Purkinje fibre action and pacemaker potentials’, *The Journal of Physiology*. doi: 10.1113/jphysiol.1962.sp006849.

Noble, D. (2002) ‘Modeling the heart - From genes to cells to the whole organ’, *Science*. doi: 10.1126/science.1069881.

Nygren, A. *et al.* (1998) ‘Mathematical model of an adult human atrial cell: The role of K+ currents in repolarization’, *Circulation Research*. doi: 10.1161/01.RES.82.1.63.

Olson, T. M. *et al.* (2006) ‘Kv1.5 channelopathy due to KCNA5 loss-of-function mutation causes human atrial fibrillation’, *Human Molecular Genetics*, 15(14), pp. 2185–2191. doi: 10.1093/hmg/ddl143.

Osadchii, O. E. (2017) ‘Role of abnormal repolarization in the mechanism of cardiac arrhythmia’, *Acta Physiologica*, 220(S712), pp. 1–71. doi: 10.1111/apha.12902.

Paci, M. *et al.* (2013) ‘Computational models of ventricular-and atrial-like human induced pluripotent stem cell derived cardiomyocytes’, *Annals of Biomedical Engineering*, 41(11), pp. 2334–48. doi: 10.1007/s10439-013-0833-3.

Page, E., McCallister, L. P. and Power, B. (1971) ‘Stereological Measurements of Cardiac Ultrastructures Implicated in Excitation-Contraction Coupling’, *Proceedings of the National Academy of Sciences of the United States of America*, 68(7), pp. 1465–1466.

Passini, E. *et al.* (2016) ‘Mechanisms of pro-arrhythmic abnormalities in ventricular repolarisation and anti-arrhythmic therapies in human hypertrophic cardiomyopathy’, *Journal of Molecular and Cellular Cardiology*, 96, pp. 72–81. doi: 10.1016/j.yjmcc.2015.09.003.

Patel, S., Churchill, G. C. and Galione, A. (2001) ‘Coordination of Ca2+ signalling by NAADP’, *Trends in Biochemical Sciences*, 26(8), pp. 482–489. doi: 10.1016/S0968-0004(01)01896-5.

Pellman, J. and Sheikh, F. (2015) ‘Atrial fibrillation: Mechanisms, therapeutics, and future directions’, *Comprehensive Physiology*, 5(2), pp. 649–665. doi: 10.1002/cphy.c140047.

Penny, C. J. *et al.* (2014) ‘A computational model of lysosome-ER Ca2+ microdomains’, *Journal of Cell Science*, 127(Pt 13), pp. 2934–43. doi: 10.1242/jcs.149047.

Pitt, S. J. *et al.* (2010) ‘TPC2 is a novel NAADP-sensitive Ca2+ release channel, operating as a dual sensor of luminal pH and Ca2+’, *Journal of Biological Chemistry*, 592(6), pp. 1181–1197. doi: 10.1074/jbc.M110.156927.

Pitt, S. J. *et al.* (2014) ‘Reconstituted Human TPC1 is a proton-permeable ion channel and is activated by NAADP or Ca2+’, *Science Signaling*, 7(326), p. ra46. doi: 10.1126/scisignal.2004854.

Pitt, S. J., Reilly-O’Donnell, B. and Sitsapesan, R. (2016) ‘Exploring the biophysical evidence that mammalian two-pore channels are NAADP-activated calcium-permeable channels’, *Journal of Physiology*, 594(15), pp. 4171–4179. doi: 10.1113/JP270936.

Platt, F. M. *et al.* (2018) ‘Lysosomal storage diseases’, *Nature Reviews Disease Primers*. doi: 10.1038/s41572-018-0025-4.

Qiu, J. (2004) ‘The calcium link of heart and mind’, *Nature Reviews Neuroscience*. doi: 10.1038/nrn1548.

Qu, Z. *et al.* (2013) ‘Early afterdepolarizations in cardiac myocytes: Beyond reduced repolarization reserve’, *Cardiovascular Research*, 99(1), pp. 6–15. doi: 10.1093/cvr/cvt104.

Rawlins, J., Bhan, A. and Sharma, S. (2009) ‘Left ventricular hypertrophy in athletes’, *European Journal of Echocardiography*. doi: 10.1093/ejechocard/jep017.

Romero, L. *et al.* (2009) ‘Impact of ionic current variability on human ventricular cellular electrophysiology’, *American Journal of Physiology - Heart and Circulatory Physiology*. doi: 10.1152/ajpheart.00263.2009.

Ruas, M. *et al.* (2015) ‘Expression of Ca 2+ -permeable two-pore channels rescues NAADP signalling in TPC -deficient cells’, *The EMBO Journal*, 34(13), pp. 1743–1758. doi: 10.15252/embj.201490009.

Sánchez, C. *et al.* (2014) ‘Inter-subject variability in human atrial action potential in sinus rhythm versus chronic atrial fibrillation’, *PLoS ONE*, 9(8), p. e105897. doi: 10.1371/journal.pone.0105897.

Sánchez, C. *et al.* (2017) ‘Atrial fibrillation dynamics and ionic block effects in six Heterogeneous human 3D virtual atria with distinct repolarization dynamics’, *Frontiers in Bioengineering and Biotechnology*, 5, p. 29. doi: 10.3389/fbioe.2017.00029.

Sarkar, A. X., Christini, D. J. and Sobie, E. A. (2012) ‘Exploiting mathematical models to illuminate electrophysiological variability between individuals’, *Journal of Physiology*, 590(11), pp. 2555–2567. doi: 10.1113/jphysiol.2011.223313.

Schmidt, C. *et al.* (2015) ‘Upregulation of K2P 3.1 K + Current Causes Action Potential Shortening in Patients with Chronic Atrial Fibrillation’, *Circulation*. doi:

10.1161/CIRCULATIONAHA.114.012657.

Schotten, U. *et al.* (2002) 'Atrial fibrillation-induced atrial contractile dysfunction: A tachycardiomyopathy of a different sort', *Cardiovascular Research*, 53, pp. 192–201. doi: 10.1016/S0008-6363(01)00453-9.

Schotten, U. *et al.* (2011) 'Pathophysiological mechanisms of atrial fibrillation: A translational appraisal', *Physiological Reviews*, 91(1), pp. 265–325. doi: 10.1152/physrev.00031.2009.

Schröder, B. A. *et al.* (2010) 'The proteome of lysosomes', *Proteomics*. doi: 10.1002/pmic.201000196.

Schwartz, P. J. *et al.* (1995) 'Long QT syndrome patients with mutations of the SCN5A and HERG genes have differential responses to Na+ channel blockade and to increases in heart rate: Implications for gene-specific therapy', *Circulation*, 92, pp. 3381–3386. doi: 10.1161/01.CIR.92.12.3381.

Scoote, M. and Williams, A. J. (2004) 'Myocardial calcium signalling and arrhythmia pathogenesis', *Biochemical and Biophysical Research Communications*, 322(4), pp. 1286–309. doi: 10.1016/j.bbrc.2004.08.034.

Seydelmann, N. *et al.* (2015) 'Fabry disease and the heart', *Best Practice and Research: Clinical Endocrinology and Metabolism*. doi: 10.1016/j.beem.2014.10.003.

Shah, J. S. *et al.* (2005) 'Prevalence and clinical significance of cardiac arrhythmia in Anderson-Dabry disease', *American Journal of Cardiology*. doi: 10.1016/j.amjcard.2005.05.033.

Shannon, T. R. *et al.* (2004) 'A mathematical treatment of integrated Ca dynamics within the ventricular myocyte', *Biophysical Journal*, 87(5), pp. 3351–3371. doi: 10.1529/biophysj.104.047449.

Simon, J. N. *et al.* (2021) 'Oxidation of protein kinase a regulatory subunit PKARIα protects against myocardial ischemia-reperfusion injury by inhibiting lysosomal-triggered calcium release', *Circulation*, 143(5), pp. 449–465. doi: 10.1161/CIRCULATIONAHA.120.046761.

Singh, B. N. *et al.* (2005) 'Amiodarone versus Sotalol for Atrial Fibrillation', *New England Journal of Medicine*, 352, pp. 1861–1872. doi: 10.1056/nejmoa041705.

Singh, B. N. (2008) 'Amiodarone as paradigm for developing new drugs for atrial fibrillation', *Journal of Cardiovascular Pharmacology*, 52, pp. 300–305. doi:

10.1097/FJC.0b013e31818914b6.

Smith, G. L. and Eisner, D. A. (2019) ‘Calcium Buffering in the Heart in Health and Disease’, *Circulation*, 139, pp. 2358–2371. doi: 10.1161/CIRCULATIONAHA.118.039329.

Sobie, E. A. (2009) ‘Parameter sensitivity analysis in electrophysiological models using multivariable regression’, *Biophysical Journal*. doi: 10.1016/j.bpj.2008.10.056.

Soltis, A. R. and Saucerman, J. J. (2010) ‘Synergy between CaMKII substrates and β-adrenergic signaling in regulation of cardiac myocyte Ca2 handling’, *Biophysical Journal*, 99(7), pp. 2038–47. doi: 10.1016/j.bpj.2010.08.016.

Sossalla, S. *et al.* (2010) ‘Altered Na+ Currents in Atrial Fibrillation. Effects of Ranolazine on Arrhythmias and Contractility in Human Atrial Myocardium’, *Journal of the American College of Cardiology*, 55, pp. 2330–2342. doi: 10.1016/j.jacc.2009.12.055.

Spada, M. *et al.* (2006) ‘High incidence of later-onset Fabry disease revealed by newborn screening’, *American Journal of Human Genetics*. doi: 10.1086/504601.

SZABO, B. *et al.* (1994) ‘Role of Na+:Ca2+ Exchange Current in Cs+-Induced Early Afterdepolarizations in Purkinje Fibers’, *Journal of Cardiovascular Electrophysiology*, 5, pp. 933–944. doi: 10.1111/j.1540-8167.1994.tb01133.x.

Tauber, A. I. (2003) ‘Metchnikoff and the phagocytosis theory’, *Nature Reviews Molecular Cell Biology*, 4(11), pp. 897–901. doi: 10.1038/nrm1244.

Trayanova, N. A. (2014) ‘Mathematical approaches to understanding and imaging atrial fibrillation: Significance for mechanisms and management’, *Circulation Research*, 114(9), pp. 1516–1531. doi: 10.1161/CIRCRESAHA.114.302240.

Tse, G. (2016) ‘Mechanisms of cardiac arrhythmias’, *Journal of Arrhythmia*, 32(2), pp. 75–81. doi: 10.1016/j.joa.2015.11.003.

Tsujimae, K., Murakami, S. and Kurachi, Y. (2008) ‘In silico study on the effects of IKur block kinetics on prolongation of human action potential after atrial fibrillation-induced electrical remodeling’, *American Journal of Physiology - Heart and Circulatory Physiology*, 294(2), pp. H793–H800. doi: 10.1152/ajpheart.01229.2007.

Voigt, N. *et al.* (2009) ‘Cellular and molecular determinants of altered atrial Ca2+ signaling in patients with chronic atrial fibrillation’, *Circulation*, 120, pp. S667–S668.

Voigt, N. *et al.* (2013) ‘Impaired Na+-dependent regulation of acetylcholine-activated inward-rectifier K+ current modulates action potential rate dependence in patients with chronic

atrial fibrillation', *Journal of Molecular and Cellular Cardiology*, 61, pp. 142–152. doi: 10.1016/j.yjmcc.2013.03.011.

Voigt, N. *et al.* (2014) 'Cellular and molecular mechanisms of atrial arrhythmogenesis in patients with paroxysmal atrial fibrillation', *Circulation*. doi: 10.1161/CIRCULATIONAHA.113.006641.

Volders, P. G. A. *et al.* (2000) 'Progress in the understanding of cardiac early afterdepolarizations and torsades de pointes: Time to revise current concepts', *Cardiovascular Research*, 46(3), pp. 376–392. doi: 10.1016/S0008-6363(00)00022-5.

Walmsley, J. *et al.* (2013) 'mRNA Expression Levels in Failing Human Hearts Predict Cellular Electrophysiological Remodeling: A Population-Based Simulation Study', *PLoS ONE*. doi: 10.1371/journal.pone.0056359.

Weiss, J. N. *et al.* (2010) 'Early afterdepolarizations and cardiac arrhythmias', *Heart Rhythm*, 7(12), pp. 1891–1899. doi: 10.1016/j.hrthm.2010.09.017.

Weiss, J. N. *et al.* (2011) 'Alternans and arrhythmias : From cell to heart', *Circulation Research*. doi: 10.1161/CIRCRESAHA.110.223586.

Wettwer, E. *et al.* (2004) 'Role of IKur in controlling action potential shape and contractility in the human atrium: Influence of chronic atrial fibrillation', *Circulation*, 110(16), pp. 2299–2306. doi: 10.1161/01.CIR.0000145155.60288.71.

Wilders, R. (2007) 'Computer modelling of the sinoatrial node', *Medical & Biological Engineering & Computing*, 45, pp. 189–207. doi: 10.1007/s11517-006-0147-9.

Wit, A. and Rosen, M. (1992) *Afterdepolarizations and triggered activity distinction from automaticity as an arrhythmogenic mechanism.* In: Fozzard HA, Haber E, Jennings RB, Katz AM, Morgan HE (eds) The heart and cardiovascular system, second edition. Raven Press, Ltd., New York, pp. 1–51.

Wu, P. L. *et al.* (2017) 'Myocardial Upregulation of Cathepsin D by Ischemic Heart Disease Promotes Autophagic Flux and Protects Against Cardiac Remodeling and Heart Failure', *Circulation-Heart Failure*, 10(7). doi: 10.1161/circheartfailure.117.004044.

Yang, J. H. and Saucerman, J. J. (2012) 'Phospholemman is a negative feed-forward regulator of Ca 2+ in β-adrenergic signaling, accelerating β-adrenergic inotropy', *Journal of Molecular and Cellular Cardiology*, 52(5), pp. 1048–1055. doi: 10.1016/j.yjmcc.2011.12.015.

Yuan, Y. *et al.* (2021) 'The lysosomotrope GPN mobilises Ca2+ from acidic organelles',

Journal of Cell Science, 134(6), p. jcs256578. doi: 10.1242/jcs.256578.

Zaza, A. (2000) 'The cardiac action potential', in *An Introduction to Cardiac Electrophysiology*.

Zeng, J. and Rudy, Y. (1995) 'Early afterdepolarizations in cardiac myocytes: mechanism and rate dependence', *Biophysical Journal*. doi: 10.1016/S0006-3495(95)80271-7.

Zhao, Z. *et al.* (2012) 'Revisiting the ionic mechanisms of early afterdepolarizations in cardiomyocytes: Predominant by Ca waves or Ca currents?', *American Journal of Physiology - Heart and Circulatory Physiology*, 302(8), pp. H1636-44. doi: 10.1152/ajpheart.00742.2011.

Zhou, X. *et al.* (2016) 'In Vivo and in Silico Investigation into Mechanisms of Frequency Dependence of Repolarization Alternans in Human Ventricular Cardiomyocytes', *Circulation Research*, 118(2), pp. 266–78. doi: 10.1161/CIRCRESAHA.115.307836.